University of Naples “Federico II”

Department of Industrial Engineering

PhD in Industrial Engineering

Environmental impact of passenger ships in port

Luigia Mocerino

Tutors:

Prof. Franco Quaranta

Prof. Enrico Rizzuto

Coordinator:

Prof. Michele Grassi

33° Cycle (2018-2021)

Summary

Summary

The ***environmental impact of ships*** *can be of different types. This thesis covers* ***air pollution*** *due to* ***chemicals*** *and concentrates on local effects due to compounds emitted in the exhaust gases of internal combustion engines and* ***acoustic pollution****. The attention has been focused on the consequences of the presence of many ships in ports located close to inhabited zones. For port-scale analyzes, the case study is the port of Naples for which traffics, geographic conformation, meteorological conditions, results of experimental campaigns both in the field of acoustic and environmental impact are available. In the field of polluting emissions, the case study for the simulations is a catamaran in service at the port of Naples for which experimental measurements at sea and bench tests are available. For the simulation of acoustic emissions, the case study is a passenger ship for which experimental measurements and forecast data are available. Experimental campaigns and simulations have been carried out on the port of Naples and most of the applications concern passenger ships, but methods and procedures can be applied to a general case. The thesis consists of six chapters, briefly introduced here. Each chapter contains a first subsection named "aims and scope" precisely to describe its main purposes in a more extended way than the summary presented here.*

The theme is first framed in the more general context of the environmental impact of anthropogenic activities and of marine transportation in particular assessment studies and documents issued by international bodies reporting targets for limiting the global environmental impact of the shipping sector are briefly summarized. Recalls on the main mechanisms of formation and reduction of pollutants are exposed.

The second chapter describes the bottom-up method aimed at estimating the emissions of passenger ships in port. To obtain an estimation of all the emissions a series of very specific steps are necessary. The main information to be collected and produced concerns: traffic, routes, arrival and departure schedules, engine loads, emissions, heights, and diameters of the funnels. The technique of data collection and its use was gradually deepened (from simple cruise calendar to AIS data). The main application on the entire port sees the use of AIS data. The starting AIS data have been processed through an "ad hoc" MATLAB code capable of managing a relevant amount of data and returning a complete calendar of all the movements of every ship arriving and operating in the port. The use of AIS data has brought about improvements in the calculation methodology for emissions as well, allowing for example a more accurate analysis of average speeds in port and idle times.

The port of Naples, where all the analysis were developed, is presented next. The traffics for the years and reference periods chosen in the subsequent analyzes are presented (2012, 2016, and 2018). A comprehensive study of the environmental impact of ships cannot be separated from the creation of atmospheric dispersion models. These models require the flow of pollutants emitted in the main operational phases in port (navigation, maneuvering, and mooring) as the main inputs. The results allow to estimate the weight that the passenger branch has on air quality also thanks to cross-comparisons with port measurements and ARPAC (Regional Agency for Environmental Protection in Campania) data.

After the analysis of the environmen0tal impact on a port scale, the problem of emissions has been approached by applying a designated simulation, with the aim to overcome the use of emission factors. The first part of the chapter describes a state of the art of simulation model and an in-depth analysis of the main emission simulation methodologies. An engine model has been created in RICARDO WAVE environment; this engine model was validated and calibrated on an engine installed onboard a passenger ship operating in the port of Naples. Bench test results in terms of power, torque, consumption, and rpm have been used to calibrate the model while experimental measurements validated it. In the dissertation, a description of the case study (ship, engine, bench tests, and sea trials), a description of the model, and an interpretation of the results are presented. The validation on sea trials shows the effectiveness of the model both in terms of main engine parameters and emissions. At the end of the chapter, a comparison between the three emission estimation methodologies (EMEP-EEA, with AIS data, simulations, and experimental campaign) has been carried out.

The next chapter of the thesis concerns the assessment of the acoustic impact of passenger ships in port. The structure of the research is typically the same: simulation and experimental results. The first part shows some experimental surveys made on a passenger ship in port that served as validation of a simulation model built in the TERRAIN OLIVE TREE LAB SUITE environment. The second and last part presents the methodology and results obtained in the context of a collaborative research project between the Universities of Naples, Genoa, and Trieste. The project aimed at characterizing the acoustic impact of a ship in light of the new additional class notation published by the Lloyds Register "Procedure for the Determination of Airborne Noise Emissions from Marine Vessels Airborne Noise Emissions from Marine Vessels".

The last chapter sets out three applications in order to keep the problem set in a global scale context. The first presents an analysis of the possible countermeasures that can be applied to the cruise ship fleet aimed at environmental safeguarding (DNV Appraisal Tool), in the wake of the EEOI and EEDI. Furthermore, in the context of the environmental impact on a port scale, preliminary measurements of polluting emissions using remote measurement instruments (LIDAR) were carried out with the aim of allowing an indirect estimate of the concentrations of pollutants in the exhausts of ships, thus significantly reducing the uncertainties related to ground-level measurements with active or passive samplers.

The last application, on the other hand, concerns the ports and the possible activities and initiatives to be implemented in order to host fleet of increasingly green and eco-sustainable ships (Environmental Ship Index).

1. The influence of the maritime sector on the environment

Aims and scope

Anthropogenic activities, i.e. all those related to human life on earth, involve an alteration of the natural balance of the ecosystem. The ***transport sector****, in particular, is one of the main causes of* ***climate change*** *(on a global scale) and of* ***air pollution*** *(on a local scale). Within the transport sector, the* ***maritime sector*** *plays a central role in terms of trade in goods and passengers. Social awareness on environmental issues is becoming increasingly greater in recent years and efforts are being made to reduce emissions with different strategies. Each sector with its means and its possibilities.* ***Identifying, quantifying, and monitoring the problem are the essential steps to address the problem of pollution in the port and propose solutions suited to the particular case.*** *In this chapter, the main introductory aspects to the problem of environmental impact due to ships will be exposed. In particular, after a state of the art regarding anthropogenic activities and their impact on the ecosystem,* ***GHG emissions*** *related to the maritime sector will be briefly described according to the two most recent reports on the subject.* ***Local-scale emissions*** *related to the maritime sector will be described in terms of causes, formation, and effects on human and the environment. Later, a quick regulatory framework will be exposed. Finally, an overall framework on the amounts of pollutants emitted by ships and possible solutions aimed at mitigating it will be presented.*

1.1. Anthropogenic emissions and the maritime sector

1.1.1. Global effects- Green House Gases (GHG)

Human activities play a central role in climate changes. Nowadays a strong attention is paid, on a global scale, to the reduction of pollutant emissions and to the fulfillment of the Paris Agreement in all industrial sectors. The production of carbon dioxide by anthropogenic activities is one of the main factors influencing climate variations on the Earth. The so-called *greenhouse effect* is the natural phenomenon by which a layer of Green House Gases (GHG) placed in the upper atmosphere of the Earth prevents a part of the heat of the earth from being radiated into space. This heat balance between the incoming solar radiation and the outgoing radiation has been altered by the introduction of pollutants related to human activities into the atmosphere. Agriculture, industry, energy production and transport are just some examples of activities, which intrinsically determine greenhouse gasses, pollution and alteration of the normal habitat and influence the energy balance of the climate scheme. Around 90% of the goods traded in the world are transported by oceans and for many countries such goods represent the main source of import and export. In latest years, the economic growth of some Asian countries (India, China and Japan in particular) has contributed to increase in the amount of maritime traffic. In 2013, the United Nations Conference on Trade and Development (UNCTAD) review of maritime transport confirmed that every year more than 80% of global trade is transported by sea (**UNCTAD, 2013**). According to the 2019 Review of Maritime Transport, the world maritime trade lost momentum in 2018, with traffic volumes still expanding at 2.7 per cent, but below the historical averages of 3.0 per cent and 4.1 per cent recorded in 2017. Total volumes are estimated to have reached 11 billion tons. UNCTAD project

2.6 per cent growth in 2019 and an annual average growth rate of 3.4 per cent for the time period 2019–2024 (estimates before the COVID19 pandemic). Cruise tourism has experienced rapid development in the same years. The reference global cruise community is Cruise Lines International Association (CLIA) that provides a unified voice for the global cruise community and its commitment to better maritime practices and responsible tourism. From 2003 to 2013, the worldwide demand for cruising has increased from 12.0 to 21.3 million passengers (+77%); and to 23.9 million passengers (+12%) from 2013 to 2015 (**CLIA, 2014; CLIA, 2016**). According to CLIA the Mediterranean is the second largest cruise market in the world and it represents 21.7% of the annual cruising capacity in 2013 (**CLIA, 2014**). According to the latest statistics of CLIA (**CLIA 2020**), the number of global ocean cruise passengers for 2018 is 28.5 million and it was predicted, to reach 30 and 32 million for 2019 and 2020 respectively, in absence of Sars-Cov-2.

Within the transport sector, the maritime sector is adopting mitigation policies for drastically reducing the emissions along with the contribution to the global production of harmful pollutants (**Mocerino et al., 2018**). Obviously, economic and population growth imply important increases in anthropogenic GHG emission. The concentration of carbon dioxide, methane and nitrous oxide in the atmosphere have reached the highest level in the last 800.000 years, although mankind is among the most recent causes of this climatic alteration (**IPCC 2014**). The continuous emission of GHG will only increase the numerous and harmful effects, with changes that could be irreversible in the long term for people and for the terrestrial ecosystem. According to Anderson and Bows report, the global emission of CO_2 in 2011, year of economic crisis for numerous industrialized nations, has increased by 3.2% compared to 2010 (**Anderson & Bows 2012**). Since 1990, an increase in CO_2 emissions is evident in the transport segment, with a total increase of 68 % between 1990–2015.

In the climate change framework, greenhouse gases are the emissions that overall contribute, although in a different way, to climate change. An updated list of the main GHG gases has been published in an amendment to the Kyoto Protocol (**UNFCC 2012**): *Carbon dioxide (CO_2), Methane (CH_4), Nitrous Oxide (N_2O), Hydrofluorocarbons (HFCs), Perfluorocarbons (PFCs), Sulphur Hexafluoride (SF_6) and Nitrogen Trifluoride (NF_3)*. Carbon dioxide is certainly the main contributor among these. The so-called CO_{2eq} is used to measure the impact of all these seven gases on global warming; this quantity converts the emissions in terms of various other gases into an amount of carbon dioxide producing an equivalent greenhouse effect in the time unit. Anthropogenic emissions produce local effects in terms of pollution and contamination of air, water, soil and therefore the food chain, in the directly affected areas. However the most important impact is on a global scale, with climate changes affecting millions of people. Global temperature rises, increase of ultraviolet radiation, extreme weather phenomena, melting of glaciers and rising levels of the ocean are some of the numerous effects of such changes on the environment (**Jinghong et al., 2018**). These changes imply a direct impact on humans and on the ecosystem: the increase in temperatures favors the spread of diseases carried by vectors and invasive species and desertification which will damage agriculture; the difficulties in the supply of drinking water and food will lead to malnutrition and illness; spatial distribution, seasonality, incidence and severity of communicable diseases could be strongly influenced by climatic variations. The World Health

Organization (WHO) estimates that between 2030 and 2050 the deaths due to these effects will increase significantly (250.000 deaths per year). Latest statistics indicate that the number of natural disasters and calamitous events in the world has tripled compared to 1960s, with an increased impact on all the life forms. In addition, the increase in the production of CO_2 will lead to an acidification of the oceans with damage to the marine ecosystems and loss of biodiversity.

Therefore, the increase of GHG content in the Earth's atmosphere does have a social cost, which the human kind will be paying for in the near future. In an attempt to establish a balance between those parts of the Society that actually contribute to the emissions, and those areas who instead mainly bear the consequences, the concept of cost for ton of CO_2 emitted was introduced. The original idea is internalization, i.e. making the economic accounting of the GHG active emitters explicitly reflect the damage caused to the environment, that will otherwise be bore by entities external to their interest. The implication of the concept is also quite evidently to provide economical means for the Society in order to try to re-establish the disrupted balance. Many institutions and groups around the world have provided a monetary evaluation of the cost of a ton of CO_2 or CO_{2eq} emitted: for example the US Environmental Protection Agency (EPA) in 2015, suggested a cost of \$37 per ton of CO_2 [1] (**Fuglestvedt et al., 2009**). Another research, carried out by the University of Stanford, estimates that this cost may reach as much as \$220 [2]. These impact estimates are overall incomplete and depend on a large number of assumptions, many of which are debatable. In fact, many estimates do not take the possibility of large-scale singular events and irreversibility into account, especially the ones that are difficult to monetize, such as loss of biodiversity (**IPCC 2014a**).

1.1.2. General- the Paris Agreement (climate changes)

The Paris Climate conference (COP21) gave a strong input to global policies aimed at reducing greenhouses gas emissions into the atmosphere. The result of this conference was the first worldwide universal and legally binding agreement on the subject of climate change, known as "*Paris Agreement*". The ratification began on 22 April 2016 and it has entered into force in 2020, only after at least 55 countries, responsible for more than 55% of global emission, will have signed it. The agreement includes [3]:

- long-term goals aimed at maintaining the average increase in global temperature below 2°C compared to pre-industrial level and strategic plans aimed at maintaining these values preferably close to 1.5°C;
- attention to developing countries: more benefits for these countries and a general willingness to reach the maximum values of global emission as soon as possible;
- research and innovation in order to continue with rapid and successive reductions, after reaching this maximum value, using the most advanced scientific and technological solutions;
- mandatory cooperation for richer countries to subsidize poor ones with a "green climate fund" of \$100 billion a year, starting in 2020, to help them reduce emission;
- monitoring five-year checks starting from 2023.

The General Secretariat of the United Nations expects both by the International Maritime Organization (IMO) and by the International Civil Aviation Organization (ICAO) incisive, pragmatic and urgent actions.

With a particular focus on the maritime sector, the upcoming IMO decisions in this respect are in the spotlight. That is clearly reflected in the "Negotiating text" for the Paris Agreement, which states (**UNFCC 2015**) [4]*:*

"In meeting the 2°C objective, Parties agree on the need for global sectorial emission reduction targets for international aviation and maritime transport and on the need for all Parties to work through the International Civil FCCC/ADP/2015/1 19 Aviation Organization and the International Maritime Organization to develop global policy frameworks to achieve these targets".

According to IMO, maritime transport annually discharges around 1000 million tons of CO_2 and it is responsible for approximately 2.5% of global greenhouse gas (GHG) emissions (**Dong et al., 2019**). The twenty-fourth session of the Conference of the Parties to the United Nations Framework Convention on Climate Change (COP24) was held in Katowice, Poland, in December 2018 [4]. This climate package aims to promote international cooperation and encourage greater ambition for implementing the Paris Agreement as of 2020 and it includes guidelines on the establishment of new finance targets from 2025 onwards to follow up on the current target of mobilizing $100 billion per year from 2020 to support developing countries.

1.1.3. Maritime sector - IPCC and IMO last assessment reports about GHG emission

When dealing with the topic of emissions related to the maritime sector, the references are the *Fifth IPCC Assessment Report* (AR5) and the *Third IMO GHG Study* Figure 1-1 and Figure 1-2. The Intergovernmental Panel on Climate Change (IPCC) is the United Nations body for assessing the science related to climate change and AR5 is the last assessment report available (AR6 will be published in 2022).

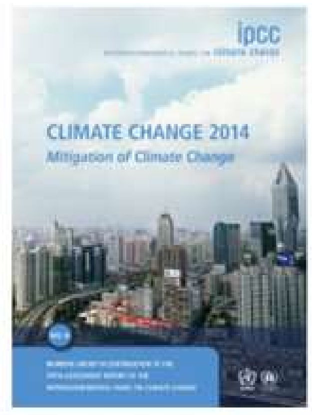

Figure 1-1 Fifth IPCC Assessment Report (AR5)

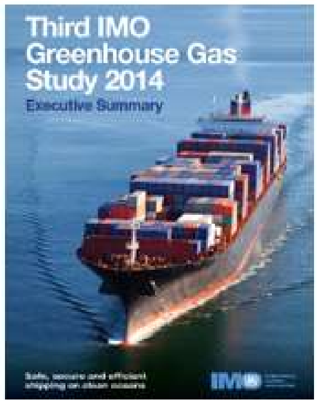

Figure 1-2 Third IMO GHG Study

The second report is the main and most recent IMO study providing a quite updated picture of the shipping emissions containing data up to 2012 (**Smith et al., 2014**). The effects of the Paris agreement will influence all sectors of anthropogenic activity, and the transport sector, in particular, will not be exempted from developing policies aimed at reducing emissions in the next years (**Larkin et al., 2017**). According to an Intergovernmental Panel on Climate Change (IPCC) report (AR5) about 23% of CO_2 emissions in 2010 is due to transports; the estimated quantities are as large as Gt of CO_2 and 7.0 Gt of CO_{2eq} (**IPCC 2014**). The perception of the severity of these increases is amplified by comparing the quantities of 1970 with the 2010 ones: direct emissions related to transport increased by 250%, going from 2.8 to 7.0 Gt CO_{2eq}. According to this report, see Figure 1-3, the transport sector is responsible of 14% of the CO_{2eq}, to following industry, agriculture and the production of heat and electricity.

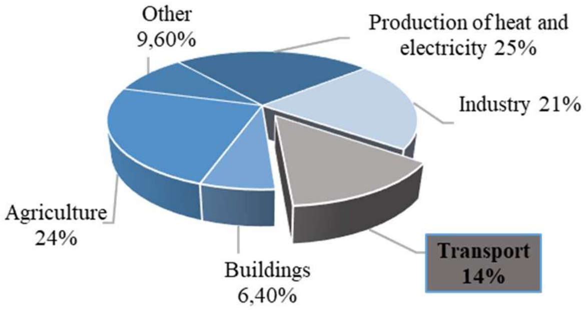

Figure 1-3 Distribution of the influence of anthropogenic activities on emissions

The maritime sector is responsible for the global emissions of CO_{2eq} for relatively low percentages compared to the other transportation modes (72% of the same emission is produced by road traffic). Of the total contribution from shipping the share between domestic and international is also available in T*a*ble 1-1. According to IMO and with the 2006 IPCC Guidelines, domestic shipping has been defined as "shipping between ports of the same country as opposed to international shipping" (**Smith et al., 2014**).

Table 1-1 Emissions of CO_{2eq} due to maritime transport referred to 2011 (IPCC 2014 & 2014a, Sims et al., 2014)

Type of transport	% referring to global	Gt Co_{2eq}
Domestic Waterborne	1.91	0.14
International Shipping	9.26	0.64

The values in T*a*ble 1-1, referred to year 2011, can be compared with those of 1990, indicating a decrease of 0.18% for "Domestic Waterborne" and an increase of 1.6% for the "International Navigation". In the same report, ranges of emission values for each category of ships are provided in

Table 1-2. For passenger ships, values are expressed in grams of CO_2 emitted per passenger and per km, while for the commercial vessels the units are grams of CO_2 emitted per tons of freight per km. When compared to air traffic (from 95 to 250 g CO_2/p-km for passengers' traffic) these ranges are very low.

Table 1-2 Emission of C_{O2} due to the maritime sector divided by type of ship referred to 2011 (Sims et al., 2014)

Ship category	Emission
Passenger ferry	25-150 g CO_2/p-km
Barge	28-55 g CO_2/t-km
Roll-on-off ferry	30-85 g CO_2/t-km
Container ship	10-47 g CO_2/p-km
Bulk	1-13 g CO_2/p-km
Tanker	5-15 g CO_2/p-km

According to Third IMO GHG Study, in 2012, the shipping sector produced about 0.938 Gt CO_2 and 0.961 Gt CO_{2eq}. If these quotas are compared with the global emissions of CO_2 and CO_{2eq}, they amount to 2.2% and 2.1% respectively. The emissions related to the maritime traffic from 2007 to 2012, are shown in *Figure* 1-4. Together with CO_2, in 2012, the emissions of CH_4 and N_2O were 9.8 and 12.71 ktons respectively.

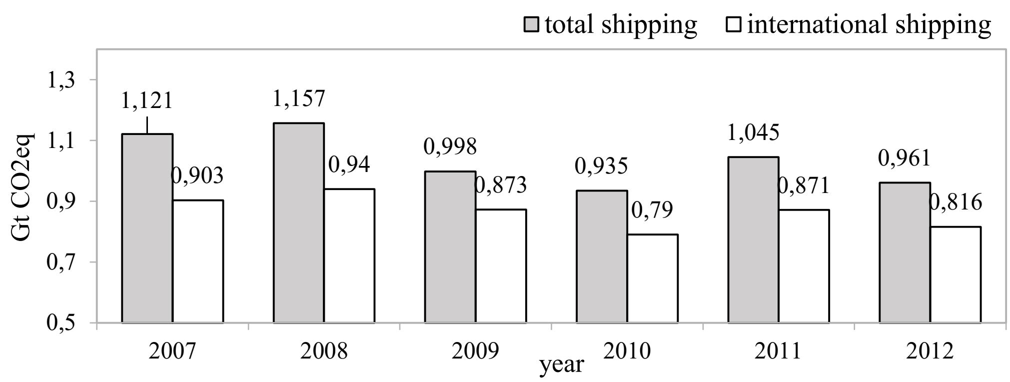

Figure 1-4 Emission of CO_{2eq} for total shipping (left) and international shipping (right) (Smith et al., 2014)

The IMO report provides a breakdown of the emissions referred to 2012 obtained through a "bottom-up" methodology for different type of ships (see Figure 1-5).

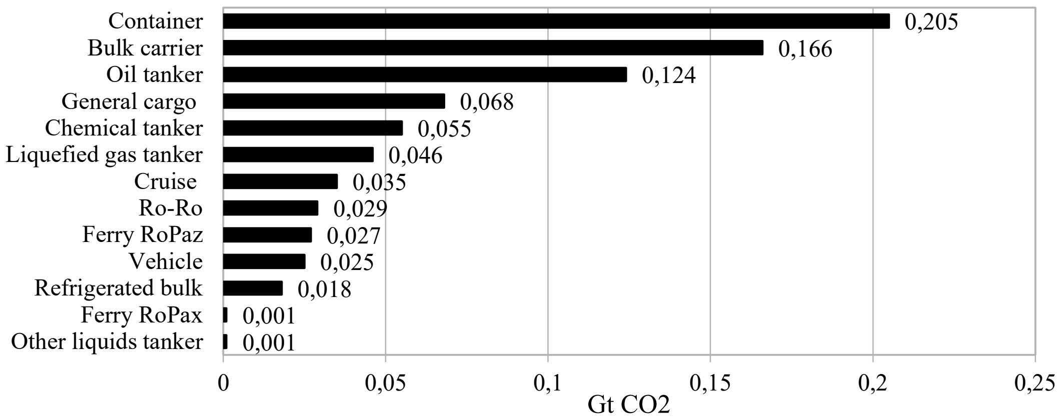

Figure 1-5 CO_2 emissions from international shipping (year 2012)-3O IMO-GHG's (Smith et al., 2014)

By comparing the two reports, the emissions values indicated in the two reports are different because of the different procedures adopted for the estimation of the annual global emissions; however, an increase in annual emissions seems confirmed. In

Table 1-2 and in Figure 1-6 the possible comparisons are reported.

Table 1-3 Comparison between the IMO and IPPC (AR5) inventory. The percentages refer to the comparison between the two IMO studies. [Gt CO_{2eq}]

Report	**AR5 (2010)**	**IMO (2010)**	**IMO (2012)**	**Increase [%] IMO 2012 vs 2010**
Total shipping	0.785	0.935	0.938	0.30
International shipping	0.648	0.790	0.796	0.8

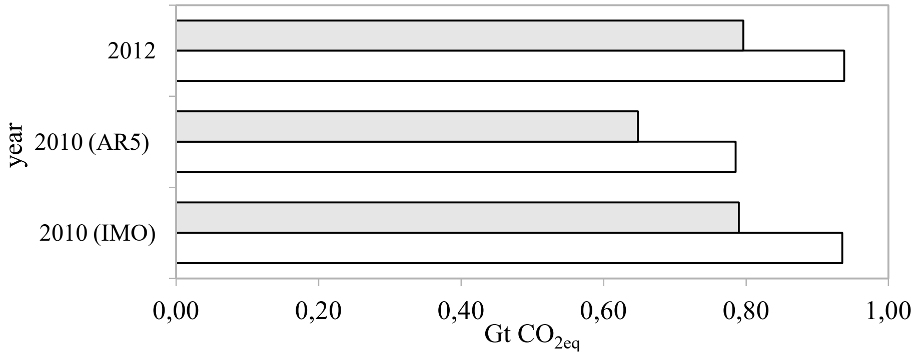

Figure 1-6 Emissions linked to maritime transport (International: full bar; total shipping: white bar)

Data updated to 2012 can be compared with a prediction of the annual emission of the maritime sector realized for 2015 through AIS data and the STEAM3 model (**Johansson et al., 2017**). According to **Johansson et al., (2017)**, about 8.3 Gt CO_2 were produced in that year by ships, of which 7.5 from IMO-registered ships, with the most significant contributions coming from container ships, carriers and takers.

Dealing with forecasts about future emissions of GHG in the shipping field, development scenarios are to be hypothesized. According to IPCC report (**Solomon, 2007**) quite worrying increases in emissions were expected; assuming a "business as usual" (BAU) economic growth and the absence of strong precautionary measures, from 2002 to 2030 an increase in emissions of about 80% was expected (**IPCC 2014; Smith et al., 2014**). This increase could occur in the absence of precautionary actions, with an average rise of 2.1% per year (with peaks of 3.65% per year for developing countries). At the same time, the potential impact of possible countermeasures was estimated. The possible reduction scenarios are reported below:

- from 5% to 30% of emission reduction on new ships with the optimization of engines, hull shape, use of alternative fuels and renewable energy, and speed optimization (**Bouman Evert et al., 2017**);
- from 4% to 20% of improvement with retrofit actions capable of providing additional efficiency;
- peak emission reductions are reported to be possibly achieved for all types of ocean-going ships, for which a wider range of technological solutions would allow reductions up to 50%.

The United Nations Conference on Trade and Development (**UNCTAD 2017**), on the other hand, stated in 2017 that there is a possibility of reducing emissions by up to 75% by implementing appropriate technical and operational countermeasures in the maritime sector. In addition, the IMO hypothesized scenarios of development covering the period from 2012 to 2050. These IMO scenarios (**Smith et al., 2014**) include the combination of two different paths: RCPs "Representative Concentration Pathways" for future demand of coal and oil in transport and SSPs "Shared Socioeconomic Pathways" for future economic growth. Both scenarios assume that the present policies on energy efficiency and emission of ships remain in force and that no restrictions or additional policies will be introduced (Business As Usual scenarios). For each BAU scenarios, the IMO developed three policy scenarios having an increased action on either energy efficiency or emission or both. Consequently, projections of emissions are made for 16 scenarios. There are four main RCPs in use: 2.6, 4.5, 6.0, 8.5 (resultant, in W/m^2, of radiative forcing by 2100). The envisaged scenarios foresee increases in the average global temperature ranging from 1.5 to 4.9 degrees. For SSPs there are five different possible scenarios ranging from sustainability to conventional development (1-5). The possible combinations are shown in Table 1-4; those considered by the IMO were RCP8.5-SSP5; RCP6-SSP1; RCP4.5-SSP3; RCP2.6-SSP4.

Table 1-4 Overview of assumptions per scenarios (Smith et al., 2014).

Scenario	**RCP scenario**	**SSP**	**Efficiency improvement 2050**	**Fuel mix (LNG, ECA)**
1	RCP8.5	SSP5	High	
2	RCP6.0	SSP1	High	High LNG – extra ECA
3	RCP4.5	SSP3	High	-
4	RCP2.6	SSP4	High	-
5	RCP8.5	SSP5	Low	-
6	RCP6.0	SSP1	Low	-
7	RCP4.5	SSP3	Low	-
8	RCP2.6	SSP4	Low	-
9	RCP8.5	SSP5	High	Low LNG – no ECA
10	RCP6.0	SSP1	High	-
11	RCP4.5	SSP3	High	-
12	RCP2.6	SSP4	High	-
13 (BAU)	RCP8.5	SSP5	Low	-
14 (BAU)	RCP6.0	SSP1	Low	-
15 (BAU)	RCP4.5	SSP3	Low	-
16 (BAU)	RCP2.6	SSP4	Low	

As example of all the possible projected scenarios, the extreme ones (3 [continuous line] and 13 [dashed lines]) are reported in Figure 1-7.

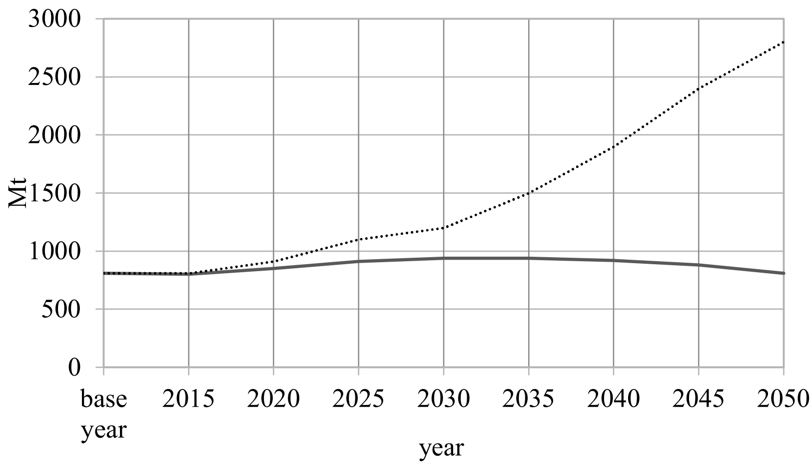

Figure 1-7 CO_2 emission (Smith et al., 2014)

1.1.4. Local effects - Exhaust emissions from ships (non-GHG)

There are other emissions, especially in the transport sector, called **non-GHG** which produce a different effect at a local level on the air quality and a negative impact on human health. The exhaust gas emissions from ships represent a key issue for the environmental impact assessment of maritime transports. Almost 70% of ship emissions are generated within 400 km of coastlines, leading to reduced air quality in coastal areas and harbors (**Fuglestvedt et al., 2009**). Although local emissions are a small fraction of global transport emissions (**Entec, 2002**), they can have serious effects on human health, especially in coastal areas and water cities. Shipping-related emissions are one of the major contributors to global air pollution, especially in coastal and port areas and these emissions contribute significantly to air quality in the proximity of harbors (**Eyring et al., 2010**).

The ships produce pollutants during the cruising, maneuvering and mooring at berth. Diesel engines used as the main power supply of marine vessels produce a range of emissions (on a local scale), including *carbon monoxide* (CO), high fractions of water vapor (H_2O), *nitrogen oxides* (NOx, mostly NO), *Sulphur oxides* (SO_x), unburned *hydrocarbons* (HC), *particulate matter* (PM) and *Volatile Organic Compounds* (VOC) and ash (**Heywood 1988; MEPC 2014**). Emissions of these pollutants vary between different engines and depend on some variables such as ignition timing, speed, and load and air/fuel ratio. Overall, the sulfur oxides are emitted depending on the content of Sulphur in the fuel while the quantity of nitrogen oxides in the exhausts depends on the inner parameters of engines and on the temperature of combustion and timing. In addition, diesel engines emit solid matter or particulate matter mostly during transient conditions of engines which can cause oncological diseases.

Generally, the pollutants related to atmospheric pollution are divided into **primary** and **secondary** pollutants. The primary pollutants are already present in the emissions while the secondary ones are substances resulting from reactions between primary pollutants or between primary pollutants and natural components of the atmosphere. CO, NO, HC and SO_2 are considered primary pollutants whereas O_3, HNO_3, SO_3 and H_2SO_4 are some examples of secondary pollutants. The term engine emissions refers primarily to pollutants in the engine exhaust. A ship funnel discharges the exhaust gases and particles into the atmosphere where, due to buoyancy effects, these exhaust masses have an early momentum of extra rise and horizontal transportation in the wind (**Simonen et al., 2020**). The turbulence occurring during this propagation will cause dispersion of the plume leading to the dilution of the embedded fumes by entrainment of air into the plume. In **Dobrucali & Ergin (2019)** a numerical study on the effects of operational conditions, design parameters and buoyancy on the exhaust smoke dispersion of a generic frigate is presented and discussed.

When leaving the funnel the hot gases have a typically temperature of almost 400^{O} K (**Simonen et al., 2020**) and contain combustion products produced during the burning of Marine Gas Oil (MGO) or diesel or Heavy Fuel Oil (HFO). The chemical reaction that takes place inside the plume has an impact on the NO-NO_2-O_3 cycle. The combination of NOx emissions with oxidized hydrocarbons would typically favor ozone formation as a result of the NO oxidation (**Simonen et al., 2020**).

The main impact of maritime sector on sulphate chemistry is the direct emission of SO_2 nevertheless, the NOx emissions increases the OH radical formation and will enhance the gaseous oxidation pathway (**Simonen et al., 2020**). SO_2 emissions are oxidized to sulphate primarily in the aqueous phase by hydrogen peroxide (H_2O_2) and ozone and then in the gas phase by the OH radical (**Simonen et al., 2020**).

The contribution of maritime traffic to global emissions is estimated in 5.6 Tg of NO_X and 5.3 Tg of SO_X (**MEPC 2014; Murena et al., 2018; Smith et al., 2014**). According to **Eyring et al., (2005)** in 2005, about 15 % of all global NO_X emissions were attributable to the shipping sector. On the other hand, the ship emissions in port areas are dispersed in the atmosphere and in many cases move to the nearby urban areas, affecting air quality and jeopardizing people's health and quality of life (**Adamo et al., 2014; Ault et al., 2009;**

Quaranta et al., 2012; Viana et al., 2014). According to **Viana et al., (2014)** the shipping emissions contribute typically with 1–7% to the annual mean PM10 levels, with 1–20% to PM2.5, and with 8–11% to PM1 in coastal areas (**Viana et al., 2014**).

The main definitions related to the major atmospheric pollutants (**non-GHG**) produced by vessels to follow.

1.1.4.1. HC

Hydrocarbons (HC) are fuel molecules that did not get burned and smaller non-equilibrium particles of partially burned fuel. HC emissions are reduced by excess air until the reduced flammability of the mixtures causes net increase in HC emissions (**Heywood 1988**).

1.1.4.2. CO

Carbon monoxide (CO) is mostly produced with fuel-rich mixtures as there will be incomplete combustion (**Heywood 1988**). This harmful compound is a colorless and scentless poisonous gas which is generated in an engine operating when there is not enough oxygen for the conversion of all carbon to CO_2. Some fuel does not get burned in the combustion chamber and some carbon ends up as CO. Poor mixing, local rich regions and incomplete combustion will create some CO. Incomplete combustion of carbon or carbon-containing compounds follows the following reactions in which the former one is about 10 times faster than the latter. CO will then be present either as an intermediate product or as a final product if the O_2 is not sufficient or well mixed with the fuel (see 1-1).

1-1 CO formation

$$2C + O_2 \rightarrow 2CO$$

$$2CO + O_2 \rightarrow 2CO_2$$

The effects of carbon monoxide on the environment are considered negligible while those on humans are very dangerous since carbon monoxide is rapidly absorbed into the pulmonary alveoli with symptoms ranging from headache to death from asphyxiation.

1.1.4.3. NO_X

The formation of *Nitrogen Oxides* is more complex since it depends on a series of reactions. Atmospheric nitrogen exists as a stable diatomic molecule at low temperatures, and only very small trace amounts of oxides of nitrogen are found. However, at the very high temperatures that occur in the combustion chamber of an engine, some diatomic nitrogen breaks down to monatomic nitrogen (N). Oxides of nitrogen are created in an engine when high combustion temperatures cause some normally stable N_2 to dissociate into monatomic nitrogen N, which then combines with reacting oxygen. This dissociation of the N and O molecules into atoms occurs as a result of the high temperatures reached by the gases in the reaction zone of the flame front, but above all by those just burned. The latter, in fact, are further compressed by the expansion of the charge that is reacting and are therefore brought to even higher temperature values. However, an engine never reaches an actual condition of chemical equilibrium between the reactants, due to the short times available and the high local and time gradients of the temperature. Thus, during the expansion phase, the reactions of destruction of NO are freezed by the rapid decrease in temperature and NO remains as a constituent of the flue gas. Its concentration ultimately depends on the maximum temperature values reached and the oxygen content of the feed mixture. At low temperatures very little NOx is created. Chemical kinetics show that the formation of NOx increases very strongly with increasing flame temperature. This would imply that the highest concentration of NO_X should be slightly rich mixtures, which have the highest flame temperature. In addition, NO_X formation will also be influenced by the flame speed. Lower flame speeds with lean mixtures provide a longer time for NO_X to form. Generally, there are several types of nitrogen oxides but the most produced one is nitrogen oxide (NO), followed by a small amount of nitrogen dioxide (NO_2), and traces of other Nitrogen-Oxygen combinations. These are all grouped together in NOx, with x representing some suitable number. In addition to the combustion temperature, the formation of NOx depends on the residence time at this temperature of the gases during combustion, the quantity of free O contained in the flame, air-fuel ratio, the ignition advance in relation to Top Dead Center (TDC), the recirculation of part of the combustion gases in the intake, the load value and the engine speed and the compression ratio. The NO emissions can be subdivided in three categories: thermal (Zeldovich), prompt and fuel. Thermal NO formation was first introduced in the 1940s. The formation of thermal NO is very sensitive to the combustion temperature, and its formation is negligible when the temperature is of 1.000 °C or lower. There are a number of possible reactions that form NO, all of which are probably occurring during the combustion process and immediately after. These include **yet** are not limited to:

1-2 NO_X formation

$$O + N_2 \rightarrow NO + N$$

$$N + O_2 \rightarrow NO + O$$

$$N + OH \rightarrow NO + H$$

Fenimore (1971) found that some of the NO formed during combustion could not be explained by the aforementioned Zeldovich mechanisms (**Heywood 1988**). When equivalence ratio is greater than 1, the nitrogen in the air reacts to form Hydrogen Cyanide (HCN). Since there are oxygen-containing compounds in the combustion system, HCN produced in the above reaction and the nitrogen atom reacts further to produce NO through several chain reactions. Prompt NO is formed only in a combustion zone of the flame where the combustion is incomplete and the hydrocarbon radicals are present. It is known as *prompt* NO because these reactions take place very fast. The formation of prompt NO does not depend on temperature as significantly as the thermal NO. The prompt NO is formed mainly under lower temperature conditions during a short residence time.

Most fuels contain nitrogen element, the NO originated from this part of nitrogen is referred to as *fuel* NO. The amount of nitrogen in fuel varies with the fuel type. Although the amount of nitrogen in fuel is relatively small, the fuel nitrogen is much more reactive compared to the nitrogen present in the combustion air. Therefore, the formation of fuel NO from a nitrogen-rich fuel is higher than that from a nitrogen-lean fuel. The fuel NO is sensitive to stoichiometry rather than the temperature because it forms quickly at quite low temperatures. According to **Ergin (2008)** the NO_X formation can be reduced in the exhaust and at the source. The first class of method belongs for example to the Selective Catalytic Reduction (SCR) and the wet Scrubber respectively with 75-95% and 15% of reduction potentiality (**Ergin, 2008**). To the second class belong, instead, delayed fuel injection (2-3%), reduced scavenged air (5%), direct water injection (20-50%), and the Emission Control System (70%) (**Ergin, 2008**). By delaying ignition, less fuel burns before Top Dead Center, so pressure and maximum temperatures decrease. It is also possible to dilute the fresh charge with part of the gases, which practically constitute a mixture inert, consisting essentially of nitrogen, carbon dioxide and water vapor. In this way the result of lowering the maximum combustion temperature is obtained, because the heat released by the oxidation of the fuel is distributed over a larger mass of fluid, therefore having a higher thermal capacity (with the same fuel burned). Finally, the load and the engine speed, as well as the value of the compression ratio and the degree of supercharging, influence the combustion temperature and therefore the concentration of nitrogen oxides produced in a known way. Released NOx reacts in the atmosphere to form ozone and is one of the major causes of photochemical smog that has become a major problem in many large cities of the world. Smog is formed by the photochemical reaction of NO_X and atmospheric air in the presence of sunlight. NO_X decomposes into NO and monatomic oxygen:

1-3 Photochemical smog

$$\mathrm{NO_X} + \text{energy from sunlight} \sim \mathrm{NO} + 0 + \text{smog}$$

Monoatomic oxygen is highly reactive and initiates a number of different reactions, one of which is the formation of ozone ($O+O_2 \rightarrow O_3$).

Nitrogen dioxide is four times more toxic than nitrogen monoxide. NO can lead to paralysis of the central nervous system and, in specific concentrations, irritation of the mucous membranes of the eyes and nose. The lowest level at which an effect on lung function in humans due to exposure to nitrogen dioxide was observed, after an exposure of 30 minutes, is 560 $\mu g/m^3$; for this reason, the World Health Organization recommends a guide limit of 1 hour for NO_2 equal to 200 $\mu g/m^3$, and a limit for the annual average of 40 $\mu g/m^3$.

In addition to the harmful effects on human health, nitrogen oxides produce damage to plants, reducing their growth, damage to material assets with corrosion of metals and discoloration of fabrics. Both also contribute to acidic precipitations which cause deterioration of buildings and works of art.

1.1.4.4. SO_X

From the combustion of any fuel containing sulfur, *sulfur oxides* (SO_2 and SO_3) are developed; the concentration of sulfuric anhydride is generally lower as the reaction that it produces is much slower.

The main type of bunker oil for ships is Heavy Fuel Oil (HFO), derived as a residue from crude oil distillation. Crude oil contains Sulphur which, following combustion in the engine, ends up in the ship's plume. The production of Sulphur oxides depends on the combustion temperature and pressure, the air fuel ratio and above all the Sulphur quantity in the fuel.

1-4 SO_X formation

$$S + O_2 \rightarrow SO_2$$

$$2SO_2 + O_2 \rightarrow 2SO_3$$

Due to the high solubility in water, SO_2 is easily absorbed by the mucous membranes of the nose and upper respiratory tract; only very small quantities reach the deepest part of the lung.

A synergistic effect with the particulate has been ascertained due to the latter's ability to convey SO_2 into the deepest respiratory areas of the lung. Sulphur oxides are known to be harmful for human health, causing respiratory problems, and for the ecosystem, leading acid rain, which can harm forests and aquatic species other than contributing to the acidification of the oceans.

1.1.4.5. PM

By atmospheric *Particulate,* we mean the set of solid and liquid atmospheric particles with diameters ranging from a few nm to 100 microns. Their classification is possible on a dimensional basis (ultrafine, fine and coarse), according to the source that originates it (natural or anthropic) and according to the chemical composition. The most common subdivision is the one on dimensions between PM 10, PM 2.5, and PM1 for particulate fractions with aerodynamic diameter less than 10, 2.5 and 1 respectively. Solid particulates (PM) are formed in compression ignition engines and are seen as black smoke in the exhaust of these engines. Other emissions found in the exhaust of engines include aldehydes, sulfur, lead, and phosphorus. According to **Corbett et al (2007)**, shipping-related PM emissions from marine shipping contributes to approximately 60.000 deaths annually at a global scale, with main impacts in coastal regions on major trade routes. Most mortality effects are seen in Asia and Europe where there are both high populations and high shipping-related PM concentrations. The majority of particles are formed inside the cylinders during the combustion, and are the result of incomplete combustion of the hydrocarbons in the fuel. Some particles originate from the lubrication oil (**Heywood, 1988**). These emissions in the exhaust gases originate from the deposition of very small particles of partially burned fuel or lubricating oil, the ash content of fuel oil and cylinder lube oil, sulfates, and water (**Heywood, 1988**). The exhaust particles emitted from ships are composed of elemental, organic and inorganic carbon, sulphate and ash, as well as nitrates (**Agrawal et al., 2008**). In **Kalender & Ergin (2017)** an experimentally investigation of the particulate emission characteristics emitted by a medium speed diesel engine installed on a ferry has been reported. The negative effects of particles on humans and environment are reduced visibility changes to ecosystems and damage to buildings, respiratory illnesses, bronchitis, asthma, and pneumonia, lung cancer, and cardiopulmonary mortality. The health effects depend on the size, shape and chemical activity of the particles. The smallest ones can penetrate the alveoli and can flow into the blood.

1.2. Regulatory framework for the maritime sector

The International Maritime Organization (IMO) is the specialized agency of United Nations organization, responsible for regulating ship safety, pollution, security and environmental matters for

International shipping. It consists of an assembly, a council and five main committees, of which the Marine Environment Protection Committee (MEPC) is in charge of the prevention and control of pollution from ships (**Zetterdahl 2016**). It is known that the key IMO Convention on the subject is the MARPOL (International Convention for the Prevention of Pollution from Ships) first issued in 1973, revised by Protocols in 1978 and 1997 and updated with amendments through the years. The focus of MARPOL is protecting the marine environment from pollution caused by ships due to operational or accidental causes. It includes six Technical Annexes setting requirements on different types of potential environmental impacts. The prevention of potential pollution derived by goods transported on board is covered by Annexes I, II (October 1983) for oil and other noxious liquid substances carried in bulk, while harmful substances carried in packaged form are regulated by Annex III (July 1992). Pollution of seawater originating from ship operations is covered by Annex IV (September 2003) for sewage and by annex V (December 1988) for garbage. Annex VI (added in 1997 and entered into force in/ May 2005), started to regulate emission in the atmosphere, dealing with the control of both local and global effects

1.2.1. Requirements about GHG emissions

Amendment to Annex VI of MARPOL 73/78 at the MEPC66 (2014) made the Energy Efficiency Design Index (EEDI) mandatory for new ships as well as the Ship Energy Efficiency Management Plan (SEEMP) for all ships. Further requirements within annex VI, formulated in terms of the Energy Efficiency Existing Ship Index (EEXI), subject to adoption at MEPC 76 in June 2021, will enter into force in 2023. During the MPEC70 (2016) a mandatory data collection system for fuel consumption of ships was formally adopted. Under global data collection scheme, collecting consumption data for each type of fuel used as well as data related to energy efficiency will be required for ships of 5000 gross tonnage and above. IMO will be required to make annual reports where individual ship data will not be recognizable. In 2013, the European Commission suggested a strategy for progressively integrating maritime emissions into the EU's policy for reducing its domestic GHG emissions. In April 2015, this strategy was adopted by the European Parliament and the 'Shipping MRV Regulation' 2015/757 came into force on 1 July 2015. The MRV (Monitoring Reporting Verification) system is expected to cut CO_2 emissions from the journeys covered by up to 2%, compared with a BAU (business as usual) situation. The strategy consists of three consecutive phases: *Monitoring, Reporting and Verification* of carbon emissions for ships exceeding 5.000 gross tonnage on all voyages to, from and between EU ports applicable from 2018; *GHG reduction targets* for the maritime transport sector. *Further measures*, including Market-Based Measures (MBM). The MRV regulations apply to all ships exceeding 5.000 GT regardless of their flag, port of registry, home port except warships, fishing vessels, wooden ships of a primitive build, ships not propelled by mechanical means, and government ships used for non-commercial purposes. Fuel consumption and carbon dioxide emissions on all voyages to, from and between EU ports during navigation and mooring phase must be reported. Generally, with only a few exceptions, data shall be reported on an annual as well as per-voyage basis; the four acceptable recognized fuel consumption monitoring methodologies are: Bunker Fuel Delivery Note (BDN), bunker fuel tank monitoring on board, flow meters if possible, and direct emissions measurements. The MEPC continues to work on the MEPC70 roadmap developing medium and long-term strategies.

1.2.2. Local pollution and non-GHG

Annex VI (added in 1997 and entered into force in May 2005) regulated air pollution from ships by dealing with SO_X, NO_X and PM from exhaust gases, shipboard incineration, emissions from VOCs. The original Annex VI of the convention has undergone successive changes aimed at reducing the limits related to the emissions of the non GHG pollutants on the basis of the technological improvements made over the years and the ever more severe need to decrease emissions (**IMO 2007; IMO 2008**). The main change to the regulation consists of a progressive reduction in emission limits of nitrogen and sulphur oxides and the introduction of Emission Controlled Areas (ECAs) with even more stringent requirements. *Regulation 13* of Annex VI sets limitations to which every engine with power *output* $\geq$ *130 kW* has to comply for the NO_X emissions. Table 1-5 and

Figure 1-8 show the formulas for calculating the limits for NO_X.

Table 1-5 NO_X emission limits

TIER	Ship construction date on or after	Total weighted cycle emission limit [g/kWh]		
		n=engine's rated speed [rpm]		
		n < 130	130 < n < 1999	n ≥ 2000
I	01/01/2000	17.0	$45\cdot(n^{-0.2})$	9.8
II	01/01/2011	14.4	$44\cdot(n^{-0.23})$	7.7
III	01/01/2016	3.4	$9\cdot(n^{-0.2})$	2.0

For each TIER the limits are calculated according to the rpm of the engine depending on the ship's operations (**IMO 2008**). The limits depend on the date of ship construction and are divided in three levels: TIER I, II and III. Tier III requirements are to be applied to engines installed on ships constructed after 01/01/2016 and operating in the North American and the United States Caribbean Sea Emission Control Areas (from 01/01/2021 the Baltic Sea and the North Sea Emission Control Areas became NO_X ECA). Nowadays, the reference is TIER II while the TIER III is to be considered valid only in the NO_X ECA (**IMO 2007**).

Regulation 14 of Annex VI sets limits for the mass sulphur content ratio in the fuel used by the ship engine. Since the sulphur generating the oxides in the exhaust gases is present in the fuel, the limits to the emissions of sulphur oxides concern the mass percentages of sulphur present in the bunkered fuel. In 2009, without stricter regulations, maritime sector was responsible for 124.000 t of SO_X emissions in the Baltic Sea (**Jukka-Pekka Jalkanen et al, 2014**). A study on the human health impacts of SO_X emissions from ships, submitted to IMO's Marine Environment Protection Committee (MEPC) in 2016 by Finland, estimated that by not reducing the SO_X limit for ships from 2020, the air pollution from ships would contribute to more than 570.000 additional premature deaths worldwide between 2020-2025. From 1 January 2020, the limit for sulphur in fuel oil used on board ships operating outside designated emission control areas is reduced to 0.50%

m/m while, from 01/01/2015 this limit is of 0.10% (**IMO 2007**) in the ECA (as mentioned: North American, US Caribbean, North Sea and Baltic Sulphur Emission Control Areas) (see Figure 1-9).

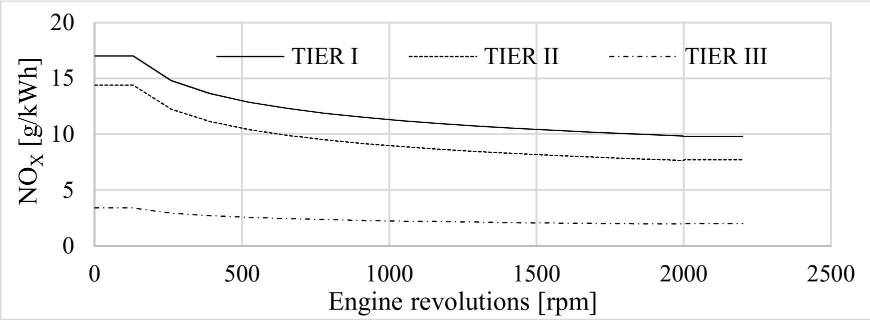

Figure 1-8 NO_X emission limits

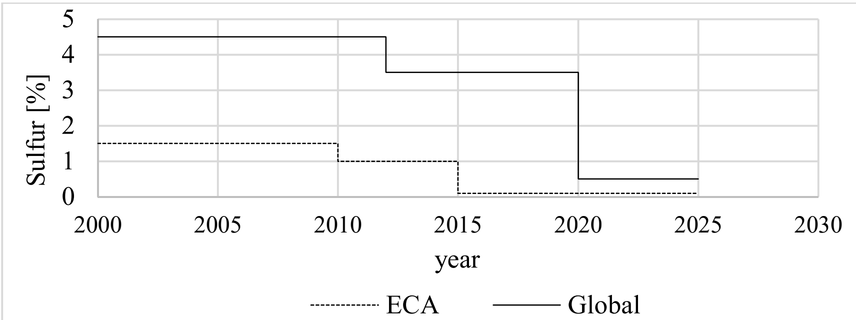

Figure 1-9 SO_X emission limits

Vessels that have exhaust gas cleaning systems installed are still allowed to use High-Sulphur Fuel Oil (HSFO). The European Union Sulphur Directive prescribes a maximum of 0.10% sulphur content for ships in EU ports.

1.3. Solutions for reducing non GHG emissions with effects on a local scale

The non GHG atmospheric pollution has particularly strong and consistent associations with mortality and with respiratory infections and asthma in young children (**WHO, 2016**). All the action aimed at significantly reducing the shipping-related non GHG emissions have as a target major health and environmental benefits for the world, particularly for populations living close to ports and coastal areas. The methods used to reduce harmful emissions include improving the technology of engines and fuels so that a better combustion takes place in the combustion chamber and fewer emissions are produced. Alternatively (or in addition) an after-treatment of the exhaust gases (using thermal converters or catalytic converters to promote chemical reactions in the exhaust flow) can be adopted. According to **UNCTAD (2019)**, two out of three of the main indicators of ship-owners' sensitivity to marine environment protection are the use of scrubbers and compliance with NO_X regulation. On a global scale, respectively 1.58% and 0.53% of the world fleet met these three requirements. If the percentages are made on the subtotal of the top 50 owners, they rise to 1.74% and 0.57% respectively. With reference to Italian ship owners, on the other hand, the percentages are 1.48% and 0.07%. According to the "2020 State of the cruise industry outlook" (**CLIA 2020**), the development and identification of new technologies and **cleaner fuels** is a top priority for the cruise industry, which continues to make significant investments in reducing its environmental impact. Moreover, $22 billion have been invested in **new energy efficiency technologies** and cleaner fuels, reduction in rate of carbon emission has been fixed, by 2030, to 40% compared to 2008 and the average age of the fleet has dropped to 14.1 vs 14.6 years in 2018. The main adopted innovations are the use of **Liquefied Natural Gas (LNG)**, with virtually zero emissions, the use of **Exhaust Gas Cleaning Systems** (ECGS), with a 98% reduction of Sulphur oxide levels and 12% reduction of Nitrogen oxides, Advanced Wastewater Treatment Systems and Shore-side Power. **Cold ironing** mainly provides social and environmental benefits. It is an anti-pollution measure, to reduce air pollution produced from diesel engine (over 30% of CO_2 emissions and more than 95% of NO_X and particulate), through the use of shore electric power as an alternative. With this process, all equipment (emergency, refrigeration, cooling, heating, lighting, etc) are still able to receive continuous electrical power (**Battistelli et al., 2012**). Some ships limit the air pollutants by installing exhaust gas cleaning systems, also known as scrubbers which are accepted by flag States as an alternative means to meet the Sulphur limit requirement; a ship equipped with a scrubber can use HFO, since the Sulphur oxides emissions will be reduced in a post processing phase.

For the 2020 deadline, there are essentially these possible choices: switching from HSFO to MGO or distillates which will lead to an increase in fuel cost and may require upgrading to a fuel treatment system due to the significantly lower viscosity of the fuel; installing scrubbers and using LNG. In **Durmaz et al., (2017)**, the effects of the Ultra-Low Sulphur Fuel Oil diesel fuel on the emissions of a ferry are investigated. The SO_2 and particles emissions for both the main and auxiliary engines are substantially reduced by using this type of diesel fuel.

2. *Bottom-up predictive method for the estimations of non-GHG emissions and their dispersion into the atmosphere on a local scale.*

Aims and scope

A first step of control of any kind of pollution is monitoring: as non GHG pollutants have mainly local effects, monitoring of ship emissions of this type at ports, where ship spend a considerable part of their emission time in the proximity of inhabited areas is crucial to quantify problems and identify and rank solutions.

The monitoring activity can be carried out by experimental methods, but predictive models are very powerful for studying in advance new situations and countermeasures and, if properly validated, can even substitute to a large extent the experimental surveys (predictive monitoring). Further, experimental surveys are prone to access problems if carried out on board in the proximity of the funnels, or to uncertainty about the actual source if carried out at quay.

The chapter describes a bottom-up predictive methodology, while chapter 6 will cover an innovative holistic experimental procedure based on Lidar remote sensors.

The chapter presents inputs and tools used to predict the emissions of numerous ships in port and the inherent dispersion of the emitted pollutant in the atmosphere. Each of the input information can be provided at different levels of accuracy and precision. The first type of input for the characterization of emissions at port is certainly the ***shipping traffic****. Chapter 3 will report prediction results with reference to the traffic in the Port of Naples in specific years, but with different degree of detail. A second set of data is represented by the* ***route*** *which the ship follows when entering the port and approaching the quay. Other key information for the characterization of emissions are represented by the* ***engine load during the operations in port.*** *Very often, this information are not available so the engine load profiles in port and in the various operational phases are derived in terms of pre-set percentages of the* ***total power installed on board****. Unfortunately, this datum, too, was missing in many cases (particularly for cruise ships), so a detailed regression analysis was carried out on a subset of ships of that category for which complete data were available. This way, missing data were forecast by regression based on other available characteristics of the ships.*

Another element of paramount importance is the link between the power delivered by the engines and the ***flow of pollutant in the exhaust gases****. A simple linear model for describing the dependency is available through emission coefficients (one for each type of ship, engine, fuel and pollutant), but the subject will be covered more in details in this chapter. Lasts, inputs to the dispersion model are the* ***height and diameter of the funnels*** *and also this topic, is covered in the chapter.*

2.1. The bottom-up prediction methodology

The primary sources of emission that can be found on a ship are the Main Engine (ME), the Auxiliary Engines (AE) and the thermal boilers. Fuel consumption and emissions vary depending on the engine's rated power output, load factor and build year. In addition, the main engine power output and load factor vary over time in function of the ship's operational phase such as cruising, at berth, anchoring, and maneuvering. In order to evaluate air emissions due to maritime transport, two variables are to be considered: the amount of air emissions and the location where they are produced. For both dimensions, two different approaches are possible: bottom-up or top-down (**Miola & Ciuffo, 2011**).

- Full top-down approach. Total emissions are evaluated without considering the characteristics of the single ships and are later geographically located and assigned to the different ships (**Miola and Ciuffo, 2011; Berechman & Tseng, 2012; Smith et al., 2014; Tichavska &Tovar, 2015**).
- Full bottom-up approach. Emissions from a single vessel are considered over a certain period of time and the aggregation of the emissions produced by all the ships gives an estimate of the total emissions. By aggregating these estimates over time and over the fleet it is possible to estimate the total emissions. The global activity carried out within a single maritime route or a single geographic cell (for example the entire port) is evaluated.

The so-called bottom-up, or activity-based method, is used to estimate the emissions of each main pollutant from a particular ship by calculating its energy consumption. The method needs information on the ship's characteristics such as ship category, mission profile, size, engine and fuel type, total power deliverd and movements, as well as the corresponding fuel consumption and emission factors. Numerous studies evaluating the emissions of ships in ports have been published (**Saxe & Larsen 2004; Battistelli et al., 2012; Chen et al., 2018; Fan et al., 2016; Merico et al., 2017**); these studies refer to the assessment of the contribution of ship emissions on air quality in port and nearby urban areas. In many cases, a limited contribution of ship emissions inside the port areas is reported. **Papaefthimiou et al., (2016)** reports the results of a bottom-up methodology based on in-port ships activity to calculate exhaust pollutant emission rates during all the phases of a cruise ship's voyages to and from 18 ports in Greece during 2013. **De Melo Rodriguez et al., (2017)** provide a regression analysis for the emission indicators depending on independent predictors such as port time, number of passenger and GT. The analyses were performed on 30 cruise vessels in the port of Barcelona, by evaluating the load factor and working time of the thrusters, type of fuel used and hoteling power demand. The highest impact of ship emissions of PM2.5 is estimated at 10 km from the coastline in a region of China. It is also generally highlighted that the influence of ship emissions on pollutant concentration at ground is statistically relevant only during ship-plume-influenced periods (**Argawal et al., 2009; Chen et al., 2018; Liu et al., 2017; Merico et al., 2016; Poplawski et al., 2001**). In order to assess the impact of ship emissions on nearby urban areas, two different kinds of approach exist: experimental approach and numerical modelling of atmospheric dispersion. Some authors carried out monitoring campaigns on selected pollutants and applied data analysis techniques to evaluate the contribution of each source (**Cesari et al., 2014**). Among gaseous pollutants, SO_2 is often indicated as tracer of ship emissions (**Prati et al., 2015**). However, the collection of monitoring data followed by data analysis is a relatively long and expensive procedure and does not always produce clear results, due to the presence of other sources of pollutants such as urban and road traffic and industry. Consequently, the use of dispersion models is recurrent. Many different dispersion models have been adopted (**Saxe & Larsen 2004; Merico et al., 2017; Chen et al., 2016; Fan et al., 2016; Lonati**

et al., 2010). **Gariazzo et al., (2007)** and used a Lagrangian particle model to assess the impact of harbour, industrial and urban activities on air quality in the Taranto area (Italy). **Merico et al., (2017)** have studied air quality shipping impact in the Adriatic and Ionian area focusing on Brindisi and Venice (Italy), Patras (Greece), and Rijeka (Croatia) and using a WRF-CAMx modelling system. The study covers all cruise ship calls during the year 2016. A complete bottom-up procedure includes the following stages:

- **traffic:** acquisition of arrival and departure schedule of the specific port and category and characterization of ships;
- analysis of the **routes** (within the port);
- determination or estimation of total **powe**r installed on board and of the power used in the different phases in port;
- estimation of pollutant **emissions** in various phases in port;
- determination of the environmental impact by using a **dispersion** of pollutants in the atmosphere.

Usually for all ports arrival and departure schedules for cruise ship terminals are available for free. Ships data such as GT, main engine power, length and so on can be found, although not easily, in various specialized databases.

Generally, for a ship in port, two different phases are identified: manoeuvring and mooring. The first one, including slow navigation in the port area, approaching/docking and departing, begins with the deceleration of the ship's speed and ends at mooring, restarting after it and then ending when the speed is reached just outside the port's edge. The mooring or hotelling phase corresponds to the time that a cruise ship stays in port and provides hotel services on board for passengers and crew. Generally, in a cruise ship, the main engine is turned off during this phase and all power requirements are covered by auxiliary engines or, the main engine works at limited load factor producing only the required energy, doing so through the use of a diesel-electric propulsion, which is common for cruise ships.

In our evaluation, the operations and the phases considered to calculate emissions in the atmosphere will be defined as **navigation in port** (as in arrival and -departure at slow speed), **manoeuvring** for berthing, unmooring, and **hoteling** at berth.

2.2. Traffic in port

The tools useful for collecting data on traffic concerning a port can be:

- calendars available online on the port's official websites (for cruise only) (applied for 2012 & 2016);
- calendars available on the websites of the shipping companies (only for passenger ships and very often the name of the ship is not provided) (applied for 2012 & 2016);
- AIS data (comprehensive and for all ship categories) (applied for inventory 2018).

The traffic should be analyzed in terms of arrival and departure times, duration of the stop, and mooring point. In the processing carried out on the case study of the port of Naples, the calendars of the cruise ships only will be obtained from the official website of the port authority, the accesses of ferries and fast vehicles will be extracted from the arrival and departure calendars available on the sites of the shipowners. This method is valid as long as only passenger ships are analyzed. In fact, the access data of the merchant fleets are not available online for the port in question, and more generally for most ports. For this reason, the use of AIS data becomes essential to extend the analysis to the entire incoming fleet. The first applications at the port of Naples (cruise for 2016 and all passenger ships for 2012) will follow the first two approaches while AIS data will be used for the realization of the inventory for a whole year and for the entire port (2018).

2.2.1. Automatic Identification Systems

The AIS, Automatic Identification System, was developed in the 1990s as global standard to avoid ship collisions accidents, and improving navigation safety and it has been used in the maritime sector for over two decades. Using VHF (Very High Frequency), the AIS system allows ships and coastal authorities to communicate at a long distance and permits to broadcast and receive messages from and to other ships or port authorities equipped with the same system (**Dong et al., 2019**). SOLAS regulation V/19 - Carriage requirements for ship borne navigational systems and equipment - sets out navigational equipment to be carried on board ships. From 2000, the IMO adopted a new requirement, which became effective for all ships by 31 December 2004, according to which all ships must carry AISs capable of automatically providing information about the ship to other ships and to coastal authorities [5] (**IALA, 2004**). The regulation applies to ships built on or after 1/07/2002 and to ships engaged in international voyages constructed before 1/07/2002, according to the following timetable (**IMO 2003**):

- passenger ships, not later than 1/07/2003;
- tankers, not later than the first survey for safety equipment on or after 1/07/2003;
- other ships of 50.000 GT and upwards, not later than 1/07/2004.

An amendment adopted by the Diplomatic Conference on Maritime Security in December 2002 states that, additionally, ships of 300 GT and upwards but less than 50.000 GT, are required to install AIS not later than the first safety equipment survey after 1/07/2004 or by 31/07/2004, whichever occurs earlier. The regulation requires AIS to be installed onboard of all ships of 300 GT and above engaged in international voyages, cargo ships of 500 GT and upwards not engaged in international voyages and all passenger ships regardless of the size. The regulation requires that AIS will automatically provide and receive information, monitor and track ships and exchange data with shore-based facilities. The AIS shall be kept active at all times unless international agreements or standards which provide for the protection of navigational information are adopted. Initially, AIS data was difficult to collect, because direct ship-to-ship, ship-to-coast, or coast-to-ship communication was limited to the VHF radio wave range, which only covered 10–20 nautical miles (**Dong et al., 2019**). Currently and since 2008, satellites equipped with AIS receivers have been able to receive data transmitted by onboard transceivers worldwide and allows a simplified data collection. Nowadays AIS data can be easily acquired from commercial websites such as *Marine Traffic* and *Spire*. With the constantly improving quality of AIS data, and acquisition technologies their applications have expanded from safety to include several aspects such as emission inventory, analysis of the impact of ships on the environment, port management and logistic, traffic monitoring (**Perera et al., 2012**), improvement in the accuracy of ship trajectory extraction and prediction (**Arguedas et al., 2018; Rong et al., 2019**). The global coverage indeed allowed extending the analysis from a specific ship to global or regional areas. Recently, AIS data has been used to map ship activities (**Kaluzaet al., 2010**) and to evaluate their environmental impact (**Winther et al., 2014**) on a global scale (**Vitali et al., 2020**). In addition, the high-resolution of data improves the accuracy of shipping behavior analysis. The growth of AIS applications is expected to continue with improvements in the quality and availability of AIS data.

The AIS transceivers are subdivided in two classes, A and B, having different numbers of reported data fields and reporting frequencies. The information recorded by a ship in Class A can be grouped into three type of data fields: static, dynamic and voyage-related information. For Class A, AIS transceivers every 2–10 s, depending on the ship's speed in navigation, and every 3 min at anchoring point, transmit dynamic information automatically. Class B transponders transmit a reduced set of data (lack of IMO number, draught, destination, ETA). The *static* data are MMSI and IMO number, name, type, ship length and width, call sign; *voyage-related information* are ETA- Estimated Time of Arrival, draught, and destination. *Dynamic* information includes ship position, with latitude and longitude, ship speed from 0 knot to 102 knots (with 0.1 knot resolution), rate of turn (ranging from 0 to 720° per minute), navigation direction with shipping course and heading and time stamp in UTC (Universal Time Coordinated) (**Dong et al., 2019**). The main problem related to AIS data is, indeed, the extremely large size of the database (see Figure 2-1). In order to get an idea of the size of an AIS database it is worth noting that a single ship with an AIS data transmitted every ten seconds produces over 3 million records in 1 year, therefore the main issue with AIS is a "big data problem". For this reason, the use of AIS data in maritime research activities involves other different skills such as statistics, environmental science and computer programming (**Dong et al., 2019**).

Figure 2-1 Marine traffic display example (https://www.marinetraffic.com/)

One of the applications of AIS data is the data mining: a data extraction process which started from raw AIS data, which includes spatial and temporal scattered points from which only limited information can be directly obtained. The most common methods for processing and mining AIS data include trajectory, clustering and trajectory prediction (**Lee et al., 2007; Arguedas et al., 2018; Wang, et al., 2017**). The two types of ship behavior are performance in open waters (**Breithaupt et al., 2017**) and performance in restricted waters such as navigation in straits, bays, ports, and inland waterways (**Mitchell and Scully 2014; Rong et al., 2020; Scully & Mitchell, 2017; Zhang et al., 2017**). The AIS data has been usually applied in the monitoring of ship emissions to derive ship activities (**Xu et al., 2019**). The impact of ship emissions on the air quality of sea and coastal areas has also been investigated using AIS data. **Winther et al. (2014)** suggested a method for estimating emission inventories for Arctic shipping starting from AIS information and other aspects related to emissions. **Kivekäs et al. (2014)** introduced a method for assessing the contribution of ship traffic to the concentration of aerosol particles in the downwind of shipping routes, which has been identified through AIS data.

AIS data has also been used to evaluate green shipping strategies aimed at reducing emissions produced by shipping activities. **Watson et al. (2015)**, for example, analyzed the possibility of using an integrated information system of AIS data, shipping agencies' database and port authorities' information to reduce and/or minimize the time at berth of ships by optimizing their sailing speed.

Although AIS offers a powerful and easy-to-access databank for researchers and academics, inaccuracies and errors may occur; for example different ships can share the same MMSI (**Mazzarella et al., 2013**), erroneous positional data may be possible if the position system is not working well (**Harati-Mokhtari et al., 2007**). Therefore, one important preliminary step for processing the AIS data is to identify and delete incorrect and or spike information.

2.3. Routes

Also for routes the levels of simplification can be different. In the absence of real data but with the possibility of visiting the port, it is possible to drawn in CAD the typical routes for each pier of interest starting from the observation of the movements and the times used in port by the ships. With the aid of AIS data, on the other hand, assumptions that are more detailed can be made on the basis of the exact position of each ship at any time spent in port. In the next analyses, both levels of simplification will be addressed.

2.4. Definition of the total installed power on board modern cruise ships: statistical analysis

Once the traffic data has been collected, attention shifts to the characterization of the emission source and it may happen that you do not have enough input data to define the load profiles in the port. In this analysis, a statistical methodology is applied to predict the total power installed on board a cruise vessel. The aim of this analysis is to provide a simple tool for a good estimate of the total power installed onboard of a cruise ship. Statistic methods in the maritime sector have provided important results on many subjects in this context: prediction of ship emissions (**Lepore et al., 2017; Fumo et al., 2015**), analysis of the ship performances, evaluation of the statistical value of ship service speed (**Szelangiewicz & Żelazny 2015**), are only a few examples. Normally, a cruise ship undertakes trips with a duration of one or two weeks, with navigation at night and stops to allow passengers to move ashore and visit new attractions every day (**Molland, 2011**).

On board a modern cruise ship, as in a hotel, numerous attractions and facilities are offered to boarders: restaurants, swimming pools, cinemas, theaters, room service etc. Many of the modern cruise ships feature a diesel-electric propulsion (DEP). Major advantages by DEP are reduced fuel consumption, improved power availability, better maneuverability, easier engine room arrangement and simplified maintenance (**Hansen et**

al., 2001). Two different actuators can provide the electric propulsion: a conventional solution with shaft line and propeller and a more modern one, with Azipods. The latter consists of a propeller that can be orientated on 360^{O}, providing high performances especially during maneuvers (**Kuiken 2008**). The choice of an Azipod solution provides high efficiency, high maneuverability, also at low speed, lower vibrations and more space on board as well. On the other hand, costs of installation and maintenance are higher.

This target has been sought by using a dataset of cruise ships belonging to the most important ship-owners in the world.

2.4.1. Dataset and predictive variables

For a good statistical analysis and for obtaining good performance in the application of the results, there are many efforts that need to be made in generating the dataset.

The dataset of cruise ships includes 129 ships, delivered on 01/01/2000 or after; the data come from sectorial studies, ship-owners, catalogues, projects, technical data sheets, articles, sector websites and similar sources. In Table 2-1, the descriptive statistics of the total power is reported.

This includes the number of ships, and the mean, standard deviation, median and quartiles of the distribution of total power installed onboard, as well as the standard error related to the mean. The same information can be derived from the cumulative distribution function in Figure 2-2. Since the aim of the analysis was to provide a rapid and efficient predictive tool, the prediction variables have been chosen among the main characteristics available for the ships. For this purpose, the following informations were collected: geometric characteristics (overall length, breadth, draft in m), max speed in knots, number of passengers, characteristics of the propulsion system (type of propulsion, number and power of AZIPOD, type of propellers, etc.), and year of launch.

Table 2-1 Descriptive statistics of the cruise ship dataset

Variable	**Total power installed on board (in MW)**
N	129
Mean	56.7
Standard error Mean	1.72
Standard Deviation	19.
Minimum	1.66
Maximum	97.0
Q_1 (first quartile)	50.6
Median	62.4
Q_3 (third quartile)	67.2

All the ship characteristics feature a range of variability in the dataset.

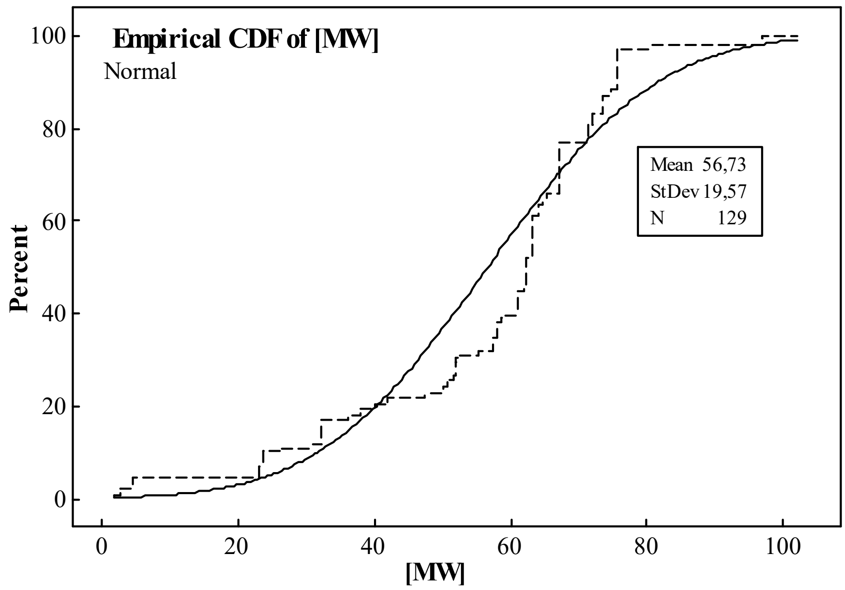

Figure 2-2 Empirical CDF of total power installed onboard for the dataset in [MW]

In Table 2-2, the mean and standard deviation values of the different variables are reported.

Table 2-2. Mean and standard deviation of the principal characteristics of the ships. GT, L_{OA} (length overall), B (beam), T (draft)

Characteristics	Mean	Standard Deviation
GT	92886	44414
L_{OA} [m]	272,32	57,10
B [m]	33,90	7,60
T [m]	7,70	1,10
Speed [kn]	22,30	2,40
Passengers	2643	1385

The data represent potentially independent variables of the regression model: in order to reduce their dispersion before the analysis, it was decided to transform these variables through standardization, i.e. by subtracting to each variable x_i the average value and dividing by the standard deviation (2-1):

2-1 Standardization of variables

$$x_{ist} = (x_i - mean(x_1, \ldots x_k))/standard\ deviation(x_1, \ldots x_k)$$

Figure 2-3 contains the scatter plots of the standardized variables. The scatterplot is a graphic tool for the exploratory analysis of data, which can exploit type and intensity of possible existing relationships between the dependent variable (power installed) and the other variables, as well as the presence of outliers in the data set.

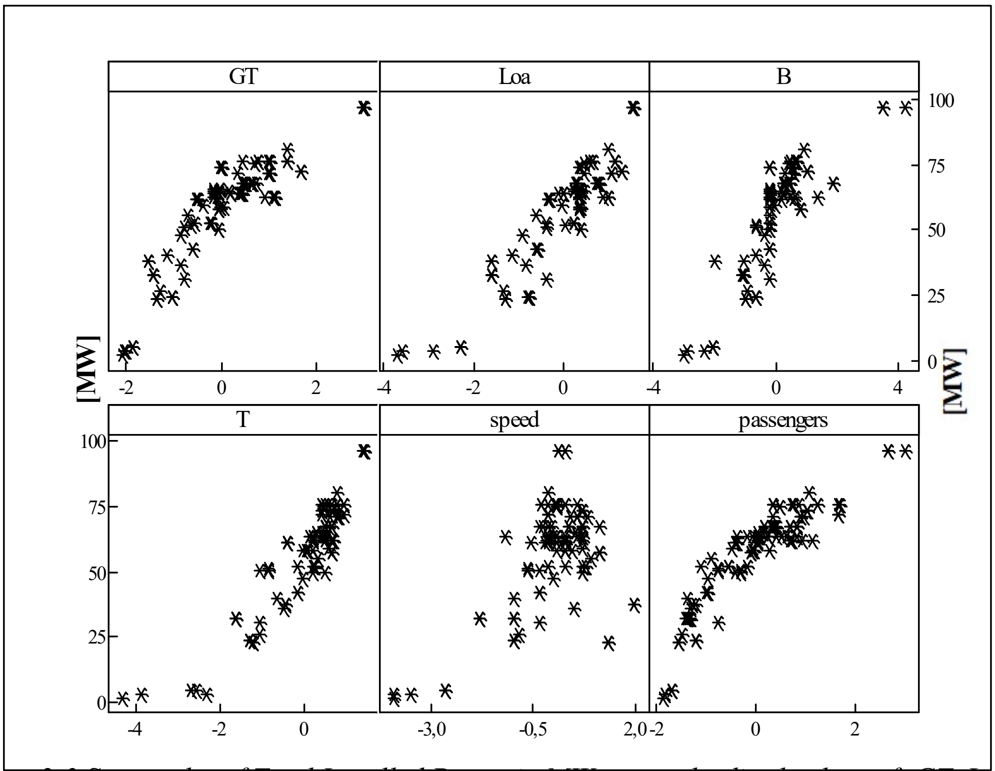

Figure 2-3 Scatterplot of Total Installed Power in MW vs standardized values of: GT, L_{oa}; B; T; Speed; Number of Passengers.

2.4.2. The selection of the regression model

A simple equation for data analysis is:

2-2 Regression model

DATA= MODEL+ ERROR

Where:

- DATA represents the total power installed on board of cruise ships; MODEL is a compact regression of data
- ERROR is the amount by which the model fails to describe the data.

Before selecting the final regression model, several models were theorized and carefully tested using the statistical software MINITAB (**Minitab, 2007**) and its main tools.

Given the need for predicting a single output variable Y, the appropriate regression model is the univariate one. The simplest form is a linear regression with single input X. The generalization is a multiple linear regression involving more input variables X_i. Applying such a model in the context of Eq. 2-2 yields:

2-3 Linear regression

$$Y_i = \beta_0 + \Sigma_j \beta_j X_{ij} + \varepsilon_i$$

Where:

Y_i represents an observed data value, ε_i the error disturbance, X_{ij} represents the value of the i^{th} observation on the j^{th} predictor variable and β_j is the partial regression coefficient for predictor j; β_0 is the intercept of the regression line or regression constant. The partial regression coefficients βj, (**Judd et al., 2011**) are estimated on the basis of sample data using the Ordinary Least Squares (OLS) method, which minimizes the sum of the squared errors. *In this work, multiple linear regressions with two predictors will be adopted.* To carry out the choice of predictors and to later evaluate the effectiveness of the regression model, the following indicators have been used.

2.4.2.1. Standard deviation

Standard deviation, which gives information on the dispersion of variable X; it is calculated as the square root of the variance of variable X (2-4).

2-4 Standard deviation

$$S = \sqrt{\frac{\sum_{i=1}^{N}(x_i - \bar{x})^2}{N-1}}$$

Where:

N is the number of ships in the dataset, x_i are the sample values of variable X and $\bar{x}$ is the mean value of X (Weisberg, 2005).

2.4.2.2. Determination coefficient (R-Sq)

R^2 (R-Sq), is the square of the correlation between predicted Y scores and actual Y scores.
The definition is (2-5):

2-5 R^2

$$R^2 = 1 - \frac{SS_{res}}{SS_{tot}}$$

Where:

- SS_{res} is the residual sum of squares and SS_{tot} is the total sum of squares (**Weisberg, 2005**).

Ranging between 0 and 1, R-Sq represents the percentage of variation of the response variable Y which is explained by the structured link between the variable itself and the predictors of the model.

High values indicate a good prediction. This coefficient grows with an increasing number of predictors and for this reason it is also assessed in its corrected form (R-Sq(adj)).

2.4.2.3. Determination coefficient (R-Sq(adj))

R-Sq(adj) is a modified version of the coefficient of determination , adjusted to the number of predictor used for the regression model; the general formula for calculating the adjusted coefficient of determination is (2-6):

2-6 R-Sq(adj)

$${R_{adj}}^2 = 1 - \left[\frac{(1-R^2)(N-1)}{N-k-1}\right]$$

Where:

- N is the number of ships in the dataset and k is the number of independent regressors, excluding the constant and R^2 is the coefficient of determination (**Weisberg, 2005**).

The predicted R-squared, R-Sq(pred), indicates how well a regression model predicts responses for new observations. Is possible to calculate the predicted R-squared by systematically removing each observation from the data set, and determining how well the model predicts the removed observation.

2.4.2.4. Mallows C_P

This coefficient is linked to statistics that evaluate the adaptation of a regression model obtained with the least squares method; for a particular set of predictors C_P is defined as (2-7):

2-7 Mallows CP

$$C_P = SSE_P/S^2 - N + 2k$$

Where:

- N is the number of the dataset; k is the number of regressors selected among the K predictors available; SSE_p is the error sum of square for a model with k (k<K) regressors; S^2 is the residual mean square after regression on the complete set of regressor.

The C_P value must be as close as possible to the number of variables to which a constant (n + 1) is added; Mallows' C_P is used to choose between multiple regression models.

2.4.2.5. PRESS

The **PRESS** indicator (Predicted Residual Error Sum of Squares) evaluates the predictive ability of the model; this parameter is the sum of the squares of all prediction errors (**Kuliken, 2008**). The PRESS statistic is calculated as the sum of the squares of all the resulting prediction errors. The general formula for calculating the PRESS is (2-8):

2-8 PRESS

$$PRESS = \sum_{i=1}^{N} (y_i - f_i)^2$$

Where:

- N is the number of ships in the dataset; y_i is the outcome of the i^{th} data, and f_i is the prediction for y_i from the model that is trained using all the data in the dataset except the i^{th} data (**Weisberg, 2005**).

For the calculation of the PRESS, a Cross Validation is necessary. The cross validation splits the dataset in two random parts: a training set and a validation set; the former one is used to estimate the parameters in the mean function and the validation set is used to test the model. In the current analysis, the LOOCV (Leave-One-Out Cross-Validation) method was preferred, using a validation set of 1 element only. The method removes one element of the dataset at a time, evaluates the error associated with the generic observation and finally calculates the PRESS. Low PRESS values, together with high predictive R^2 (R-Sq(pred)), indicate the absence of predictive problems.

2.4.2.6. VIF

The Variance Inflation Factors (VIF) is the ratio of variance in a model with multiple terms, divided by the variance of a model with one term alone. The general formula for calculating the VIF is (2-9):

2-9 VIF

$$VIF = \frac{1}{1 - R_j^2}$$

Where:

- R_j^2 is obtained when the j^{th} variable is removed and the model is calibrated with the k-1 regressor (**Weisberg, 2005**).

VIF values << 10, according to standard practice in statistical analysis, demonstrate the absence of multi-collinearity.

2.4.2.7. Pearson correlation index

ρ is a measure of the linear correlation between two variables. The general formula for calculating the ρ is (2-10):

2-10 Pearson correlation index

$$\rho = \frac{\mathrm{cov(X, Y)}}{\sigma_X \sigma_Y}$$

Where:

- Cov(X,Y) is the covariance of variables X and Y and σ_x and σ_y are respectively the (**Weisberg, 2005**) standard deviations of X and Y.

2.4.2.8. Anderson-Darling test

The **Anderson-Darling** test measures how well the data fit into a particular statistical distribution (normal, in this case).

Given the data to be analysed, the better the hypothesized distribution fits the data, the lower this indicator results to be. In our case, the Anderson-Darling statistic was used to verify the normal assumption of the residuals of the chosen regression. The general formula for calculating the AD is (2-11):

2-11 Anderson Darling Statistic

$$AD = -N - \frac{1}{N}\sum_{i=1}^{N}(2i-1)\left[\ln F(X_i) + \ln\left(1 - F(X_{N-i+1})\right)\right]$$

Where:

- N is the number of ships in the dataset, F(x) is the Cumulative Distribution function (CDF) for the specified distribution (normal in this case), i is the i^{th} sample, calculated when the data is sorted in ascending order (**Weisberg, 2005**).

2.4.2.9. P-value

The p-value is another check aimed at establishing if a set of data follows a given distribution. The formula for calculating the p-value is a function of the result of the Anderson Darling statistic. If the p-value is less than a given figure (generally 0.05 or 0.10), the data follow that distribution (**Weisberg, 2005**).

2.4.3. Selection of the model

The aim when adopting any type of model is represented by the choice of actually representative variables and by the need for excluding possible mutual dependencies between them. The procedure used in this work for the selection of the model was structured in two steps (**Olive, 2017**): the first skimming analysis was carried out by a best-subset approach, by which the combinations of regressors with very weak performances have been discarded; in this phase, one of the indexes taken into consideration, in addition to the standard deviation and the coefficient of determination R^2, has been the coefficient proposed by Mallows (C_P), able to address the issue of over fitting, i.e. the trend of the residual sum of squares to get smaller as more variables are added to a model. A second phase of analysis was carried out following a stepwise approach for inclusion and elimination of variables, among those available. As it is known, two collinear variables (i.e. variable with a strong correlation, indicating a linear relationship between the two) do not provide additional information to the model in comparison with a single one.

At the end of the first step, a table similar to Table 2-3 has been analyzed.

Table 2-3 Best subset analysis

Model n.	R-Sq	R-Sq(adj)	C_P	σ	Predictors
1	0,84	0,84	106,3	7,81	T
2	0,83	0,82	129,5	8,20	L_{OA}
3	0,92	0,91	0,60	5,73	T, Pax
4	0,89	0,88	43,1	6,65	GT, T
5	0,92	0,91	1,90	5,74	T, speed, Pax
6	0,92	0,91	2,30	5,75	T, B, Pax
7	0,92	0,91	3,70	5,76	T,B, speed, Pax
8	0,92	0,91	3,70	5,76	GT, T, B, Pax
9	0,92	0,91	5,20	5,77	GT, L_{OA}, T, B ,Pax
10	0,92	0,91	5,40	5,77	GT, T, B , speed, Pax
11	0,92	0,92	7,00	5,79	GT,L_{OA},T, B, speed,Pax

As an example, the number 5 model of Table 2-3 is explained as follows. Predictors are the draft (T), the speed and the number of passengers; the model features a coefficient of determination of 0.916, an adjusted coefficient of determination of 0.914, a Mallows C_P of 1.9 and a standard deviation (σ) of 5.74 MW.

The combinations of variable with high Mallows C_P were eliminated; other combinations of variables were tested but then showed weaknesses concerning the residuals. In a second phase, to avoid the choice of collinear variables, a discriminating indicator in choosing the combination of predictors was the VIF (Variance Inflationary Factor) giving information on the multi-collinearity between variables.

The matrix plot above, Figure 2-4, derived for five variables from the dataset, highlights this multi-collinearity: strong ties exist, for example, between length, breadth and draft and between gross tonnage and number of passengers. The correlation analysis supports the choice of the variables in the model.

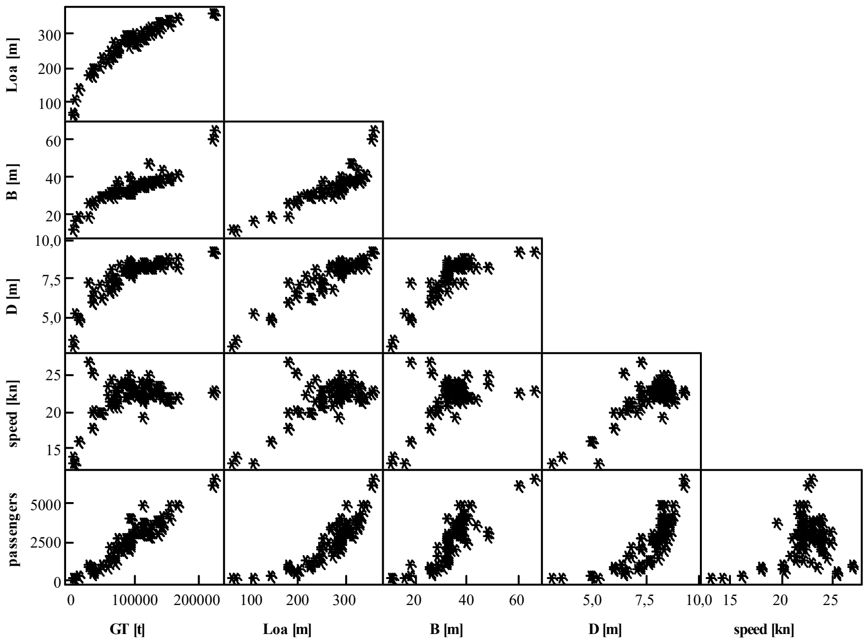

Figure 2-4 Matrix Plot of the following 5 variables: GT [t]; Loa [m]; B [m]; D [m]; speed [kn]; pax

A more detailed analysis of the correlation was made possible, after a first selection obtained from the graph in Figure 2-4, with the calculation of the Pearson correlation coefficients that support the results shown in graphic form (see Table 2-4).

Table 2-4. Correlation analysis (Pearson correlation indexes)

Characteristics	GT [t]	L_{OA} [m]	B [m]	D [m]	Speed [kn]
L_{OA} [m]	0,912				
B [m]	0,900	0,853			
D or T [m]	0,842	0,933	0,820		
Speed [kn]	0,408	0,619	0,500	0,732	
Passengers	0,937	0,869	0,834	0,819	**0,398**

Possible outliers in the dataset have been sorted out through the identification of unusual observations within the software [6].The last but fundamental analysis carried out on the model was on residuals, to evaluate their distribution on a probability card. In this context, the Anderson-Darling statistics and the p-value were calculated [7]. At the end of this step, there were still several combinations of variables: a major part of regressions has been eliminated for problems associated to distribution of the residuals or for physical incompatibility. The final choice for the predictive variables of the regression was maximum speed and the number of passengers on board of the cruise ships. From a purely engineering point of view, speed is linked to the fraction of power installed for propulsion, while the number of passengers is linked to the power installed for hull services and hoteling. Similarly, the gross tonnage GT could be an effective metrics for hotel power. The former parameter was actually the first choice when carrying out the study. However, the regressions obtained by using GT (in place of the number of passengers) did not have normally distributed residues and had worse predictive performances, so the latter parameter was preferred in the end. Overall, the target of finding a simple regression for the total power installed has been sought by the twofold strategy of enhancing the statistical properties of the regression while keeping a clear (even though not optimal) adherence with the physics of the represented power components.

The regression model selected is the following:

2-12 Regression

$$Total\ power\ installed\ onbard = 56{,}7 + 5{,}28 * speed + 15{,}7 * pax\ [MW]$$

It must be kept in mind that in the terms *speed* and *pax* speed values and number of passengers must be entered, standardized through the values of mean and standard deviation presented in Table 2-2 (see also 2-1). Once the regression has been identified, it is possible to compare the predicted power with the actual values from the dataset (see Figure 2-5).

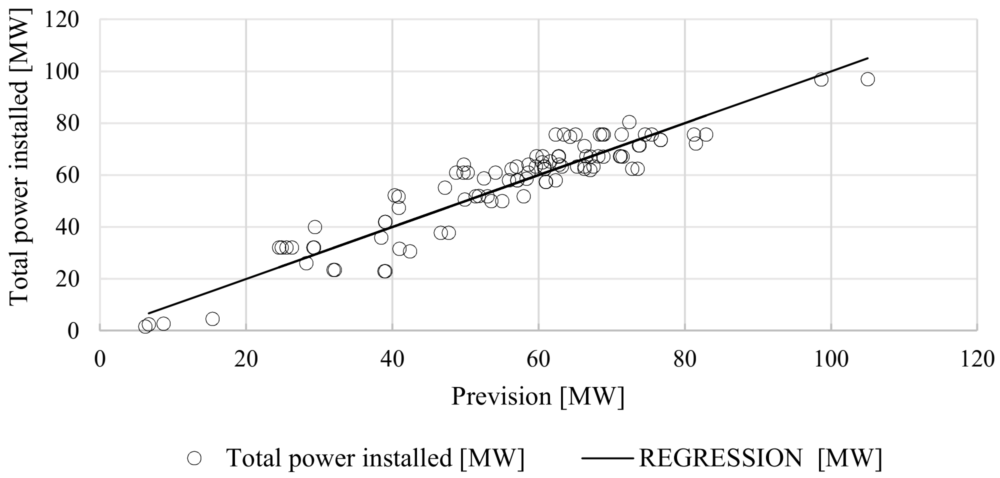

Figure 2-5 Comparison between actual and predicted values of power installed. On the X-axis the prediction and on the Y-axis the actual total power

2.4.4. Analysis of the model and comparisons

In Table 2-5, results obtained for the computed indicators on the selected regression are reported:

Table 2-5. Analysis of model

C_P	VIF speed	VIF pax	σ [MW]	R-Sq	R-Sq(adj)	PRESS	RSq(pred)
3,0	1,188	1,188	6,705	0,884	0,883	6042,8	0,868

Results in Table 2-5 show:

- proper value for the Mallows C_P coefficient;
- low *VIF* values (<10), indicating absence of collinearity between the variables;

- relatively low standard deviation σ, considering that over 60% of cruise ships have more than 60 MW installed;
- the Pearson correlation index between speed and passengers, which expresses the possible linearity relationship between them, is the lowest among all the pairs of predictors available as shown in Table 2-4;
- very high *coefficients of determination* for the projected phase as well.

An important verification was obtained by plotting the data on a normal probability plot, where the standardized predicted values and the observed values are compared. To confirm the of the residuals, it is enough to visualize in the graph that the data (points), which represent the obtained residuals, are not standing far from the straight line (see Figure 2-6a).

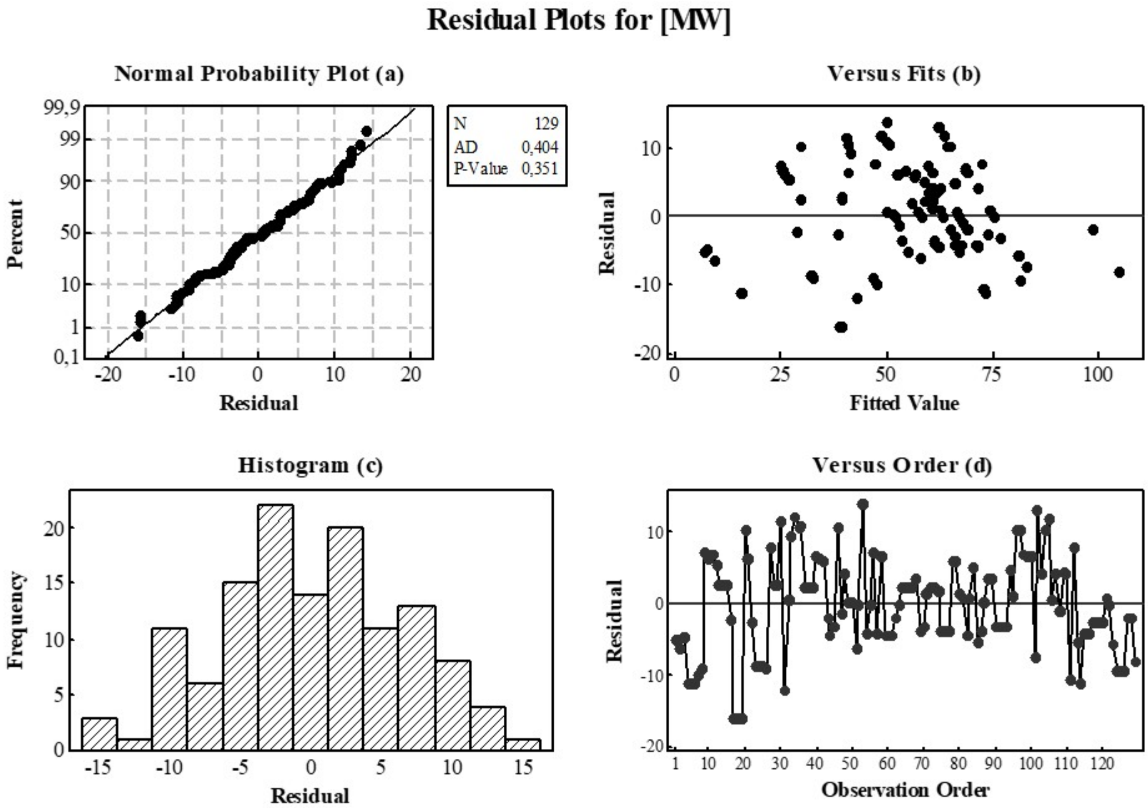

Figure 2-6 Residual plot for total power installed: (a) normal probability plot; (b) and (d) check of homoscedasticity and independence; (c) histogram of residual

The box in the graph of the normal probability plot (see Figure 2-6a) shows the values of the Anderson-Darling statistics (AD) and the p-value (see Figure 2-6a). In our case, the p-value, equal to 0.351, is considerably higher than the level of significance normally set at 0.05.

Relatively low values of the AD statistic and a high p-value confirm the good result obtained. A graphic check was carried out for the assumptions of homoscedasticity and independence. The residuals are, in fact, laying approximately as a cloud of points randomly arranged within a horizontal band confirming homoscedasticity (see Figure 2-6b).

A histogram is reported to analyze the residuals (see Figure 2-6c); the plot shows very few cases of high residues: the residuals are expressed in [MW] on the x-axis, it is noted that the higher frequency occurs around 0 MW (see Figure 2-6c). By considering the quartiles of the histogram of the residuals it appears that 50% of the observed residuals are contained between +-4 MW. In the graph of Figure 2-6d the ships are ordered according to the Gross tonnage, i.e. sorted by increasing size: the trend is random and no particular patterns are shown.

The model has been compared with two different prediction models available in the literature.

2.4.5. EEA (alternative) model

Through the use of this model, it is possible to estimate the power of the main engines, starting from the knowledge of the ship tonnage. The proposed regressions providing estimates of the main power installed are different depending on the type of ship: cruise vessels are included in the category "passenger ships". The regression is based on a dataset updated to 2010, it features an exponential form and uses the tonnage of the ship as a predictor. In Table 2-6, the formula proposed by **EMEP-EEA (2013).**

Table 2-6. The proposed method of EMEP/EEA for passenger ship category

Installed main engine power as a function of GT in kW	$9.55078 \cdot GT^{0.7570}$
Estimated average vessel ratio of Auxiliary engines/ Main engines.	0,16

The regression model proposed by EMEP/EEA, has been tested (see Figure 2-7) on the available dataset and the results, in terms of residues and standard deviation have been compared with the linear regression obtained in this study.

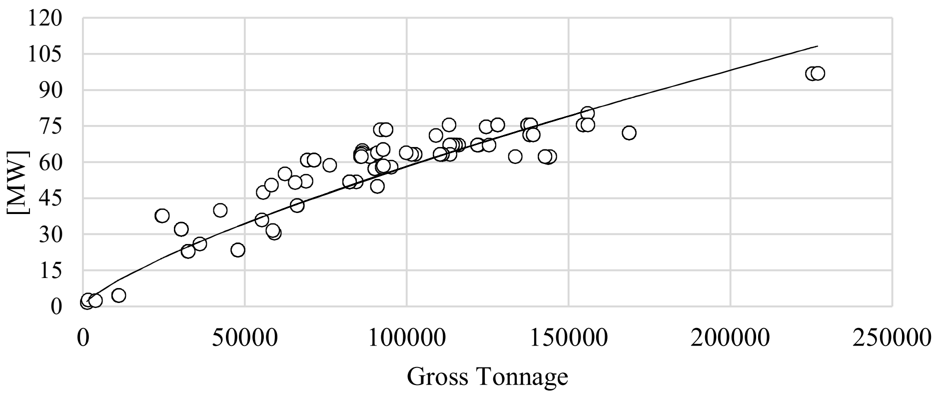

Figure 2-7 Fitted line plot for total power installed in function of gross tonnage (EMEP/EEA)

The results show that the standard deviation of these methods (EMEP/EEA) is larger than the proposed linear regression and that the residues usually grow higher when the size of the vessel increases (see Figure 2-8).

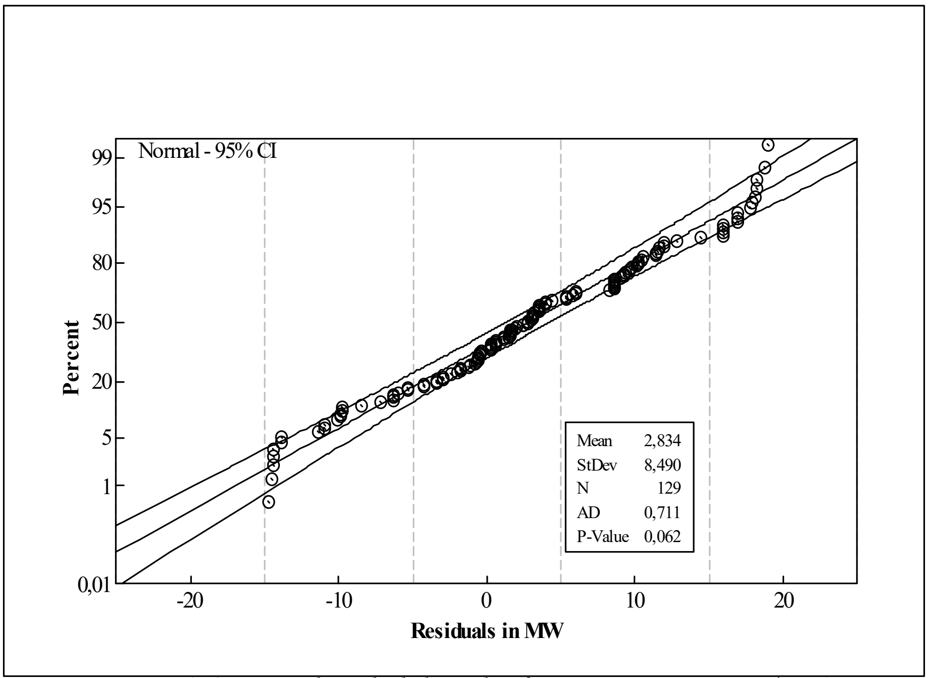

Figure 2-8 Normal probability plot for regression EMEP/EEA

2.4.6. Alternative model by Giernalczyk et al.

The method of **Giernalczyk et al. (2010)**, is based on regressions that allow, to estimate the propulsive and electrical power of different categories of ships, knowing the displacement and speed, (**Giernalczyk et al., 2010**). The proposed regressions are reported in Table 2-7 where D is the displacement in tons and v is the speed in knots:

Table 2-7 The regression proposed by ***(Giernalczyk et al., 2010)***

Main propulsion shaft power [kW]	$(1{,}1896 + 0{,}00002051 \cdot D)\ v^3$
Total electric power [kW]	$3044 + 0{,}24048 \cdot D$

To use this regression it is necessary to know the displacement of the ships, which was not available in the dataset. Assuming, a block coefficient C_B of 0.65 (**Lamb, 2003**) for all the ships available and knowing the main dimensions, the displacement was obtained. Results show that the standard deviation of the power predicted for the available dataset, is about three times the one obtained by the proposed linear regression.

2.4.7. Comparisons

The three methods have been finally compared on a single graph, according to the size of the vessel (see Figure 2-9). The trend lines of the four clouds of point were inserted in the graph for a quick comparison: the suggested linear regression based on speed and passengers, the **EMEP-EEA (2013)** method and the method based on **Giernalczyk et al (2010)**.

The graph shows that, for the analyzed dataset, the linear suggested regression is closer to the actual data, while the two methods of **EMEP-EEA (2013)** and **Giernalczyk et al. (2010)** respectively overestimate and underestimate the total power values installed on board for a large part of the ships.

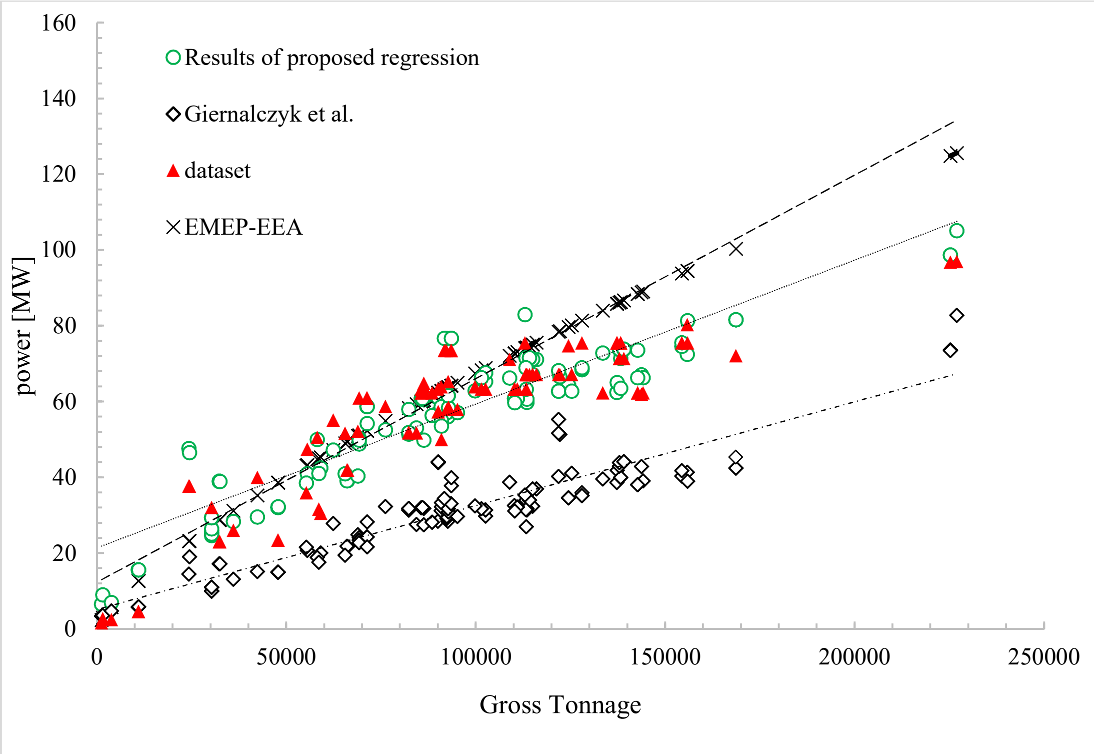

Figure 2-9 Comparison between the available methods and the proposed method

In conclusion, it can be said that the obtained tool is easy to use: by knowing the number of passengers and the speed of a cruise ship, it is possible to obtain an estimate of the on-board total power installed. The model is suited for application whenever an estimate of the power installed on board is necessary.

The good results obtained suggest the possibility of an extension of the model to other classes of vessels, for example ferries and high-speed vessels. It is noted, however, that the higher dispersion in the characteristics of these latter classes of ships could prevent to obtain regressions with the same quality.

2.5. Emission rates: EMEP-EEA Methodology

The main basis on which the emissions have been estimated is the EMEP-EEA (European Monitoring and Evaluation Programme-European Environment Agency) methodology. The EMEP/EEA "Air pollutant emission inventory guidebook" provides guidance on estimating emissions from both anthropogenic and natural emission sources.

Our reference in particular is the part called "International maritime navigation, international inland navigation, national navigation (shipping), national fishing, military (shipping) and recreational boats" in its most updated version of 2016 and 2019 (**Trozzi & De Lauretis, 2016 and 2019**). This methodology starts from a series of assumptions and necessary general information for its application. In particular, for each ship or, more generally, any category of ships, it must be defined with a combination of engine type and fuel type. The types of engine and fuel to choose from are shown in the Table 2-8. The combination of engine type and fuel type first defines a typical consumption (see

Table 2-9).

Table 2-8 Type of engines and fuels

Engine
HSD (High Speed Diesel), **MSD** (Medium Speed Diesel), **SSD** (Slow Speed Diesel)
Fuel
BFO (Bunker Fuel Oil), **MDO** (Marine Diesel Oil), **MGO** (Marine Gas Oil)

Table 2-9 Specific fuel consumption according to type of engines and of fuels

Engine	Fuels	Consumption [g/kWh]
HSD/MS	BFO	213
	MDO/MGO	203
SSD	BFO	195
	MDO/MGO	185

In the absence of available information about the on-board auxiliary's engines, the methodology provides an estimate of the average power values of these engines through the load factors reported in Table 2-10.

Table 2-10 Average power for auxiliary's engines

Categories of ships	2010 world fleet
Liquid bulk	0,30
Dry bulk	0,30
Container and cargo container	0,25
General cargo	0,23
RoRo cargo and RoRo container	0,24
Passenger, RoRo pax and Yacht	0,16
Fishing	0,39
Other	0,35
Tugs	0,10

For the estimate of the loads to the main and auxiliary engines in the three phases of navigation (at sea), maneuvering and hotelling, the estimated % of load to the engines shown in the Table 2-11 can be used.

Table 2-11 Load factors for main and auxiliary motors according to the operating phase

Phase	%load of MCR Main Engine	% load of MCR Auxiliary Engine
Cruise	80	30
Maneuvering	20	50
Hotelling	20	40
Hotelling (tankers)	20	60

Lastly, the Table 2-12 (updated to the 2019 version) shows the emission factors, available according to the type of engine, type of fuel and pollutant chosen:

Table 2-12 Emission factor for NO_X and PM (updated at 2019)

		HSD BFO	HSD MDO/ MGO	MSD BFO	MSD MDO/ MGO	SSD BFO	SSD MDO/ MGO
EF NO_X [g/kWh] (2010 fleet)							
Main	Cruise	11,8	11,2	13	12,3	16,9	15,8
	Maneuvering/ hotelling	9,5	8,9	10,4	9,9	13,5	12,7
Auxiliary	Cruise/ Maneuvering /hotelling	10,8	0,2	13,7	13		
EF PM 10 e PM 2,5 [g/kWh]							
Main	Cruise	0,8	0,9	0,8	0,3	1,7	0,3
	Maneuvering/ hotelling	2,4	0,9	2,4	0,9	2,4	0,9
Auxiliary	Cruise/ Maneuvering /hotelling	0,8	0,3	0,8	0,3		

Further available data allows estimating the total installed power on board through regressions, upstream and in the absence of actual data, taking the tonnage of the ship as a predictable variable. This method, as announced, will be used as guidance for estimating the emissions, although it will undergo changes aimed at improving the results by getting as close to the actual case as possible.

2.6. Diameter and height of the funnels, flow speed and temperature of the plume

The main characteristics of the funnel, which are necessary for studying the dispersion of airborne pollutants, are the height above sea level and diameter. In the elaborations applied to the case study, two approaches were used: a first approach (for 2012 and 2016) provided for the assignment of a single value to the height and diameter of the chimneys for the categories of passenger ships only, while in the second (for 2018) a regression analysis allowed a more detailed estimate of both parameters and for the entire incoming fleet. Data on funnel height from sea level and diameter are difficult to obtain for each cruise ship.

Therefore, the following average values have been assumed in a first approximation (**ARPAV, 2014**). The height of the funnels on the baseline is generally not available. **For the simulation on 2012 and 2016**, in lack of alternative data, funnel height from sea level and diameter for each vessel category are assumed and reported in Table 2-13; for ferries three different funnel heights were assumed depending on the gross tonnage.

Table 2-13. Diameter and funnel height from sea level for each vessel category

Type of vessels	Funnel height	Funnel diameter
	[m]	[m]
Hydrofoils	5	0.5
Cruise ships	40	1
Ferries	15-25-40	1

This approach needed to be revised if we will dealing with the whole port. **For the 2018 inventory**, 46 general arrangement plans were collected including: cruise, ferry, ro-ro cargo, bulk, general cargo, oil tanker, product tanker, pax-cargo ship, fishing trawler, chemical tanker, supply, tug, and container vessels. In these drawings, the height of the upper side of the funnel on the base line and the design depth were measured. The difference between these two heights provides the height of the funnel above the sea level, obviously, when the ship is in full load conditions. By varying the immersion according to the load of the ship, this difference will change. By analysing the measured data, it has been concluded that the best way to simulate the height of the diameter above sea level is by using an estimate, by linear regression, of the height with respect to the baseline. For a more accurate estimation of the H_{BL}, data for each macro-category have been fitted by linear regression equations using L_{BP} as predictive variable. Table 2-14 shows the parameters of the regression equations and the determination coefficients (m is the slope and q is the intercept).

Table 2-14 Coefficients of regression equation (H_{BL} = m L_{BP} + q)

Category	**m**	**q**	**R^2**
Bulk and General cargo	0,16	2,25	0.77
Passenger (cruise, ferry and Ro-Ro)	0,19	6,50	0,92
Fishing	0,22	9,79	0,88
Tanker	0,19	-6,65	0,84
Container	0,06	24,9	0,47
Supply and tug	0,36	0,05	0,40

Next, to obtain the height of the funnel above sea level from the obtained H_{BL} value, the ship depth value, available from the database, is subtracted. For the estimation of the diameters of the funnels starting from the estimation of a design funnel's diameter based on max power of engines and assuming an exhaust temperature and speed of exhausts set to 400 °C and 12 m/s respectively (**Badeke et al., 2020**) the project diameter has been estimated. These values are confirmed by the literature. In **Durmaz et al., (2017)**, for example, exhaust gas temperatures and velocity have been measured on a ferryboat. Results are respectively between 250°C and 350°C while the velocity values are between about 10 m/s and 17 m/s for the engine load considered. Since there are often several funnels on board, an abstraction rather than the actual design diameter was obtained. Next, the flow rate and speed of the exhausts gas have been estimated for partial loads to the engines in port in the various phases. For example, during the hotelling phase, the speed is reduced by 20%.

3. *From operations of ships in port to dispersion of pollutants in the atmosphere*

Aims and scope

In this chapter, the bottom-up methodology for the prediction of pollutants dispersed in air from ships at port that was reported in the previous chapter 2 is applied with reference to the port of Naples. First of all, the port of Naples will be presented and described with the newest statistics and traffic data. Input data with a different degree of precision and inherent results are described. The chapter will therefore address each aspect of the problem: traffic, routes, power and load to the engines, speed in port, diameters and heights of the funnels and emissions. Traffic data will also be deepened thanks to an AIS data management code developed in Matlab. Dispersion maps in output allow to quantify the dispersion of pollutants in the atmosphere, the impact on air quality and seasonal variations.

3.1. The port of Naples: history, morphology and chacteristics

The city of Naples and its port were funded in IX B.C. in the East bay of the homonymous gulf. With 954.244 residents, the Municipality of Naples occupies 119,02 km^2 with a density of 8.017 inhabitants/km^2 (**www.ISTAT.it, 2019**), and is the third-largest city in Italy after Rome and Milan. More than 3 million people live in the "Metropolitan Area" of 1.171 km^2 with a density of 2.672 inhabitants/km^2 (**www.ISTAT.it**, **2020**). The area includes several sources of risk for human health such as common anthropic sources, ports and airports, road traffic and industries and natural sources like active volcanoes. Located in the center of the Mediterranean Sea, the Port of Naples is one of the main points of arrival and passage in commercial traffic and, with 75 berths (11 km) it is also one of the largest ports of the Mediterranean in terms of quantity and diversity of traffics, see Figure 3-1. Together with the port of Salerno and Castellammare di Stabia it constitutes the Authority of Port System of the Central Tyrrhenian Sea. From the tourist zone of the port, located in the center of Naples, connections by fast vessel and ferries depart for the islands of the Gulf (Capri, Ischia and Procida) and for the Sorrento and Amalfi coast; the main archaeological sites (such as Pompei, and Ercolano) are also easily reachable from the port. The port represents an important hub from and to Sicily and Sardinia [8]. In the cabotage sector, the port is the Italian leader, accounting for 50% of Italian traffic. In 2015 the port ranked 12th among the busiest European ports in terms of number of passengers, and the 2017 rankings place it 35th for tourist cruises worldwide. On a local scale, the port was confirmed third in Italy (after Civitavecchia and Venice) for cruise traffic in 2019. The passenger traffic is certainly one of the strengths of the port: according to the latest statistics, in 2019 cruise passengers were 1.266.704 (22.659 in 2020 due to the restrictions related to the COVID-19) and the total number of passengers (cruise, local and ferry) was as large as 7.386.689 (3.301.347 in 2020) [9]. The data updated to 2019, compared to those of 2018, show an increase of + 16.9% in the number of TEUs (681.929), + 4.39% in the tons of liquid cargo transported by bulk carriers and a -2.63% for the tons of solid cargo. In the first ten months of 2020 (COVID-19), the number of containers in transit in the port has been 537.206 (-6.23% compared to the 2019) and between January and October 2020, the number of Ro-Ro unit has been 162.770 (-24.32% compared to 2019) [9]. A 2015 deliberation of the Port

Authority of Naples forces all the vessels entering the port to use fuel with a maximum of 0.1% weight of Sulphur.

Figure 3-1 The port of Naples [10]

The port is divided into two main areas, with different types of traffic and different geographical position. The west end, closer to downtown, is dedicated to passenger traffic and features three sub-areas [8]:

- pier Beverello, with hydrofoil service connecting the town to the main islands in the Gulf;
- pier Angioino, pier for cruise ships;
- Quay Porta di Massa and Piliero, piers used for long-range ferryboats.

The eastern area is dedicated to commercial vessels and is equipped with several spaces for handling and storage of liquid and dry cargo and containers. In the next paragraphs, the traffic of the three reference period chosen for the simulation will be presented

3.2. Traffic data

3.2.1. Passenger ship traffic in 2012

2012 data on cruise ships traffic (date of arrival, departure and berthing time) in the port were obtained by consulting the official website of the Port Authority of Naples [8]. The main characteristics of the ships have been collected in accordance with what is described in chapter 2 (see 2.2). The total power installed on board and the maximum speed of the ship are shown below, Figure 3-2, to describe the incoming fleet. The graph shows how the maximum speed of these vessels does not vary with varying tonnage, while what grows strongly as tonnage increases is the power destined for hotelling services.

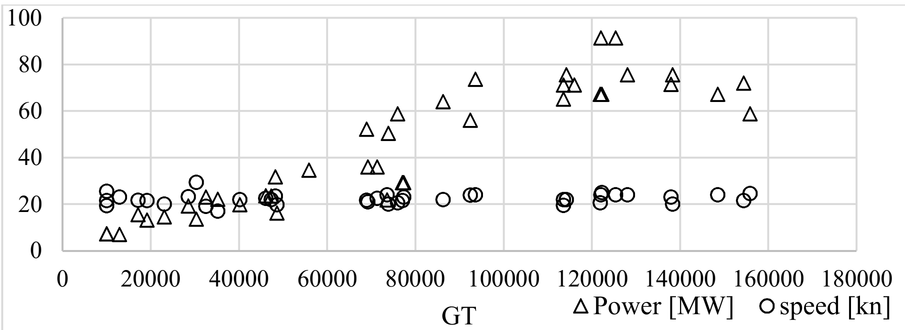

Figure 3-2 Distribution of total power installed on board and of the max speed for each cruise ships (2012)

As for the small boats, intended as ferries and HSC, the available calendars for the port of Naples do not indicate the name of the particular vessel which, for a specific day, will make the connection with the islands. In the absence of specific data, the speeds and the total power installed on board of the fleet were, therefore, collected for each ship-owner in service at the port of Naples. In particular, for each incoming fleet are shown in Table 3-1 the "typical" vessel generated.

Table 3-1 Typical ship for all HSC vessels arriving in Naples

Category	Shipowner	Power [kW]	Speed [kn]
Ferry	Caremar	6148,0	23,1
	Medmar	3388,6	16,8
	TTTLines	19800,0	24,3
	GNV	20746,7	21,9
	Siremar	4824,0	16,7
	Tirrenia	6100,0	25,3
HSC	Caremar	3733,3	35,3
	NLG	3510,0	31,0
	SNAV	3972,3	34,3
	Alilauro Gruson	3650,1	32,4

3.2.2. *Cruise ship traffic in 2016*

The cruise ship fleet arriving in 2016 was treated in the same way as the one arriving in the first elaboration, which has been previously explained. In Figure 3-3 the distribution of total power installed on board and of the max speed for each cruise ships according to the gross tonnage of the ship.

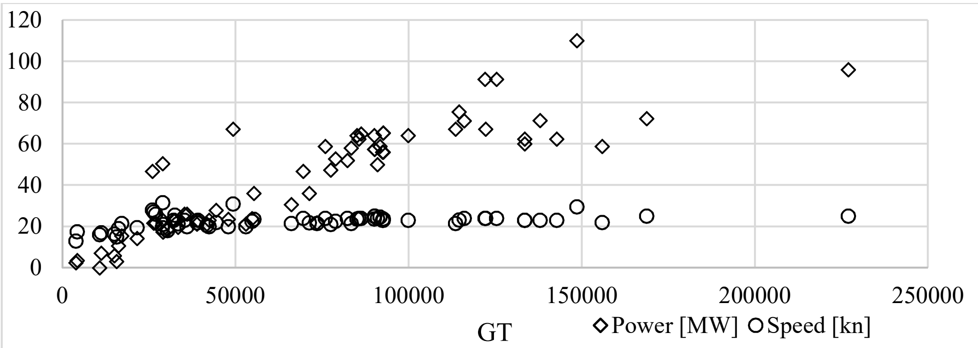

Figure 3-3 Distribution of total power installed on board and of the max speed for each cruise ships (2016)

Generally, according to the Port Authority, the cruise ship activity in the port of Naples is at its highest from May to October with about 60 calls per month with a peak in September (67 calls for 2016). A medium activity is registered in April and November (about 36 calls per month for 2016), while there is a minimum activity from November to April with only about 15 calls per month. According to **Papaefthimiou et al., (2016)**, this indication could have some consequences on the assessment of the impact on air quality due to the increase of hoteling emissions in summer period. The total number of cruise ships arriving at the port of Naples in 2016 is 73. In the following figure (Figure 3-4), instead, the monthly variation in call and number of passengers. Usually cruise ships are at berth from 7 am to 8 pm and the average time at berth is about 13 hours per day.

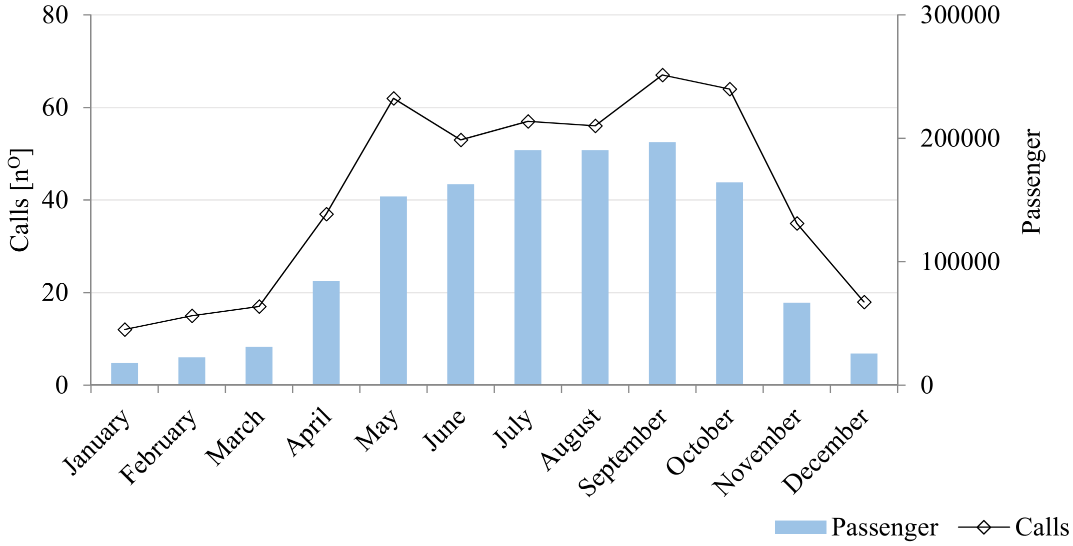

Figure 3-4 Monthly variation of cruise ships calls and passenger traffic (reference year 2016)

3.2.3. Traffic in the whole port of Naples (2018)

The AIS data used in this study has been obtained from Spire: Satellite, Terrestrial, and Dynamic™ AIS, a company dedicated to providing real-time data on the locations and movements of vessels, which offers a one-stop-shop for AIS tracking data. Satellite-AIS (S-AIS) allows for enhanced coverage in remote areas, such as oceanic and Arctic regions and complements Terrestrial-AIS (T-AIS) coverage [12]. Spire's constellation of nanosatellites, for example, picks up AIS signals to increase visibility of vessels in remote areas of the world. The data has been obtained as directly decoded in CSV (Comma Separated Values) format, as in Figure 3-5.

```
created_at,timestamp,mmsi,msg_type,latitude,longitude,speed,course,heading,rot,imo,name,call_sign,flag,draught,ship_and_cargo_type,length,width,eta,destination,status,maneuver,accuracy,collection_type,to
2020-02-17 16:12:22.905695 UTC,2020-02-17 16:12:22 UTC,247273400,5,,,,,,,9376854,DOMINIA,ICFW,IT,8.3,80,176,31,2020-02-17 16:00:00 UTC,IT NAP,,,,terrestrial,,,,
2020-02-17 16:12:23.133089 UTC,2020-02-17 16:12:23 UTC,247273400,5,,,,,,,9376854,DOMINIA,ICFW,IT,8.3,80,176,31,2020-02-17 16:00:00 UTC,IT NAP,,,,terrestrial,,,,
2020-02-17 16:12:30.806091 UTC,2020-02-17 16:12:30 UTC,247166800,5,,,,,,,9322645,ATTILIO IEVOLI JR,IBYI,IT,6,80,105,16,2020-02-18 06:00:00 UTC,ITNAP-ITLIP,,,,terrestrial,,,,
2020-02-17 16:12:30.860197 UTC,2020-02-17 16:12:30 UTC,247166800,5,,,,,,,9322645,ATTILIO IEVOLI JR,IBYI,IT,6,80,105,16,2020-02-18 06:00:00 UTC,ITNAP-ITLIP,,,,terrestrial,,,,
2020-02-17 16:12:37.330778 UTC,2020-02-17 16:12:37 UTC,247223400,3,40.84229,14.26331,0,0,511,-128,,,,IT,,,,,,,5,0,0,terrestrial,,,,
2020-02-17 16:12:50.99146 UTC,2020-02-17 16:12:50 UTC,247043100,3,40.841886666666667,14.268076666666667,0.1,191.7,271,0,,,,IT,,,,,,,5,0,0,terrestrial,,,,
2020-02-17 16:12:58.798204 UTC,2020-02-17 16:12:58 UTC,247273400,3,40.806,14.315316666666666,0.2,15,78,0,,,,IT,,,,,,,1,0,0,terrestrial,,,,
2020-02-17 16:13:18.824805 UTC,2020-02-17 16:13:17 UTC,247376900,3,40.842475,14.265083333333333,0,343.3,168,0,,,,IT,,,,,,,5,0,0,terrestrial,,,,
2020-02-17 16:13:46.079175 UTC,2020-02-17 16:13:45 UTC,247376900,5,,,,,,,9821237,VIVARA,IJUR2,IT,5,52,22,11,2020-01-11 08:15:00 UTC,NAPOLI,,,,terrestrial,,,,
2020-02-17 16:13:46.121228 UTC,2020-02-17 16:13:45 UTC,247376900,5,,,,,,,9821237,VIVARA,IJUR2,IT,5,52,22,11,2020-01-11 08:15:00 UTC,NAPOLI,,,,terrestrial,,,,
2020-02-17 16:14:23.973806 UTC,2020-02-17 16:14:23 UTC,247074100,5,,,,,,,8881345,MARINA PICCOLA,IOBC,IT,2.6,80,65,11,2020-02-17 14:45:00 UTC,NAPOLI,,,,terrestrial,,,,
2020-02-17 16:14:24.097475 UTC,2020-02-17 16:14:23 UTC,247074100,5,,,,,,,8881345,MARINA PICCOLA,IOBC,IT,2.6,80,65,11,2020-02-17 14:45:00 UTC,NAPOLI,,,,terrestrial,,,,
2020-02-17 16:14:24.876859 UTC,2020-02-17 16:14:24 UTC,247590000,5,,,,,,,8117988,BILLTON,ISFX,IT,4,70,57,11,2020-02-17 19:00:00 UTC,NAP<>PROC<>CASAM,,,,terrestrial,,,,
2020-02-17 16:14:24.988385 UTC,2020-02-17 16:14:24 UTC,247590000,5,,,,,,,8117988,BILLTON,ISFX,IT,4,70,57,11,2020-02-17 19:00:00 UTC,NAP<>PROC<>CASAM,,,,terrestrial,,,,
2020-02-17 16:14:29.048516 UTC,2020-02-17 16:14:28 UTC,247326000,3,40.840833333333336,14.2815,0.1,154,14,0,,,,IT,,,,,,,5,0,1,terrestrial,,,,
2020-02-17 16:14:36.412333 UTC,2020-02-17 16:14:34 UTC,247372400,3,40.84133,14.276693333333334,0,166.5,204,0,,,,IT,,,,,,,5,0,1,terrestrial,,,,
2020-02-17 16:14:39.636555 UTC,2020-02-17 16:14:38 UTC,247441000,3,40.841026666666664,14.261666666666667,0,287.9,127,0,,,,IT,,,,,,,5,0,0,terrestrial,,,,
2020-02-17 16:14:39.420695 UTC,2020-02-17 16:14:39 UTC,247441000,5,,,,,,,9144732,VINCENZO FLORIO,ICFQ,IT,6.3,60,180,29,2020-02-17 05:45:00 UTC,ITNAP,,,,terrestrial,,,,
2020-02-17 16:14:39.360939 UTC,2020-02-17 16:14:39 UTC,247441000,5,,,,,,,9144732,VINCENZO FLORIO,ICFQ,IT,6.3,60,180,29,2020-02-17 05:45:00 UTC,ITNAP,,,,terrestrial,,,,
2020-02-17 16:14:39.703749 UTC,2020-02-17 16:14:39 UTC,247441000,3,40.841026666666664,14.261666666666667,0,287.9,127,0,,,,IT,,,,,,,5,0,0,terrestrial,,,,
```

Figure 3-5 Example of CSV file for the AIS data

The rates of emission have been calculated using a bottom-up activity-based methodology, using AIS data. The flow sheet describing the use of the AIS data is reported in Figure 3-6.

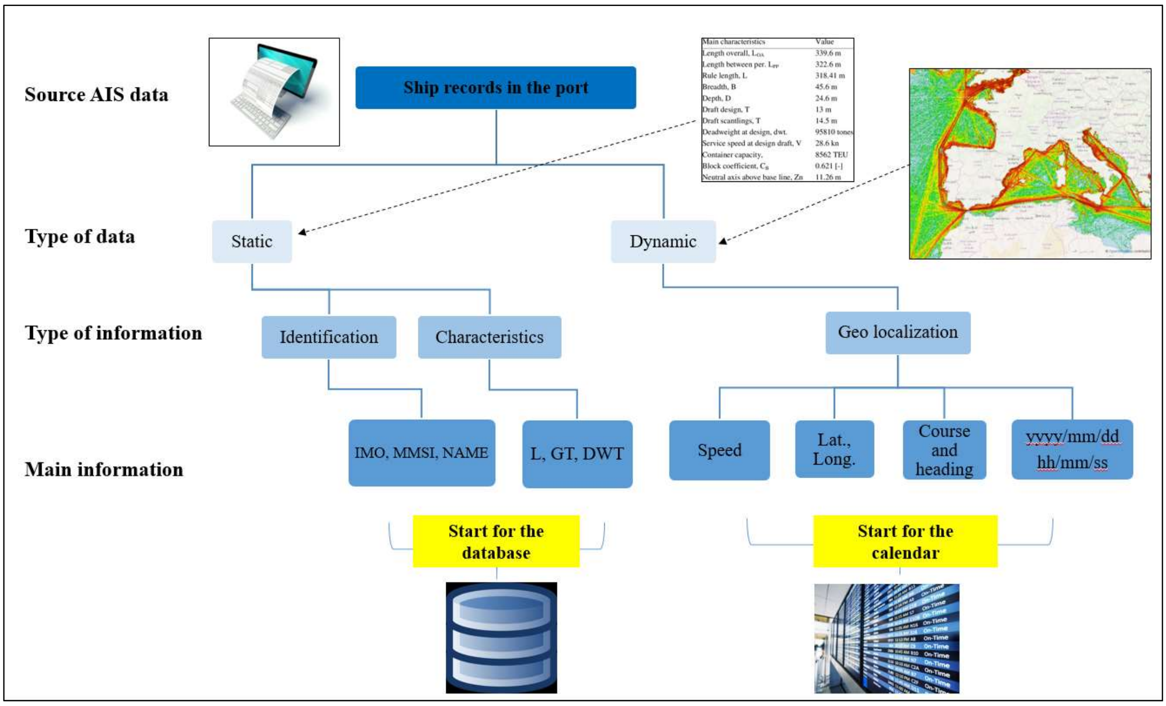

Figure 3-6 Flow sheet of the use of AIS data

The **innovations and improvements** introduced in this inventory are: use of AIS data and coverage of the **entire port**, the development of a MATLAB code for the making of **calendars**, improvements in the estimation of power in the various phases, use of **average speeds in port** and therefore exclusion of the approximation of a single speed, identification of **actual routes**.

The AIS database used includes more than 1.000.000 records associated with 922 objects, generally identified by their MMSI and grouped in categories. Among them, those belonging to seven categories have been removed because they corresponded to stationary objects or to ships lacking adequate information and therefore were not relevant for our scopes. For these reasons, null category containing ships without data, law enforcers, military Offshore Power Supply, and Salvage and Rescue (SAR) Aircraft, pleasure craft, sailing vessels and port tender has been excluded from the analysis since their influence on emissions is null or not relevant at all. Overall deleted elements has been141 (84965 records equal to 7.95% of the total records). The static portion of the AIS data was used as the starting point for the data collection. In order to quickly present the database, the information resulting from the carried out processing is shown in the Table 3-2. The **main average data** such as max speed, power, Gross Tonnage, and number of ships of the fleet visiting the port of Naples in 2018 sub-dived into 45 categories are reported in Table 3-2. These data has been obtained through the construction of a specific database which will be explained in the next paragraphs. The first column "Group" indicates the first of five macro categories in which all ships have been grouped for the successive dispersion model: **C**ommercial, **F**ishery, **P**assenger, **T**anker, **O**ther. The last column of the same table counts the number of calls for each category; this is one of the results of the MATLAB Code explained in the next paragraph.

Table 3-2 Average data of the fleet arriving at the port of Naples in 2018

Group	Category	Speed [kn]	Power [kW]	GT	Number of ships	Calls
O	Aggregates Carrier	11,6	1790	995,0	1	1
O	Anchor Handling Vessel	12,0	4050	1471	1	2
T	Asphalt/Bitumen Tanker	14,0	2981	5774	3	17
C	Bulk Carrier	16,2	6830	22045	32	36
T	Bunkering Tanker	8,50	892,0	775,3	3	94
O	Cable Layer	12,0	6005	9024	2	3
C	Cargo	10,0	625,5	311,0	1	5
C	Cargo/Containership	16,7	6728	8017	5	11
T	Chemical Tanker	15,0	8179	24996	1	40
C	Container Ship	22,2	33811	45043	131	503
O	Crane Ship	7,50	526,0	505,0	5	7
C	Deck Cargo Ship	10,0	3180	2770	2	2
F	Fish Carrier	8,50	1600	206,0	1	1
F	Fish Factory	12,0	1194	1085	1	1
F	Fishery Research Vessel	12,0	1600	398,0	1	1
F	Fishing Vessel	13,5	666,5	170,4	13	17
C	General Cargo	15,0	4826	11427	153	270
O	Grab Hopper Dredger	10,0	1102	481,0	1	2
O	Heavy Load Carrier	17,3	4300	6295	3	4
O	Hopper barge	8,00	882,0	1192	1	2
P	HSC	32,3	5864	1006	9	2960
P	Hydrofoil	38,0	4000	196,0	1	8
P	Inland	18,5	34241	62750	3	30
T	LPG Tanker	17,8	6093	11135	23	118
T	LPG-Chemical Tanker	15,5	6000	9835	1	7
O	Motor Hopper	12,0	2388	1469	1	39
O	Offshore power Supply Ship	13,2	4457	1973	8	415
T	Oil Products Tanker	14,0	6145	17794	4	78
T	Oil-Chemical Tanker	16,2	6269	15250	100	230
O	Other	19,5	28151	113216	3	38
P	Passenger Ship	23,8	22178	38916	130	12798
P	Passenger-Cargo Ship	13,0	648,0	196,0	1	90
O	Patrol Vessel	32,0	9440	550,0	1	1
O	Research-Survey Vessel	14,2	5616	2442	2	4
C	Ro-Ro-Cargo	19,2	16150	29773	14	62
C	Ro-Ro-Container	20,3	18251	33718	7	37
P	Ro-Ro-pax	20,1	15013	15653	54	8133
O	Salvage-Rescue	13,6	2942	1204	4	58
O	Special Vessel	16,0	8000	4201	1	1
F	Trawler	14,0	665,6	177,3	6	12
O	Tug	12,6	3110	344,1	14	89
O	Unspecified	19,5	1333	367,0	5	61
T	Water Tanker	11,9	1219	1200	7	174
T	Wine Tanker	11,9	1219	1200	3	71
P	Yacht	18,7	3152	470,0	8	6

3.2.4. The MATLAB code

The dynamic AIS data was largely processed using MATLAB code strings created ad-hoc in-house. The spatial coordinates were used for the reconstruction of the routes while speed and time data were used for the making of the calendars, see Figure 3-7.

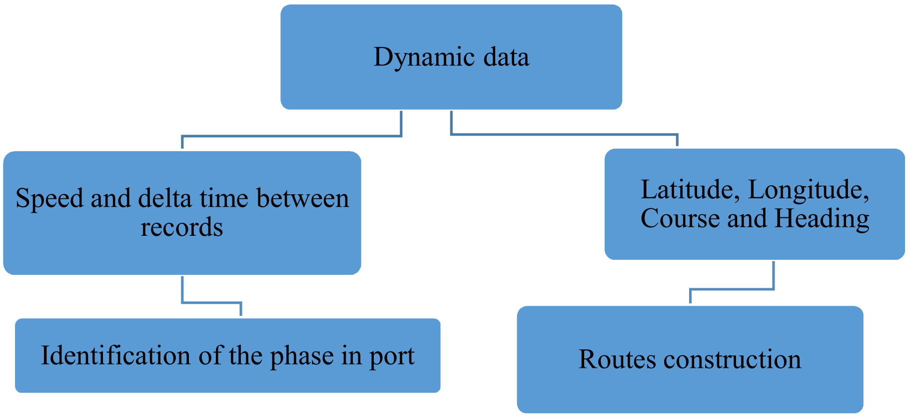

Figure 3-7 Flow sheet for dynamic data

The built Matlab code allows the organization of the arrival and departure calendars of the ships and the definition of the various phases in port. In particular, the lines of code analyze every single ship in terms of time data, position data, and speed. The variations in speed during the acceleration and deceleration phase of the ship and the moments in which the records have zero speed are also classified depending on the time that elapses between two consecutive tics. Overall, the code is able to distinguish between:

- arrival in port (in);
- port navigation (navigation);
- start stop on the quay (mooring);
- possible starting and stopping of the engines;
- end stop on the quay;
- exit from the port (out).

For example, the image of a simple route of a small passenger ship is shown in Figure 3-8; the points of entry and exit from the port (1 and 4), the stopping points (3) and the navigation (2) points are highlighted. Each of these phases is characterized by a unique combination of speed and time delta related to neighboring records and locations.

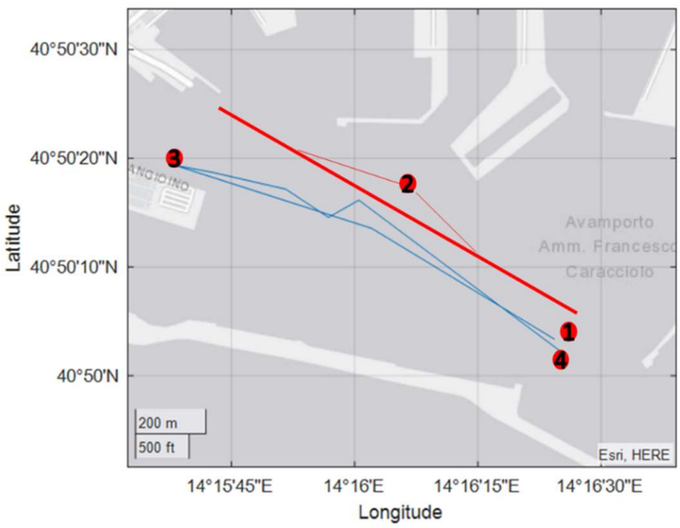

Figure 3-8 Example of route analysis

In order to better understand the results of the code, Table 3-3 shows an example of result obtained for a particular container ship. In Table 3-3 each record is marked with a particular wording. Each record of each ship has been characterized by latitude, longitude, route's angle, time, speed and phase. The detailed articulation of the AIS data has allowed the subsequent accurate estimation of emissions.

Table 3-3. Example of MATLAB results

Ship name	Lat.	Long.	Course	Heading	Timestamp (UTC)	Speed [kn]	Phases
Ship 1	40.833	14.275	319	346	21/04/2018 10:51	5,7	in
Ship 1	40.835	14.274	16	39	21/04/2018 10:53	4,0	navigation in port
Ship 1	40.837	14.276	50	74	21/04/2018 10:55	4,3	navigation in port
Ship 1	40.838	14.279	86	108	21/04/2018 10:57	3,7	navigation in port
Ship 1	40.838	14.282	86	134	21/04/2018 11:00	1,3	navigation in port
Ship 1	40.839	14.282	4	169	21/04/2018 11:03	1,9	mooring phase (start)
Ship 1	40.840	14.282	220	187	21/04/2018 11:07	0,0	0…………………
Ship 1	40.839	14.283	164	195	21/04/2018 20:27	1,8	mooring phase (end)
Ship 1	40.838	14.281	258	270	21/04/2018 20:30	2,5	navigation in port
Ship 1	40.830	14.279	273	257	21/04/2018 20:33	3,7	navigation in port
Ship 1	40.837	14.276	242	214	21/04/2018 20:35	3,7	navigation in port
Ship 1	40.836	14.274	199	176	21/04/2018 20:37	3,8	navigation in port
Ship 1	40.835	14.274	188	170	21/04/2018 20:37	3,9	navigation in port
Ship 1	40.833	14.274	160	149	21/04/2018 20:39	5,3	out

The lines corresponding to mooring records, so the lines between "mooring start" and "mooring end" are obviously not reported in Table 3-3. Starting from the data available in Table 3-3, the Figure 3-9 reports the routes obtained with the speed values in some typical points. Clearly, the dwell time physically passes between the last data in input speed (blue circle in Figure 3-9) and the first in output speed (orange circle in Figure 3-9).

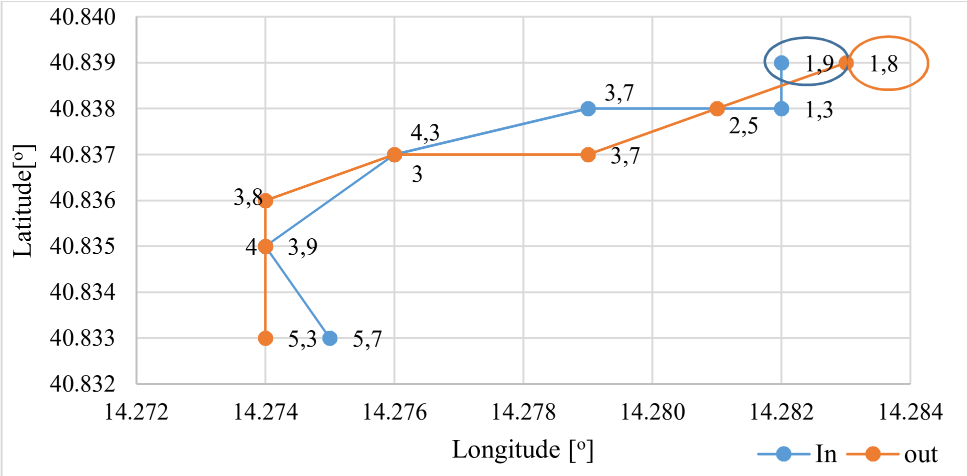

Figure 3-9 Example of in and out routes

3.2.5. Static information Database

For an accurate estimation of the emission rates, a necessary database of all the ships visiting the port of Naples in 2018 was realized. The collected informations are:

- category, name/ IMO number, gross tonnage (GT) and deadweight (DWT) from static AIS data (Yang et al., 2019);
- length (L), width (B), and draft (T) [m];
- total power installed on-board (P) [kW] and type of engines;
- maximum speed (v) [kn];
- number of passengers, cars, containers and similar if present.

Below there are the graphs, for each group of ships (Commercial, Fishing, Other, Passengers, Tanker as grouped in Table 3-2) that describes the power and the max speed.

- COMMERCIAL

a)

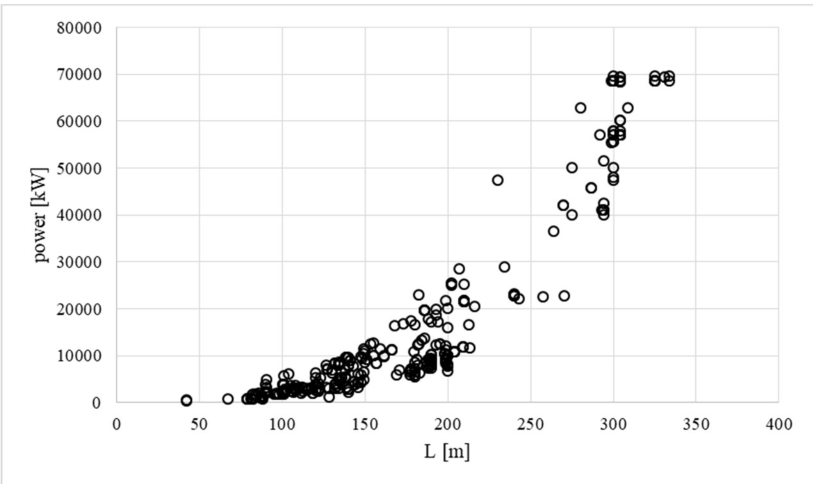

b)

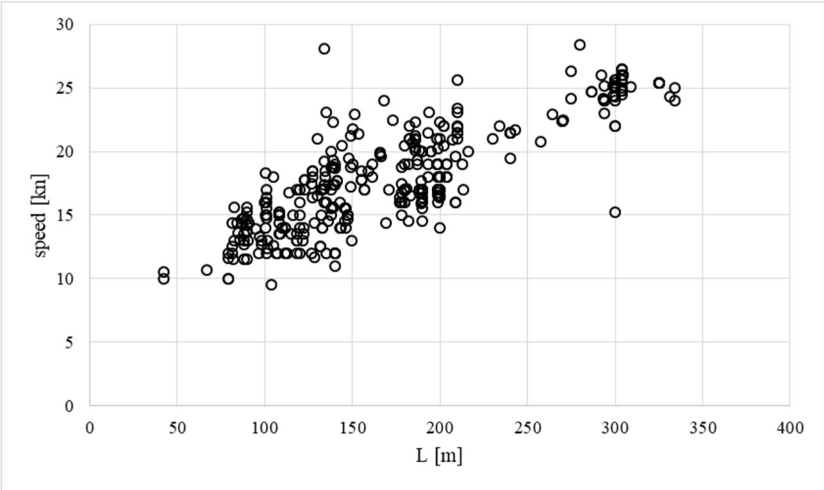

Figure 3-10 Commercial ships: total power installed on board (a) and max speed (b)

- FISHING

a)

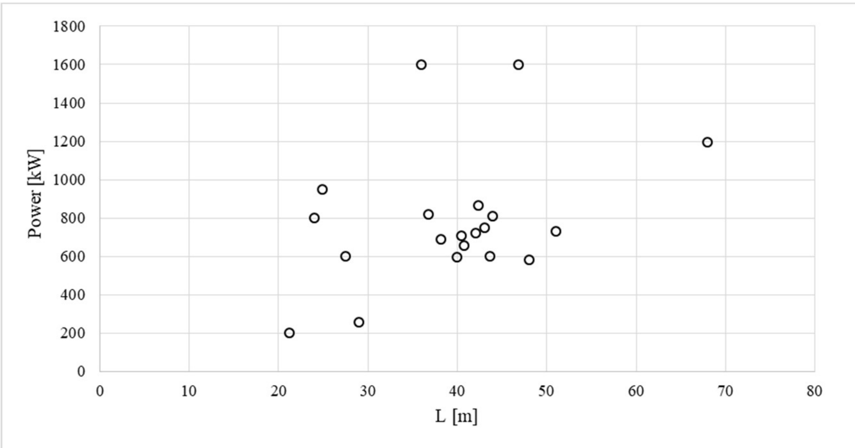

b)

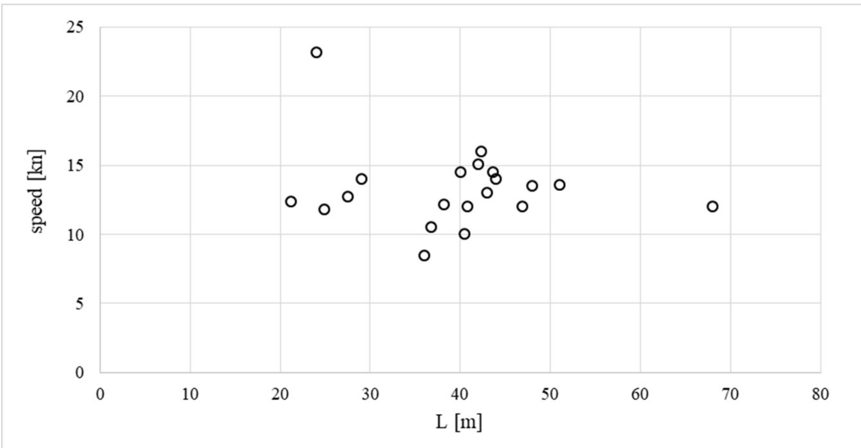

Figure 3-11 Fishing ships: total power installed on board (a) and max speed (b)

- PASSENGER

a)

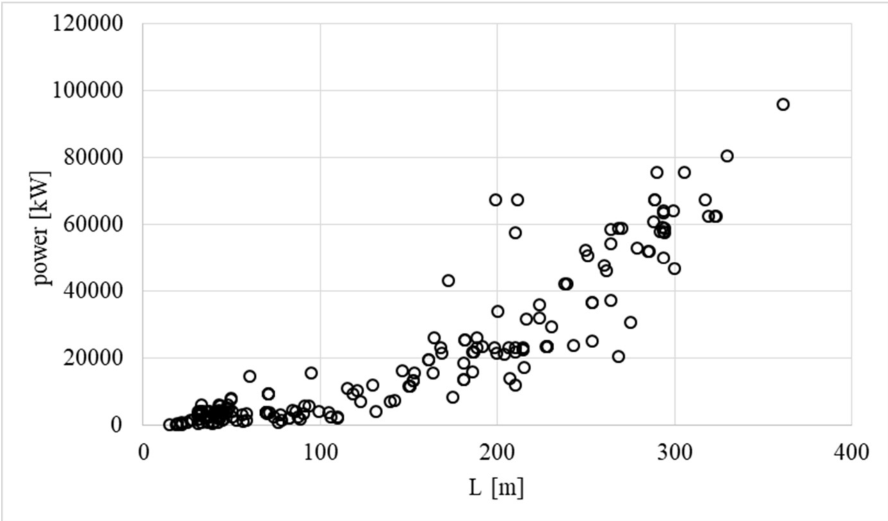

b)

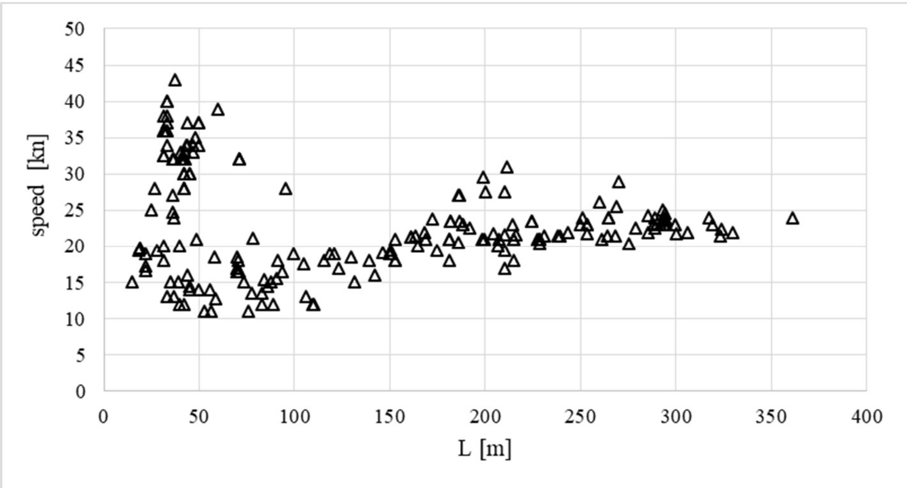

Figure 3-12 Passengers ships: total power installed on board (a) and max speed (b)

- OTHER

a)

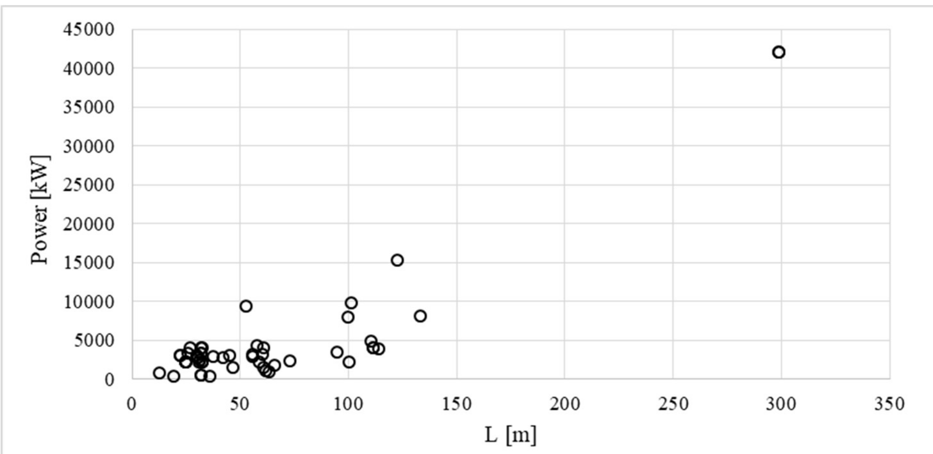

b)

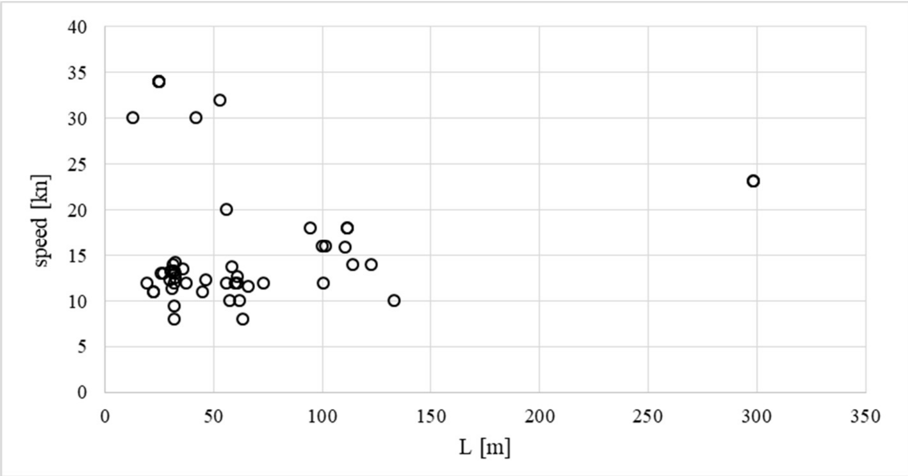

Figure 3-13 Others ships total power installed on board (a) and max speed (b)

- TANKER

a)

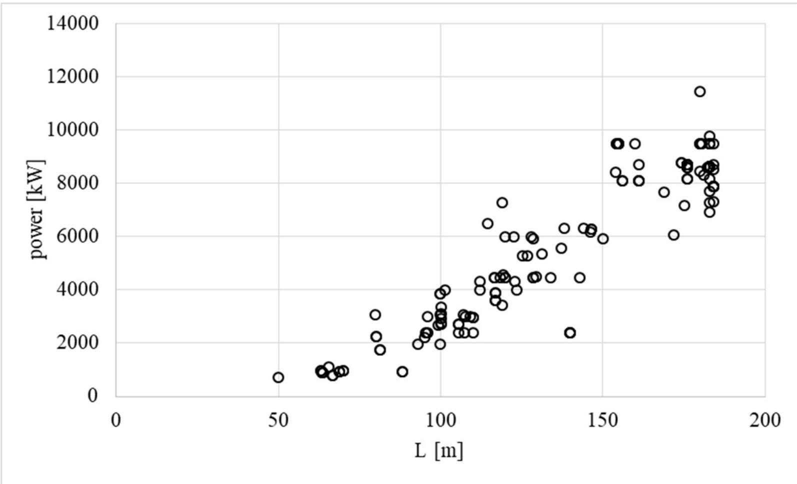

b)

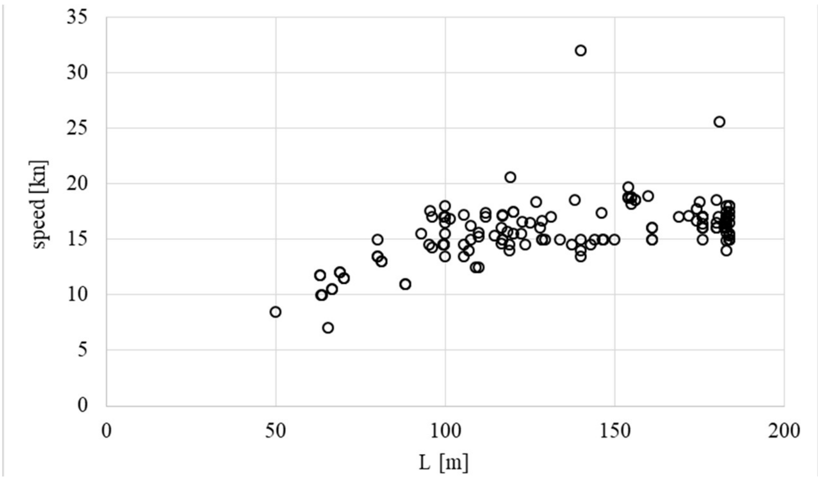

Figure 3-14 Tanker ships: total power installed on board (a) and max speed (b)

3.2.6. Handling the missing data

Unfortunately, data for the calculation of emission rates are not entirely available for all ships. In particular, the percentage of missing data was 10.5% and 5.7% for power installed on board and for maximum speed respectively. Table 3-4 shows the categories for which the percentage of missing data is different from zero (Categories without missing data are not reported, and - indicates to 0% of missing data).

Table 3-4 Percentage of missing data

Category	Depth (%)	Power (%)	Speed (%)
Bulk Carrier	21,8	12,5	12,5
Cargo	100	-	100
Cargo/Containership	20,0	-	-
Chemical Tanker	-	100	-
Container Ship	36,6	3,82	-
Deck Cargo Ship	100	50,0	-
Fish Carrier	100	100	-
Fish Factory	100	-	100
Fishing Vessel	38,5	69,2	15,4
General Cargo	1,96	5,23	-
Grab Hopper Dredger	-	-	100
Inland	33,3	-	33,33
LPG Tanker	8,70	4,30	-
Oil Products Tanker	25,0	-	-
Oil-Chemical Tanker	13,0	15,0	3,00
Other	46,2	46,2	46,2
Passenger Ship	12,3	6,90	5,40
Ro-Ro-Cargo	21,4	14,3	14,3
Ro-Ro-Container	-	28,6	-
Salvage-Rescue	-	25,0	-
Special Vessel	-	100	-
Trawler	50,0	83,3	50,0
Tug	14,3	21,4	21,4
Unspecified	20,0	-	20,0
Yacht	12,5	12,5	12,5

In order to fill these missing data, regressions have been realized. Generally, these regressions are structured as a function of L_{BP} (length between perpendiculars) in m or as function of GT. For each category, the type of egression (***linear***: $y= mx+q$ or ***power*** $y = mx^q$), the coefficient *m* and *q* used and the determination coefficient obtained (R^2). The categories of ships with only one ship have been grouped with categories of similar mission profile (for example fish factory, fishing vessel and fish carrier). Table 3-5 report the main parameters and characteristics of the regressions for power and max speed. For the definition of missing data in max speed the distribution of the data did not allow, in some cases, the realization of good quality regressions (see Table 3-6); in these cases, a constant value equal to the average of the speeds or the specific category was assigned. For example, for bulk carrier two constant values have been chosen: 13kn for ships smaller than 130m and 17kn for longer ships.

Table 3-5 Main parameters of regressions for total power in kW

Category	Type of regression	Coefficient		Predictor	R^2
		m	q		
Bulk	Linear	64,8	-4534,5	L [m]	0,78
Container Ship	Linear	314,2	-38524,0	L [m]	0,90
Crane ship	Linear	14,0	35,4	L [m]	1,00
Deck cargo	Power	0,0495	2,30	L [m]	0,82
Fishing vessel	Linear	-3,00	1327,9	GT	0,87
General cargo	Linear	78,00	-5501,7	L [m]	0,82
LPG Tanker	Linear	103,6	-7638,3	L [m]	0,92
Oil Chemical tanker	Linear	64,4	-3157,9	L [m]	0,76
RoRo cargo	Linear	0,40	5159,9	GT	0,75
Passenger (L<50m)	Power	0,0029	3,10	L [m]	0,54
Passenger (L>50m)	Power	0,0058	2,80	L [m]	0,94
RoRo container	Linear	0,20	12084,0	DWT	0,41
Salvage rescue	Linear	-72,9	4633,6	L [m]	1,00
Trawler	Linear	-3,00	1327,9	GT	0,87
Tug	Linear	6,30	930,3	GT	0,74
Yacht	Linear	2,80	771,6	GT	0,70

Table 3-6 Main parameters of regressions for max speed in kn

Category	Type of regression	Coefficient		Predictor	R^2
		m	q		
Bulk	Constant	13 kn for L<130 m and 17 kn after		L [m]	
Fishing	Constant	12			
Container ship	Linear	0,034	14,20	L [m]	0,62
Oil chem. tanker	Two constant	11 kn for L< 80 m and 15 kn after		L [m]	
Passenger (L<50m)	Power	3,69	0,569	L [m]	0,24
Passenger (L>50m)	Linear	0,039	11,92	L [m]	0,65
RoRo cargo	Constant	20 kn			
Trawler	Constant	14 kn			
Tug	Constant	13 kn			
Yacht	Constant	15 kn			

3.3. Routes

3.3.1. 2012 & 2016

For the 2012 and 2016 simulations, the docks for cruise ships have been summarized to simplify the simulations in 7 points marked in the Figure 3-16 by the letters A-G. At each ship a unique mooring point, generally the most frequent one, has been assigned. In Figure 3-15 the position assumed for A (high-speed vessel), C (cruise) and T (ferry). The routes in the Figure 3-16 have been elaborated by observing the typical maneuvers carried out in port and strongly reflect the actual behavior. For hydrofoils and small passenger ships, the close mooring points have been simplified in a single mooring point since differentiating points that are very close to each other is useless to our purposes.

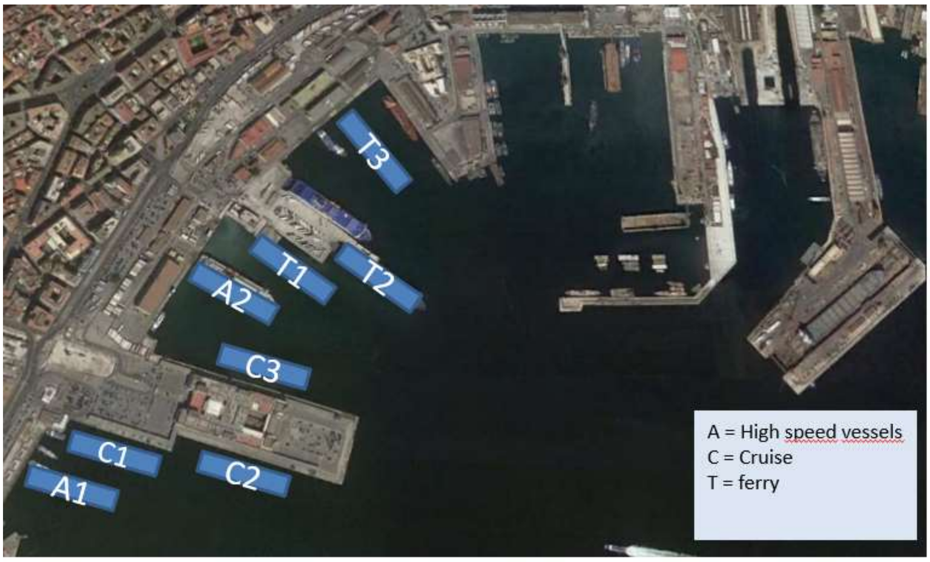

Figure 3-15. Berthing zones for cruise, ferry and HSC

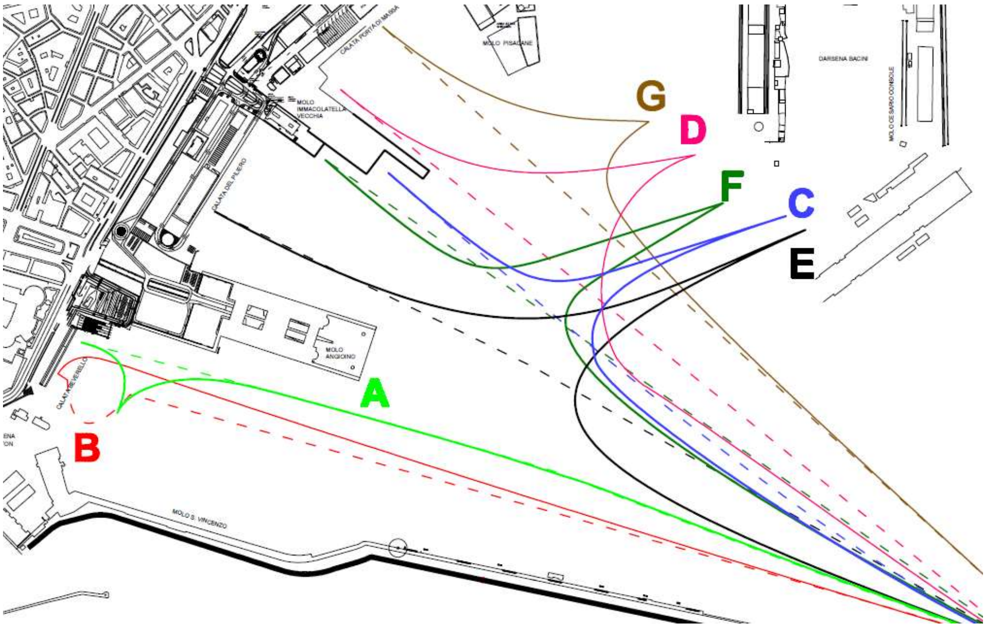

Figure 3-16 Routes in port (continuous line for arrivals and dotted lines for departures)

3.3.2. 2018

These routes have been replaced, in the following analyses, by the actual ship routes acquired through AIS data (**inventory 2018**). By analysing AIS data of each ship category, similar routes on the same dock were identified. Sequentially, piers and routes that are very close to each other, and dedicated to a particular ship category have been grouped (see

Figure 3-17) with the aim to simplify the number of sources in dispersion model input file. In the Figure 3-18 actual piers and merged piers are reported (inside the red lines the piers that have been merged).

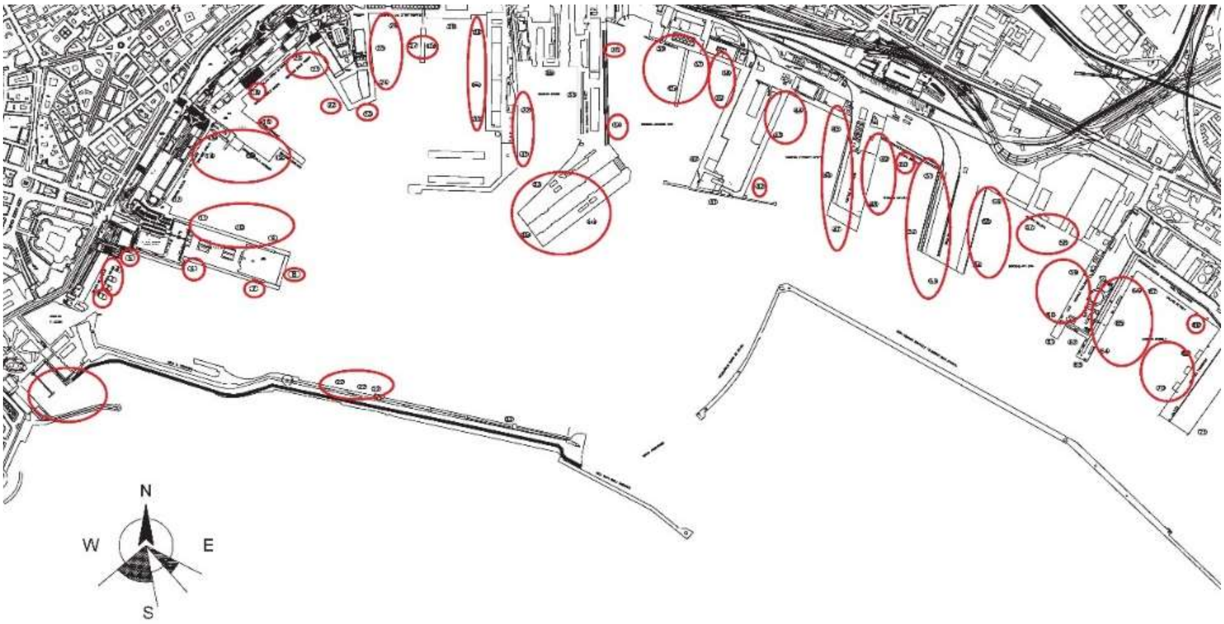

Figure 3-17 Grouping of piers

Figure 3-18 Reference piers

In the Table 3-7, instead, the combination of ship and pier category. Some large categories have been assigned to several piers in order to not stray too far from the real case.

Table 3-7 Combination of piers and ship category

Category	Pier
SAR-AIR CRAFT	-1
HSC, Hydrofoil, Unspecified	2
Research survay vessel	5
Special vessel	7
Inland vessel	9
Salvage rescue	15
Deck cargo ship	21
Water T	22
Trawler	23
Anchor Handling, Cable Layer	24
Bulk carrier, Fish factory	27
Passenger cargo	29
RoRo container	33
Fish carrier, Fish research,	34
Patrol vessel, Yacht	35
Crane ship, Hopper barge	37
Cargo container ship, Other	42
Offshore power supply	44
Heavy load carrier	46
Aggregate	49
RoRo cargo	54
Asphalt bitumen tanker, Grab Hopper Dredger	60
LPG chemical tanker, Oil product tanker	64
LPG and chemical tanker	68
Passenger ship	2-7-9-15
Ro-Ro pax	9-15-18-21-29
Sar Air craft	22 SV
General cargo	22-27-44
Oil chemical tanker	46-60-64
Container	49-52-54
Cargo	50-58
Wine and water tanker	5-21-46

In order to provide a measure of the amount of data available for each category, the raw data for routes of all the passenger categories are reported in figures from Figure 3-19 to Figure 3-22.

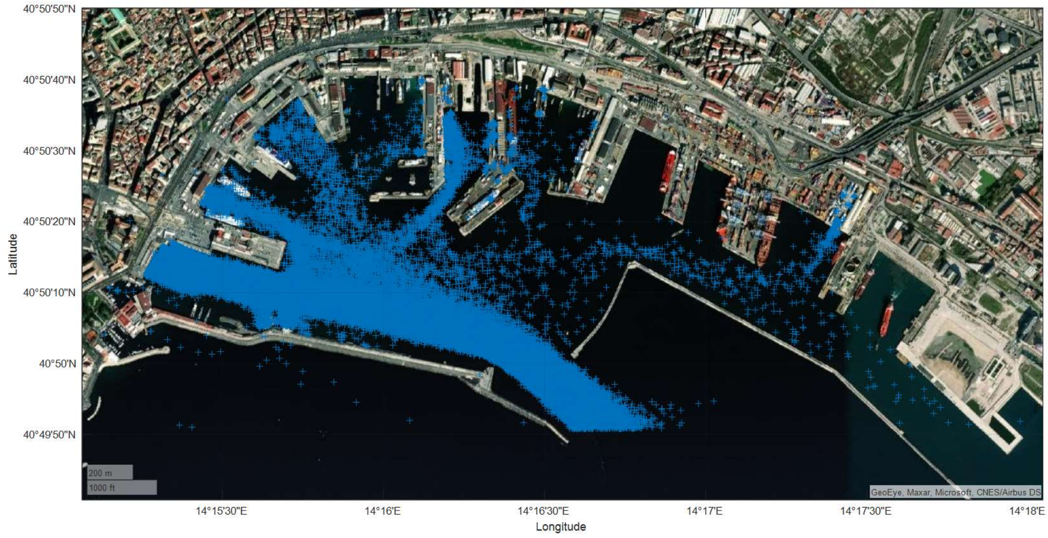

Figure 3-19 Passenger ship routes

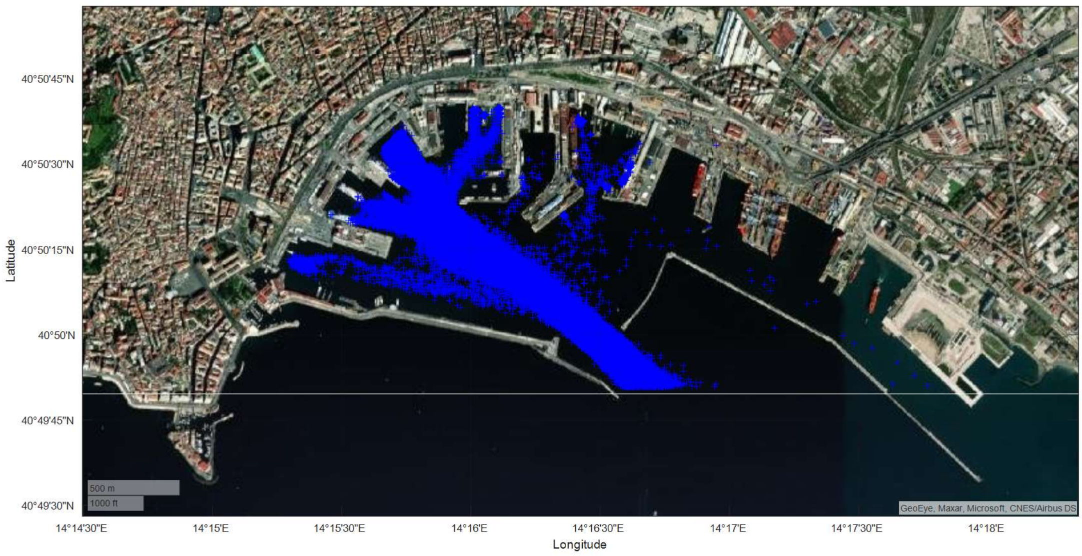

Figure 3-20 RoRo pax routes

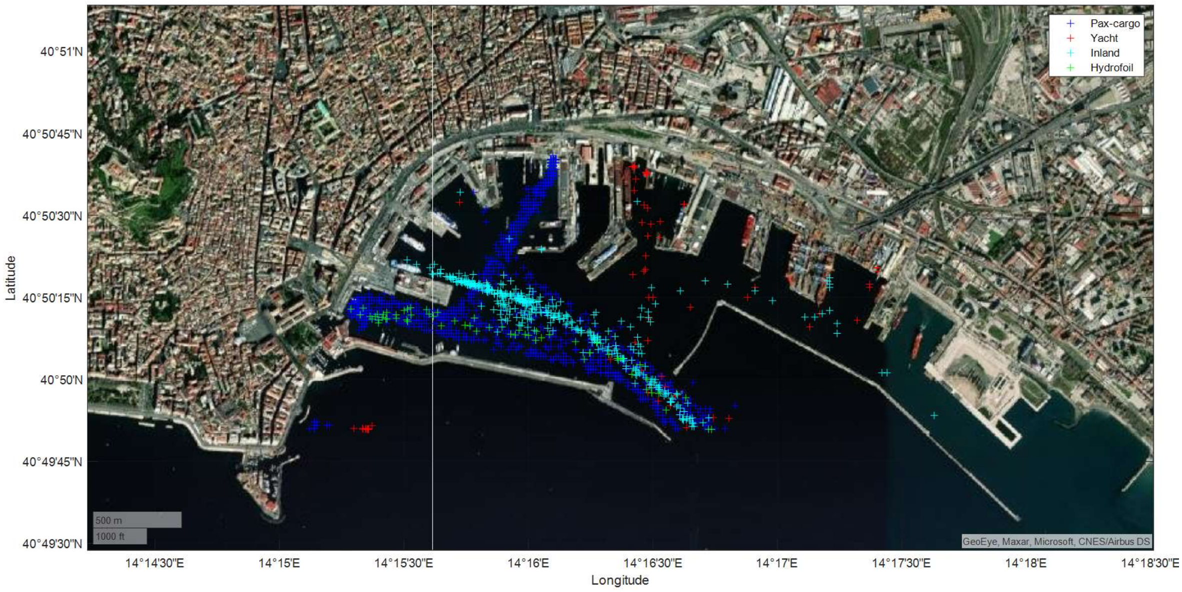

Figure 3-21 Pax-cargo (blue), Yacht (red), Inland (light blue), and Hydrofoil (green) routes

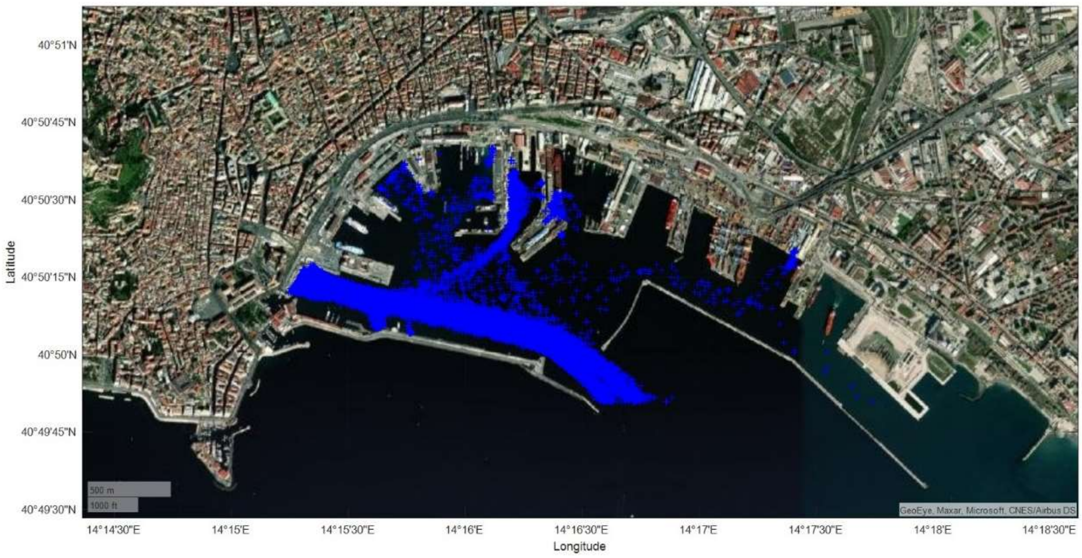

Figure 3-22 HSC routes

These graphs show how the use of all the actual routes for positioning the funnels would have been complicated to carry out throughout the port. For this reason, as previously mentioned, the actual routes of ships belonging to a specific category were selected for each of the piers; this route has become the standard route for all ships arriving at that pier. From the study of raw data, an arrival pier was associated with each category on the basis of the vast majority of arrivals and departures in that position. Here are some defined standard routes for each single passenger categories (figures from Figure 3-23 to Figure 3-30).

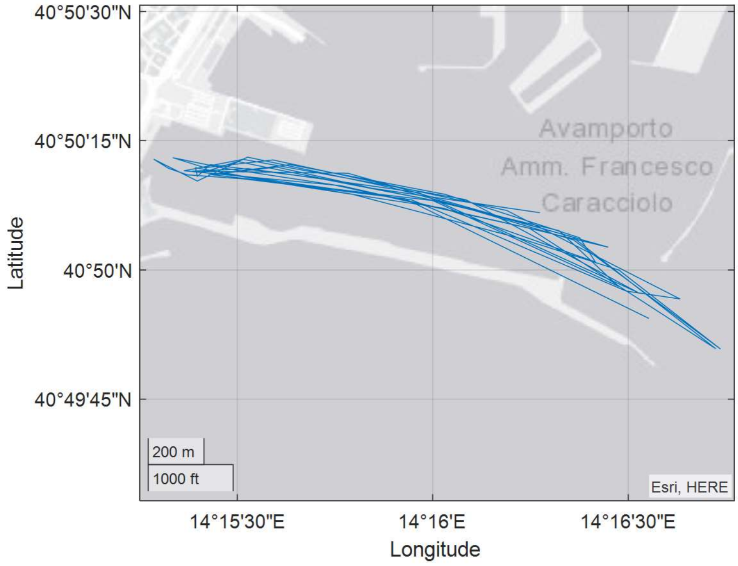

Figure 3-23 Pier nr. 2 for HSC, Passenger and Hydrofoil

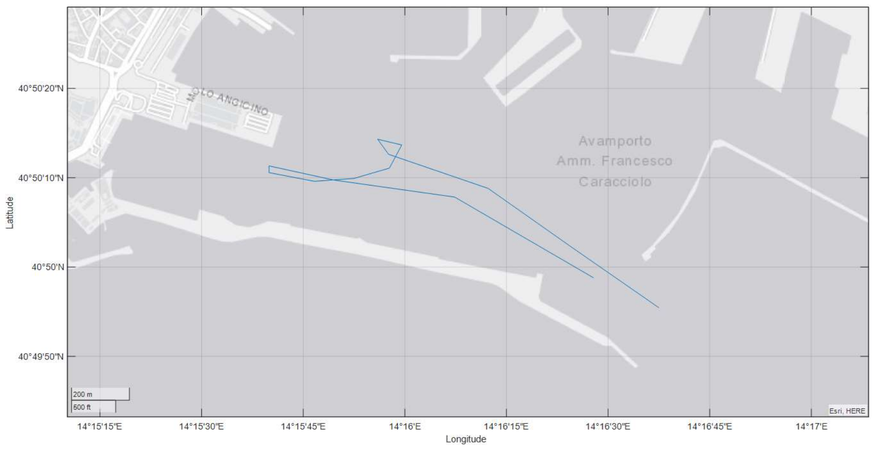

Figure 3-24 Pier nr.7 for Passenger ship

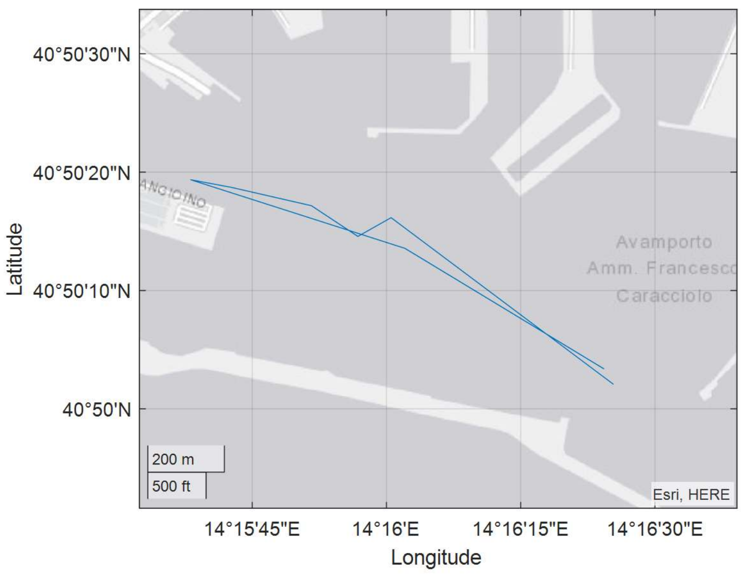

Figure 3-25 Pier nr.9 for Passenger and Roro pax ship

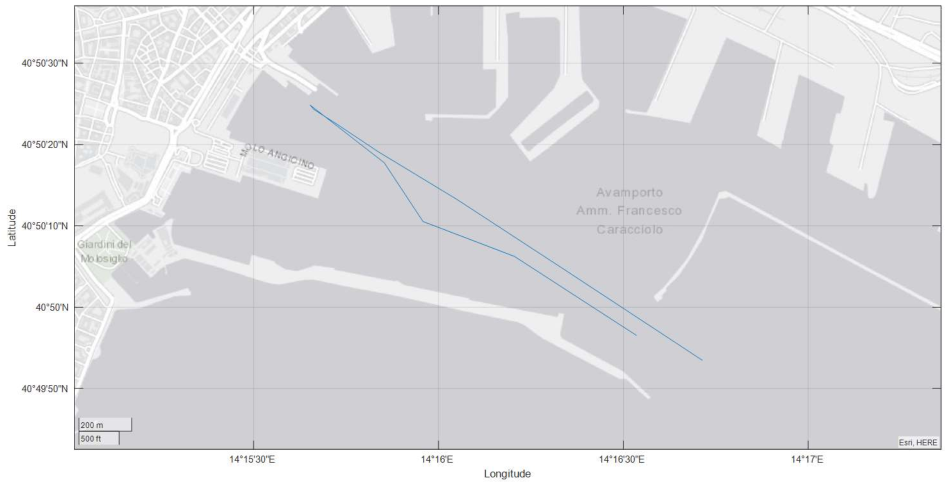

Figure 3-26 Pier nr.15 for Passenger and Roro pax ship

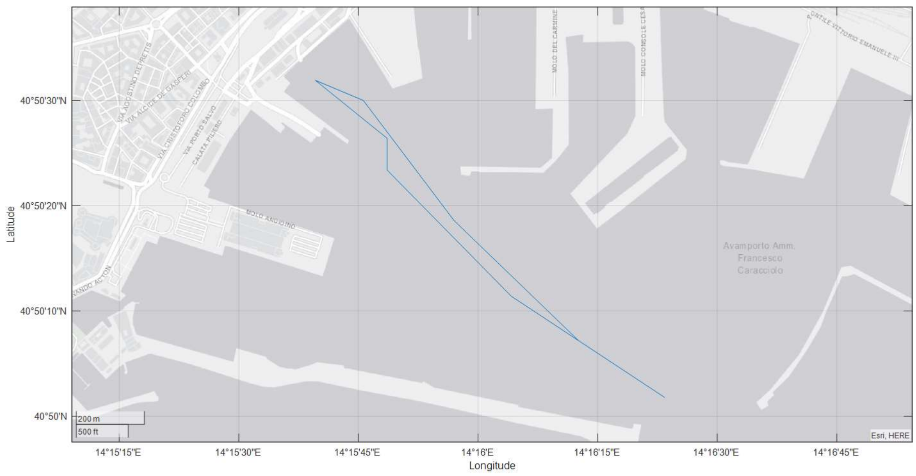

Figure 3-27 Pier nr.18 for Passenger and Roro pax ship

Figure 3-28 Pier nr.21 for Passenger and Roro pax ship

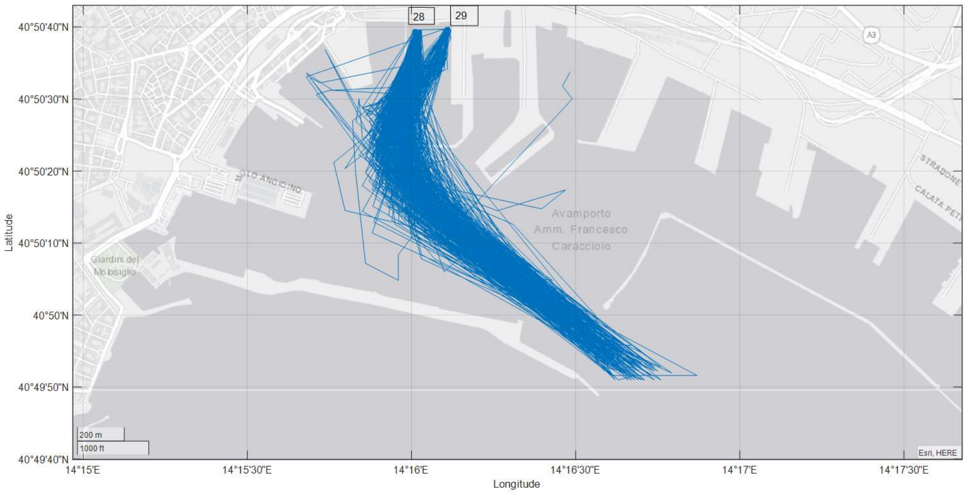

Figure 3-29 Pier nr.29 for Passenger and Roro pax ship

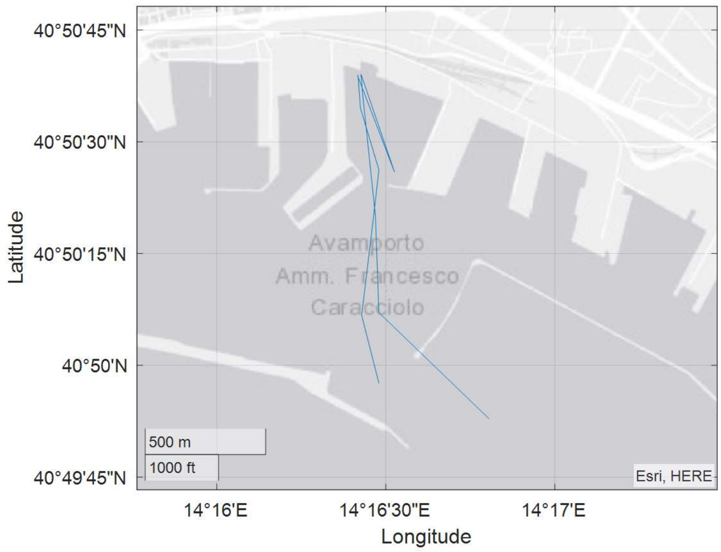

Figure 3-30 Pier nr.35 for Yacht

3.4. Emission rates

In this paragraph, the application of the bottom-up methodology part that returns the flow rates of the main pollutants will be exposed. For the total tons produced during the year, see the next chapter where for each year the emissions of passenger ships will be declared and for 2018 the same emissions, obtained with higher accuracy, will be compared with the other macro-categories of ships arriving at Naples.

3.4.1. 2016

For 2016, each ship was characterized in terms of principal characteristics using database provided by websites and ship-owners. After establishing that the emissions were strictly related to power produced by the engine, the second step was to determine the power released from the engines onboard during the various operations in port. As a first step of accuracy, even though the load on engines changes during the various phases in port, the evaluation of the mean value e for each single phase has been deemed sufficient.

Using a method that will be shown later, the reference overall power installed was considered as the overall electric power released by all the engines onboard in the Diesel Electric systems (usual for cruise ships), or as the sum of powers from AE and ME for conventional propulsion power plants. In order to evaluate the power rate during mooring phase, actual data of three large cruise ships, consisting of datasheets with more than 800 calls in several European ports, including Naples, have been used.

Available data for each ship and each stop includes: total power installed onboard, required power during the hoteling phase (as % of the overall power installed onboard, and in absolute terms), and overall time spent at berth (about 9h in the port of Naples). In Table 3-8, all significant parameters related to these ships are reported:

Table 3-8 Main parameters of three ships used to evaluate power rate during hoteling phase

	Ship 1	**Ship 2**	**Ship 3**
Required power (min) [%]	9.40	9.70	12.8
Required power (max) [%]	19.0	15.6	20.4
Required power (average value) [%]	11.7	11.8	15.0
Variance	1.80	1.80	2.30
Overall power [MW]	71.4	58,0	31.7
Length [m]	333	294	275
Speed [kn]	22.9	23,0	21,0
Number of data	267	265	271

In order to predict the load on engine when the ships are berthed in port, an average percentage of the overall power was evaluated from Table 3-8 (12.9%). This percentage is not deemed as varying significantly with size of the vessels, so the same number was used for all cruise ships. The power released during the in port navigation phase, has been considered as a sum of two components: required power for hoteling, the same of when the ship is effectively at berth and power dedicated to the propulsion at reduced speed. The evaluation of the propulsive power has been made by considering a cubic correlation between the power needed for the propulsion and the ship speed, assumed as **6 kn**. For the maneuvering phase, the "reduced" EMEP-EEA method has been implemented (also for transient states) by using both the load factors of the main and auxiliary. The time spent in maneuvering has been deemed of 20 min; the specific consumption of engines has been fixed by following the recommendations of the EMEP-EEA method (see
Table 2-9). Some uncertainties in the EMEP-EEA method have been eliminated. The mere knowledge of the power installed onboard allowed eliminating a first approximation of the method: indeed, EMEP-EEA suggests an exponential regression, based on the tonnage of the ship that can supply the value of the power released by engines of passenger ships (without distinction among ferries, cruise ships, Ro-Ro pax, etc). For the hotelling phase in port, the evidence of the average value of 12.9 for cruise ships meant that we did not use the 20% value foreseen by the method, certainly getting closer to the actual case since that 20% applies to all the categories of ships. Regarding the emissions of SO_2, a content of sulphur in fuel equal to 0.1% in port was assumed according to the deliberation of the port Authority.

A summary of the parameters adopted to evaluate the emission of cruise ships arriving in the port of Naples is reported in Table 3-9.

Table 3-9 Parameters adopted to evaluate emissions in arrival, departure and maneuvering phases

	Main Engines	**Auxiliary Engines**
Load Factors [%]	Power required for low speeds during navigation	30 (Navigation)
	20 (Maneuvering)	50 (Maneuvering)
	12.9 (Hotelling)	40 (Hotelling)
SFOC [g/kWh]	223,0 (for HSD and MDO/MGO)	217,0 (for HSD and MDO/MGO)
EF NOx [g/kWh]	9.90	13,0
EF SOx [kg/fuel ton]	20	
Maneuvering times:	20 min (0.33 h)	

3.4.1.2012

For HSC and ferries (reference year 2012), the necessary power for navigation in the port at 3 kn as well as the power required for maneuvering and finally the pollutant flow rate typical of the specific fleet have been obtained (set at a reasonable value considering how much time, small ferries, and hydrofoils take to navigate).

The manoeuver phase has always been inserted in the entrance route of each ships. For the cruise ships the duration of the maneuver has been fixed at 20 min while for the ferries and fast vessels at 10 min. For small vessels, the emissions during the mooring phase have been neglected compared to those of the cruise due to the very high demands for electric power. For the phase of navigation in port, the propulsion power has been obtained starting from information about total propulsion power available on board and sets a typical speed of 3 or 6 kn. Finally, during the navigation in port, the required total power was calculated as the sum of the power necessary to maintain that speed and the power needed for the same on-board services present in the mooring phase. As for the hoteling phase, based on the already carried out simulations, about 13% of the total installed power was considered for the cruise ships. After evaluating the rate power in the various phases, the emission rates in g/s of NO_x has been estimated by the emission factors of EMEP/EEA (presented earlier). Regarding the emissions of SO_2, a content of sulphur in fuel equal to 0.1% in port was assumed according to the deliberation of the port Authority.

3.4.1.2018

For the inventory 2018, once the database is completed, emission rates of NO_x, SO_x and PM are calculated. The reference adopted is the recent EMEP-EEA guideline (updated 2019, **Trozzi & de Laurentis, 2019**). As already mentioned, the necessary input data are total power installed on board, type of engine and type of fuel use. So far, the elaborations required the assignment of a fixed speed value in port with which to obtain the load from the engine in navigation in the port. This time, the ability to use AIS data allowed us to bypass this assumption. Elaborations made with AIS data, through the Matlab Code, provide three typical speeds for each category of ships. In addition to a reduced speed in port, two values have been chosen which correspond to the arrival and departure speeds. The following figures (from Figure 3-31 to Figure 3-35) show the three speeds for all groups of ships (average value). In general, as expected, there is a difference between the speed in the central points of the route in port and the extreme points of the routes. For almost all categories of ships, the in and out speeds roughly coincide. The average speeds reported in the graphs (from Figure 3-31 to Figure 3-35) are used to calculate the actual power of main engines in each of the three phases. The adopted procedure allows a more accurate estimation of the actual power when ships are moving in port compared to the power estimated while using the typical load factors corresponding to the cruise phase. According to **Trozzi & de Laurentis (2019),** the total power of auxiliary engines was evaluated for the load factor of main and auxiliary engines for all the phases in port and has been chosen according to the EMEP-EEA procedure. Finally, the emissions for each ship in the navigation and in the mooring phase have been estimated using the emission factors shown in Table 2-12. Due to the lack of precise data about the duration of the individual manoeuvring phases for all the categories, and the possible presence of tugs, the emissions occurring during the manoeuvres have been incorporated into the pure navigation phases defined.

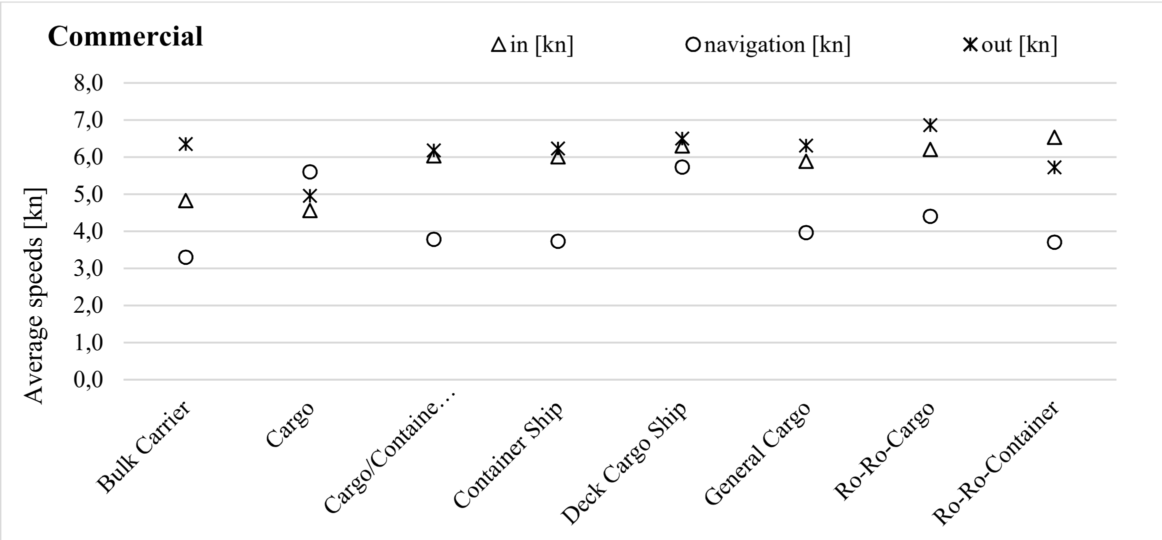

Figure 3-31 Average speeds for the commercial category

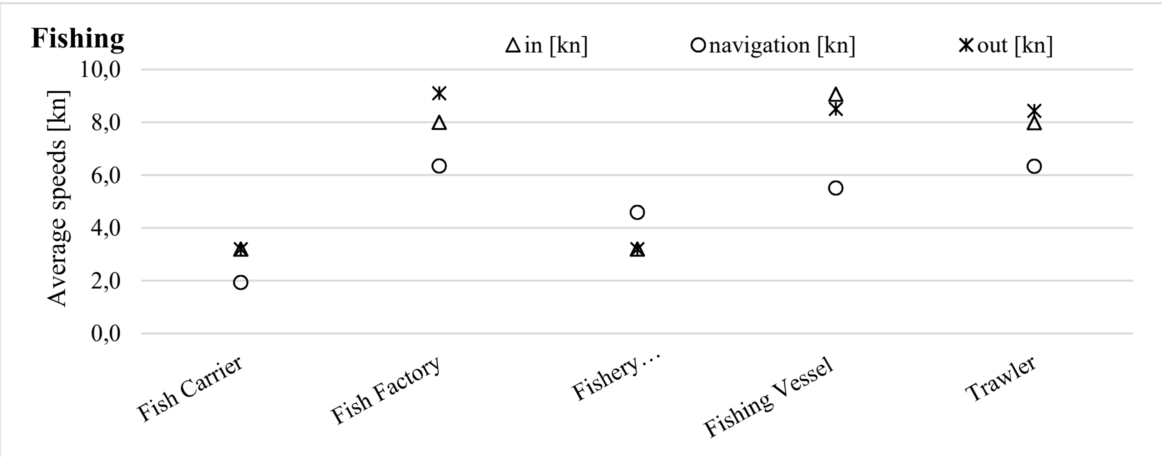

Figure 3-32 Average speeds for the fishing category

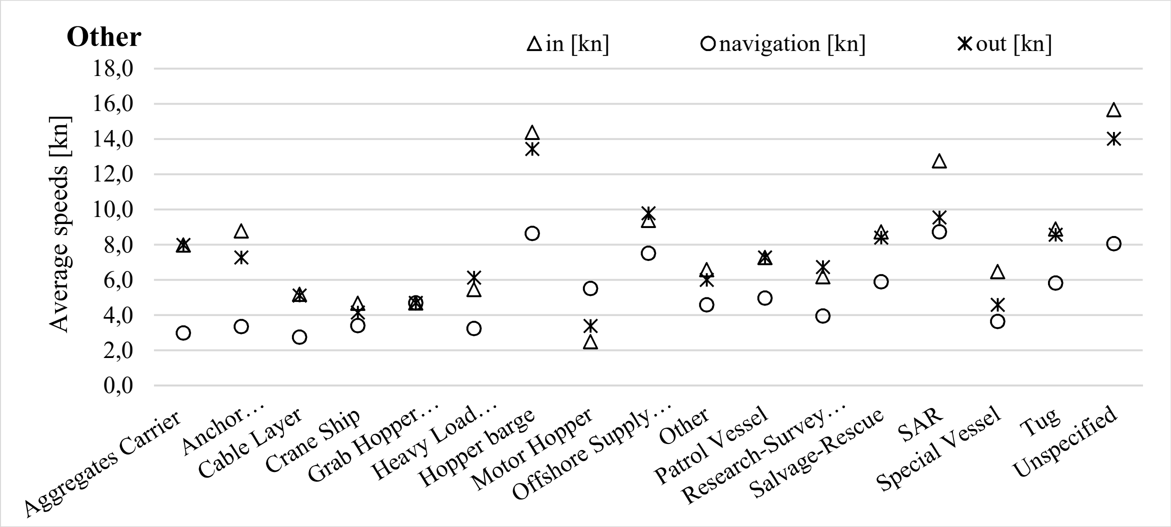

Figure 3-33 Average speeds for the other category

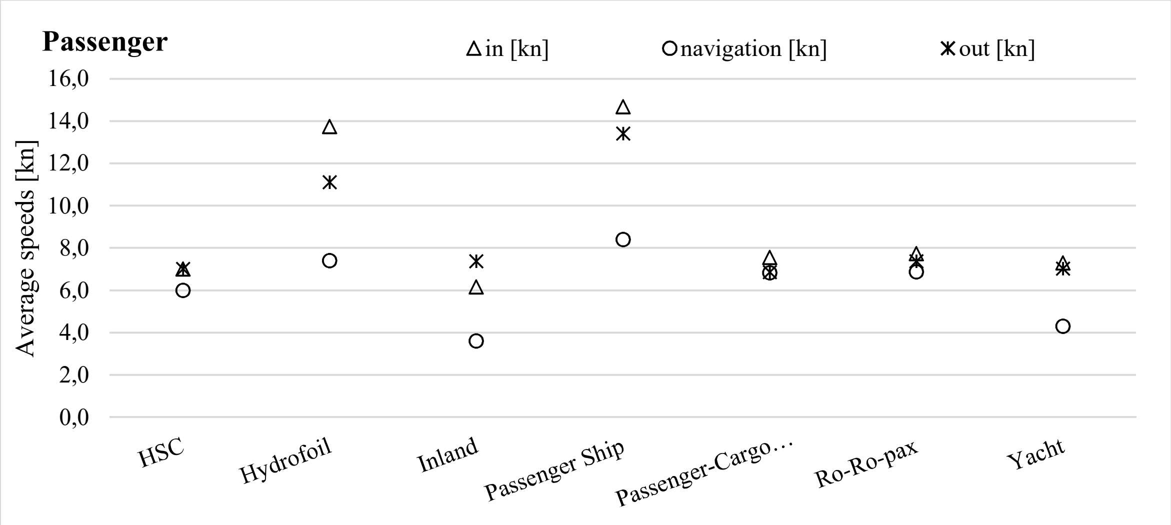

Figure 3-34 Average speeds for passenger category

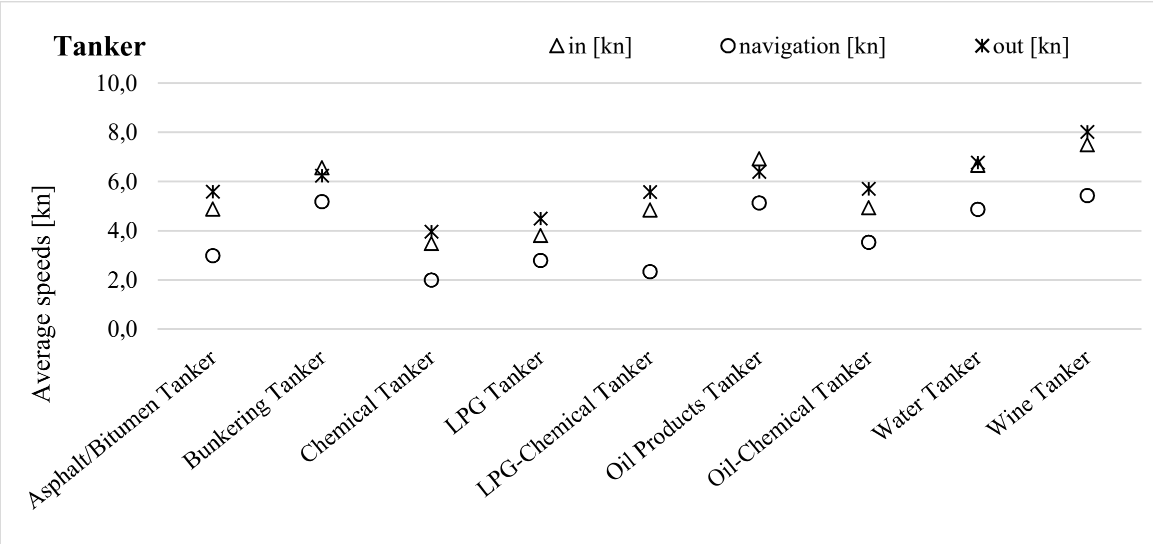

Figure 3-35 Average speeds for tanker category

As an example of the result obtained, the next diagrams show, for the entire fleet arriving in Naples In 2018, the emissions in g/s of NO_x, PM and SO_X during navigation and hotelling phase according to the length overall of the ships.

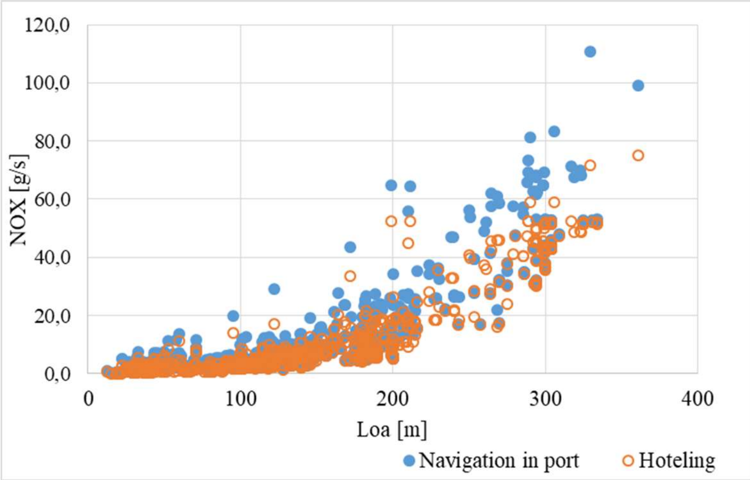

Figure 3-36 Emission rates estimated for NO_X during navigation in port and hotelling

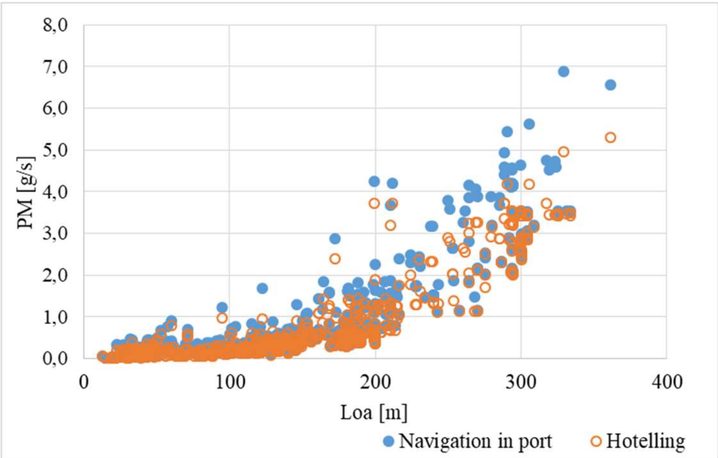

Figure 3-37 Emission rates estimated for PM during navigation in port and hotelling

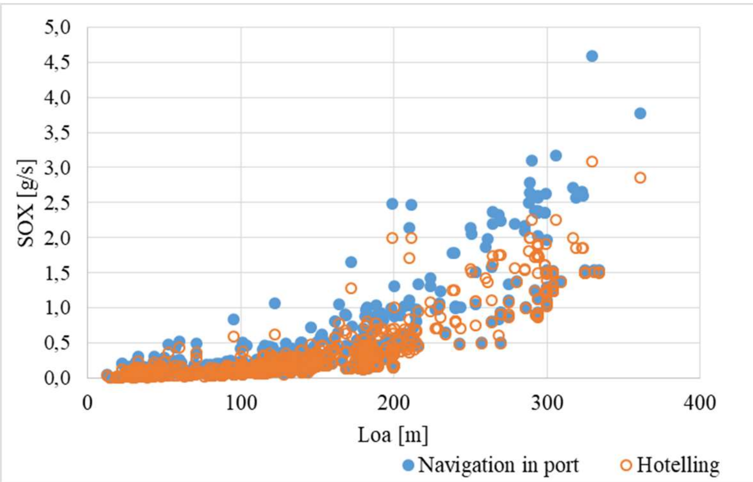

Figure 3-38 Emission rates estimated for SO_X during navigation in port and hotelling

Below, on the other hand, for all categories of Passengers, the emissions during the hotelling phase divided by category (Figure 3-39-Figure 3-41) respectively for NO_X, PM and SO_X.

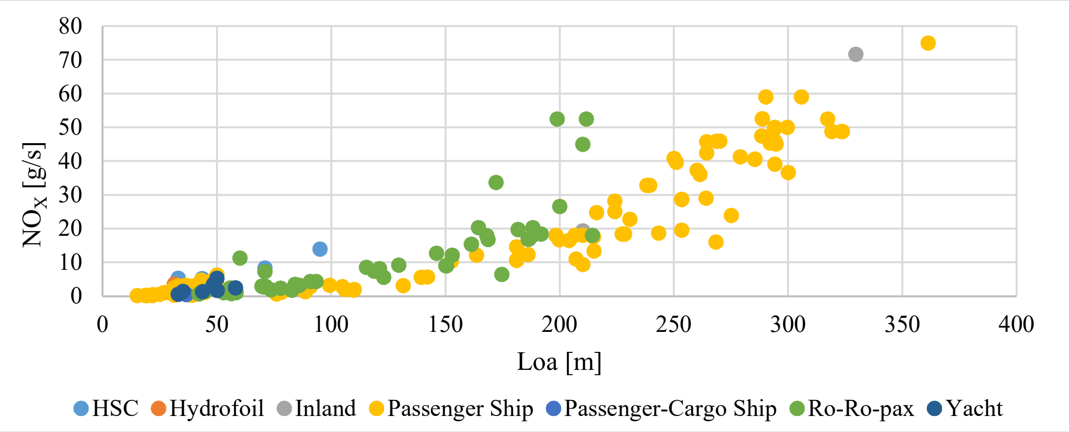

Figure 3-39 NO_X emission rates, for passenger ships, during mooring phase

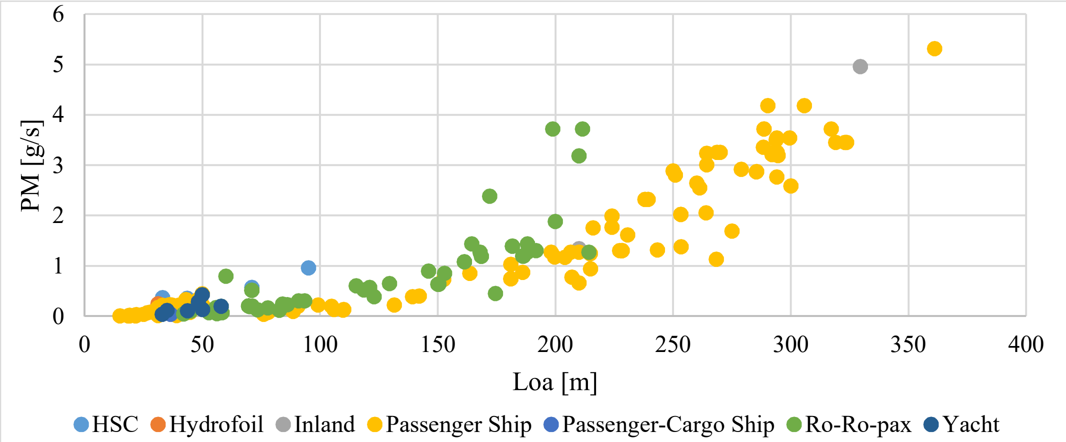

Figure 3-40 PM emission rates, for passenger ships, during mooring phase

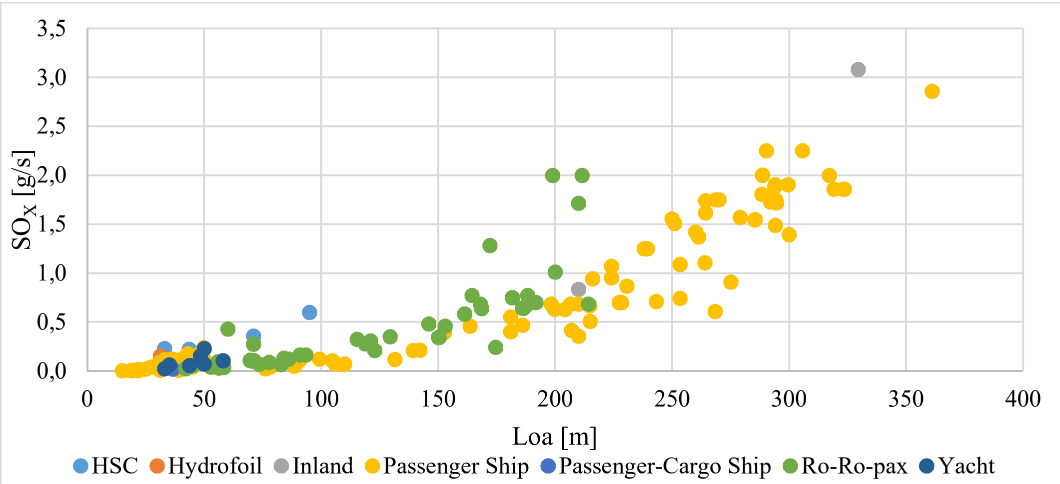

Figure 3-41 SO_X emission rates, for passenger ships, during mooring phase

3.5. Diameters and height

As previously explained in the dedicated subsection (2.6), in the elaborations for **2012 and 2016** the heights and diameters of the passenger ship funnels were set in accordance with Table 2-13. For the **2018 inventory**, on the other hand, by following what is described in the same paragraph, the following results are obtained. In Figure 3-42 the values of H_{BL}, for all the macro-categories of ships, which have been obtained are reported according to the total power installed on board.

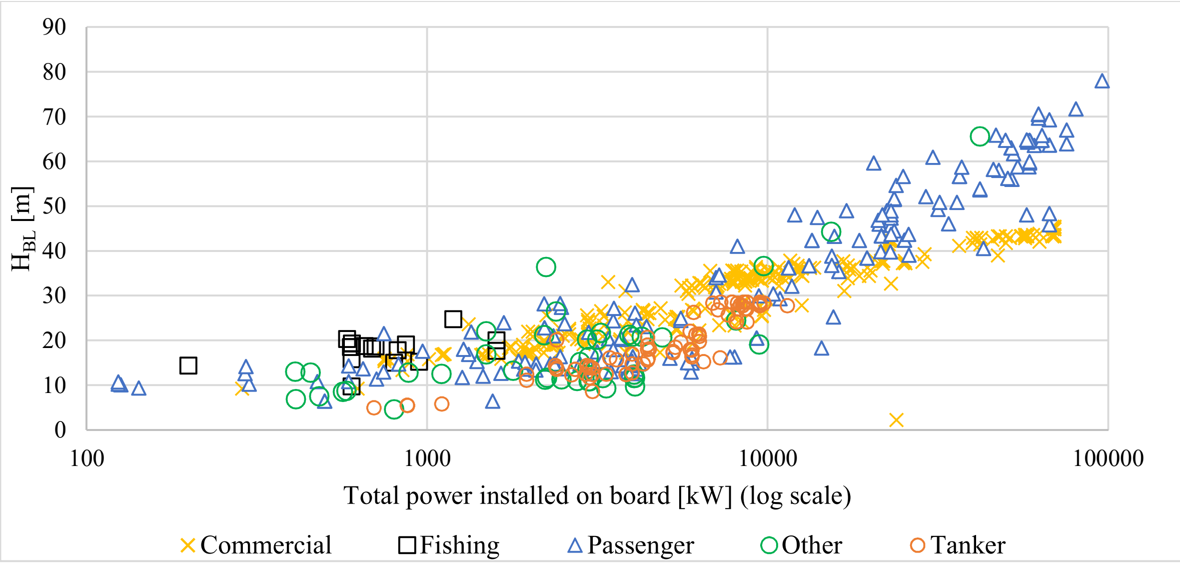

Figure 3-42 Height over base line (H_{BL}) according to the total power installed on board for macro-categories

3.6. Analysis for 2016

3.6.1. Fixed stations and passive samplers

The monitoring of air quality in the Metropolitan Area of Naples is guaranteed by a network of fixed stations of the Regional Agency of Environmental Protection (ARPAC) [11] with equipment and measurement methods based on the standards established by European Community (2008/50/CE). There are no fixed stations inside the port area. A complete map of all receptors corresponding to fixed stations and passive samplers inside the urban area is reported in Figure 3-43 where NA06 and NA07 are receptors corresponding to fixed stations of the Regional Air Quality Network. Passive samplers used during the monitoring campaign, located inside the urban area, are indicated with letters from A to Q (**Murena et al., 2017**). Due to the high spatial density points corresponding to passive samplers inside the port area, they have been assembled in two areas: P1-P2, see Figure 3-44. Area P1 (12 receptors) includes terminals for high-speed vessels, cruise ships and ferries. Area P2 with 20 receptors includes commercial terminal. Three receptors (BW1-BW3) were located at breakwaters and this area is indicated as P3.

Figure 3-43 Metropolitan area of Naples with fixed stations of Regional Air Quality Network (in yellow is the boundary of Municipality). Down - Map of the port of Naples with berthing areas

Figure 3-44 Receptors inside the port and the urban area whose data were compared with simulations: monitoring areas and single receptors.

Data on SO_2 from Regional Air Quality Network were not available in the urban area but only at suburban stations (see Figure 3-43 and Figure 3-44). Therefore, the same passive samplers used during the experimental campaign **(Murena et al., 2017**) have been used in port and city for this pollutant. Data from fixed stations were analysed to obtain statistics of hourly average values (max and percentiles) and long-time averages on a chosen period or on the whole year. Generally, the time periods correspond to the duration of the monitoring campaign or to a time interval of particular interest. Data from passive samplers only gave period averages. In the last five years (2012-2016) limit values established by European Community to protect human health in urban areas have been exceeded by: NO_2, PM10, Ozone and Benzene as documented by the Italian Institute for Environmental Protection and Research (ISPRA) in its annual report on the Quality of the Urban Environment (**Murena et al., 2018**). For NO_2 in particular, the annual limit value of 40 μg/m³ (Table 3-10) has been exceeded non-stop from 2012 to date, with values higher than 50 μg/m³ in 2015, while the hourly limit (less than 18 excesses of 200 μg/m³ in the solar year) was exceeded only in 2015. The situation for SO_2 is better. In fact, due to reduction of sulphur content in fuels, emissions of this pollutant decreased, and EU limits in ambient air (Table 3-10) have never been exceeded since 2012.

Table 3-10 NO_2 and SO_2: limit values established by EC for the protection of human health. Maximum number of exceedances in one solar year

Pollutant	1-hour [μg/m³]	24-hour [μg/m³]	Year [μg/m³]	Alert threshold [μg/m³]
NO_2	200[a]		40	400[d]
SO2	350[b]	125[c]		500[d]

a =18; b = 24; c = 3; d = 3 consecutive hours.

To analyse the air quality in the zone of interest, concentrations measured at receptor points indicated in Figure 3-44 are reported in Table 3-11 as average and 1-hour maximum values. The time periods during which the averages have been calculated correspond to: year 2016, June-September high cruise traffic season and January 20th–March 8th (date of monitoring campaign). Values in correspondence of areas P1-P3 have to be interpreted as spatially averaged values, since they were obtained as average on all the passive samplers present in the zone. The average of data collected at Acerra, Pomigliano d'Arco and Casoria stations, are the concentrations reported as urban periphery (UP) (Figure 3-44).

Table 3-11 Field data from fixed stations and monitoring campaign in 2016. CA= continuous analyser; PS= passive sampler. a) Murena et al., 2017

Period	Receptor		Period average		1-hour maximum	
			NO_2 [µg/m^3]	SO_2 [µg/m^3]	NO_2 [µg/m^3]	SO_2 [µg/m^3]
Year	NA06	CA	44.0		178.6	
	NA07	CA	56.2		198.8	
	UP	CA	28.2	2.7	154.9	53.2
Jun-Sep	NA06	CA	39.5		149.7	
	NA07	CA	56.4		174.5	
	UP	CA	20.3	2.2	80.4	44.6
20th Jan - 8th Mar	P1[a]	PS	7.87	3.46		
	P2[a]	PS	10.3	1.83		
	P3[a]	PS	6.57	7.23		
	U1[a]	PS	7.94	1.35		
	U2[a]	PS		1.23		
	NA06	CA	45.7		178.6	
	NA07	CA	53.3		155.8	
	UP	CA	36.5	2.4	124.7	9.5

Annual average limit value of 40 µg/m^3 for NO_2 (Table 3-10) is exceeded both at NA06 and NA07 with 44.0 µg/m^3 and 56.2 µg/m^3 respectively, while there is no exceeding of limit value of 200 µg/m^3 for 1-hour averages. The limit is also exceeded from June to September at NA7 (56.4 µg/m^3) and from 20/01/2016 to 08/03/206 at NA06 and NA7 (at 45.7 µg/m^3 and 53.3µg/m^3 respectively). For SO_2, data are not available in these two stations. However, considering results of monitoring campaigns of the previous years, it can be argued that this pollutant is largely below both the 1 and 24-hour limit values of 350 µg/m^3 and 125 g/m^3 respectively.

3.7. Dispersion model: 2016

In this first approach to the environmental impact of ships in port, three types of approach have been compared: for 2016 the field data measured at selected fixed stations, the ones collected during monitoring campaigns performed from 20/01/16 to 08/03/16 (**Murena et al., 2017**) and the simulation model results. The considered fixed stations are inside the urban area (NA06, NA07) and in the surroundings (Acerra, Pomigliano d'Arco, and Casoria) **[11]**. Data of some stations (NA01, Pozzuoli, Portici) were analysed to obtain information on background concentration of O_3 which is necessary to model atmospheric reactions of NO_X and SO_X. CALPUFF was adopted as model to simulate transport and chemical reactions in atmosphere of NO_X and SO_X emitted by cruise ships.

3.7.1. Numerical simulation model

Numerical simulations were achieved by DICMAPI (Department of Chemical Engineering, Materials and Industrial Production of University of Naples Federico II), by using the four softwares of the modeling chain: **LANDUSE®, CALMET, CALPUFF** (California Puff Modeling System) and **CALPOST** (a post-processing package). The orography in the calculation domain has been evaluated with LANDUSE. The orographic file, together with files containing hourly average values of meteorological parameters measured at Naples Airport of Capodichino (including wind speed and direction, cloud height, sky cover, temperature, pressure and relative humidity, precipitations and vertical profiles of wind velocity, direction and temperature) are given in input to CALMET for producing the 3D weather file.

CALPUFF is a multi-layer, multi-species, and non-steady state Lagrangian Gaussian puff dispersion model that can simulate the effects of temporally and spatially variable meteorological conditions from point, line, area or volume sources (**Scire et al., 2000**). It contains modules for complex terrain and coastal interaction effects, overwater transport and simple chemical transformation. Input meteorological data for the CALPUFF model are the 2D/3D fields of the main local meteorological parameters such as wind speed and direction, atmospheric stability parameters, temperature, and precipitation rate. Such input data are the output of the **CALMET** diagnostic meteorological pre-processor that can simulate local effects like kinematic terrain effects and sea breeze circulations. These latter effects can be reproduced only by running CALMET based on local meteorological input data and on a detailed description of the terrain properties in the simulation domain.

In this case study meteorological fields for reference year were generated by CALMET model for an about 35 km^2 Cartesian grid centered on the port and subdivided into a 36 × 24 cells grid system with 200 m cell spacing; these vertical grid system considers 10 layers up to 3 km height. In order to generate the input of emissions in the calculation domain, 38-point sources corresponding to ships funnel have been defined: 4 for each mooring point and the remaining 34 were placed along the routes in port to simulate emissions during navigation in port. All ships are considered at berth by the bow (almost true for all cruise ships berthing in Naples) with a manoeuvre done during the arrival. The hourly variation of emission rates was taken as input for creating a PTEMARB (Point Source Emissions File with Arbitrarily Varying Emissions) model file according to detailed ship schedules for the whole year. For the entire chemical transformation module, RIVAD/ARM3 has been used to simulate chemical reactions of NO_X and SO_X in the atmosphere (**Morris et al., 1988**). The PTEMARB file contains time-invariant and time-dependent records. The first contains the funnel height and diameter for each source, and UTM (Universo Traverso Mercatore) coordinates. The second one contains the outlet air velocity (m/s), the temperature of the funnel flue gas outlet (K), and pollutant emission rate (g/s) for each hour and for each sources.

3.7.1.1. Meteorological conditions

As in most coastal regions, meteorology in Naples is characterized by breeze regime with prevailing wind directions from SSW-W, especially during summer and from N-NE in winter (see Figure 3-45 for 2016). The most frequent classes of wind velocity are 1-2 m/s and 2-3 m/s.

The occurrences of wind directions from E to SSE are very rare. Considering that, the city center is mainly located downwind of port in the directions from W to N fortunately typical wind directions luckily minimize the impact of ship emissions on the city.

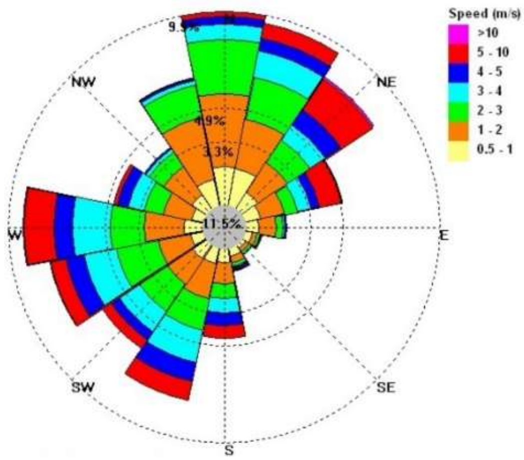

Figure 3-45 Wind rose of meteorological file at 10m of height (2016)

3.7.2. Results

In Table 3-12, the annual and seasonal emissions of cruise ships for both NO_X and SO_X were evaluated. The partition of annual emissions of NO_X and SO_X among the different activities are, respectively:

- mooring phase (98.1% and 98.1%);
- navigation in port (1.45% and 1.29%);
- dock approaching (0.48% and 0.57%).

According to other authors, emissions during hoteling represent the largest part of total emissions in port: for **Papaefthimiou et al., (2016)** the NO_X and SO_X, due to cruise ships at hoteling are equal to 89.2% of total emissions as average values for several Greek ports. The very high percentage of emissions due to the hoteling phase reported in Table 3-12 also depends from the limited navigation zone within the port area (about 2 km).

Table 3-12 Annual emissions from cruise ships in the port of Naples in year 2016

Activity	**NOx**		**SOx**	
	[t/y]	**[%]**	**[t/y]**	**[%]**
Navigation in port	6.09	1.45	0.18	1.29
Docking approach	2.02	0.48	0.08	0.57
Hoteling	411	98.1	13.7	98.1
Total cruise ship	**419**	100	**14.0**	100

Total emissions were evaluated using other methods as well (**Melo Rodriguez et al., 2017; Papaefthimiou et al., 2016**) to verify the correctness and reliability of the adopted methodology (see **Murena et al., 2018**).

Since **Melo Rodriguez et al. (2017) and Papaefthimiou et al. (2016)** assumed in their studies, respectively, a S=3% wt and S=1.5% wt in fuel, the emission calculated with their procedures has been modified in our study in order to consider the directive of the Port Authority of Naples (S=0.1% wt).

The evaluated annual emissions therefore are:

- NO_X = 687 t/y and SOx = 19.4 t/y according to **Melo Rodriguez et al. (2017)** (1.64 for NO_X and 1.39 for SO_X compared to our estimation);
- NO_X = 352 t/y and SO_2 = 7.3 t/y according to **Papaefthimiou et al. (2016)** (1.19 for NO_X and 1.92 for SO_X compared to our estimation).

These differences show the uncertainties inherent to such calculations. Contour maps of annual average modelling simulations for both NO_2 and SO_2 are reported in Figure 3-46 and Figure 3-47. Direction of the impact for annual average is strictly related to the wind rose diagram in Figure 3-45 and land orography. As evident, areas of maximum concentration are indeed along NE-E and SW directions from cruise terminal. The area of maximum impact of NO_2 is inside the port area and in the industrial area to the east of the city centre of Naples. However, there is a clear impact on the urban area as well. However, values are well below the limit of 40 µg/m^3 (Table 3-10). Map of SO_2 shows some differences due to the different chemical reactions occurring in the atmosphere and a maximum value is reached in proximity of emission sources. However, annual average for NO_2 values are well below the limit of 40 µg/m^3 (Table 3-10). The difference in absolute values is mainly due to different emission rates between the two pollutants (Table 2-12). To show the impact at short averaged time (1-hour) contour maps of modelling simulations of 10th maximum value of 1-hour average of NO_2 and SO_2 are reported in Figure 3-48 and Figure 3-49. As expected, the values are much higher than those reported in Figure 3-46 and Figure 3-47. Once again, the maximum value is reached inside the port area. Nevertheless, a large part of the town is affected by possible high contribution to 1-hour averaged concentration for both NO_2 and SO_2. Emissions are larger during summer period, due to higher electrical consumption for air conditioning and ventilation system on board. Both this and the fact that during summer cruise traffic is very high (see Figure 3-4) suggest that seasonal variation of emission factors should be taken into account.

Figure 3-46 Simulations: maps of annual average of NO_2 [µg/m^3]

Figure 3-47 Simulations: maps of annual average of SO_2 [µg/m^3]

Figure 3-48 Results of simulations: maps of 10th maximum value of 1-hour average of NO_2 [µg/m^3]

Figure 3-49 Results of simulations: maps of 10th maximum value of 1-hour average of SO_2 [µg/m^3]

3.7.3. Comparison of simulations with experimental data

To assess the contribution of cruise ship emissions to air quality concentration levels, surface concentrations calculated by simulations are compared with those obtained from field measurements and the results is expressed through a relative contribution calculated as percentage of actual concentration by the following formula (see Table 3-13 CA= continuous analyzer; PA= passive sampler. a) **Murena et al. 2017**):

3-1 Surface concentration due to cruise ship emissions

$$SC\%_{ij} = \frac{C_{sij}}{C_{mij}}$$

where SC% is the percentage of surface concentration due to cruise ship emissions; C_m is the concentration measured and Cs is the concentration obtained by simulations, i and j correspond to pollutant and averaging time respectively.

Table 3-13 Contribution of cruise ship emissions to actual concentration levels – Period average

Period	**Area/Receptor**		**Monitoring**		**Cruise contribution**	
			NO_2	**SO_2**	**NO_2**	**SO_2**
			[µg/m^3]	**[µg/m^3]**	**[%]**	**[%]**
2016	NA06	CA	44.0		0.74	
	NA07	CA	56.2		2.47	
	UP	CA	28.2	2.74		
Jun-Sep 2016	NA06	CA	39.5		1.17	
	NA07	CA	56.4		3.58	
	UP	CA	20.3	2.24		
20th Jan – 8th Mar 2016	P1[a]	PS	7.87	3.46	2.65	0.89
	P2[a]	PS	10.3	1.83	6.10	1.53
	P3[a]	PS	6.57	7.23	6.06	0.62
	U1[a]	PS	7.94	1.35	2.78	1.00
	U2[a]	PS		1.23		1.46
	NA06	CA	45.7		0.27	
	NA07	CA	53.3		1.33	
	UP	CA	36.5	2.38		

The NO_2 cruise contribution depends on the average period considered and on the position of the receptor (distance from source, in particular). As expected, maximum contribution at NA06 and NA07 is observed from June to September: 1.17% at NA06 and 3.58% at NA07 (see Table 3-13), since this time period has the maximum number of calls per month of cruise ships (see Figure 3-4). Regarding distance, the monitoring campaign data from January 20th to March 8th (**Murena at al., 2017**) show that maximum contribution is observed in the port area (6.10% at P2) but not in the area near cruise moorings (2.65% at P1) (see Figure 3-4). This is due to the joint effects of prevailing winds from SW (Figure 3-45), atmospheric reactions converting NO to NO_2 and the height of the funnels. A high contribution is also observed at breakwaters area (6.06% at P3) almost certainly due to emissions during navigation at low speed in port. Lower contributions are observed inside the urban area (2.78% in U1; 1.33% at NA07 and 0.27% at NA06). As for the prevalence of wind from W-SSW, contribution at NA07 is always higher than at NA06 in all the time periods examined. In order to evaluate the contribution of ship emissions when high concentration levels are measured 99° percentile of NO_2 of short averaging time data (1-hour) concentration measures were evaluated at NA07 for solar year; months of high and low traffic of cruise ships (respectively June-September and January-March and December). Then SC% was evaluated for each hour when 1-hour concentration was higher than 99° (C_{mNO2}> 99°). Maximum and average SC% were then reported in Table 3-14. As shown, 99° of NO_2 is 133 µg/m^3 in solar year and for C_{mNO2}> 99° maximum and average value of SC% was respectively 86.2% and 3.65%. Results shows that only in rare days of the year the cruise ships emission contribution can be important to determine high concentration levels of NO_2 and generally their contribution is limited. Similar results are obtained for the time period June-September. The 99° percentile is 140 µg/m^3 the maximum SC% was the same while average SC%=5.18% is higher than that observed in the whole year. In the months of lowest cruise ship traffic SC% both maximum and average are respectively 1.77% and 0.10% so very low. As a conclusion, maximum average SC% occurs in Jun-Sep and minimum in Dec-Mar, in accordance with cruise ship traffic (Figure 3-4). Due to the absence of data, the same analysis was not possible for SO_2.

Table 3-14 Contribution of cruise ship emissions at NA07 for NO_2 1-hour peak concentration (C > 99° percentile)

Period	**Receptor**	**99°**	**Maximum cruise**	**Average cruise**
-	-	[µg/m^3]	[%]	[%]
Year	NA7	133	86.2	3.65
Jun-Sep	NA7	140	86.2	5.18
Dec-Mar	NA7	130	1.77	0.10

Cruise ship emissions contribution to NO_2 emissions in the city area depend on wind direction. In Figure 3-50 1-hour SC% occurrences in the year at NA7 are organized according to the wind sectors. Data with very low SC% (SC%< 0.1%) representing 87% of the cases have been excluded and neglected. In the remaining hours it is evident that significant contribution occurs only when the wind blows from sectors S to W, specifically when NA07 is downwind of cruise passenger terminal. When the wind blows from other sectors, instead, the contribution of cruise ship emissions to hourly average concentration at NA07 is negligible.

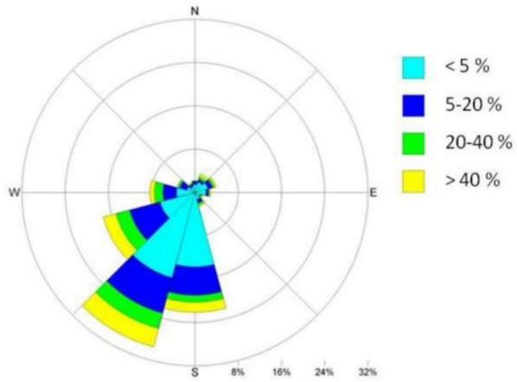

Figure 3-50 Distribution of SC% occurrences of NO_2 at NA07 in 2016 (occurrences with SC% < 0.1% are not considered)

Cruise ship contributions on air quality reported in Table 3-13 are generally lower than the ones reported in literature. **Merico et al. (2017)** evaluate a 16.7-32.5% for Brindisi and 2.8-9.1% for Venice for the ship emission contribution for NO_2 while for SO_2 the contribution are respectively 23.5-46.3% and 5.2-16.5% Such differences with our results have more than a few reasons:

- first of all, in this first study we have considered only cruise ship emissions;
- in addition, the city of Naples has about ten times more residents than Venice and Brindisi and as a consequence it has higher emissions from other sources such as road traffic;
- **Merico et al. (2017)** calculated SO_2 assuming 0.1% wt of S content in fuel for hoteling phase, 1.5% in manoeuvring phase for passenger ships and (and 3.5% for all other ship typologies);
- lastly, a few considerations on meteorological situation. The center of Naples is rarely downwind of the cruise terminals. Therefore, for more than 50% of hours in the year pollutants are mainly transported by the wind from W to NE on the sea. Calm wind represent about 11.5% of the observations. Consequently, pollutants emitted by cruise ships are transported toward the town only for about 35% of hours.

3.7.4. Discussions

The results of this first important study represent an important achievement in the purpose of analysing of the impact of cruise ship emissions to air pollution in Naples. The simulation results have been compared with data from the fixed stations and with data from a monitoring campaign. Even though results do not represent the whole impact of ship emissions of the port of Naples, cruise ships represent an important part of the total fleet in port. While considering the annual averages, cruise ships contribution seems limited but non-negligible. At fixed station NA07, (about 2 km in NE direction from the cruise terminal), the contribution to annual average is estimated at 2.47% for NO_2. It reaches the value of 3.58% during the period of maximum cruise ship traffic (Jun-Sept). Higher contributions are observed inside the port area (6.10% at commercial ships terminals). When short-time averages are analysed, the contribution of cruise ship emissions on pollutant concentration levels can be significantly high. In particular, if 1-hour peak concentrations are considered (values > 99° percentile) the contribution can reach 86.2 % while on the average it is 5.18% during high season

(June –September) and 3.65% in the whole year. For SO_2 concentration, the contribution of cruise ship emissions is lower than ≈ 1 % for long time averages. This may be due to the low S content of fuel (0.1% wt) used inside a distance of minimum 2 miles from the port of Naples as a consequence of a directive of the Port Authority. Obliviously the uncertainties of the whole process should be taken into account. The first one concerns the exact evaluation of emission rates of each pollutant: many informations are necessary to assess more accurate emission rates for each pollutant and each ship. Although the reduced time of the manoeuvring in port, the unsteady state working conditions of the engines during this phase could make the emission factors of exhaust gases vary significantly from the ones measured in steady state conditions (**Winnis & Fridell 2010**).

3.8. Air quality-monitoring network in port areas (2012)

Generally, during the monitoring campaign the assessment of the impact of ship emissions is measured by a network of receptors at ground level inside the port area or in the nearby urban canopy. In addition to the emissions of cruise ships, those related to small passenger ships (ferries and high speed craft) have been estimated with the aim of both measuring the impact of all three categories and proposing an optimization of the position of the receptors in port in order to identify and quantify emissions associated with ship traffic.

Therefore, in accordance with the methodology exposed so far, we have come to the estimate of the dispersion in the atmosphere, with some different basic hypotheses and some different criteria that will soon explained. Subsequently, for illustrative purposes, the SO_2 concentrations at different heights (0-60 m) were assessed at selected points within the port area. Results shows how is possible to better identify and quantify the air pollution due to ships by positioning the receptors in the port area at different heights. In addition, the results obtained give useful indication for designing an optimum on-site air quality-monitoring network able to quantify the emissions due to maritime traffic and to determine the contribution of single ships or categories of ships. As a matter of fact, the actual emission height (height of funnels plus the plume rise) for cruise vessels and the largest ferries may reach 60-70 meters and their emissions impact the ground level at a distance of about hundred meters from the releasing point. Information on vertical profiles of pollutant concentrations in the port of Naples is not available. Anyway, the port area is undoubtedly the best choice to locate receptor points of a monitoring network to assess and control ship emissions: this choice minimizes the need for authorization and the overlap of all the typical gas pollutants sources normally present in an urban area such as traffic, heating and industrial emissions. The monitoring campaign used for this purpose was realized during two time slots of about 15 days in 2012 (**Prati et al., 2015**): these two periods are characterized by relatively low (March 28th 2012 – April 10th 2012) and high (2nd and 14th of November 2012) presence of cruise ships. In both cases, ships were located mostly between the piers n.5 and n.11, and only in some case in n.21 and n.22; in Figure 3-51, the instrumented van is reported. More details on data about the instruments and the results of the monitoring campaigns are in (**Prati et al., 2015**).

Figure 3-51. Instrumented van

The results are shortly reported in table; the hourly concentration averages for NO_X, SO_X, PM10 and CO have been obtained. Comparisons with limit values, established by European Directives, cannot be exhaustively done due to the limited time of monitoring campaigns. However, it can be observed that short time averaged values (1, 8 and 24 h) never exceed the limits (see Table 3-15); period averages measured may be compared with annual average limit values (in March-April campaign the value of concentration of NO_2 raised up to 48.4 $\mu g/m^3$ so exceeding the limit of 40 $\mu g/m^3$). The results obtained showed that the average daily concentrations of NO_2 and PM10 were always lower than the respective limit values (LVs). Period average concentrations of PM10 were lower than the annual average Limit Values. On the contrary, period average concentration of NO_2 (41.1 $\mu g/m^3$) slightly exceeded the annual limit value (40 $\mu g/m^3$). SO_2 concentrations were much lower than the hourly and daily average LVs. Finally, concentration levels of NO_2 and PM10 were comparable to those recorded in the urban area of Naples in the same period.

Table 3-15 Results of the monitoring campaigns

Pollutants	Averaging Time	Statistical Parameter	Period	
			March - April	**November**
NO_2	1h	Maximum	156.6	84.2
	Period	Average	48.4	35.8
SO_2	1h	Maximum	26.6	35.5
	24 h	Maximum	3.70	2.50
PM_{10}	24 h	Maximum	40.8	44.2
	Period	Average	27.2	31.6
CO	8 h mobile	Maximum	0.10	0.90

A simulation study for the optimization of receptor sites inside the port area has been carried out. According to the first methodology used, 3D wind field data have been obtained starting from the orography of the area (**Skamarock et al., 2005**). In this way, 3D hourly average values of meteorological parameters were obtained. From the wind rose graphs in the monitoring days reported in Figure 3-52 it can be seen that the prevailing directions are SSW and NE in March-April and in November respectively.

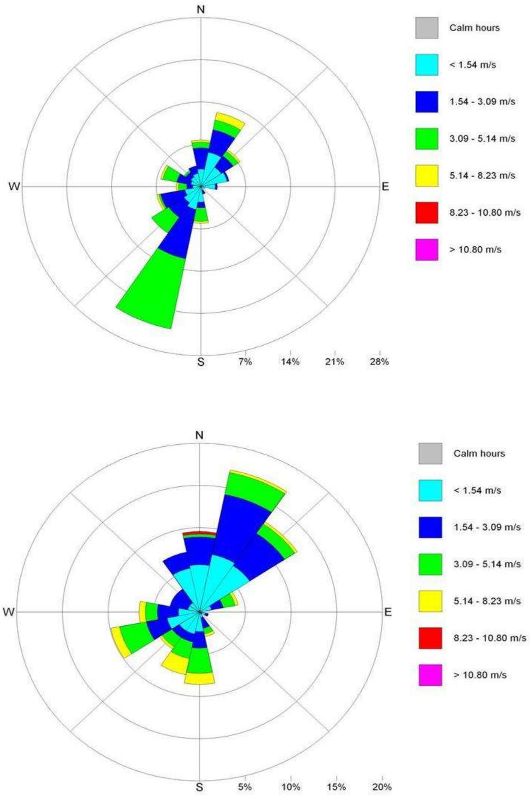

Figure 3-52. Rose Wind respectively for March-April and November (2012)

In this case meteorological fields for reference year were generated by CALMET model for a Cartesian grid, centered on the port site and subdivided into a 200×200 cells grid system with 50m cell spacing. The CALMET vertical grid system considers 10 layers up to 3km height.

To model the input of emissions in the calculation domain, 85 point sources have been defined. 77 point sources were placed along the routes of arrival and departure to simulate emissions during maneuvering and navigation in port and 8 point sources have been positioned near the mooring points. The exit gas velocity was assumed at 10 m/s for all vessel categories. All these data created, along with hourly emission rates of each source point, a PTEMARB file and have been given as input to CALPUFF (same procedure). In Figure 3-53 the point chosen for the calculation of the concentrations inside the port area.

In order to better show how the pollutants emitted by ship funnels are transported in the atmosphere, vertical profiles of SO_2 are reported in Figure 3-54 and Figure 3-55; similar results are obtained for NO_2. The results clearly show that for all designated points concentrations at ground level are at a minimum value compared to those at higher height.

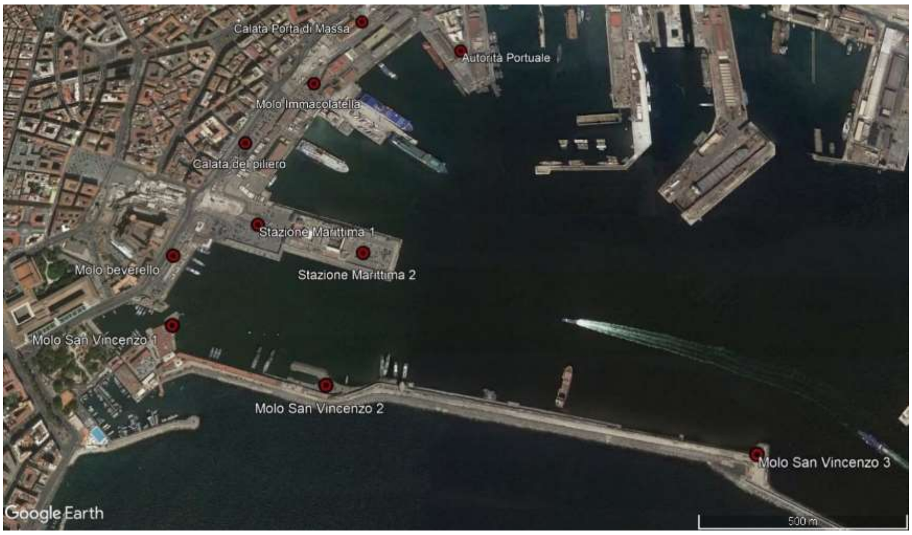

Figure 3-53 Selected points for SO_2 vertical profiles.

These results suggest a limited impact of ship emissions at ground level inside the port area and confirm that ground level is not the best choice for receptors' position inside the port zone. It is possible to observe, in fact, that the impact increases with height. However, there are some differences among the different positions.

With respect to SO_2 concentration profile, selected points can, in fact, be classified into three categories: moderately affected by height, highly affected by height and showing more than a maximum. The points where the impact of ship emissions is limited belong to the first category (e.g. *Quay Piliero* in March-April). The points most affected by emissions from elevated funnels of cruise and ferry vessels are in the second one (e.g. *Stazione Marittima 1* and *2* in November); in the third one there are the points affected from emissions of both cruise or ferries and fast vessels (e.g. *Molo San Vincenzo 3* in March-April).

It can be observed that the vertical profiles for the same point in the two periods may be different (e.g. *Molo Immacolatella*).

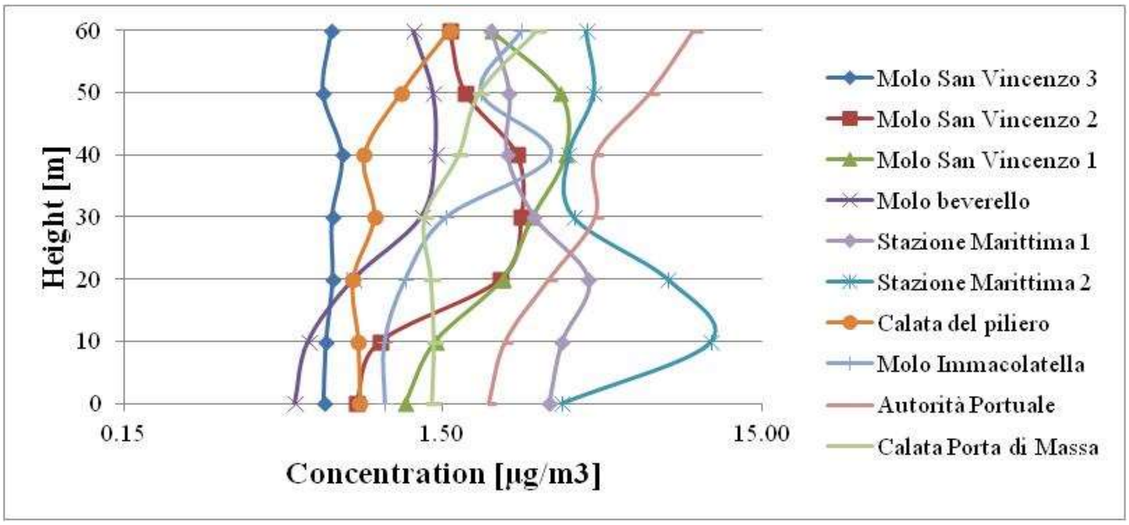

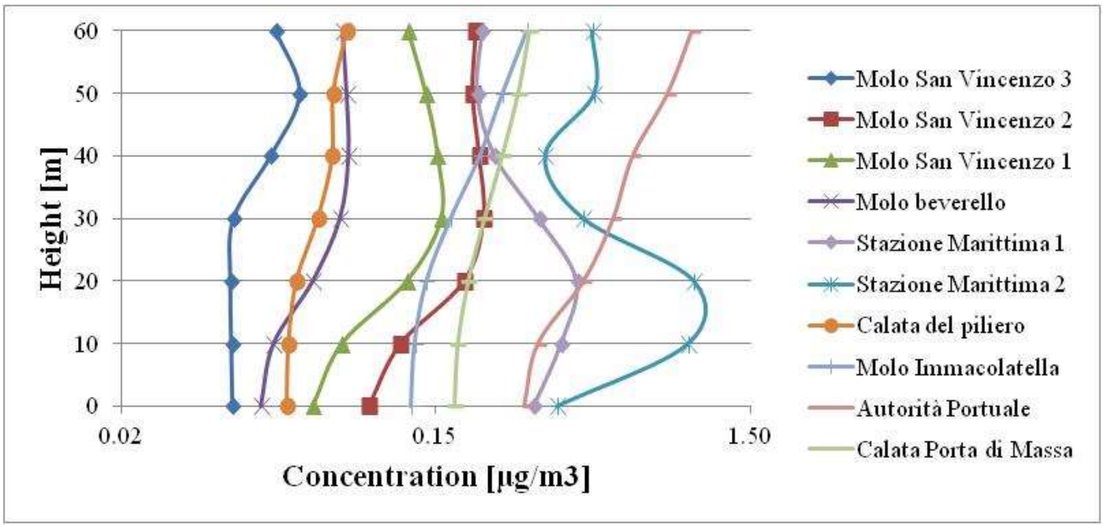

Figure 3-54 SO_2 vertical profile concentration, March-April: Period Average and 98° Percentile

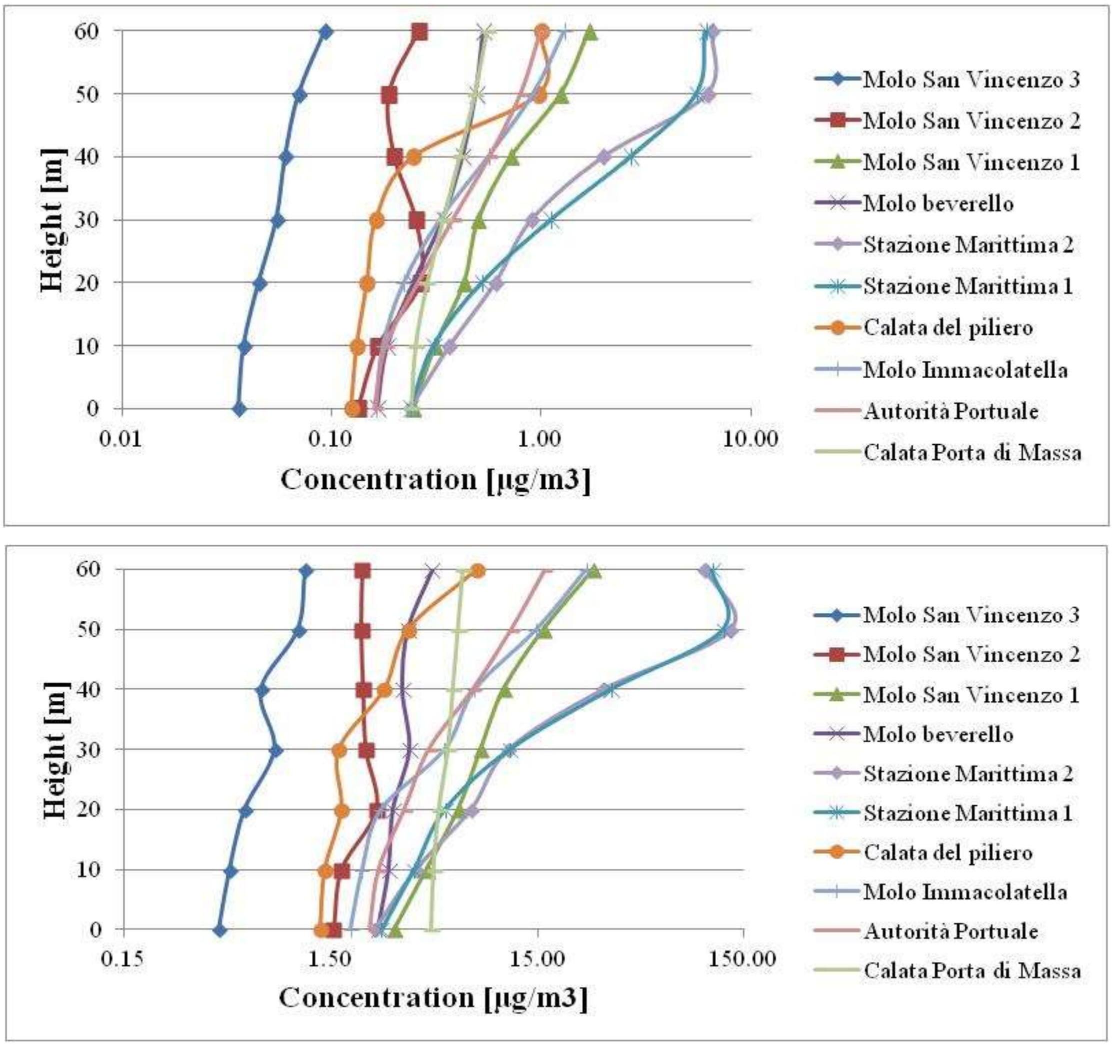

Figure 3-55 Vertical profiles of SO_2 concentration in November: Period Average and 98° Percentile

Overall, in spring period the concentration values are lower than in November: the maximums vertical profiles are about 10 μg/m^3 in March-April and 128 μg/m^3 in November for the 98° percentile and the period average is of 1 μg/m^3 in March-April and 7 μg/m^3 in November. This may be due to the quantity of calls of cruise ships in the two time periods, 19 calls in 14 days of March-April time period and 26 calls in 12 days of November. The different shapes of vertical profiles depends on the rose wind pattern in the time period. The results of the vertical profiles show that the receptor with the highest concentration level in the spring period is "*Stazione Marittima 2*", at 20 m, while in November the receptors with maximum concentration are: "*Stazione Marittima 1*" and "*Stazione Marittima 2*", both at 50 m. The different height of the maximum concentration is probably due to the different contribution of the ship categories and of the rose wind pattern in the time period. Specifically, during spring period the prevailing wind direction is from SSW and the receptor at the "*Stazione Marittima 2*" is downwind respect the emission of hydrofoils in A1; while in autumn the prevailing wind direction are from NNE and NE and the receptor is downwind as compared to the emission of cruise ships C3 and anchored ferries (T1 and T2, see Figure 3-15). A confirmation of the different contribution of vessel's categories on vertical profiles is obtained performing specific simulations for each category of vessels: cruise, ferries and fast vessels. Results for the receptor point "*Stazione Marittima 1*" are reported in Figure 3-56. Even though the emissions of cruise ships are much higher than those of others, their contribution at SO_2 concentration is lower in March-April and limited in November. The highest contribution is due to fast vessels emissions that are the most difficult to model. Mooring point and maneuvering route of these ships are, indeed, often variable and the emission height is generally unknown because in many cases a real funnel does not exists.

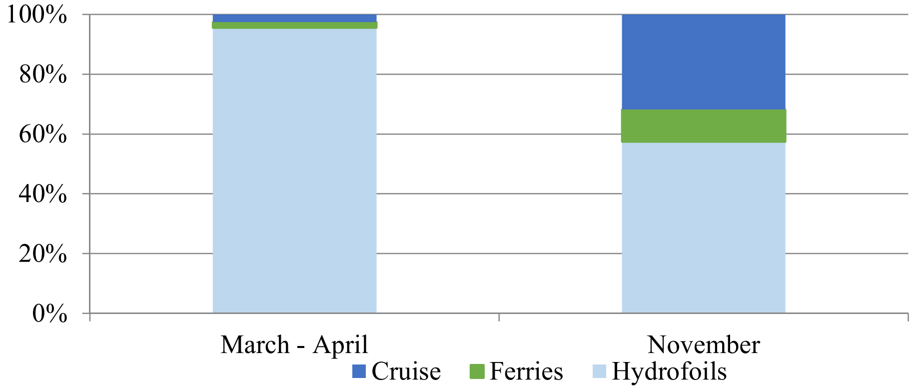

Figure 3-56 Contribution at SO_2 airborne concentration of vessel categories at ground level ("Stazione Marittima 1")

The results clearly show that for all chosen points the concentrations at ground level are very low if compared to those at higher height. The ratio between maximum concentration/concentration at ground level ranges are, indeed, between 1 and 52. In some cases, the highest concentration level is at 20 m, in other cases the maximum calculated concentration is at 50 or 60 m. This is mainly due to the different height of funnels of ship categories. Fast vessels determine a maximum of about 20 m due to the small effective height of emission plume, while it is about 50-60 m for cruise ships and ferries. Therefore, where the impact of HSC emissions is predominant the maximum concentration is at 20 m, while where cruise or large ferries emissions prevail the maximum is at 50-60 m height. Results show that the best choice is between 20-50 m. The suggested methodology can be applied to other ports to obtain very useful information for defining the best position of receptors during monitoring campaigns or the developing of a monitoring network.

3.9. Dispersion model: 2018 (AIS data)

3.9.1. The dispersion model

The necessary computing domain is highlighted in Figure 3-57. As usual, the orographic file together with hourly average values of meteorological parameters (Naples Airport of "Capodichino", Caserta, Acerra, Grazzanise and Casarea (Blu indicators in Figure 3-57), the overwater sea file containing air-sea surface temperature, air temperature, wind speed and direction, wind condition are given as input to CALMET to produce the 3D weather file. In this case, meteorological fields for reference year 2018 were generated by CALMET model for an about 3000 km2 Cartesian grid subdivided into a 265 × 265 cells grid system with 200 m cell spacing (Figure 3-57, Black boundary); the CALMET vertical grid system considers 10 layers up to 3.50 km height. In order to model the emission of ships in movements, each continuous route of every ship was discretized into a series of virtual geo-referenced sources and it was assumed that, pollutants were emitted at the time corresponding to the vessel's navigation. In this way, a point source emission file of time dependent emissions was created to simulate actual emissions when ships are in the port.

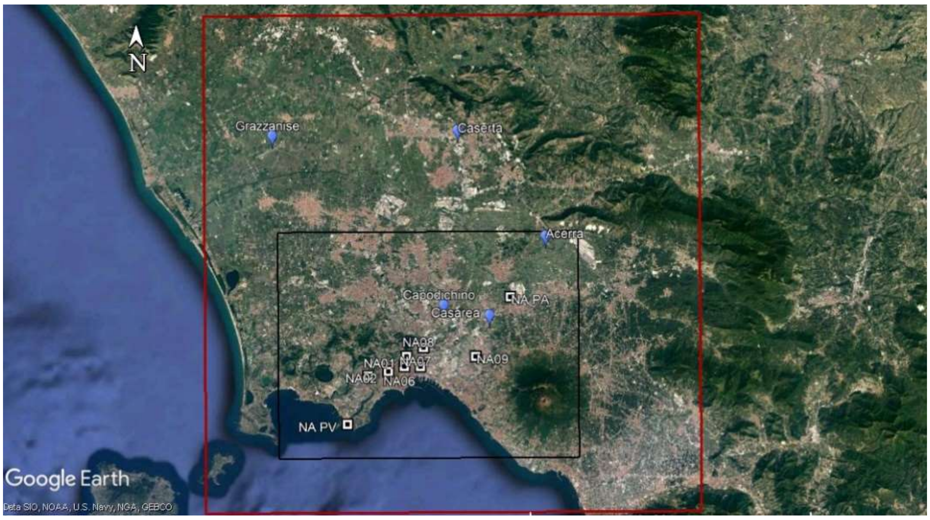

Figure 3-57 CALMET and CALPUFF domain and position of meteorological and air quality-monitoring stations

The CALPUFF domain was nested in the CALMET domain and is about 32 x 24 km^2. The computational domain is 160 × 120 cells, with 200 m cell spacing (Figure 3-57, red boundary). Ambient ozone monitoring data for 2018 from the ARPAC monitoring station are used to develop the hourly ozone monitoring data file (OZONE.DAT) for the modelling simulation. Since field data for NH_3 were not available, default values were assumed. Calculations were performed for NO_2, SO_2, PPM (Primary Particulate Matter), SIA (Secondary Inorganic Aerosols) resulting from emissions of NO_x and from emissions of SO_2, and the sum of PPM and SIA below 10 μm (PM10). The results obtained are the maximum of 24-hour average, the maximum of 1-hour average concentrations, and the annual average concentrations of pollutants. The wind rose of year 2018 (Figure 3-58) shows that winds blown predominantly from WNW (16.4 %) followed by South (13.1%) and East (10%). The ranges of most frequent velocities are 1-2 m/s (27%), 0.5-1 m/s (19.6%) and 2-3 m/s (17.1%).

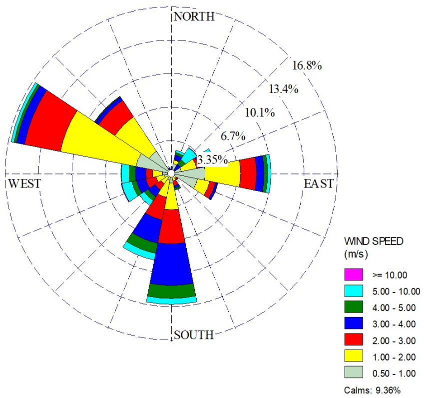

Figure 3-58 Wind rose of 2018 data

Air quality data have been provided by the Regional environmental Agency and have been studied for a comparison with simulation results. The chosen stations are the ones obviously located inside the study domain but particularly the ones continuously measuring NO_2 and SO_2 (hourly average) and PM10 (daily average). Specifically they are: NA01, NA02, NA06-09, Napoli Parco Virgiliano (NA-PV), Napoli via Epomeo (NA-VE) and Pomigliano d'Arco (NA-PA) (see Figure 3-57 square indicators). The analysis of data from the monitoring stations in 2018 are reported in Table 3-16 ([a] number of exceedances of 1-hour limit value; [b] number of exceedances of daily limit value). The results show that for SO_2 both hourly and daily limit are respected (350 μg/m^3 should not be exceeded more than 24 times a year, 125 μg/m^3 not be exceeded more than three times per year, EC Directive, 2008). For NO_2 the annual limit has been exceeded in NA06-07-08-09 while the maximum hourly average concentrations of NO_2 are in accordance with the EU established limit for the protection of human health (200 μg/m^3 cannot be exceeded 18 times a year, EC Directive, 2008). The situation of PM10 was more critical: the number of exceedances of the daily limit (established 50 μg/m^3 cannot be exceeded more than 35 times a year, EC Directive, 2008) was exceeded at NA07 and NA-PA. The NA-PA monitoring site showed the highest number of exceedances of the daily limit value (99 times) and is the only monitoring station that does not comply with the annual limit value of 40 μg/m^3 for the protection of human health during 2018.

Table 3-16 Annual mean concentration for NO_2, SO_2 and PM10 [$\mu g/m^3$], number of exceedances of daily limit values and efficiency of single sites. In bold the measurements exceeding the limit value

		NA01	**NA02**	**NA06**	**NA07**	**NA08**	**NA09**	**NA-PV**	**NA-VE**	**NA-PA**
NO_2	Annual man	21.97	38.03	44.47	56.69	45.53	45.38	11.15	29.59	22.99
	Number of exceedances[a,b]	0	0	2	0	0	0	0	0	0
	Efficiency	93%	96%	94%	94%	95%	94%	92%	63%	90%
SO_2	Annual mean				1.12		6.03		0.92	4.73
	Number of exceedances [a,b]				0		0		0	0
	Efficiency				94%		84%		85%	86%
PM10	Annual mean	31.65	21.25	31.12	34.64	25.94	30.22	16.41		44.63
	Number of exceedances [a,b]	17	4	17	40	29	31	3		99
	Efficiency	93%	100%	99%	99%	94%	96%	84%		93%

3.9.2. Shipping emissions and results

Following the methodology reported in the previous chapter the total ship emissions of the Naples port estimated in 2018 are 5418 t/year for NO_x, 193 t/year SO_2 and 602 t/year for PM10. Emissions during hotelling-phase represent about 95% of the total emissions, while about 5% is emitted during navigation in port. This result is in agreement with previous study (**Murena et al., 2018**). The small contribution of emissions during navigation compared to other ports (**Papaefthimiou et al., 2016**) depends on the small distance of ship routes in the port of Naples. The emission in t/year of NO_X, SO_X and PM are subdivided for phase in port and macro categories of ships and reported below (see from

Figure 3-59 to Figure 3-61).

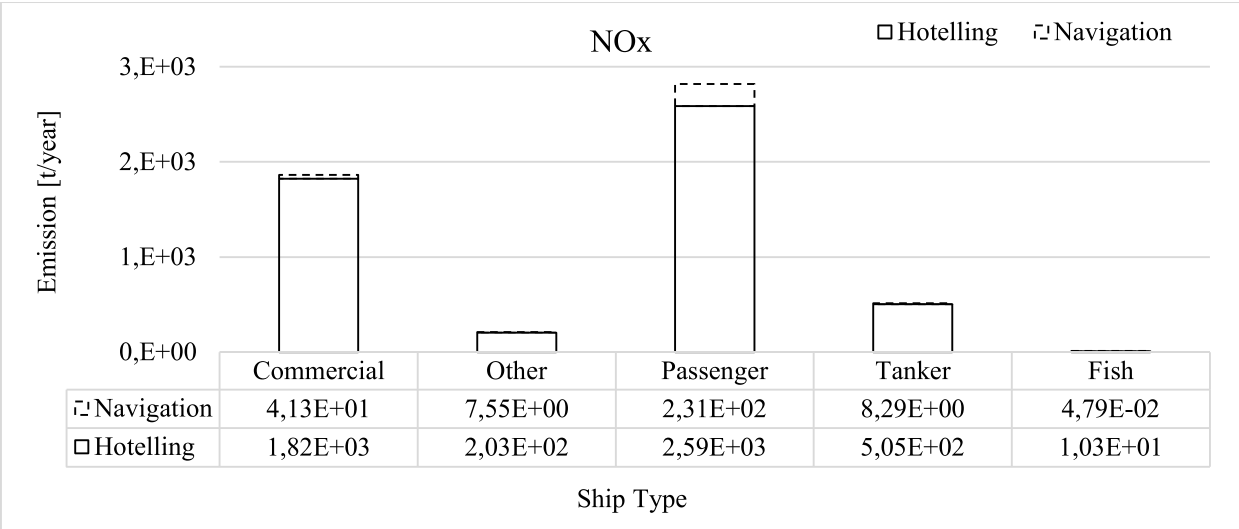

	Commercial	Other	Passenger	Tanker	Fish
Navigation	4,13E+01	7,55E+00	2,31E+02	8,29E+00	4,79E-02
Hotelling	1,82E+03	2,03E+02	2,59E+03	5,05E+02	1,03E+01

Figure 3-59 Emissions of NO_X for all categories and all phases

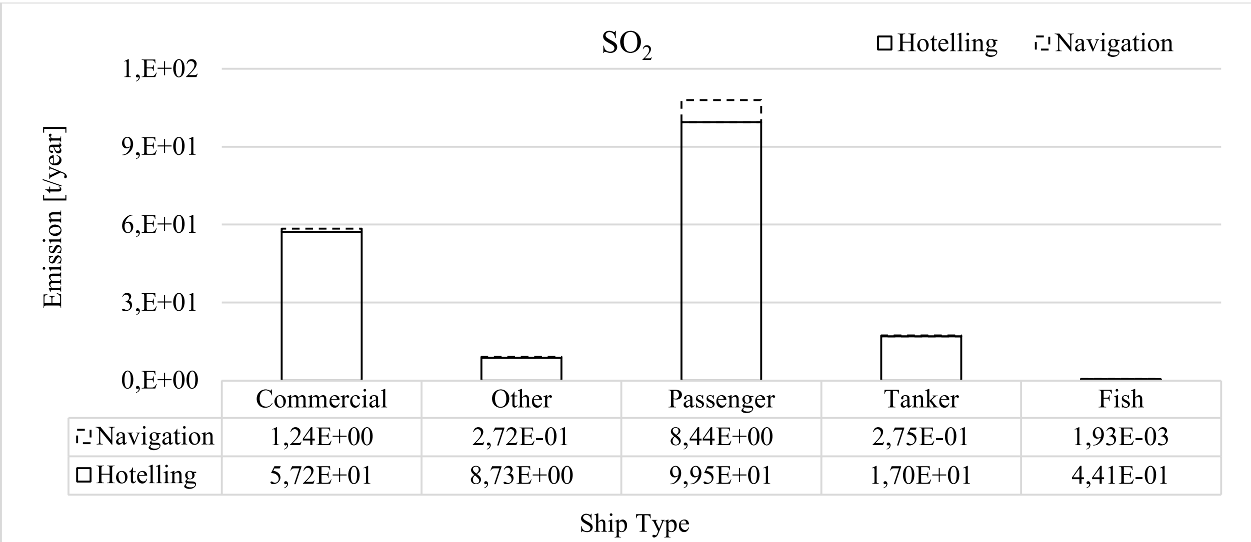

	Commercial	Other	Passenger	Tanker	Fish
Navigation	1,24E+00	2,72E-01	8,44E+00	2,75E-01	1,93E-03
Hotelling	5,72E+01	8,73E+00	9,95E+01	1,70E+01	4,41E-01

Figure 3-60 Emissions of SO_2 for all categories and all phases

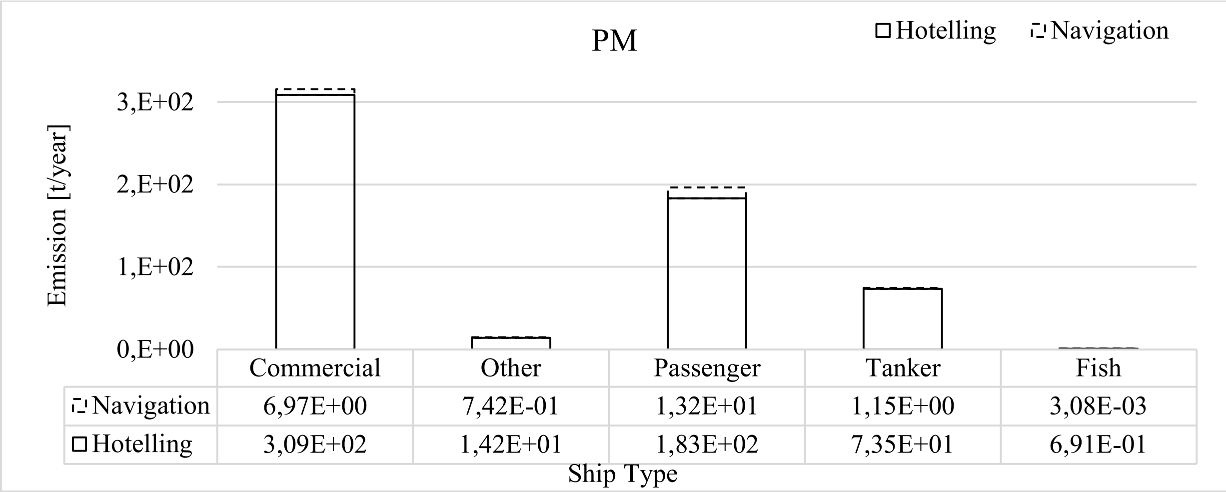

Figure 3-61 Emissions of PM for all categories and all phases

The distributions of annual emissions are shown in the three figures below (

Figure 3-62-

Figure 3-64). For NO_x and SO_2 the passenger ships produce the biggest percentage of emissions (52-56%), followed by commercial (30-34%), tanker (9-10%), other (4-5%) and fishing ships (<1%). For PM10 the largest amount of emission is from commercial ships (52%), followed by passenger ships (33%), tanker (12%) and other 5%).

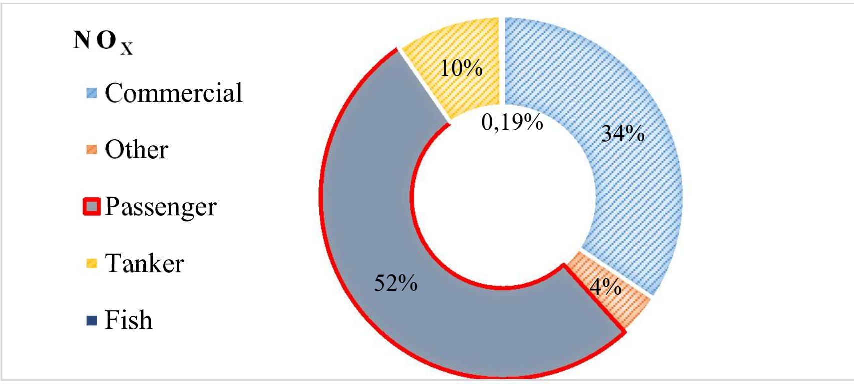

.

Figure 3-62 Ship types contribution to total emissions of NO_X in the port of Naples during year 2018

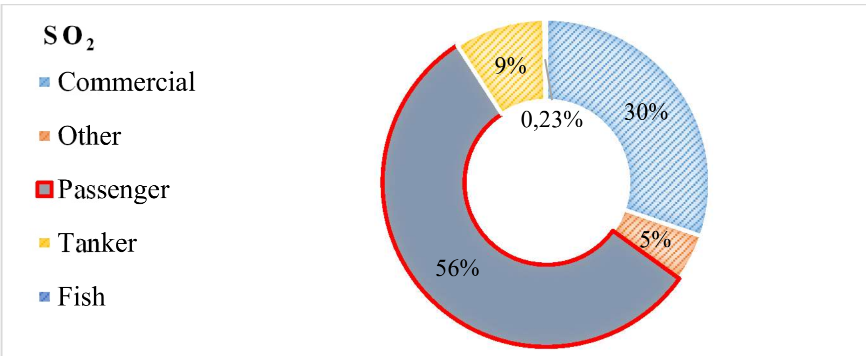

Figure 3-63 Ship types contribution to total emissions of SO_2 in the port of Naples during year 2018

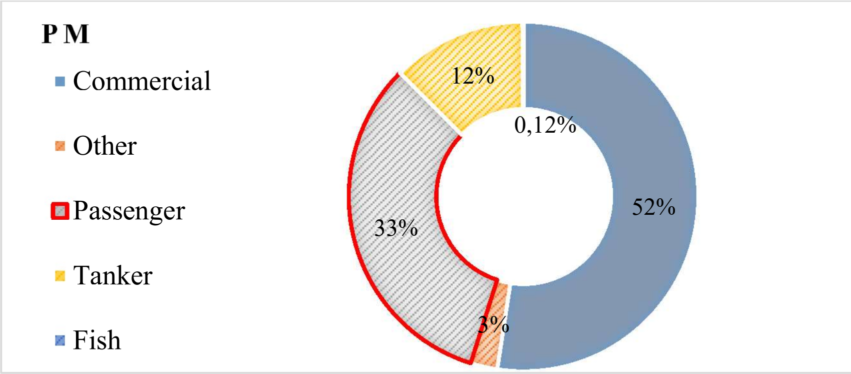

Figure 3-64 Ship types contribution to total emissions of PM in the port of Naples during year 2018

Contour maps of annual average concentration for the chosen pollutants are reported in Figure 3-65. The port area, and the near industrial area east of the centre of Naples are the areas of higher impact of all the pollutants considered. However, a portion of the urban area is also affected by some impact. The impact of ship emissions steeply decreases at larger distances from the port. Assuming that NOx is mainly emitted as nitrogen oxide (NO), in this work, NO_2 was considered as 5% of NO_x (**Jalkaneen et al, 2009**). In the atmosphere, NO is quickly converted to NO_2 in reaction with ozone, so further from the source the atmospheric NO_x is dominated by NO_2. Map of modelled annual mean atmospheric concentrations of NO_2 is shown in Figure 3-65a. The annual concentration of NO_2 spatially averaged on the entire model domain is 3.3 µg/m^3 (5.7 µg/m^3 in the area in Figure 3-65a). Passenger and commercial ship contribute with 27% of emissions, tanker and other ships with 12% and 9% respectively and fishing vessels with of <1%. The highest NO_2 contributions were found in the port area (Figure 3-65a).The modelled SO_2 concentrations are relatively low (Figure 3-65b). The annual mean concentration of SO_2 spatially averaged on the entire model domain is about 0.1 µg/m^3 (0.16 µg/m^3 in the area considered in Figure 3-65b). The relative contribution of each ships category is similar to that of NO_2.The concentration levels obtained in this study are much higher than those reported in the previous study in Murena et al., (2018a) where the maximum values of annual concentration estimated of NO_2 and SO_2 were 4 µg/m^3 and about 0.15 µg/m^3 respectively. In this study, the maximum concentrations of annual average of NO_2 and SO_2 are about 140 µg/m^3 and 5 µg/m^3 respectively. The results of SO_2 concentration in this study are comparable with some results obtained in **Merico et al. (2019)** of 5 µg/m^3.

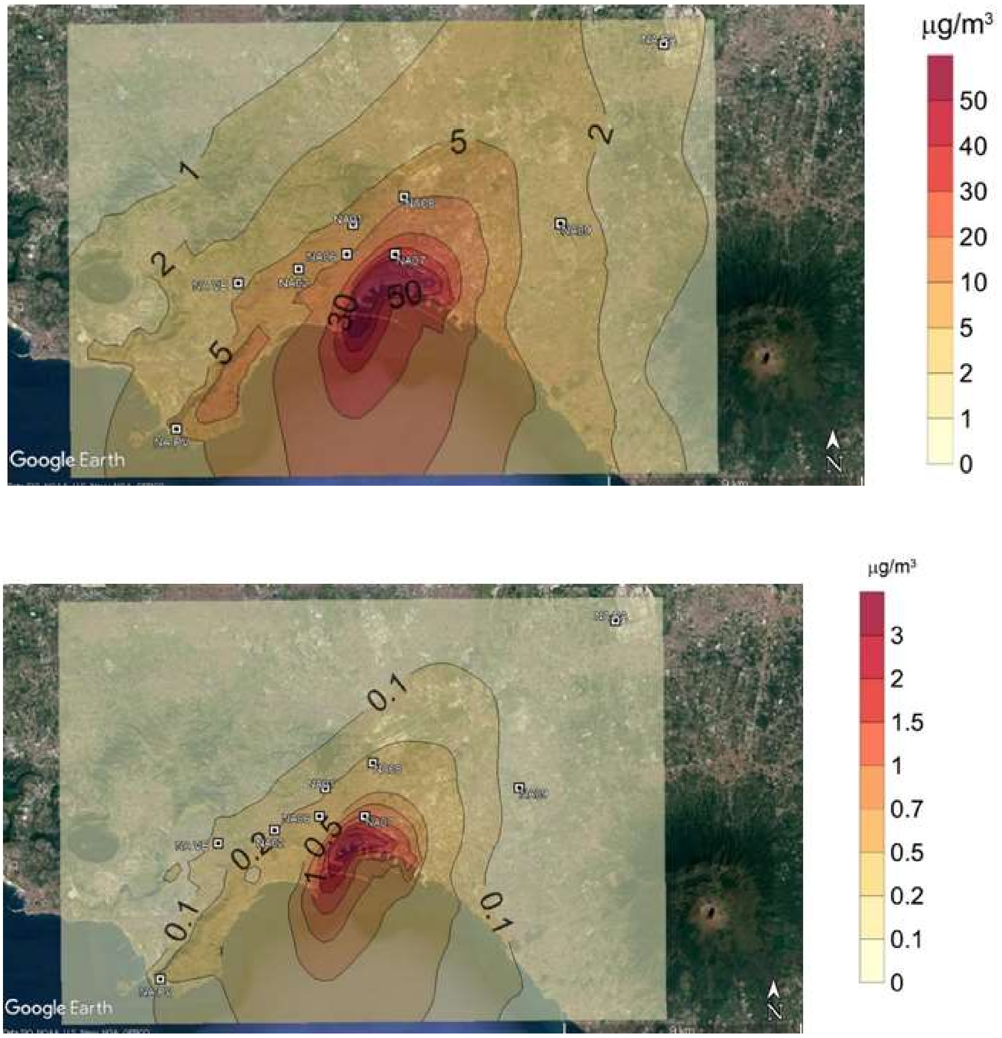

Figure 3-65 Simulations: maps of value of annual average [µg/m^3]. a) NO_2 and b) SO_2

The secondary aerosol formation in CALPUFF is parameterized by RIVAD/ARM3 chemical schemes; it calculates the secondary particle formation, such as the formation of sulphate and nitrate following SO_2 and NO_2 oxidation. The maximum concentrations of PPM (Figure 3-66a) are located in the harbour area with a max value of about 12 µg/m^3; secondary PM concentrations were reported in Figure 3-66b. The secondary PM, mainly formed far from the sources, tends to disperse and accumulate in the eastern part of the city due to the prevailing wind. The results obtained for PPM are comparable with results obtained by **Kuzu et al. (2020)** (13.1 µg/m^3).

a)

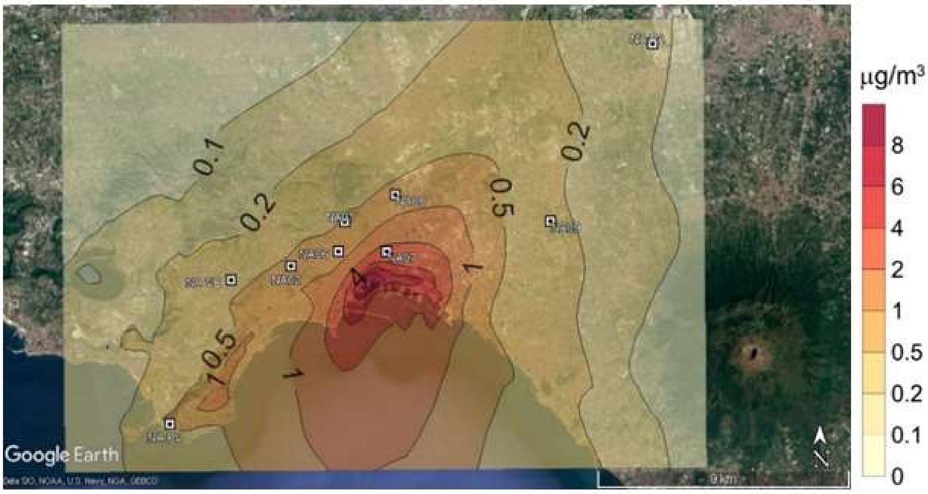

b)

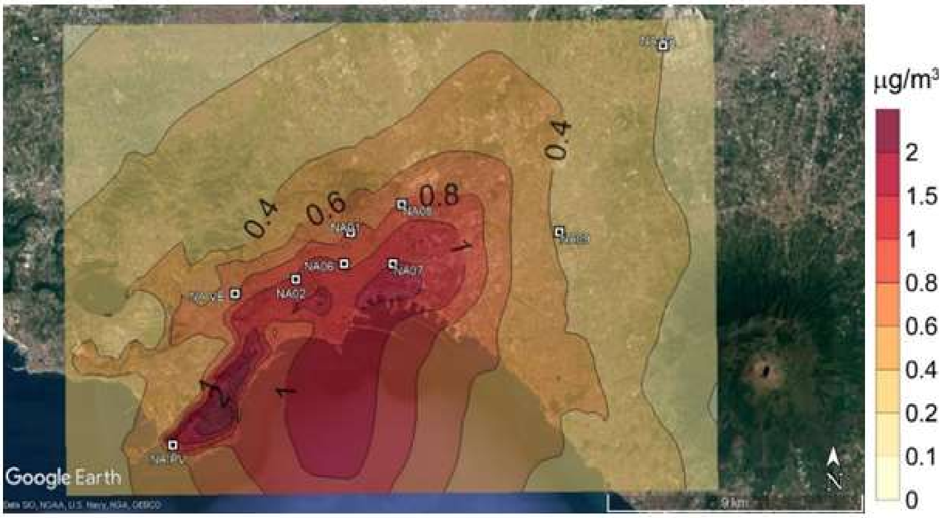

c)

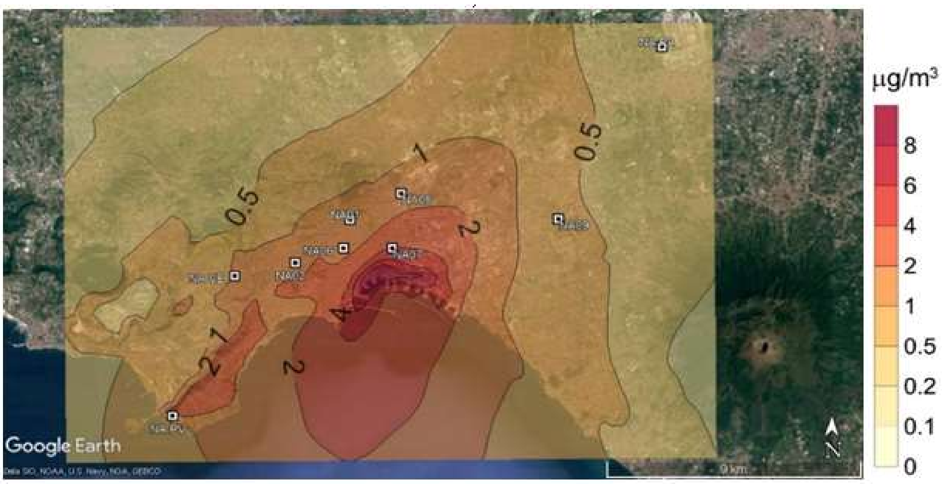

Figure 3-66 Simulations: maps of value of annual average [µg/m3]. a) Primary PM10 (PPM); b) Secondary PM10 and c) total PM10

3.9.3. Impact on air quality

The relative impact of ship emissions (concentration due to the ships obtained from simulations compared to the measured concentration) could be estimated in the location in which the monitoring stations are installed. Ground concentrations calculated by simulation models are compared with those obtained from air quality monitoring data and the relative contribution were calculated ($C\%$ is the percentage of ground concentration due to ship emissions). To have an indication of the contribution to long and short -term exposures to NO_2 and SO_2 annual averages and 98° percentile of 1h-averages obtained from simulation results are compared with air quality data measured at 9 NO_2 and 4 SO_2 receptor points (Table 3-17). The results obtained point out a possible more significant contribution of ship emissions to peak-values events.

Table 3-17 Contribution of ship emissions to hourly concentration levels measured at monitoring stations: annual mean and 98° percentiles of 1-hour averages of NO_2 and SO_2

Monitoring station	**Percentage contribution of ship emissions**			
	NO_2		**SO_2**	
	Annual mean	**98° percentile**	**Annual mean**	**98° percentile**
NA01	27%	82%		
NA02	13%	54%		
NA06	20%	93%		
NA07	64%	>100%	92%	>100%
NA08	18%	58%		
NA09	6,0%	26%	1,0%	5,0%
NA-PV	33%	86%	11%	38%
NA-VE	10%	42%		
NA-PA	5,0%	23%	1,0%	3,0%

Table 3-17 shows that the contribution of ship emissions is greater for the receptors near the port area (NA06-07 Figure 3-57) and lower for receptors located far from the port area, (see also the ground concentration maps (Figure 3-65a-b). In fact, compared to annual averages, the modelled impact of shipping on NO_2 concentrations is responsible for 64% of the measured concentration for station NA07, which is closest to the port area, while for other stations in the city the impact ranges from 6% to 33%. At NA-PA, far away from the city centre, the contribution to the annual mean is 5%.

For SO_2, the annual mean concentration at station NA07 is 92%. The contributions for the peak events (98°) are greater than those to the annual mean. This effect was also observed in Murena et al., (2018). In some cases the contribution is very high (> 80%) and for NA07 greater than 100%. The last is an unrealistic result and is an indication that the model overestimates the impact of ship emissions probably due to a certain degree of overestimation in the estimation of emissions or also due to the model underestimating the dispersive properties of the atmosphere in some conditions. Simulation results have been compared to air quality data from the ARPAC in 8 measurement sites (Table 3-18).

NA07 shows the highest contribution regarding the annual mean concentrations, (7% for PPM10, 4% SIA and 11% total PM10) in the other stations contributions are in range of 1-2% for PPM10, 2-7% for SIA and 2-5% for, total PM10 respectively. The contribution of ship emissions at NA-PA station is relatively negligible, with a contribution of 1%.

Table 3-18 Contribution of ship emissions to concentration levels measured at monitoring stations: annual mean and 98° percentile for primary PM10, secondary PM10 and total PM10

Monitoring station	**Percentage contribution of ship emissions**					
	PPM10		SIA		Total PM10	
	Annual mean	98° percentile	Annual mean	98° percentile	Annual mean	98° percentile
NA01	1%	3%	2%	5%	3%	8%
NA02	2%	4%	3%	7%	5%	10%
NA06	2%	4%	3%	6%	5%	11%
NA07	7%	11%	4%	10%	11%	18%
NA08	2%	3%	3%	5%	5%	7%
NA09	1%	1%	1%	2%	2%	3%
NA-PV	2%	4%	3%	6%	5%	9%
NA-PA	0%	0%	0%	1%	1%	1%

3.9.4. Seasonality variations

Regarding the effect of seasons on the impact of ship emissions, important differences were found and the higher contribution of shipping emissions to the concentration levels is registered during summer period. The average NO_2 concentration calculated over the entire domain in summer is 3.12μg/m^3 (5.51 μg/m^3 if urban area near the port area is considered); in winter, the average concentration is 2.83 μg/m^3 (4.83 μg/m^3). For SO_2, on the other hand, an average concentration of 0.09 μg/m^3 (0.16 μg/m^3) for the warm season and of 0.08 μg/m^3 (0.13 μg/m^3) for the cold season was calculated. The seasonal difference for PPM is less evident, in fact the average concentration over the entire domain are 0.27 μg/m^3 and 0.24 μg/m^3 respectively in summer and in winter (0.47 μg/m^3 vs 0.41 μg/m^3 in the port area). For the SIA the values are 0.36 μg/m^3 (0.55 μg/m^3) and 0.18 μg/m^3 (0.28 μg/m^3) for summer and winter respectively. Table 3-19 shows the average contributions for all the considered receptors and for all pollutants in winter and summer.

Table 3-19 Contribution of ship emissions to concentration levels measured at monitoring stations for winter and summer season for NO_2, SO_2, primary PM10, secondary PM10 and total PM10

Monitoring stations	**Seasonal percentage contribution of ship emissions**									
	Winter					**Summer**				
	NO_2	**SO_2**	**PPM10**	**SIA**	**Total PM10**	**NO_2**	**SO_2**	**PPM10**	**SIA**	**Total PM10**
NA01	14%		1%	1%	2%	34%		1%	2%	4%
NA02	11%		2%	3%	4%	15%		2%	4%	6%
NA06	11%		2%	2%	3%	23%		2%	3%	5%
NA07	29%	60%	3%	1%	4%	85%	100%	10%	6%	16%
NA08	7%		1%	1%	2%	27%		4%	6%	10%
NA09	4%	1%	1%	1%	1%	7%	3%	1%	2%	3%
NA PV	29%	11%	3%	3%	6%	29%	6%	1%	3%	5%
NA VE	9%					12%				
NA PA	4%	1%	0%	0%	0%	4%	0%	0%	0%	1%

On average, the contributions are shown in the Table 3-20 as the season changes.

Table 3-20 The contribution of NO_2, SO_2, and PM10 in winter and summer

	Winter	**Summer**
NO_2	13% (14%)*	27% (29%)*
SO_2	24%	36%
Primary PM10, SIA and total PM10	2%;2%;3%	3%:4%;7%

* if we exclude NA-PA monitoring site due to its being far away from the port area, the contribution increases.

On NA07, there is a contribution of 29% to NO_2 emissions in winter and a contribution of 85% in summer. It is important to note that for NA07 the contribution of SO_2 goes from 60% in winter to 100% in summer. This pattern seems to be related to the increase in ship traffic during summer. In fact, an average increase in emissions in summer compared to winter was calculated by 17%, 18% and 16% for NO_X, SO_2 and PM10 respectively.

4. Simulation: from engine to emissions

Aims and scope

In this thesis, so far the problem of the transition from power to emissions has been solved through the use of emission factors which, although specific to the type of ship, engine and fuel, are still a solution that simplifies the problem and represents it with a link linear between power and emissions. Obviously, the problem is more complicated than that especially with regard to transients, low loads and port operations.

For this reasons, after the analysis of the environmental impact on a port scale, the problem of emissions has been approached by using a dedicated ***simulation on a marine diesel engine****. The aim is to investigate the* ***link between engine characteristics and emissions****, with a dynamic model capable of taking into account the operating conditions of the engine for the purpose of quantifying emissions. An engine model has been created in* ***RICARDO WAVE environment****; it was validated and calibrated on an engine installed onboard a passenger ship operating in the port of Naples. Bench tests results in terms of power, torque, consumption, and rpm have been used to calibrate the model while experimental measurements validated it. The validation on sea trials shows the effectiveness of the model both in terms of main engine parameters and of emissions.*

4.1. Diesel engine simulation models: state of the art

Simulation has been used in engineering for many years as a support for design and manufacturing. Marine propulsion system simulations can be used for many purposes such as ship performance analysis, maneuvering analysis, machinery control systems development and machinery performance analysis. The elements within a classic propulsion simulation model are hull model, propeller model, engine model and governor. The engine model normally consists of the following main subsystems: cylinder, inlet and outlet manifold and intercooler, compressor, turbine, and shaft dynamics. Diesel engine simulation models can be classified into three categories, 0D single-zone models, quasi-dimensional multi-zone models and multi-dimensional models (**Chidambaram et al., 2016**).

0-D single-zone models (**Heywood 1988**) assume that the cylinder charge is uniform in both composition and temperature at all times during the cycle. Although this model has the capability of predicting engine performance accurately, it is lacking in the prediction of exhaust emissions. Multi-dimensional models, like KIVA (**Amsden et al., 1985; Amsden et al., 1987**), solve the space of the cylinder on a fine grid, providing a considerable amount of special information. However, the results may vary according to the formulation of initial or boundary conditions, which takes a lot of computational time. As an intermediate step between 0D and multi-dimensional models, multi-zone models can be effectively used to model diesel engine combustion systems (**Chidambaram et al., 2016**). The quasi-dimensional models combine some of the advantages of 0D models and multi-dimensional models. They solve mass, energy and species equations but do not explicitly solve the momentum equation. These models can provide the spatial information required to predict emission products and require significantly less computing resources compared to multi-dimensional models. In the multi-zone model, the simplest and most effective one is the two-zone model that splits the cylinder contents into a non-burning zone of air and another homogeneous zone where fuel is continuously supplied from the injector and burned. According to **Ishida et al. (1996)**, a significant improvement in the prediction of in-cylinder phenomena is represented by the "two-zone" approach, which provides distinct calculations for the burning and non-burning zone. This combustion model, unlike the 0D, allows evaluating gaseous emissions with the semi empirical equations and is used for predicting the performance and emission characteristics of a conventional engine. In particular, the "single-zone" combustion scheme is not suitable for the evaluation of exhaust emissions, because it does not calculate the flame temperature, whose value is required by the semi empirical relations yielding NO_X formation and soot formation and oxidation rates (**Altosole et al., 2017**).

4.1.1. Emission modeling

In addition to the above-mentioned simulation blocks, the purpose is to complete them with those related to the pollutant emissions. Essentially, the focus is on the NO_X, not only because of its associated impact on human health and on the environment, but also because other species such as CO_2 or SO_X can be adequately estimated using Emission Factor and/or stoichiometric combustion (**Trozzi & de Laurentis, 2016; Trodden et al., 2018**). According to **Trodden et al. (2018)**, NO_X production is predominantly a function of engine speed (or residence time) and loading. **Zel'dovich (1946)** provides a mechanism to estimate the thermal NO formation; this approach has a limited number of reactions, it can be challenging for estimating required oxygen concentration and it is relatively fast in computation. The formation of NO_X is controlled by chemical kinetics and, as well known, according to the thermal Zel'dovich mechanism (**Zel'dovich 1946**), a higher combustion temperature is responsible for an increase of the production of nitrogen oxides (**Raptotasios et al., 2015; Altosole et al., 2017**). Some authors, as **Raptotasios et al. (2015)**, approach the problem of NO_X production through the adoption of the extended Zel'dovich mechanism (**Lavoice et al., 1970; Heywood 1988**). An interesting approach is the chemical kinetics analysis; this analysis can accurately model the production of NO_X, as well as of many other species and can be embedded into a numerical engine model to provide estimates of emissions under varying loading conditions. The use of chemical kinetics solvers allows an analysis of how different conditions can influence the speed of reactions and yield details about mechanism and transition states of the reaction. A number of chemical kinetics solvers exists, including ChemKin (**Kee et al., 1996; Reaction Design, 2017**), Cantera (**Goodwin et al., 2017**) and the Kinetic PreProcessor (**Damian et al., 2017**). **Guedes Soares et al. (2015)** uses an engine model of two-stroke Diesel engine in conjunction with a chemical kinetics routine to estimate exhaust emissions; the results obtained are validated through data from real engines.

In the simulation carried out by **Trodden et al. (2018)** an emission factor is developed using a numerical engine model coupled with chemical kinetics computations. The same model, coupled to a ship's maneuvering simulator has then been used to compare NO_X formation during maneuvering operations. The results demonstrated that during maneuvers, the developed simulator shows significant differences in NO_X formation, compared to the commonly used emission factor approaches. In **Benvenuto et al. (2000)** a methodology to predict the amount and composition of exhaust gas emissions (NO and Soot) from ships has been presented. The aim of said paper was to evaluate the quantity and composition of the exhaust gas emissions of a ship during different maneuvers by the numerical simulation. For this purpose, the in-cylinder phenomena are evaluated by means of an actual-cycle two-zone combustion scheme (**Benvenuto et al., 1998**).

Furthermore, by means of the two-zone calculation scheme, the work permits the use of correlations for NO and soot prediction during the combustion process (**Wade et al., 1988**). Regarding the CO_2 emissions **Benvenuto et al. (2000)**, estimated the carbon dioxide mass of the engine for each working point of the engines maps, from the respective fuel mass consumption and fuel type, following the procedure suggested by the MEPC. In **Tadros et al. (2015)** the method of element potential (**Kristensen, 2012**) is used to calculate the chemical equilibrium of the combustion equation to determine the mole fraction equilibrium combustion product of all species (CO_2 and N_2), and then to calculate the NO_X and the CO_2 rates. The results show a good fitting between the rates of NO_X calculated from the combustion process and the rate of NO_X calculated using the emission factors, **Kristensen (2012)**, according to the specific fuel consumption. Lastly, the NO_X emission shows a total dependence on the maximum temperature of combustion process. In **Tadros et al. (2016)** the CO_2 and NO_X emissions are calculated from the equilibrium of the equation of combustion for different start angles of combustion. In **Tadros et al. (2018)** and in **Vettor et al. (2018)**, a fourth-polynomial regression model implemented in MATLAB is used to generate equation of CO_2 and NO_X emissions from two four-stroke marine turbocharged diesel engine. Another interesting research development found in literature is represented by ANFIS (Adaptive Neuro-Fuzzy Inference System) models able to solve nonlinear problems. ANFIS, a hybrid intelligent system coupling a fuzzy logic system with an Artificial Neural Network (ANN), has the advantage of being adaptable and effective for non-linear complex problems. **Hosoz et al. (2013)** have developed an ANFIS model to predict the performance parameters and exhaust emissions of a diesel engine. For this purpose, a diesel engine was equipped with various instruments for measurements and tested for varying engine speed, engine load, and different fuel. Then, the model has been tested by using some of the input-output pairs gathered in the experiments. The results show a good agreement with the experimental data. In **Tadros et al. (2019)**, the ANFIS model is recommended to be further used to investigate the exhaust emission of engines and to be coupled with other softwares for optimization procedures. In **Tadros et al. (2016)**, an optimization tool was adopted in order to monitor and optimize a few engine performance parameters without the need for tests and experimental measurements. In **Tadros et al. (2019a)** a numerical optimization model is developed to simulate the performance of a large 4 Stroke marine turbocharged diesel engine in the entire operating range and to identify optimal values for the adjustable parameters such as speed of the turbocharger and start angle of injection. Target of the optimization process is a minimization of the fuel consumption while complying to exhaust emissions limitation. In this model, the amount of carbon dioxide (CO_2) emissions is calculated according to the SFC using the emission factor while the generation of NO_X is computed by the extended Zeldovich mechanism, taking into account the two zones of combustion (burned and unburned zone). In **Tadros et al. (2020)** an engine optimization model is developed to fit the calculated in-cylinder pressure diagram to the experimental data by finding the best-fitting values of the start angle of injection and of the amount of injected fuel for different engine loads. The same methodology can be used for fitting the performance characteristics of numerical models of further engines.

4.2. The software Ricardo Wave

WAVE is a state-of-the-art 1D gas dynamics simulation tool. It is used worldwide in industry sectors including rail, marine, and power generation. WAVE enables performance and acoustic analyses to be performed for virtually any intake, combustion, and exhaust system configuration. The simulation software solves the 1D form of the Navier-Stokes equations governing the transfer of mass, momentum, and energy for compressible gas flows and includes sub-models for combustion and emissions. WAVE contains advanced combustion models for diesel engines and includes secondary models specifically for the study of engine-out emissions and knock. The main capabilities of the simulation model are:

- diesel Wiebe semi-predictive combustion sub-model;
- diesel3D: Computational Fluid Dynamics (CFD) predictive injection/combustion visualization;
- nitrogen oxides (NO_X), carbon monoxide (CO), and hydrocarbon (HC) emissions formation;
- cylinder pressure heat-release analysis for individual cylinders;
- library of fuels and custom fuel generator – ethanol, hydrogen, natural gas, E85; arbitrary blends and oxygenated fuels.

In the next subsection, the main theories underlying the construction of the model will be exposed. The same will then be particularized for the case study.

4.2.1. Model structure: basic theory and assumptions for the construction of the model

A diesel engine model built within the Ricardo Wave environment, generally, has the following elements: engine, cylinders, valves, injector, charge air cooler, turbocharger (turbine, compressor, and shaft), ducts and y-junctions. The gas follows the ideal gas equation of state. The thermodynamic properties of the mixture of air, fuel, and combustion products are calculated in WAVE as a function of temperature, pressure, and composition. There are three options for how these calculations are done: interpolation, the equilibrium of six species or the equilibrium of eleven species:

- **Interpolation** (used in this model)

This is the traditional method and is the standard one. It was chosen as the best compromise between speed and accuracy. Wave uses rapid and accurate interpolations from pre-calculated property maps which are stored in the fuel file. The maps are generated for each specific fuel as a pre-processing step to the simulation. The properties are calculated over a wide range of parameters using a comprehensive equilibrium program which is applicable to any general CCHHOONN fuel.

- **Direct (6-Species)**

The equilibrium properties are calculated directly at each timestep instead of being pre-processed into maps. This option uses a reduced 6-species scheme in order to run as fast as possible. The species used are CO, CO_2, H2, H_2O, N_2, O_2.

- **Direct (11-Species)**

The equilibrium properties are calculated directly at each timestep instead of being pre-processed into maps. This option uses the standard 11-species scheme that is used in the interpolation maps. The eleven species are (CO, CO_2, H, H_2, H_2O, N_2, NO, O, O_2, OH, N). This option is considerably slower than the other options but it is also the most accurate one. The interpolated scheme works well in general but can introduce errors where there are sharp kinks in the map surfaces.

Typically, the pressure of 1 bar, the temperature of 300 K, and initial velocity of 0 m/s is used as the initial conditions of a fluid used within a cylinder.

4.2.2. Engine and cylinder

Engine data refers to all dimensions and characteristics associated with the actual engine itself. Typical data required for an engine are inlet and exhaust wall temperatures, engine operating speed, fuel flow rate or fuel/air ratio, piston, head, and liner average surface temperatures, ambient conditions and combustion data.

Below, Figure 4-1, a simplified cylinder geometry is reported.

Cylinder elements are typically used to model the cylinders of a standard IC engine.

Inputs of the engine system are (see Figure 4-13):

- **number** of ports and valve intakes count,
- **engine shape**: *V* or inline;
- **mixture type:** Spray guided DI, typical for compression-ignition (*diese*l);
- firing order and timing.

All cylinders are connected to the engine in the predetermined firing order.

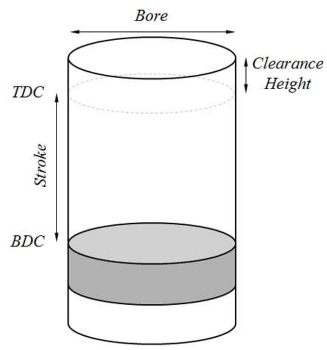

Figure 4-1. Cylinder geometry

Inputs of the cylinder system are (see Figure 4-1 and Figure 4-12):

- **geometry:** bore; crank stroke, clearance height between the top of the piston at TDC and the head deck, used to determine the exposed liner surface area at TDC;
- **Compression ratio**, the geometric ratio of the volume of the combustion chamber when the piston is at BDC to the volume of the combustion chamber when the piston is at TDC (a number greater than 1);

- **ignition delay**: for diesel combustion of cylinder measured as the time between the start of injection and the start of combustion.

In addition to these inputs, and in order to define boundary conditions the following data are necessary (see Figure 4-12):

- The average surface temperature of the piston top or crown (T_{piston}), the average surface temperature of the cylinder liner ($T_{cylinder}$) and head (T_{head});
- The average surface temperature of the intake and exhaust valve(s);
- Swirl ratio of the bulk flow in the cylinder: normally 0 for a non-swirl port design. If a turbulence and flow sub-model is applied, this serves only as of the initial value at the start of the simulation and will be updated by the sub-model during the analysis;
- The ports of cylinders require more detailed information, which can only be collected from testing the ports. Typical information needed is valve diameters, valve event timings, valve lift, or Cam profiles (see 4.2.4).

4.2.3. Engine friction

Not all the work transferred to the piston from the high-pressure gases contained inside the cylinder is available for use at the drive shaft. That transferred and not available portion of the work, is called friction work. It is dissipated in a variety of ways within the engine and engine auxiliaries. The friction work or power is a sufficiently large fraction of the indicated work or power—varying between about 10% at full load and lower speeds, through 50% at light load. Friction losses affect the maximum brake torque and minimum brake specific fuel consumption directly. A large part of the friction losses appears as thermal energy in the coolant and oil which must be removed in the radiator and oil cooler system. In particular, the friction work is expended:

- to draw the fresh mixture through the intake system and into the cylinder, and to expel the burned gases from the cylinder and out of the exhaust system;
- to overcome the resistance to the relative motion of all the moving parts of the engine such as the piston rings, piston skirt, and cylinder wall etc.;
- to drive the engine accessories such as the water, oil and fuel pump, the fan, and the generator.

Because of the different sizes of engines operating at many different rpm, the most meaningful method of classifying and comparing friction and engine losses is in terms of mean effective pressure (mep).

Frictional mep can be defined as the work lost to internal friction and to drive necessary engine equipment such as the oil pump (4-1):

4-1 Frictional mep

$$fmep = imep - bpem$$

where

- imep is the net work generated in the combustion chambers and bmep is the work done by the engine crankshaft.

Two different approaches to this problem can be followed: complex or simplified. The first one estimates the instantaneous torque but normally requires the estimation of several constants by means of accurate and detailed experimental data. The second one, instead, uses a few global variables, specifically one related to the engine load and the other related to the engine speed, in order to separately account for both the energy dissipated by friction due to gas thrust and the energy losses influenced by the speed. The Chen & Flynn model is one of the most employed models in commercial software for the second category. According to this method, the fmep depends on the cylinder's maximum pressure and engine speed by means of the following law (4-2):

4-2 Chen & Flynn model

$$fmep = ACF + BCF\, P_{MAX} + CCF\, n + QCF\, n^2$$

The correlation has a constant term (for accessory friction), a term, which varies with peak cylinder pressure (for load dependence), a third term linearly dependent on mean piston velocity (for hydrodynamic friction) and a fourth quadratic term with mean piston velocity (for windage losses):

- *ACF:* Constant portion of the Chen-Flynn friction correlation;
- *BCF:* Term that varies linearly with peak cylinder pressure in the Chen-Flynn friction correlation. This accounts for the variation of friction with engine load;
- *CCF:* Term that varies linearly with the piston speed in the Chen-Flynn friction correlation. This is to account for hydrodynamic friction in the power cylinder;
- *QCF:* Term that varies quadratically with the piston speed in the Chen-Flynn friction correlation. This is to account for windage losses in the power cylinder.

The scavenging model is required for 2-stroke engine simulations and is optional for 4-stroke engine simulations. If not activated, fully mixed scavenging is assumed. Activating this sub-model in a 4-stroke engine is normally not needed, but may improve accuracy in long overlap engine simulations. The sub-model is based on tracking of "old" and "new" mass in the cylinder.

At EVO, the entire contents are initialized to "old" mass, and as fresh charge enters, the incoming mixture is accounted as "new" mass. If there are oscillating flows or reversing flows out of the cylinder, the summation of new and old masses may drift.

The scavenging sub-model contains a thermal mixing model that assumes that the "new" zone gas will gradually mix with the exhaust gas during the scavenging event.

4.2.4. Valves

The typical parameters needed for the setting of the intake and exhaust valves are:

- IVO (Intake Valve Opening), the crank angle at which the first intake valve opens for this cylinder;
- IVC (Intake Valve Close), the crank angle at which the last intake valve closes for this cylinder;
- EVC (Exhaust Valve Close), the crank angle at which the last exhaust valve closes for this cylinder;
- overlap duration of intake and exhaust valves of the cylinder;

The software has two typical patterns of inlet and exhaust valve lifts.

The valve sub-models in WAVE requires additional input of either forward/reverse flow coefficients or pressure-ratio dependent flow coefficients. Flow coefficients are used to describe the complex behavior of flow through a valve due to a combination of factors, including port geometry and finish, valve seating, valve position, etc. They simplify all of these factors into a multiplier (0 to 1, reduction factor) of the geometric area to create an effective area through which flow can pass. Two different types of coefficients are commonly used in industry: Flow and Discharge. In this case, a typical flow coefficient profile value has been used see Figure 4-2. The Valve Flow Coefficient Profile object defines the lift profile for a lift type valve (see Figure 4-2).

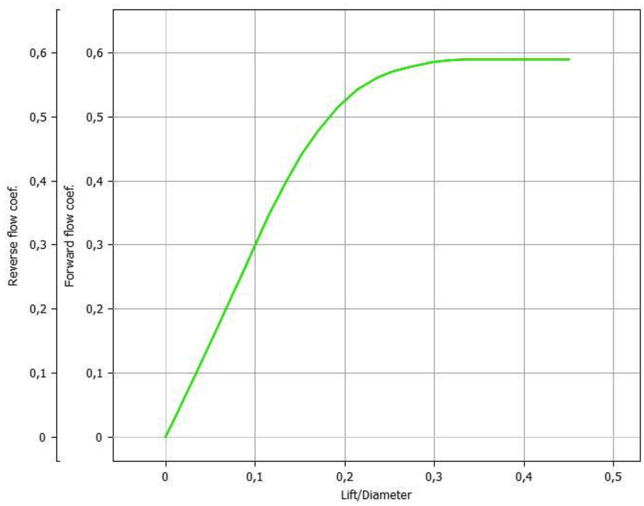

Figure 4-2 Flow coefficient profile

4.2.5. Injector

The fuel injector type used in this case is a Mass flow rate. A Mass Flow Rate injector element delivers a specified amount of fuel per unit time, following a user-defined profile. WAVE normalizes the profile and calculates the injection rate required to achieve the desired fueling per unit time. The operating point is set through the start of injection and the initial injection rate in kg/h; this is used to calculate the total injected mass per event, using the current engine speed at the Start of Injection (SOI) time. Other parameters are the temperature of the injected mass, the injector nozzle diameter (this should be entered as the effective diameter of a single injector nozzle, regardless of how many holes the injector has). The model automatically calculates the initial fuel injection velocity. Injection rate and injection pressure are added for providing a profile of injection rate and pressure versus crank angle.

4.2.6. Turbocharger

Turbochargers (TC) are modeled in the flow network with a combination of compressor and turbine elements. These are planar junctions with no specific volume of their own. They use maps to model their effects on flow behavior. The turbocharger elements are connected by a shaft element that controls the gearing of the turbines corresponding to the compressors. The shaft can be used to add power to or remove it from the turbocharger. Turbo-compressor map requires turbine and compressor input data in the form of discrete operating points. The variable geometry compressor performance is represented by one or more maps, each representing one of the internal vane positions, with respective mass flow, pressure ratio, rotational speed, and efficiency. This also allows optional scaling of the turbocharger in order to match it to an engine. The operating point of the compressor may be controlled by specifying multiple vane positions of the variable geometry, allowing increased/decreased flow back pressure from the device. The variable geometry turbine performance is represented by one or more maps, each representing one of the internal rack positions, which relates mass flow, pressure ratio, rotational speed, and efficiency. This also allows optional scaling of the turbocharger in order to match it to an engine. The software uses turbine data in the form of discrete turbine operating points. This data is generally available from the manufacturers in the form of performance maps or tabulated data. Four input values are required for each operating point: pressure ratio, speed, mass flow and efficiency. The standard units for this data are dimensional (rpm, kg/s) corrected to a reference inlet temperature and pressure. For turbines, these maps are usually presented in one of two forms: corrected mass flow and efficiency plotted against the corrected speed along lines of constant pressure ratio, or against pressure ratio along lines of constant corrected speed. In this model, a TC group, available in the library of the software, has been scaling with the aim of satisfying the engine requirements.

4.2.7. Combustion

The basic engine model is a time-dependent simulation of in-cylinder processes, based upon the solution of equations for mass and energy. The mass equation accounts for changes in in-cylinder mass due to flow through valves and due to fuel injection. Separate accounting is made for fluxes of air, vaporized fuel, liquid fuel and products of combustion. The energy equation is based on the first law of thermodynamics and equates the change of internal energy of in-cylinder gases to the sum of enthalpy fluxes in and out of the chamber, heat transfer, and piston work. There are two zonal options: single-zone and two-zone. The two-zone model is used to capture the processes taking place during the combustion period in detail. The Combustion sub model defines how the in-cylinder temperatures are tracked during combustion – either using a single zone or two zones which separately track burned and unburned species. The two-zone setting is required when the in-cylinder emissions or knock models have been activated, and also for the radiation heat transfer sub-model. The two-zone model is used to capture the chemical processes taking place during the combustion period in more detail. All combustion models may be used with either single or two-zone engine cylinders, but emission models generally require the two-zone modes. The basis of this model is a standard Wiebe non-predictive curve-fit correlation. However, the Cetane number and reference speed parameters can be calibrated to enable a semi-predictive Diesel combustion model that predicts ignition and responds to changes in the trapped mixture conditions as well as in the engine operating speed. The Wiebe combustion model uses functions which are similar to the correlations for pre-mixed and diffusion burn regimes as determined by **Watson et al (1980)**. This empirical formula is suitable for the combustion in the diesel cycle and did not require any calibration unlike the single and multi-Wiebe functions. The concept of a double Wiebe function based on the combustion simulation is suggested as an alternative to the single Wiebe function in order to model the different phases of the combustion process. An additional third function has been added to represent the slow late burning (referred to as tail burning) at the end of the diffusion burning regime. W, which is the model used in WAVE for the mass fraction burned, is (4-3):

4-3 Weibe combustion

$$W = p_f\{1-[1-(0.75\tau)^2]^{5000}\}+d_f\{1-[1-(cd_3)^{1.75}]^{5000}\}+t_f\{1-[1-(ct_3\tau)^{2.5}]^{5000}\}$$

Premix + ***Diffusion*** + ***Tail***

where:

- p_f, d_f, t_f are the mass fractions of the premix, diffusion, and tail burn curves, respectively;
- cd_3, ct_3 are the burn duration coefficients for the diffusion and tail burn curves, respectively;
- t the burn duration term.

The mass fraction of the premixed burn is obtained from the ignition delay model. The mass fractions of the diffusion and tail burn curves are obtained once the trapped equivalence ratio and the mass fraction of the premix are calculated.

The burn duration coefficients for the diffusion and tail burn curves are determined using the following equations (4-4):

4-4 Burn duration coefficients for the diffusion and tail burn curves

$$\tau = \frac{\vartheta - \vartheta_b}{125\left(\frac{RPM}{BRPM}\right)^{0.3}}$$

where:

- θ is the crank angle and θ_b is the crank angle at start of combustion;
- *RPM* is the Engine speed and *BRPM* is the Reference speed.

The burn duration varies inversely with BRPM; higher values of result in a shorter burn duration and lower values result in a longer burn duration. In addition, the mass fraction burned at which combustion is halted may be selected by the user via profile control.

In summary, the inputs are:

- The Reference Speed (BRPM), for burn duration, which is used to calibrate the burn duration; this is typically the engine RATED speed;
- Burn fraction at completion and the ignition delay (1). If "Ignition delay" is on, as in this simulation, the start of combustion timing and premixed burn fraction are automatically computed from cylinder conditions during fuel injection and the user-entered Cetane number (52).

Using the first law of thermodynamics (**Heywood, 1988**), the change in pressure (4-5):

4-5 Pressure

$$\frac{dP}{d\vartheta} = \frac{K-1}{V}\frac{dQ}{d\vartheta} - \frac{KP}{V}\frac{dV}{d\vartheta}$$

and in temperature (4-6),

4-6 Temperature

$$\frac{dT}{d\vartheta} = (K-1)\frac{T}{PV}\left[\frac{dQ}{d\vartheta} - P\right]\frac{dV}{d\vartheta}$$

along the crank angle are calculated by 4-5 and 4-6, where *K* is heat specific ratio, *V, P, T* are the cylinder volume, pressure and temperature respectively, $dV/d\theta$ is the change in volume and dQ is the total heat added. Diesel combustion models in WAVE calculate the amount of air burned at each time step using an empirical relation. Ignition delay prediction is also based on the work by **Watson et al (1980)**. In this formulation, an ignition delay is calculated using the in-cylinder temperature and pressure. In addition to the in-cylinder temperature and pressure histories, this extended correlation includes an additional dependency on the fuel Cetane number. As expected, increasing the fuel Cetane number decreases the ignition delay, and this can be used as a tuning parameter. The premixed fuel mass fraction corresponds to the amount of cumulative fuel vaporized during the calculated ignition delay period.

The correlation can be calculated as follows (4-7):

4-7 Ignition delay

$$\Delta\vartheta_{delay} = 323\ exp^{\min\left(2100\cdot\frac{C}{T_{sum}},80\ /P_{sum}\right.}$$

Where:

$$C = \frac{67}{25 + Cetane}$$

$$T_{sum} = \sum_n \frac{T_c^n + T_c^0}{2} \cdot \frac{\Delta\vartheta_n}{\vartheta_{n+1} - \vartheta_0}$$

$$P_{sum} = \sum_n \frac{P_c^n + P_c^0}{2} \cdot \frac{\Delta\vartheta_n}{\vartheta_{n+1} - \vartheta_0}$$

Where

- T_c^n, P_c^n are current cylinder temperature and pressure;
- T_c^0, P_c^0 are current cylinder temperature and pressure;
- $\Delta\vartheta_n$ is the time step size;
- ϑ_0 is the crank angle at SOI.

4.2.8. Heat transfer

The Original Woschni heat transfer sub-model views the charge as having a uniform heat flow coefficient and velocity on all surfaces of the cylinder and calculates the amount of heat transferred to and from the charge based on these assumptions. It is the most commonly used heat transfer sub-model and can be applied to all cylinder elements (see Figure 4-20). The Woschni heat transfer coefficient is calculated using the following equation (4-8):

4-8 Woschni heat transfer

$$h_g = 0.0128 D^{-0.2} P^{0.8} T^{-0.53} C_{enht}$$

where:

- D is the cylinder bore;
- *P,* and *T* are the cylinder pressure and temperature;
- v_c is the characteristic velocity;
- C_{enht}, multiplier.

The characteristic velocity is the sum of the mean piston speed and an additional combustion-related velocity that depends on the difference between the cylinder pressure and the pressure that would exist under motoring conditions. It is given by Woschni's original correlation as (4-9):

4-9 The characteristic velocity

$$v_c = c_1 v_m + c_2 \frac{V_D T_r}{P_r V_r}(P - P_{mot})$$

where:

- v_m , Mean piston speed;
- V_D, Cylinder displacement;
- T_r , P_r, V_r, Reference temperature, pressure and volume;
- P_{mot}, Motored cylinder pressure.

The coefficient, c is dimensionless quantity calculated as:

$c_1 = 6{,}18 + 0{,}417 \frac{v_s}{v_m}$ during scavenging, $c_1 = 2{,}28 + 0{,}308 \frac{v_s}{v_m}$ when valves are closed (vs is the swirl velocity). The coefficient, c_2 is a constant given as $3.24*10^{-3}$ [m/(s·K)] during combustion and 0 before combustion and during scavenging.

4.2.9. Emissions

At each step during the combustion phase, the mole fractions of WAVE's eleven species are calculated for the unburned and burned zones (based on thermodynamic equilibrium) and then averaged. When combustion ends, the single-zone model is used. The NOx emissions sub-model predicts NOx production during combustion and exhaust in an engine cylinder element. At any instant of the combustion process, there is mass flux into the burned zone associated with the instantaneous fuel-burning rate and the stoichiometry of the incremental burned mass. The composition of the fresh air inducted into the engine is needed as data, in terms of molar fractions of oxygen, nitrogen, carbon dioxide and water. Nitrogen oxide formation is calculated separately for each fuel/air package separately by taking the local temperature. The formation of NOx emissions is calculated using the extended Zeldovich mechanism, taking into account the two zones of combustion (burned and unburned zone). The Arrhenius multipliers of the chemical reactions in the NOx emissions model are calibrated depending on the data of NOx emissions provided from the datasheet of the manufacturer. The NOx model accounts for the "prompt" or "flame formed" NO, which is due to the over equilibrium radical concentration in the flame zone. This quantity is obtained from a correlation, which gives the ratio of prompt NO to equilibrium NO according to equivalence ratio (between the two zone). The overall burned zone is treated as an open and stratified system in which further NOx formation takes place in function of pressure, temperature and equivalence ratio of the burned packet. All the NOx is assumed to be in the form of NO during the prompt formation phase as well as the thermal phase described by the Zeldovich mechanism of NOx formation (1-2). The steady state assumption is used for highly reactive N atoms. The concentration of NO versus time is solved using an open system in which the above elementary reactions are used with those rate constants reported by **Heywood (2018).** For the first reaction equation, the rate constant, R_1, is given by (4-10):

4-10 Rate constant, R_1

$$R_1 = A \cdot ARC1 \cdot e^{\left(T_a \cdot \frac{AERC}{T}\right)}$$

For the second and third reaction equations, the rate constant, $R_{2/3}$, is given by (4-11):

4-11 the rate constant, $R_{2/3}$

$$R_{2/3} = A \cdot e^{(T_a/T)}$$

where:

- A is the Pre-exponential constant;
- $ARC1$ is the pre-exponent multiplier (input);
- T_a is the activation temperature for the reaction;
- $AERC1$ is the exponent multiplier (input);
- T is the burned-zone temperature.

The calculation stops when the temperature in the burned zone reaches a low enough level so that the kinetics become inactive and total NO no longer changes. The HC emissions sub-model for diesel engines predicts HC emissions in an engine cylinder element using a simple correlation to injector sac volume. The sac volume fraction is the fraction of injector sac volume that contributes unburned hydrocarbons to the exhaust. This requires an applicable setting for the “Sac Volume” in the attached injector element. The emissions sub-model predicts CO production during combustion and exhaust in an engine cylinder element; this sub-model functions only on the contents of the cylinder, meaning that the relevant chemical equilibrium and kinetic reactions work only while the charge is in the cylinder. It is necessary to specify the passive scalar to which the CO is produced by this emissions sub-model.

4.3. Case study: engine and ship data

The RICARDO software has been used for the construction of a simulation model capable of predicting the performance and the emissions of a marine diesel engine (MTU39616VTE74L) for which measurement at the test bench and experimental measurement, during navigation of the ship (see Figure 4-3), are available.

Figure 4-3 Case study

The experimental campaign has been carried out on board a catamaran owned by Caremar. Below, in Table 4-1, the main characteristics of the ships [13] .

Table 4-1 Main characteristics of the ship

Achernar	Data	Units
Owner	Caremar	-
Hull	Catamaran	-
GT	623,95	[tons]
Loa	43,7	[m]
Breadth	10,9	[m]
Max Draught	1.64	[m]
Main Engine	2 – MTU16V396TE74L	-
Engine Power	2x2000	[kW]
Max speed	34	[kn]
Number of passengers	354	-

The total power installed on board is due to two diesel engines MTU39616VTE74L. In the acronyms: MTU corresponds to the manufacturer; 16 to the cylinders; V to the shape; 396 is the Series- as well as the displacement of one cylinder x 100; T is for turbocharger with exhaust gas; E for the type of air cooling; 7 indicates the use of the engine in maritime application; 4L is the serial number.

Table 4-2 Main diesel engine parameters

MTU39616VTE74L	Data	Units
Engine shape	V	-
Mixture type	Spray guided (DI)	-
Strokes per cycle	4	-
Number of cylinder	16	-
Power	2000 at 2000 rpm	[kW]
Bore	165	[mm]
Stroke	185	[mm]
One cylinder displacement	3,96	[l]
Total displacement	63,3	[l]
Compression ratio	12,3:1	-
Mean piston speed	12,33	[m/s]
Reference air temperature	305	[K]
Reference pressure	1000	[mbar]
Type of injection	Direct	
IVO - Intake valve open	36 BTDC (before top dead center)	[deg]
IVC - Intake valve close	68 ABDC (after bottom dead center)	[deg]
EVO - Exhaust valve open	75 BTDC	[deg]
EVC- Exhaust valve close	28 ATDC	[deg]
Overlap	64	[deg]
Valve intakes/exhaust count per cylinder	2 intakes +2 exhaust (4)	-
Specific fuel consumption	220 (max 231)	[g/kWh]

Analyzing the data in the Table 4-2, it is clear that the engine is a 4-stroke V 16-cylinder with a compression ratio of 12.3 and a consumption of 220 g/kWh. The power delivered at 2000 rpm is 2000 kW, injection is direct and each cylinder has 4 valves, two for inlet and two for exhaust. The turbocharger group consists of a turbine, driven by the exhaust gases of the engine, and a compressor mounted on the same axis. The exhaust gases which are coming from the cylinders, are conveyed to the turbine and, acting on the turbine blades, move the compressor. The compressor impeller sucks in the combustion air, compresses it and sends it to the cylinders.

4.3.1. Bench test

Bench tests have been carried out on both the engines on board and the main parameters acquired are revolution in rpm, torque in kNm, power in kW, mass flow rate in kg/h as well specific fuel consumption in g/kWh. Below the main results for one of the two diesel engines (Figure 4-4 and Figure 4-5).

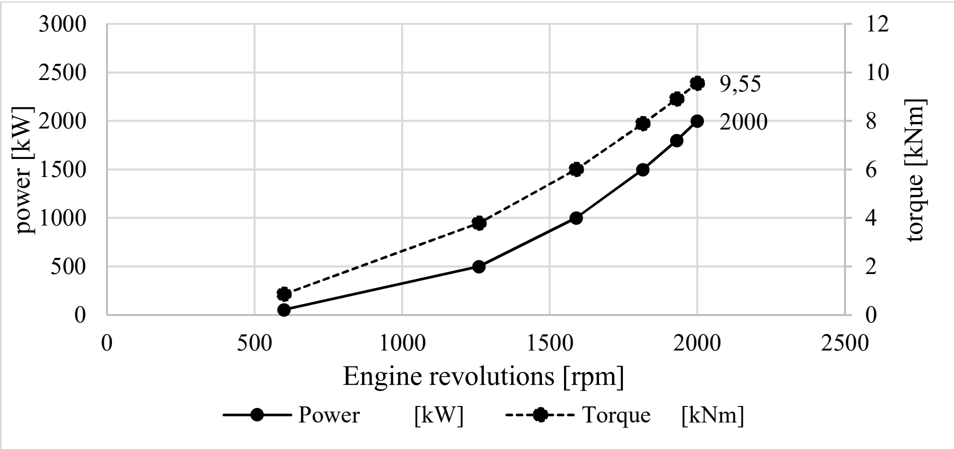

Figure 4-4. Test bench: power and torque

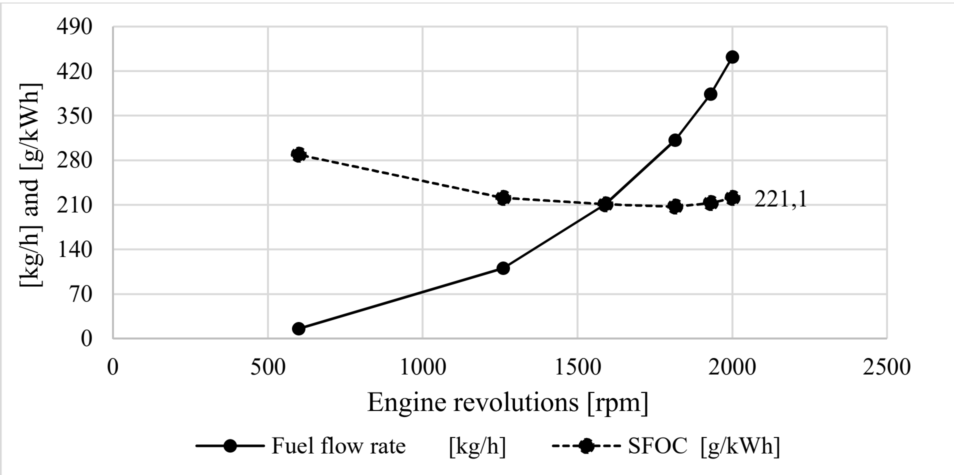

Figure 4-5. Test bench: fuel flow rate and specific fuel consumption (SFOC)

As highlighted in the graphs, at 2000 rpm, on the measurement bench, 2000 kW for engine power with specific fuel consumption of 221 g/kWh and a torque of 9.55 kNm are confirmed.

4.3.2. *Experimental campaigns*

The data logging campaigns were carried on the routes to and from the islands of Procida, Ischia and Capri, see Table 4-3 for timetable. A data logging system was capable to register the main parameters of propulsion and navigation; in some cases, an exhaust gas analyzer was used in order to log the concentration of the main pollutants in the exhausts. The main characteristics of the data logging system used for the campaigns are reported in the Table 4-4.

The monitored parameters were torque on the propeller shaft (kNm), power (kW), rpm (g/min), fuel consumption (cm^3/s) and exhaust gas temperature (^{O}C). The pollutants measured are, HC (ppm), CO (%vol), CO_2 (%vol), NO_X (ppm) were measured together with the concentration of O_2 in the air. Since both vessels work with low-sulphured fuels, SO_x was not recorded (**Cooper 2001**).

Below the main parameters recorded are reported as example of the available measures: torque and power (in Figure 4-6), speed (in Figure 4-7), specific fuel consumption (in Figure 4-8) and emission of NO_X (in Figure 4-9) during an entire route.

Table 4-3 Timetable (Na= Naples, Is= Ischia, Pr= Procida)

Voyage	Route and departure time	Date
1	Is-Na 08,50	26/06/2003
2	Na-Pr-Is 09,55	“
3	Na-Is 13,10	“
4	Is-Na 14,10	“
5	Na-Is 07,50	27/03/2003
6	Na-Is 09,50	“
7	Is-Na 12,05	“
8	Na-Is 13,10	“
9	Is-Na 14,10	“

Table 4-4 Data logging system

Parameter	Sensor and Manufacturer	
Torque	Extensimetric torque meter	Binsfeld Eng.
RPM	Magnetic pick-up	
T_{AIR} [^{O}C]	J thermocouples	Tersid
T_{WATER} [^{O}C]	J thermocouples	Tersid
$T_{EXHAUST}$ [^{O}C]	K thermocouples	Tersid
Ship speed	DGPS	
Ship position	DGPS	
NO_X, HC, CO, CO_2, O_2	Gas Analyser	TecnoTest
Data logger		Nat. Instruments

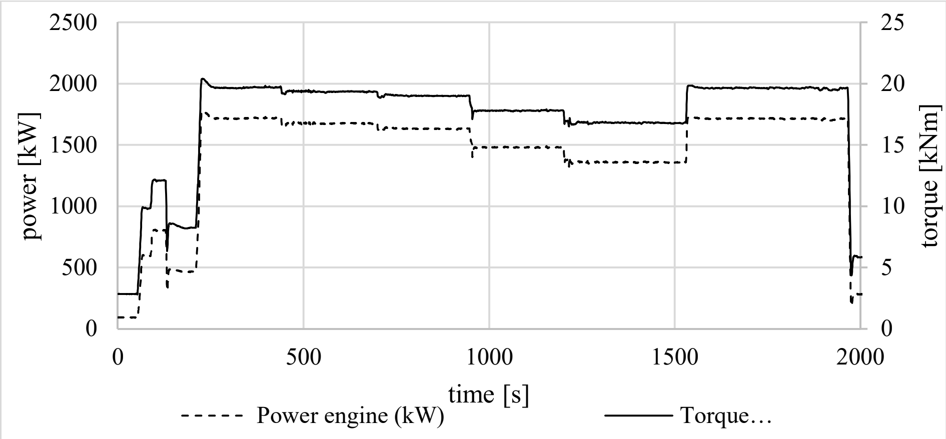

Figure 4-6. Temporal acquisition for power and torque

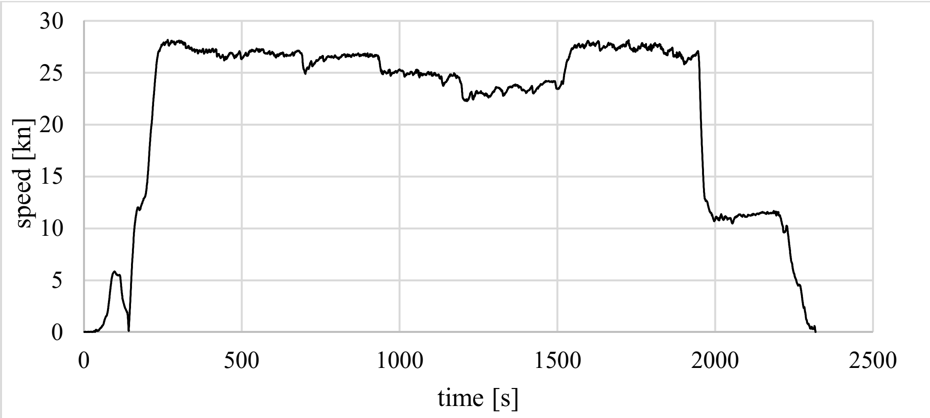

Figure 4-7 Temporal acquisition for speed

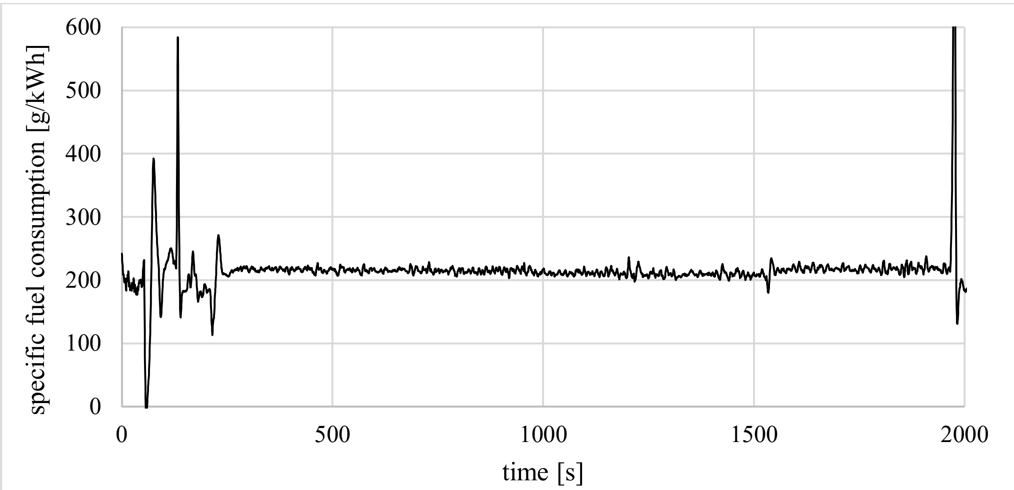

Figure 4-8 Temporal acquisition for specific fuel consumption (SFOC)

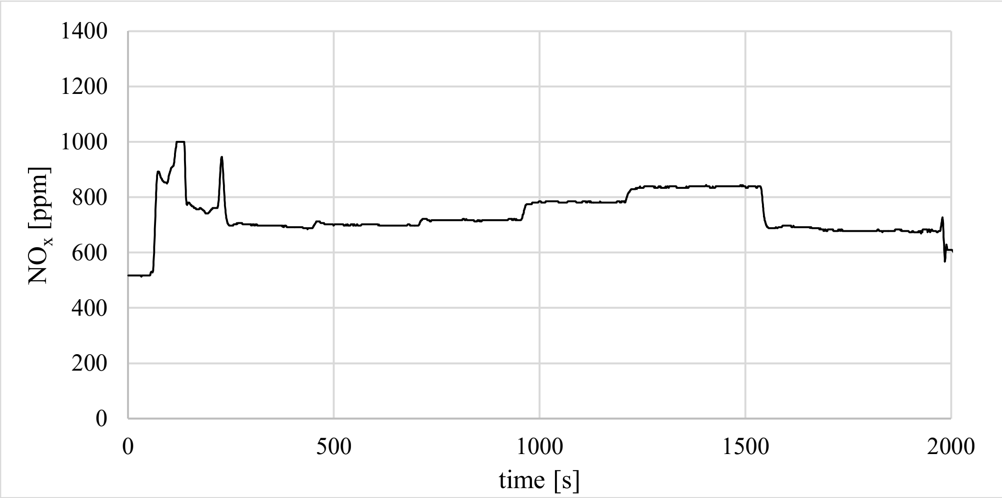

Figure 4-9 Temporal acquisition for NO_X emissions

The validation of NO_X emissions has been made both on the direct ppm measured on board and on the g/kWh obtained through a conversion. The aim of this check is to test the conversion method based on the calculation of the ratio Air-fuel through the measuring of the concentrations of all species in the exhausts gas. By this conversion method, NO_x emission is depending on the airflow rate, which can be considered depending on the air fuel flow ratio (A/F), estimated downstream of the emission measures by **Heywood (1988)** (4-12):

4-12 Air Fuel flow ratio

$$\frac{A}{F} = 4.773\left(\frac{\mu_{air}}{\mu_f}\right) \cdot \frac{(CO_2) + \left(\frac{CO}{2}\right) + \left(\frac{H_2O}{2}\right) + \left(\frac{NO}{2}\right) + (NO_2) + (O_2)}{(HC) + (CO) + (CO_2)}$$

Where

- μ_{air} is the air molecular weight; μ_f is the fuel molecular weight fixed to 13.89.

Between brackets, the measured concentrations of the single chemical compounds.

The concentrations of NO and NO_2 have been neglected, while the molar percent water in the combustion products has been estimated as (4-13):

4-13 Molar Percent water

$$(H_2O) = 0.5y \cdot \frac{(CO_2) + (CO)}{(CO)/(K[\,(CO_2)] + 1}$$

where

- K is a constant value equal to 3.50, and y = H/C ratio of the fuel (1.87).

Thus, it is possible to assess the flow rate of air (m_a) (4-14):

4-14 Flow rate of air

$$\dot{m}_a = C_s \cdot P \cdot (A/F) \cdot 10^{-3}$$

where

- C_s is the specific fuel consumption measured is g/kWh, P is the engine power measured kW, and A/F is the air fuel ratio obtained through the previous formula.

The final relationship for NO_x conversion into g/kWh is (4-15)

4-15 NO_X in g/kWh

$$NO_x = (\dot{m}_a \cdot NO_x \cdot 10^{-6})/(\rho_{air} \cdot P)$$

where

- m_a is the air flow rate in kg/h, NO_X the concentration of NO_X in μg/m^3 obtained from the ppm, ρ_{air} is the air density in kg/m^3 and P is the engine power in kW.

4.4. Diesel engine model

An overall of the diesel engine model is reported below Figure 4-10.

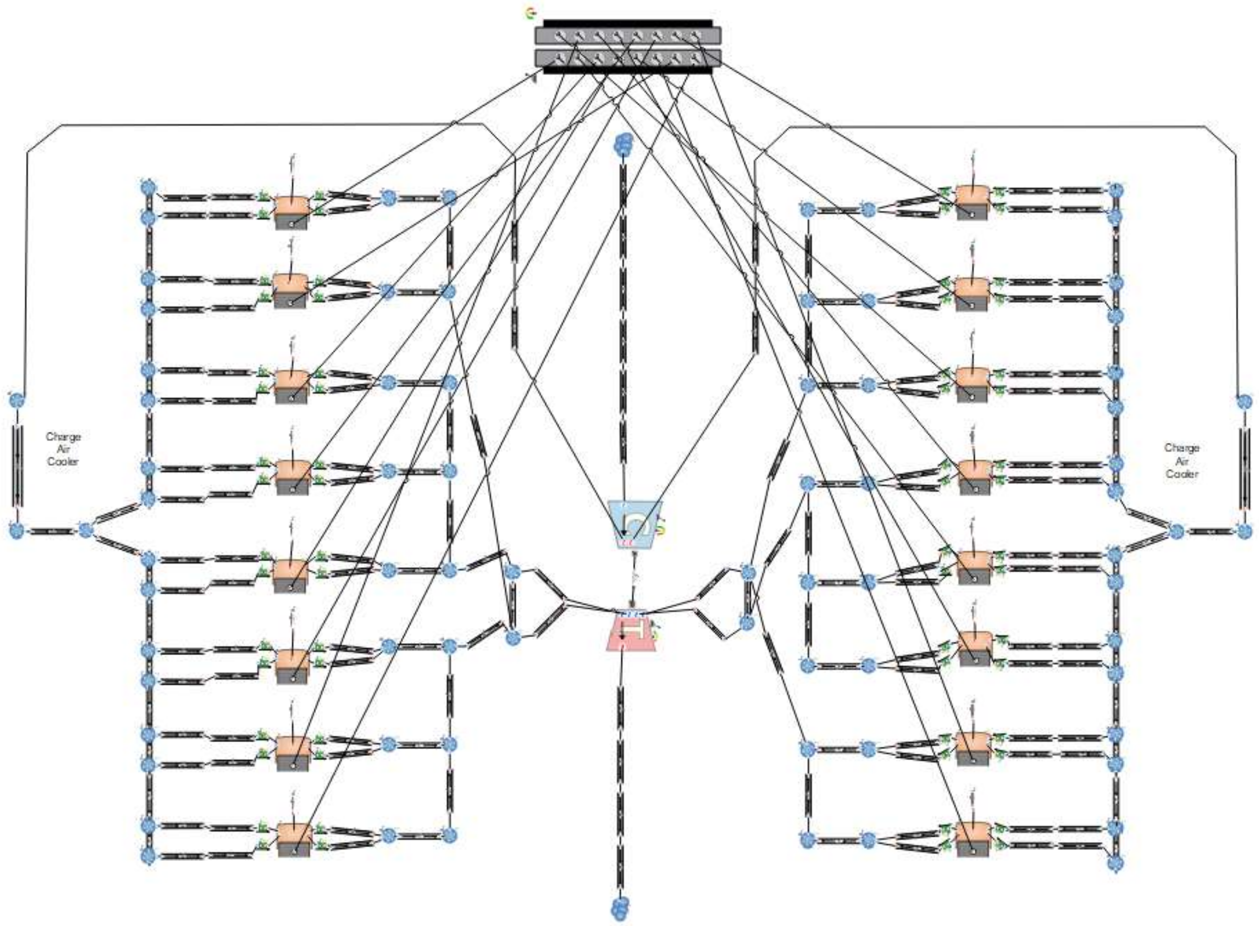

Figure 4-10 overall of the diesel engine model

In the top center area is the engine block connected to all the cylinders, which are distributed on two banks, left and right (Figure 4-11). Each cylinder has four valves and one direct injector on the top. The turbocharger group is linked to the ambient (clouds on the top center), the compressor is linked to the intercooler while the turbine is connected to the exhaust gas manifold and the ambient (clouds on the down center) (Figure 4-11). For the initial conditions of a fluid used within a cylinder, the unique parameter set in a different way, than the defaults values, is the temperature, which has been set according to an average value measured during the experimental campaign equal to 305 K. Therefore, the parameters, used as the initial conditions of a fluid used within a cylinder, are pressure of 1 bar, the temperature of 305 K, and initial velocity of 0 m/s. In the figures Figure 4-12 and Figure 4-13, the input parameters for engine and cylinders, such as for example number of valves, firing order, bore, stroke. All these inputs are available, for the case study, in Table 4-2.

Figure 4-11. Scheme of the model

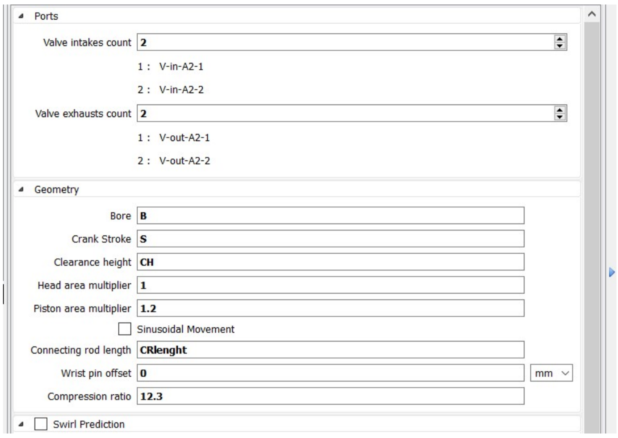

Figure 4-12 Screenshot of the edit sheet for cylinder in the software

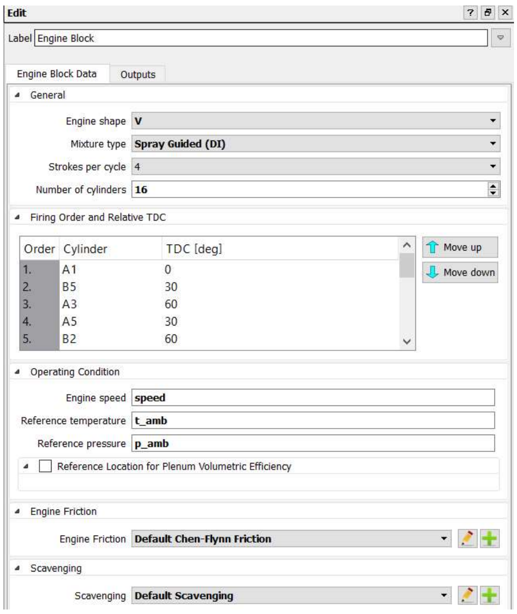

Figure 4-13 Screenshot of the edit sheet for engine in the software

A modified form of the **Chen-Flynn correlation (engine friction)** is used to model friction in the WAVE engine (see Table 4-5).

Table 4-5 Chen-Flynn correlation

ACF	BCF	CCF	QCF
0.5 bar	0.006	600 Pa.min/m	0.2 Pa.min^2/m^2

For the **scavenging**, in this model, a “fully mixed” configuration, where the mass leaving the cylinder is a perfect mixture of the mass in the cylinder, has been chosen. In absence of data about the lift (in mm) of the four **valves**, the same data of an engine present in the software library has been redistributed on the correct crank angle values available for the engine modeled (see Figure 4-14 and Table 4-6). This engine is an engine with the same number of cylinders, the same V shape but different displacement compared to our case study (50L instead of 63.3L) and will also be used in the characterization of the turbocharger. In table and in figure the characterizations of the lifts of intake and exhaust valves.

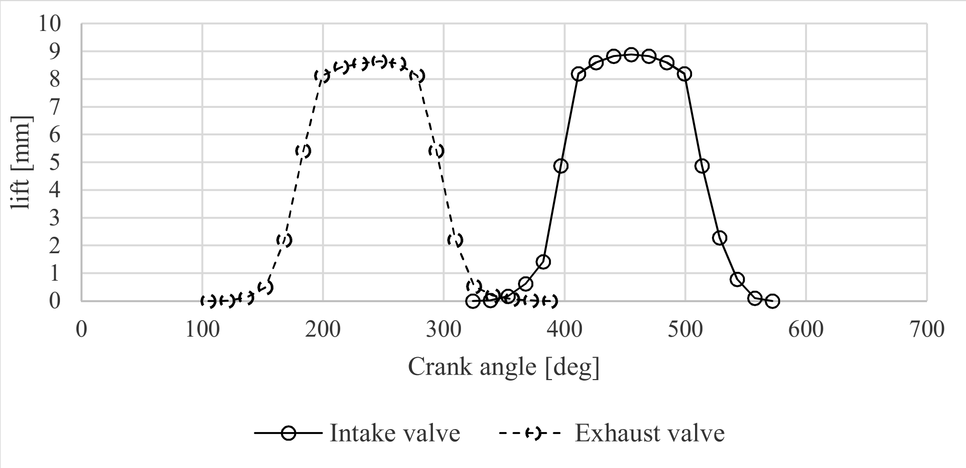

Figure 4-14. Lift of the valves

Table 4-6 Lift of the valves

Intake valve		Exhaust valve	
Crank angle [deg]	lift [mm]	Crank angle [deg]	lift [mm]
324	0	105	0
338,59	0,02	120,7	0,01
353,18	0,17	136,4	0,13
367,76	0,62	152,2	0,5
382,35	1,42	167,9	2,2
396,94	4,87	183,6	5,42
411,53	8,19	199,3	8,13
426,12	8,6	215,1	8,44
440,71	8,83	230,8	8,56
455,29	8,89	246,5	8,64
469,88	8,83	262,2	8,56
484,47	8,6	277,9	8,13
499,06	8,19	293,7	5,42
513,65	4,87	309,4	2,2
528,24	2,28	325,1	0,53
542,82	0,78	340,8	0,19
557,41	0,1	356,6	0,07
572	0	372,3	0,02
		388	0

In the model, fuel **injectors** can be attached to cylinders, see Figure 4-15.The nozzle diameter is set at 1.1 mm and the spray spread angle at 152^{O}, according to the manufacturer, is used to evaluate the spray wall impingement area, see Figure 4-15.

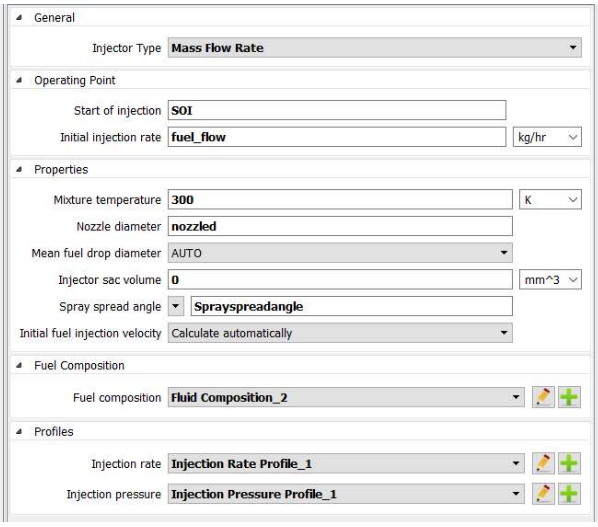

Figure 4-15 Screenshot of the edit sheet for injectors in the software

For **turbocharger** (Figure 4-16), data are generally available from the manufacturers in the form of performance maps or tabulated data. The dimensionless balance parameter is used for a balancing process where the torque balance on the shaft is done only once per engine cycle, using cycle averaged torque values; in this configuration the balancing calculation is an approximation as it ignores fluctuations in shaft speed throughout the cycle, and will not accurately predict turbocharger lag due to the shaft inertia. It is useful however, because with this process the turbocharger speed can rapidly converge to a steady state operating point (Figure 4-17). Four input values are required for each operating point: pressure ratio, speed, mass flow and efficiency. Unfortunately, in this case, no data from the manufacturers are available except the max speed of the TC.

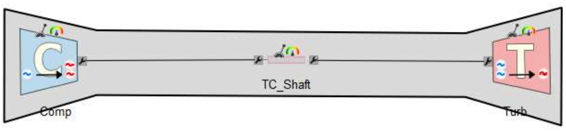

Figure 4-16. Turbocharger group

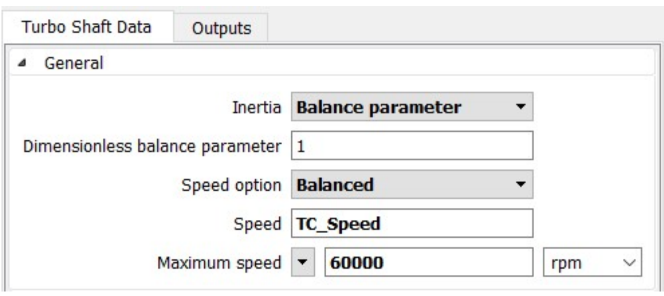

Figure 4-17 Screenshot of the edit sheet for turbo shaft in the software

The turbine and the compressor setting panel contain the following details:

- the reference temperature and pressure for input data (293 K and 100 kPa);
- the ratio of specific heats for input data: ratio between the specific heat at constant pressure, Cp, and the specific heat at constant volume, Cv. The specific heat ratio is used for the calculation of the reference diameter and for curve fitting;
- gas Constant: 287 J/kgK;
- for turbine setting panel, the highest Blade Speed Ratio: the maximum blade speed ratio value to which the map is extrapolated (1.8);
- blade Speed Ratio at Point of Maximum Efficiency: this value must be smaller than the "Highest Blade Speed Ratio" entry and is close to 0.7 in most turbocharger turbines.
- the maximum pressure ratio to which the map is extrapolated (7);
- for compressor setting panel, the highest speed curve: 60000;
- scaling factor;
- point of maximum efficiency for the two map; pressure ratio, mass flow and speed at the point of maximum efficiency.

In the absence of details about the turbocharger, except for a max speed of 60.000 rpm, the developed procedure used turbine and compressor scaled maps (starting from those belonging to another engine, the same used for the valves), as usual in this application when no data are available from the manufacture. The carried out scaling affected the following parameters:

For the compressor, see Figure 4-18: Highest Speed curve from 80.000 to 60.000 rpm; Mass flow data scaling factor from 1 to 4; Speed data scaling factor from 1 to 0,7;

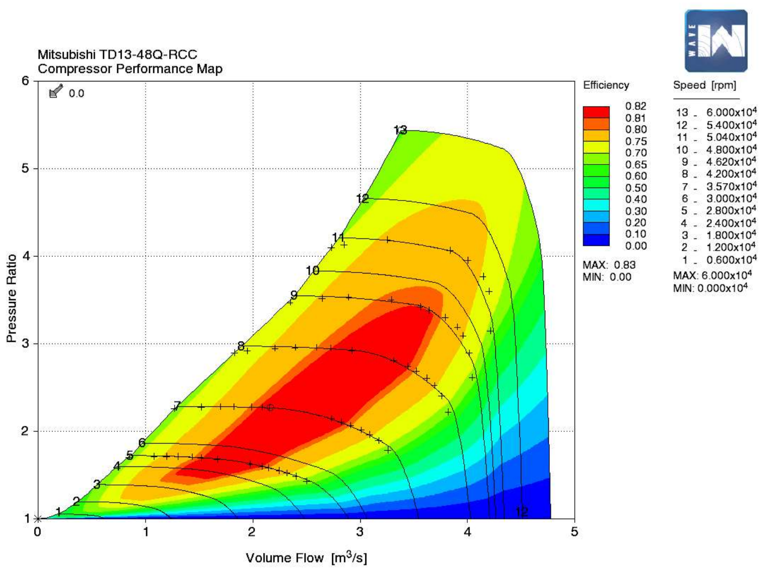

Figure 4-18 Compressor map

- For the turbine, see Figure 4-19: Mass flow data scaling factor from 1 to 4.0; Speed data scaling factor from 1 to 0,75;

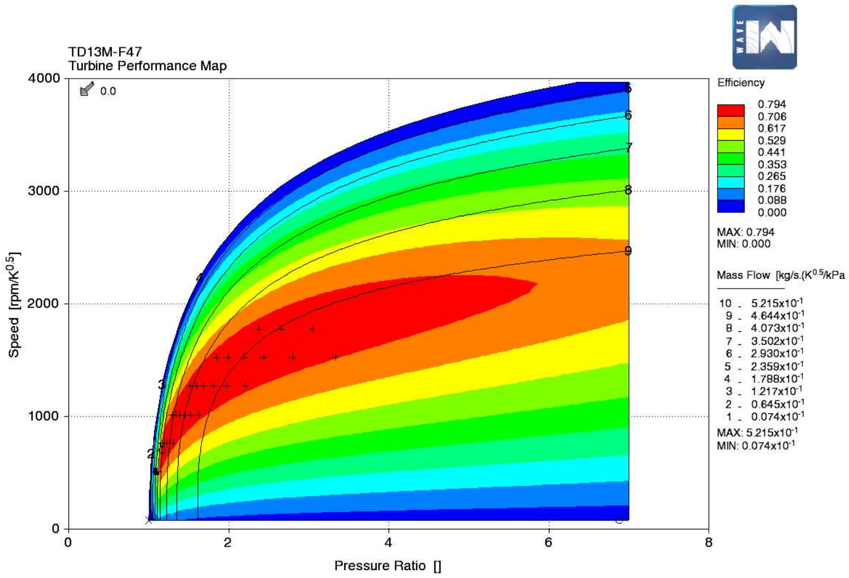

Figure 4-19 Turbine map

In this model**, two zone Diesel Wiebe and Original Woschni heat transfer** have been chosen (see Figure 4-20).

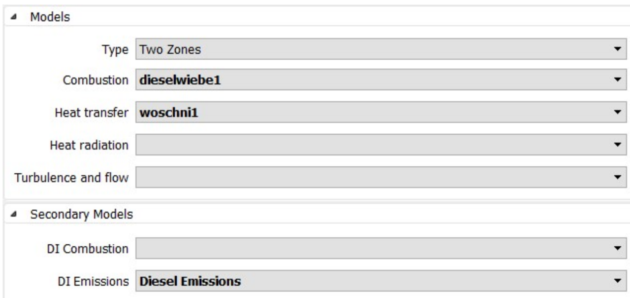

Figure 4-20 Combustion, heat transfer and emission setting in the software

For the **emissions** of NO_X, according to the input are:

- Arrhenius pre-exponent multiplier: 1.5.
- Arrhenius relationship rate constant multiplier: 1.0.

For HC, he recommended value, also used in this model, is “0.2”.

4.4.1. The simulations results: calibration with bench tests and validation with sea trials

These are the minimum conditions required to get the basic model running. It is necessary to have temperatures in several locations in the exhaust system since it varies greatly and it also has a significant effect on predicted performance. If a complete range of temperatures is not known, then it is recommended that WAVE structural conduction model is activated. This module allows the exhaust ducts to reach an equilibrium temperature during the engine simulation. In case of lack of measured data available, a range of typical operating temperatures for various parts of the engine is given in tutorial an example model. In-cylinder temperatures are rarely measured but typical values can be found. Combustion data should be measured from and correlated to a test engine. The Figure 4-21 shows the diagram of the pressure in the cylinder as a function of the crank angle at 2000 rpm.

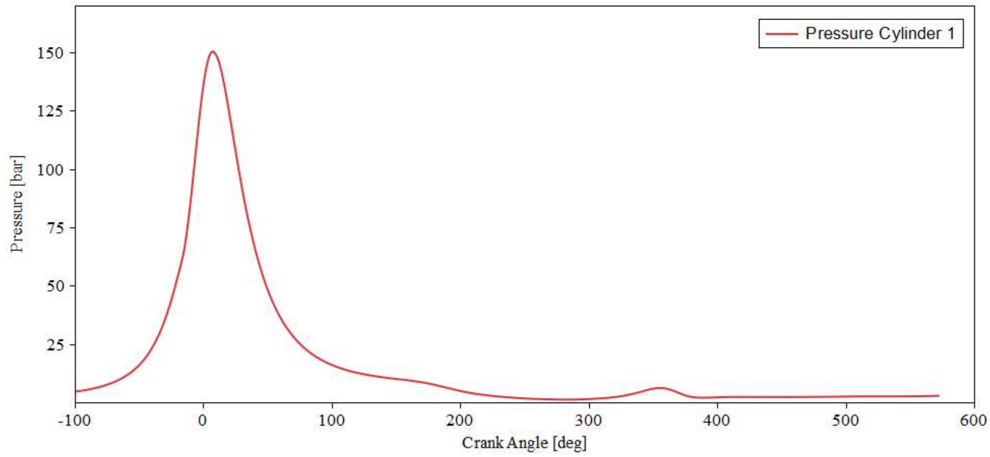

Figure 4-21 Pressure in the cylinder as function of the crank angle

4.4.2. Comparisons with test bench

After building the model, several runs were performed in order to calibrate the model with the bench test data. In the the marked data are not data from the engine product guide and were used as tuning for the construction of the model. The diameters of the inlet and outlet valves were taken from engine drawings and were found to be equal to 75 and 70 mm respectively. Below are reported the results of the comparisons between the test bench results for power and torque and specific fuel consumption (SFOC) (see figs. from Figure 4-22 to Figure 4-24). It is clear that the results are with good approximation acceptable.

Table 4-7 Model input

Parameter	Units	Value at 2000 rpm
Duration of simulation	sec	30
Ambient Pressure	bar	1
Ambient Temperature	K	305
Duration of Ignition*	deg	30
Speed	rpm	2000
Turbocharger speed	rpm	60000
Fuel/air ratio*	-	0.033
Fuel flow	kg/h per cyl	27.625
Inlet valve diameter	mm	75
Outlet valve diameter	mm	70
Spray spread angle	deg	152
T piston*	K	500
T cylinder*	K	540
T head*	K	550
Compression ratio	-	12.3

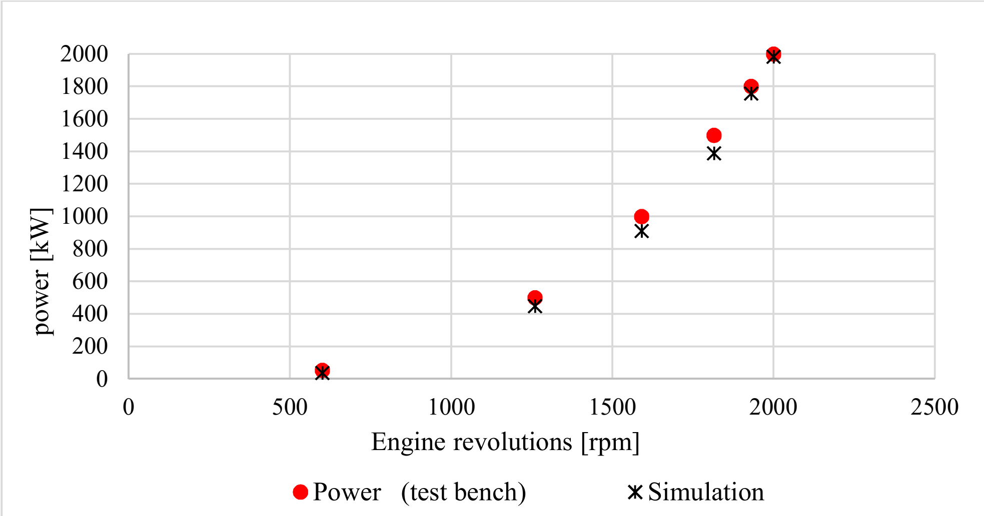

Figure 4-22 Engine power. Comparison between test bench results and simulation

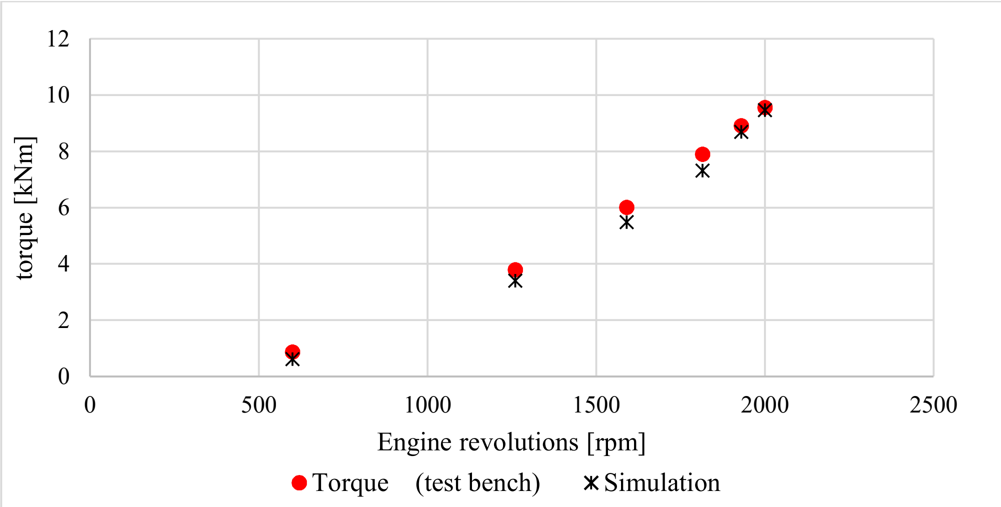

Figure 4-23 Engine torque. Comparison between test bench results and simulation

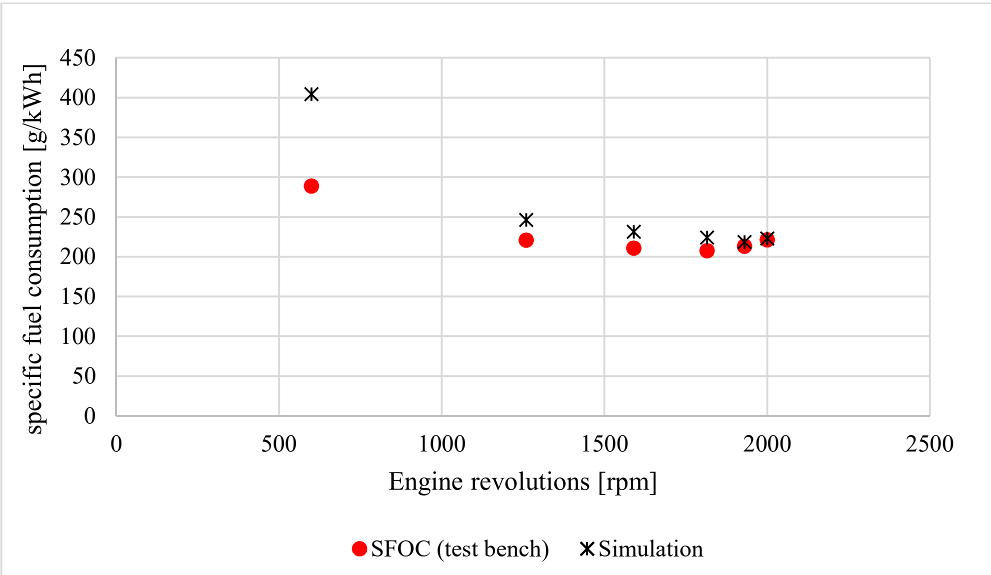

Figure 4-24 Specific fuel consumption. Comparison between test bench results and simulation

The graph in Figure 4-25 shows the absolute values of the errors but the model always underestimates torque and power and overestimates consumption.

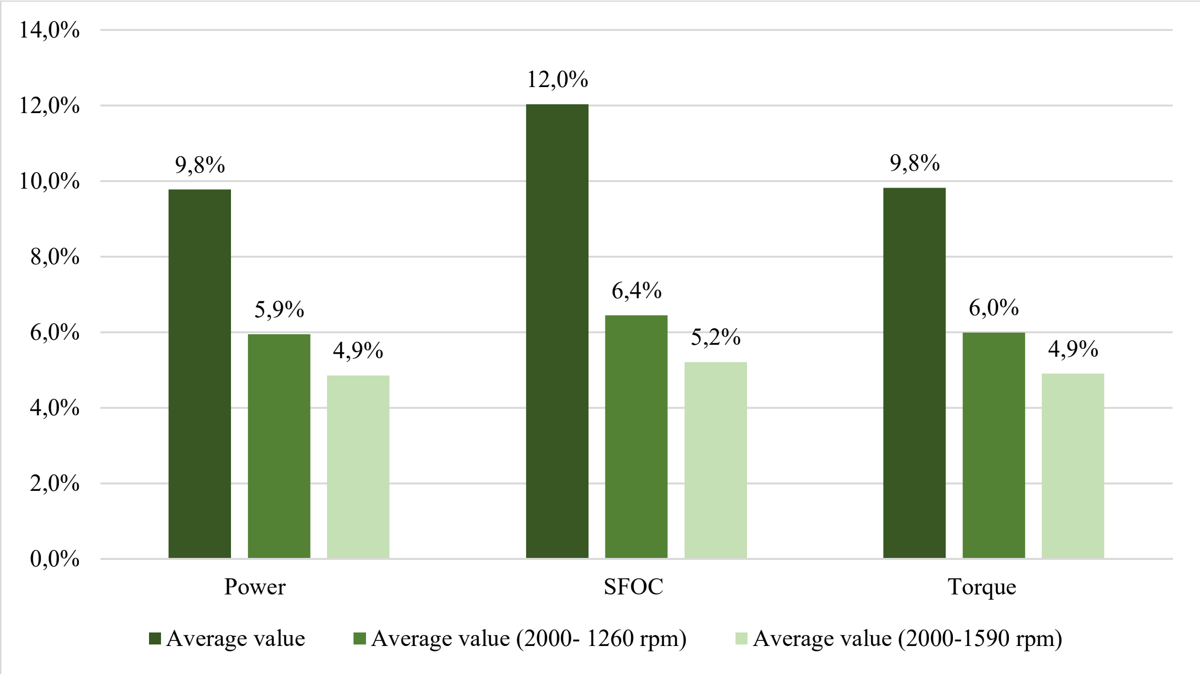

Figure 4-25 Absolute errors (%) for power, torque and consumption (bench tests and model)

Both the graphs (in figs. from Figure 4-22 to Figure 4-24) and the percentage errors (in Figure 4-25) show how the model simulates the engine well in terms of typical parameters such as power, consumption, and torque. Clearly, the error increases with decreasing engine load but as an average value we are on 9.8% for power or torque, and 12% for consumption. This error is reduced if the average values in the 2000-1260 rpm intervals are calculated and even more if it is reduced to the results obtained between 2000 and 1590 rpm up to an error of 5% for all three quantities. The error on the power clearly affects the specific consumption itself.

4.4.3. Validation with sea trials

Once the model was chosen, the second validation step involved simulations of the engine at different rpm aimed at verifying the congruence of the simulated data compared to those measured in the experimental campaigns. For the validation of the model through the measurements carried out at sea, given the large amount of data, the areas of steady-state of the engine have been used to extract an average behavior of the engine. Starting from these data, an average value (in rpm range with a step of 100 rpm) was then calculated for each of the parameters involved. The Table 4-8 shows the average values calculated in the temporal transients acquisitions. Each line therefore represents the behavior of the engine averaged over time in a particular section of the route in which the rpm remained substantially constant. To validate the model, it was decided to group this data in six cases. The average behavior obtained, has been used as input for the simulation model. Starting from the consumption in g/kWh, and the relative power the hourly flow rate for each cylinder has been obtained. This flow rate together with the rpm correspond to the simulation inputs.

Table 4-8 Steady-state data obtained from sea trials

	rpm [rpm]	Power [kW]	Consumption [g/kWh]	SFOC [kNm]	NOx [ppm]	NOx [g/kWh]
Case 1	664,0	3,5	425,0	0,1	183,2	1,1
	664,1	6,4	217,1	0,1	205,1	1,3
	693,0	83,1	178,5	1,1	565,2	15,6
	693,0	83,9	179,5	1,2	541,4	3,5
	693,1	80,5	233,2	1,1	493,8	19,2
Case 2	1033,5	254,9	214,1	2,4	741,0	12,9
	1118,0	325,0	203,4	2,8	812,8	12,5
Case 3	1400,7	638,3	206,0	4,4	862,4	5,5
Case 4	1707,8	1174,5	204,7	6,6	988,6	5,4
	1799,1	1379,3	208,6	7,3	950,9	5,4
	1799,2	1359,2	209,1	7,2	837,5	5,0
Case 5	1851,2	1481,1	211,4	7,6	781,1	4,8
	1855,3	1504,6	210,2	7,7	909,2	9,8
	1858,9	1501,6	212,4	7,7	752,6	6,9
	1898,1	1610,9	212,5	8,1	838,7	4,8
Case 6	1901,6	1613,3	213,6	8,1	739,8	8,5
	1903,2	1627,3	212,7	8,2	811,2	8,9
	1911,1	1633,4	214,8	8,2	717,3	4,4
	1916,3	1662,1	213,6	8,3	773,5	8,5
	1916,5	1655,5	214,6	8,2	728,8	8,4
	1927,5	1676,8	215,6	8,3	700,0	4,3
	1942,3	1729,0	217,1	8,5	723,5	8,3
	1942,5	1719,3	216,2	8,5	697,1	4,3
	1942,6	1720,3	217,3	8,5	687,2	7,9
	1942,6	1720,5	216,5	8,5	698,8	8,0
	1942,6	1736,2	215,7	8,5	749,2	5,7
	1942,7	1722,9	216,8	8,5	690,8	8,0
	1942,8	1730,8	215,2	8,5	727,0	8,2
	1942,9	1732,6	215,1	8,5	779,6	6,2
	1942,9	1715,0	218,0	8,4	684,7	4,3
	1942,9	1717,8	218,1	8,4	666,9	7,8
	1942,9	1732,5	215,1	8,5	755,4	8,3
	1943,0	1731,8	215,8	8,5	729,9	8,2
	1943,0	1728,9	215,5	8,5	722,7	13,8
	1943,2	1728,3	215,4	8,5	765,6	8,3
	1943,7	1728,3	215,0	8,5	750,0	14,5

In Table 4-9, the average value extracted.

Table 4-9 Behaviours averaged over the rpm

	rpm [rpm]	Power [kW]	SFOC [g/kWh]	NO_X [ppm]	NO_X [g/kWh]	Torque [kNm]
Case 1	681,4	51,5	246,7	397,8	9,9	0,7
Case 2	1075,7	290,0	208,8	776,9	10,0	2,6
Case 3	1400,7	638,3	206,0	862,4	5,5	4,4
Case 4	1768,7	1304,3	207,5	925,7	5,3	7,0
Case 5	1865,9	1524,5	211,6	820,4	6,5	7,8
Case 6	1934,2	1703,0	215,6	728,5	7,8	8,4

Extracting an average behavior in steady-state involves an error resulting from the quality of the measured data; the graphs below, Figure 4-26, show the standard deviations obtained for each of the six intervals from which they were extracted the cases in Table 4-9.

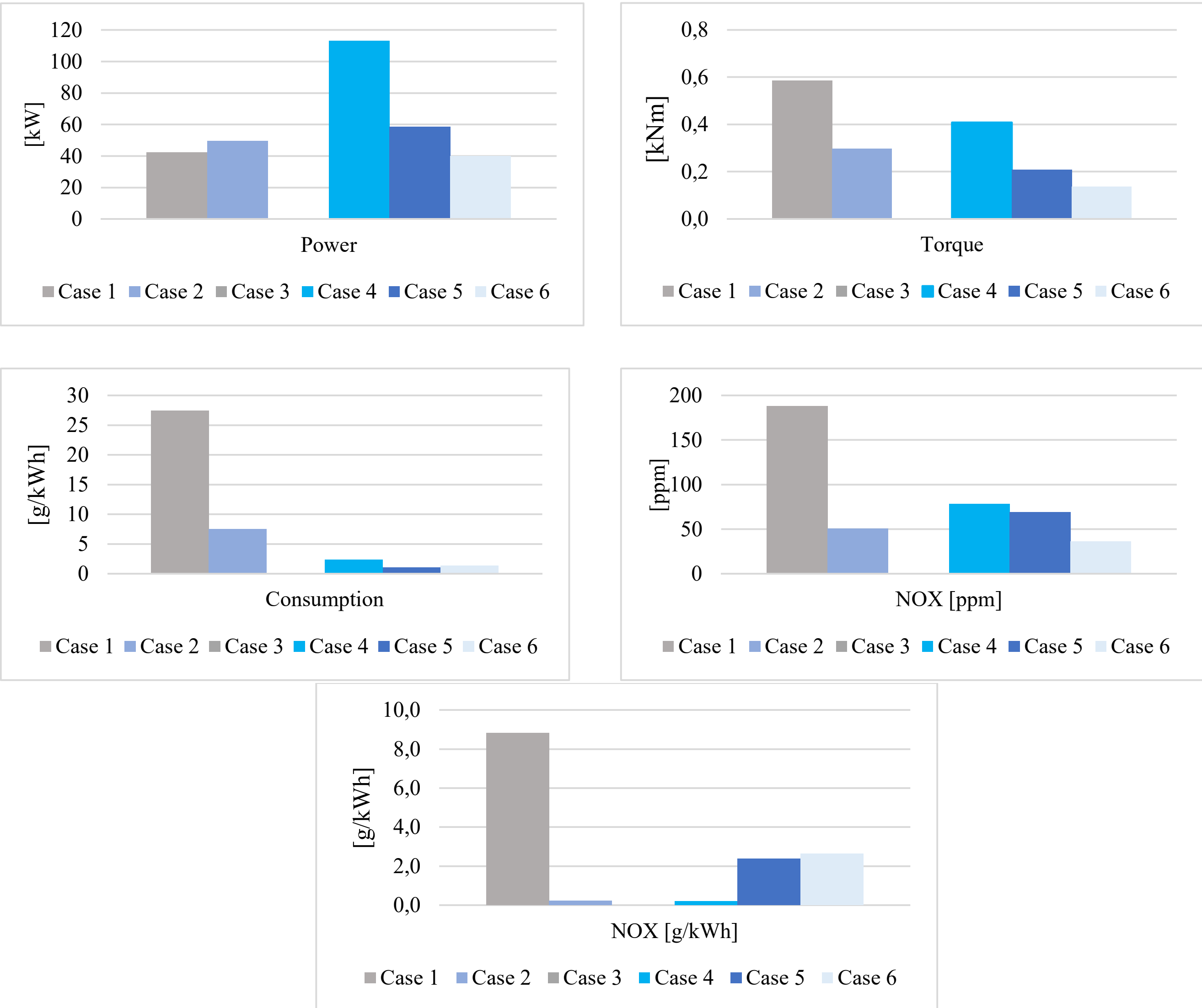

Figure 4-26 Standard deviation in the six steady state cases for power, torque, consumption and emissions

The power and torque data in Figure 4-26 show an anomaly in Case 4 (1701-1799 rpm) probably due to a small acceleration or deceleration phase while the consumption data show a high deviation of the data relating to Case 1 (601-699 rpm); this high standard deviation is the result of measurement errors of the fuel flow meter at low revs and the not too stationary behavior of the engine at low revs. As evident in the graph, however, this deviation is greatly reduced for subsequent cases. Both the measurements in ppm and the g/kWh of NO_X have a very high deviation in Case 1: this behavior is also linked to transients and measurement errors, see Figure 4-26. The simulation results, especially the percentage errors will be calculated in comparison with an average behavior first in time and then in the number of revolutions interval. For this reason, it is useful to know the criticalities and weaknesses of these experimental data at the outset. Having identified the points in which to carry out the simulations, the results obtained are reported below, having obviously kept the model calibrated on the bench tests unchanged.

4.4.4. Results

Below are reported the simulations results compared to these steady state conditions. In particular, power in Figure 4-27 , consumptions in Figure 4-28, torque in Figure 4-29 and emissions of NOx in Figure 4-30 and Figure 4-31 are reported.

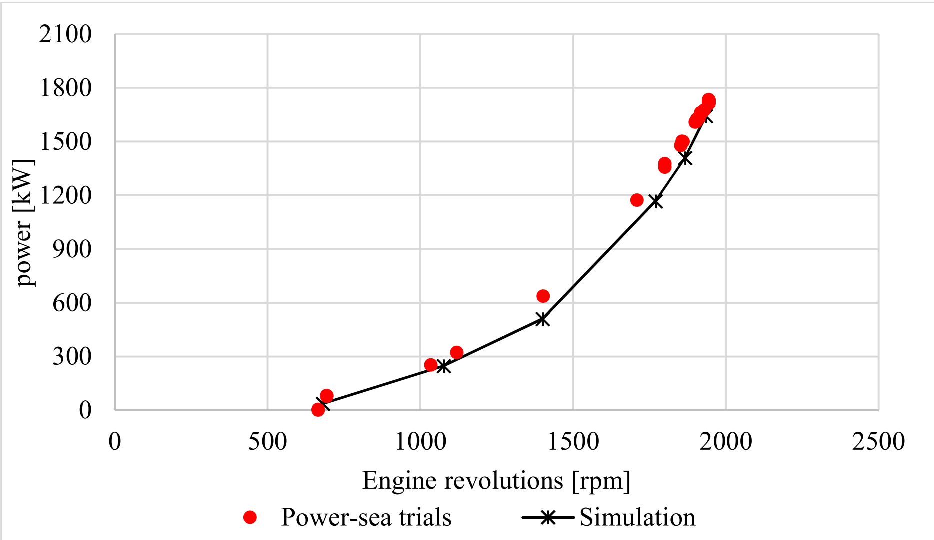

Figure 4-27 Comparisons between sea trials and simulation results: power

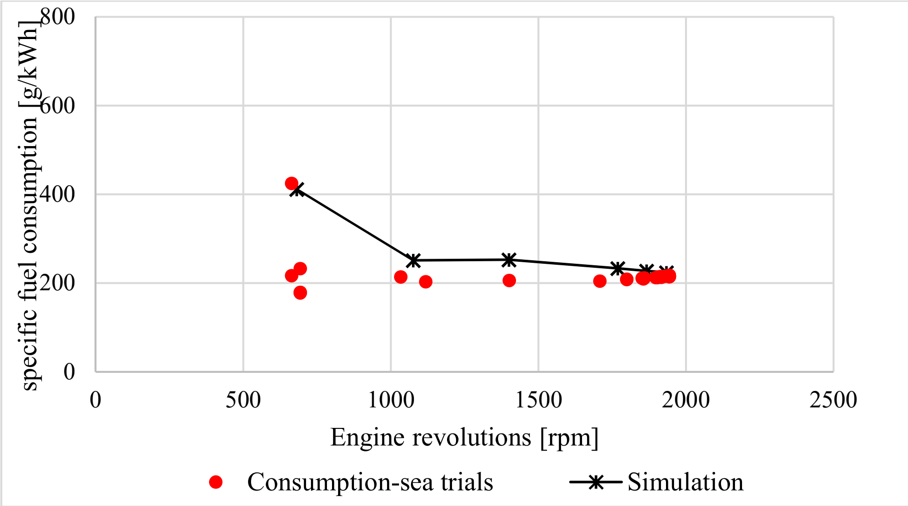

Figure 4-28 Comparisons between sea trials and simulation results: specific fuel consumption

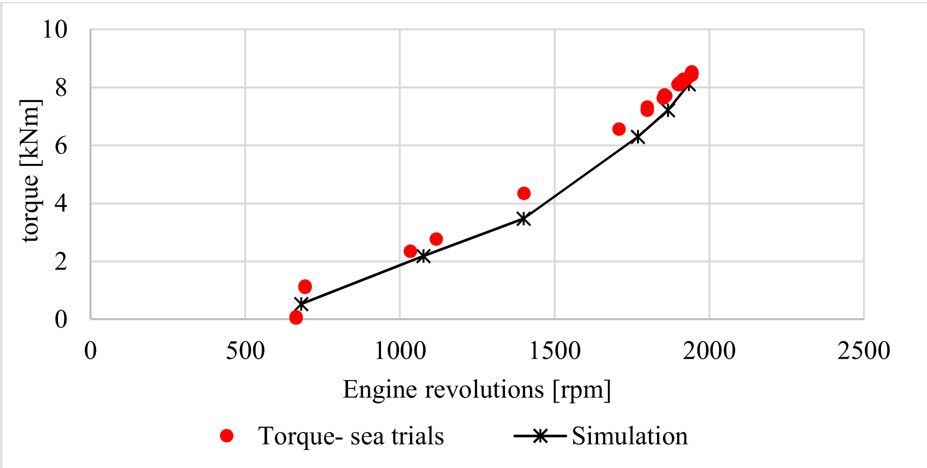

Figure 4-29 Comparisons between sea trials and simulation results: torque

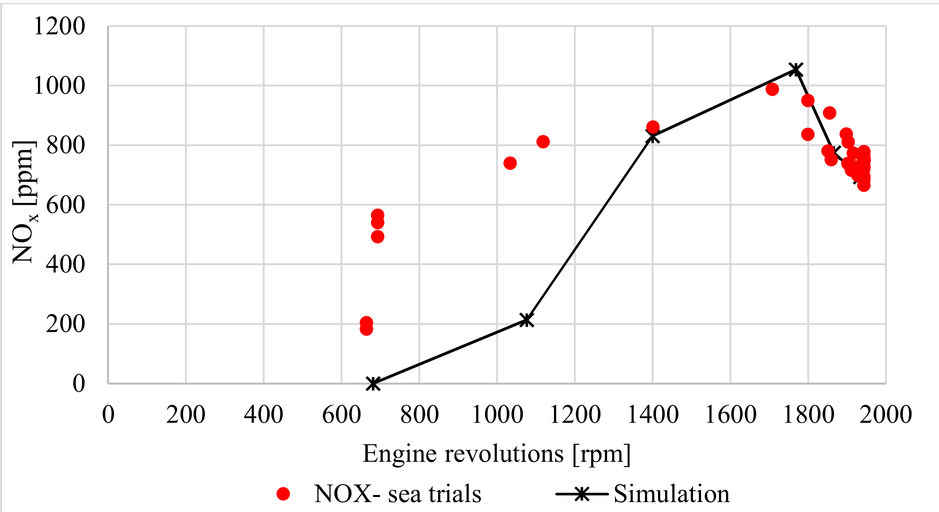

Figure 4-30 Comparisons between sea trials and simulation results: NO_X in ppm

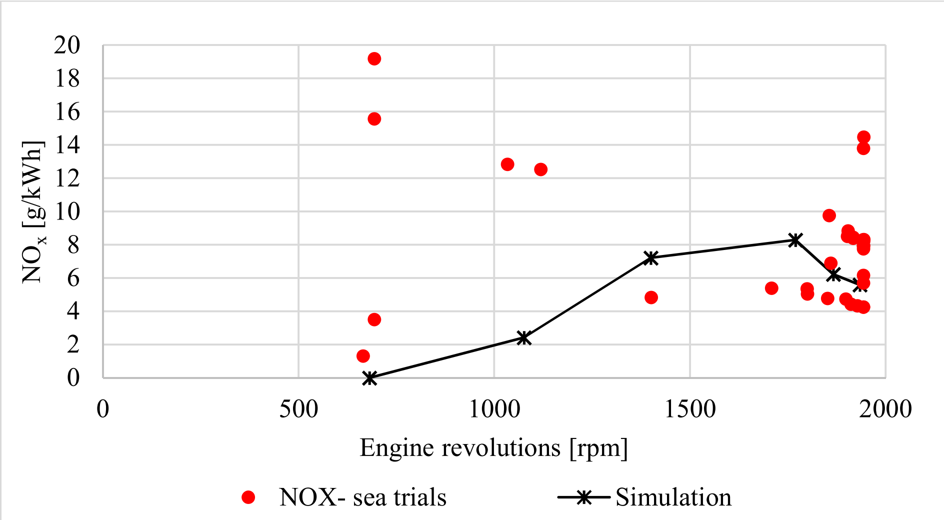

Figure 4-31 Comparisons between sea trials and simulation results: NO_X in g/kWh

The dispersion of the NO_X emission data in g/kWh (see Figure 4-31) absent in the measurements in ppm (see Figure 4-30), shows how the data is very influenced by the measurements of the other pollutants in the exhausts which are not always correct especially at the low load of the engine. In graph of Figure 4-32 the absolute errors for each case have been reported. Also in this case the model underestimates torque and power, overestimates consumption and on average underestimates the ppm of NO_X produced. As evident, power, torque and specific fuel consumption from maximum load to the motor and up to about 65% have relatively small errors. At a reduced rpm the simulation errors increase due to transient behavior at low loads that both the measuring instruments and the simulation are unable to consider overall.

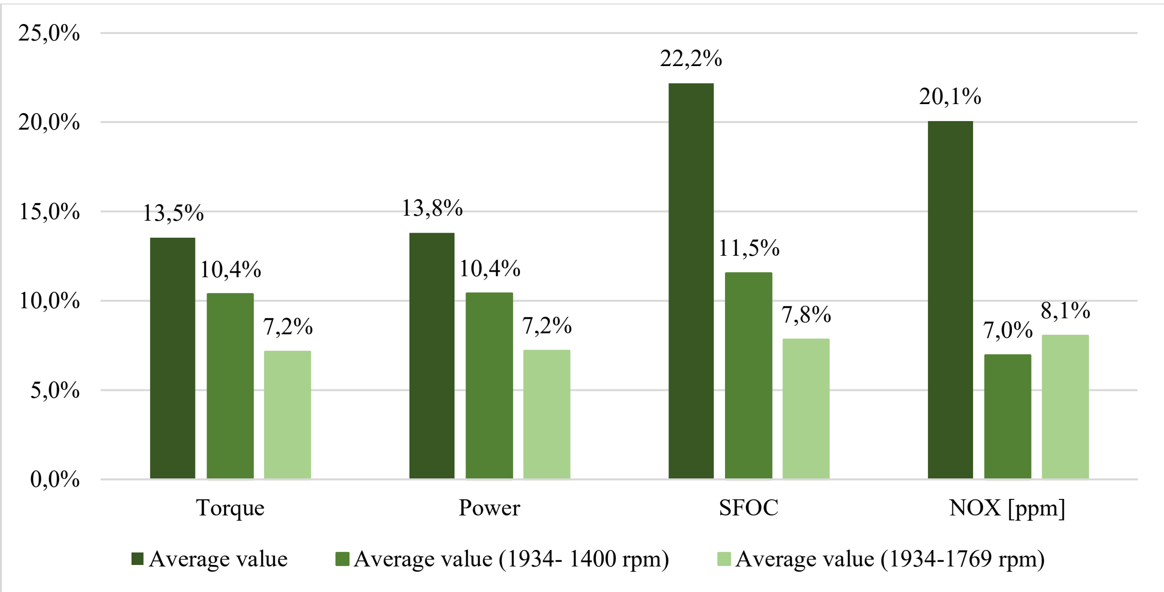

Figure 4-32 Absolute errors (%) for power, torque and consumption (sea trials and model)

From the graph in Figure 4-32 it is clear how the error increases with decreasing engine load, as expected. In particular, the average values of error related to torque, power, SFOC and ppm of NO_X are 13,5%, 13,8%, 22,2% and 20,1%; however, if these average errors are evaluated up to 1400 rpm (about 32% of the engine load), these average errors are reduced to 10,4%, 10,4%, 11,5%, and 7% respectively and if these average errors are evaluated up to 1764 rpm (about 65% of the engine load), these average errors are reduced to 7,2%, 7,2%, 7,8%, and 8,1% respectively.

These errors, together with the trend of the points on the graphs, make us consider the behavior and response of the model to the validations as acceptable. Another way to analyze the fit of the results compared to the totality of the stationary data is the graph of Figure 4-33 that relates the ppm of NO_X and the power. Two second-order polynomials estimated for the two point clouds have been inserted in the graphs to highlight how both the trend and the absolute values of the two curves are very similar.

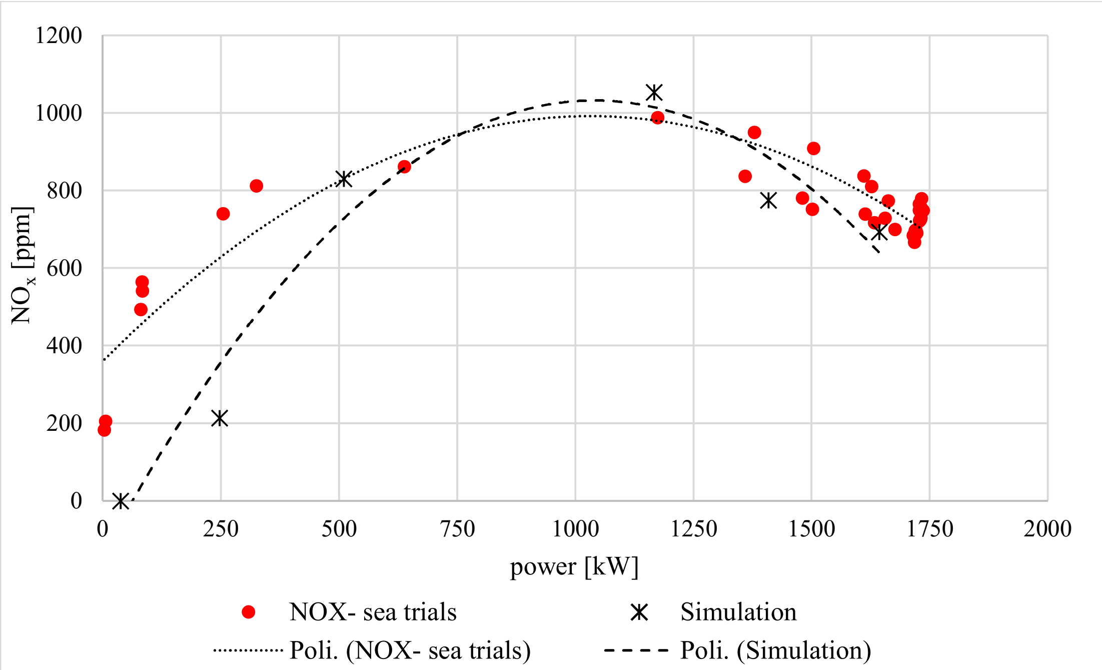

Figure 4-33 Emissions of NO_X vs power

Both graphs show that when the rpm is reduced, the simulation provides lower results than those measured. This phenomenon, for the ppm, is to be attributed to any errors made in the choice of the typical temperatures in the cylinders. For the emissions in g/kWh, instead, the differences can have numerous causes:

- Errors in power estimation done by the engine simulation model (see Figure 4-27 and Figure 4-32);
- Errors in the methodology and in the assumptions made for calculating g/kWh starting from the ppm measured at sea;
- Measurement errors of the instrumentation on board not only concerning the ppm of NO_X but also concerning the other pollutants given that these emissions in g/kWh have been estimated starting from the whole composition of the exhaust gas.

The quality of HC and CO measurement does not allow easy comparisons with the simulation results. The results obtained through the simulations are shown in the graph of Figure 4-34. These results are comparable with the indications of [14] which in the case of HSD powered by MGO associates consumption of 203 g/kWh and an emission factor for HC of 0.2 g/kWh.

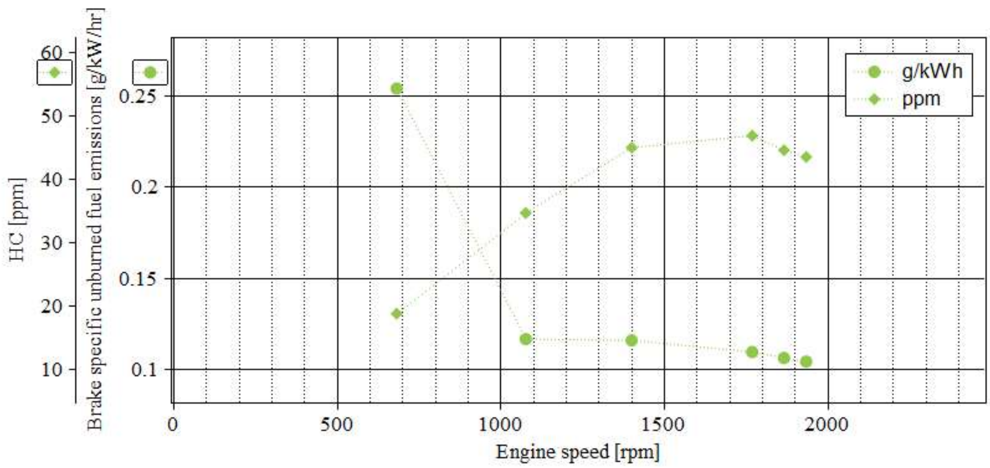

Figure 4-34 Results for HC emissions

4.4.5. Simulation with equilibrium of 11 species

The thermodynamic properties of the mixture of air, fuel, and combustion products are calculated according to temperature, pressure, and composition. For a further study, the simulations on the six cases were remade, no longer with the interpolation method (the default one) but with the equilibrium method of 11 species (as described above). A first comment concerns the time machine: with the default method we are able to do 6 simulations in about 12-15 min while with the equilibrium of 11 species, the simulation of a single case takes at least 15 min. To analyze the differences between these two approaches, the results obtained through this calculation method and the percentage differences compared to the previous method are shown in Table 4-10 and in Figure 4-35.

Table 4-10 Differences between results of default simulations and simulations with the equilibrium method of 11 species

Cases	Equilibrium	**SFOC [g/kWh]**	**Torque [kNm]**	**Power [kW]**	**NO_X [g/kWh]**	**NO_X [ppm]**
Case 1	Interpolation	411	0,53	38	-	-
Case 1	11-Species	401	0,55	39	-	-
	Δ%	**-2,52%**	**2,58%**	**2,58%**	**-**	**-**
Case 2	Interpolation	251	2,19	247	2	214
Case 2	11-Species	260	2,18	246	1	104
	Δ%	**3,69%**	**-0,41%**	**-0,41%**	**-51,23%**	**-51,41%**
Case 3	Interpolation	253	3,48	510	7	831
Case 3	11-Species	253	3,46	507	6	745
	Δ%	**-0,03%**	**-0,65%**	**-0,65%**	**-10,11%**	**-10,38%**
Case 4	Interpolation	233	6,30	1.167	8	1.054
Case 4	11-Species	234	6,27	1161,74	8	1055
	Δ%	**0,45%**	**-0,45%**	**-0,45%**	**0,13%**	**0,06%**
Case 5	Interpolation	227	7,21	1.409	6	775
Case 5	11-Species	228	7,18	1403	6	806
	Δ%	**0,40%**	**-0,39%**	**-0,40%**	**3,86%**	**3,99%**
Case 6	Interpolation	224	8,11	1.643	6	694
Case 6	11-Species	225	8,09	1.639	6	710
	Δ%	**0,26%**	**-0,26%**	**2,35%**	**-0,26%**	**2,32%**

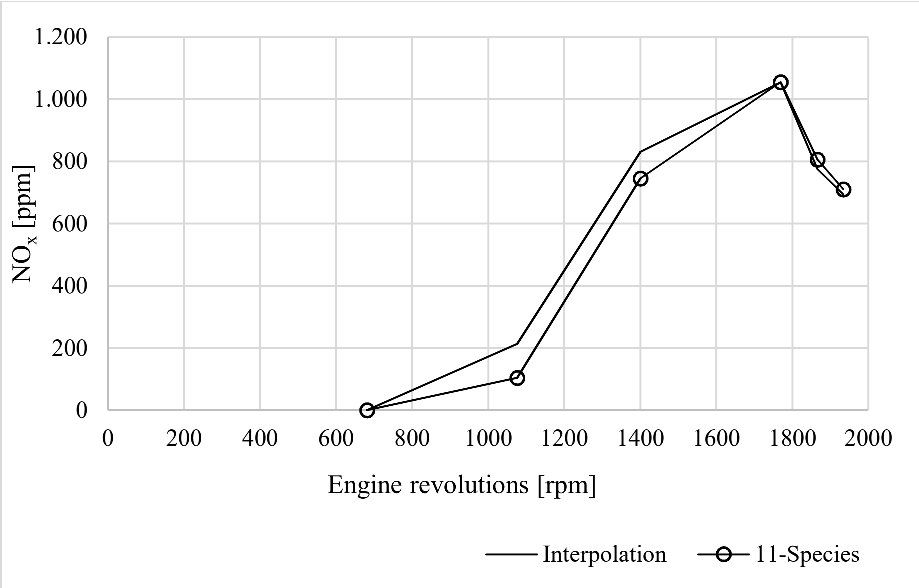

Figure 4-35 Results obtained for NO_X emissions with the two equilibrium resolution methods

Ultimately there is an average 0.79% difference in torque and power results, 1.22% error on consumption and about 11.3% error on NO_X emissions but if the first two are excluded in cases, this difference drops to 1.5% The results obtained through this type of simulation endorse those previously obtained and the choice to use interpolation as a method for calculating the balance of species.

4.5. Comparisons between the estimated emissions with the EMEP-EEA method (plus AIS data) and the results of the simulations

The last approach used in the context of the thesis to address the issue of the environmental impact of ships was that of simulation. The case study was chosen on the basis of the availability of engine data, bench tests, and experimental measurements at sea. Obviously, the results obtained cannot be globally extended to all passenger ships, much less to all ships. Certainly, however, important and useful information about the implementation of this type of analysis can be deduced from the results and the methodology applied to obtain them. Starting from the case study data, we intend to make a useful comparison between the results obtained from the **simulations** and those obtained, in the first analysis, from the processing of the **AIS data** with the Matlab code, and then from the application of the **EMEP-EEA method**. The estimation of global emissions in the port of Naples has seen the application of the EMEP-EEA estimation methodology which assumes, as has been extensively described in the 2.5 subsection of chapter 2, the assumption of a series of parameters such as typical consumption, load factors at engines, and emission factors for the main pollutants treated. These parameters are different depending on the type of ship and the combination of the type of engine type and type of fuel used (as can be seen from Table 2-12). The subdivision, made by EMEP-EEA, of the maritime fleet by macro categories clearly has the first effect that the cruise, ferry, HSC, yachts that by definition have very different behavior and mission profiles will fall into the Passenger category. For these reasons, some differences are expecting. Cross-validation of the methodologies used (**AIS, EMEP-EEA, and simulations**) is possible through the comparison between the data available from sea trials and simulations in the Ricardo environment with the results obtained from the application of the bottom-up method to the particular ship, the case study of the simulations. The possible comparisons are on speed, consumption, power and emissions.The first possible comparison is on the difference between the **average speeds** acquired in port during the measurements and the ship speeds acquired from the AIS data. The typical speeds in port identified thanks to the Matlab code that characterize the operational phases in the port were compared with two typical operating routes of the ship. The following average speeds result from the calendars made for the ship (**AIS data**):

Table 4-11 Average speeds extracted with Matlab code from AIS data (2018) for Achernar

AIS	**Average speeds [kn]**
Average speed in	15,30
Average speed out	14,50
Average speed navigation	9,58
Average speed start navigation in port	5,5

From the time acquisitions in the Figure 4-36 and Figure 4-37, typical **speeds** have been extracted in the phases of entry and exit from the port. In particular, the average values found are respectively 9.7 and 9.5 kn with peaks of over 13 kn (**experimental campaign**) (see Figure 4-36 and Figure 4-37), in accordance with the **AIS data** in the Table 4-11. It should also be noted that even the choice of an average speed of about 8 kn for the entire passenger macro-category (**EMEP-EEA**, see Figure 3-34) is not too far from the average behavior of this boat when navigating in port.

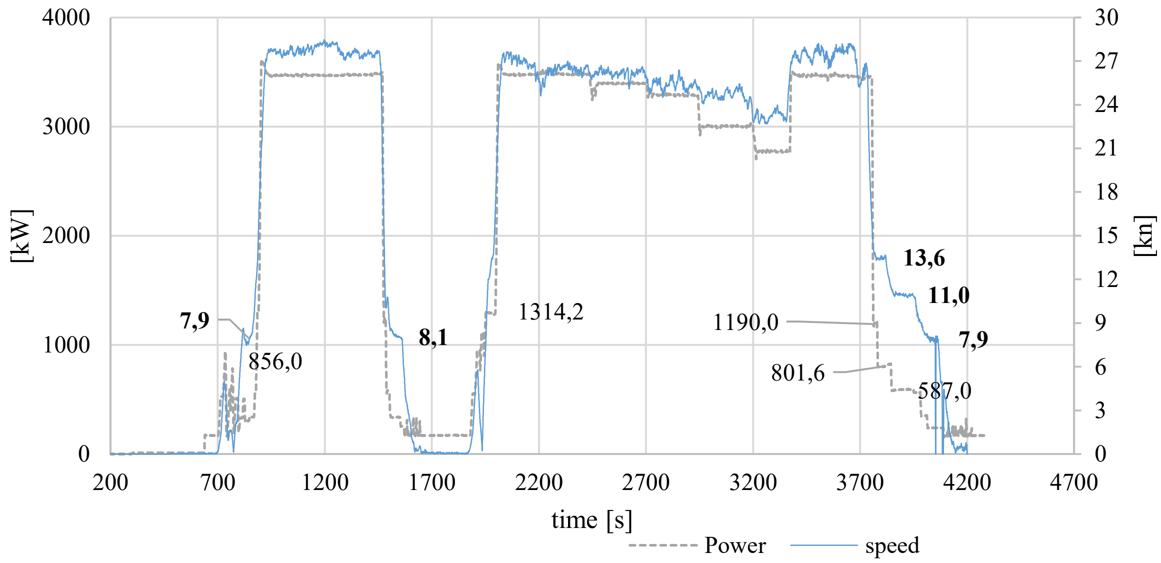

Figure 4-36 Example of a experimental data acquired with labels for power and speed (one intermediate stop)

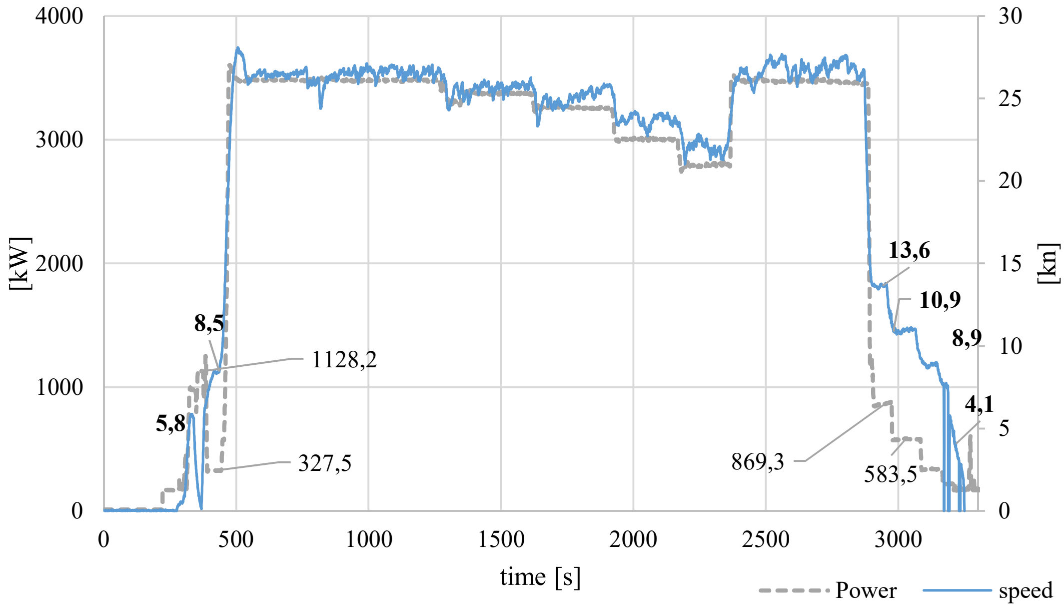

Figure 4-37 Example of a experimental data acquired with labels for power and speed (no intermediate stop)

The comparison between the **consumption** value used in the estimation of the emissions for the inventory and the actual consumption available from the measurements is greatly influenced by the fact that the EMEP-EEA method provides only one consumption value for all ships belonging to the passenger category (including of cruise, hsc, and ferries) regardless of operating conditions. In particular, for ships with MGO and MSDs on board, the consumption envisaged by the **EMEP-EEA** method is 203 g/kWh, while in reality this boat at 2000 kW has a consumption of 221 g/kWh (about 8% less). This nominal consumption value obviously varies, as the operating conditions vary, with an average value measured on the routes in the figure (Figure 4-8, **experimental campaigns**), respectively of 209 g/kWh and 207 g/kWh, therefore not too far from the assumed value. The **power** of 850 kW estimated using the **EMEP-EEA** method with a speed of about 8.6 kn (average value assigned to the ship category) should be compared with the average behavior of the ship in the navigation phases in port (**experimental campaign**). In particular, from the data shown in the figures, there is an average value of approximately 950 kW and 740 kW respectively (±12% deviation from the estimate made in the inventory). Finally, the **NO_X** hourly flow rates estimated in the inventory were compared with the hourly flow rates both measured on board and simulated at a similar engine load. By interpolating between the available stationary data (between the values of 290 and 638 kW of power measured at sea) an average value of 3.4 kg/h NO_X for each engine (6.8 kg/h total) has been obtained. The EMEP estimation method, therefore, overestimates the NO_X flow rate by about 24% (8.48 kg/h).

This error is strongly linked:

- the methods for estimating emissions with the EMEP-EEA methodology in terms of engine load factors;
- measurement errors at sea that could have altered the measured data (especially in transients at low rpm).

As regards instead, in comparison with the simulation, it must be said that the simulation result also worsens as the load on the engine decreases; despite this, the estimated NO_X flow rate at 850 kW is 7.15 kg/h.

This cross-validation of the emissions in port clearly starts from the known assumption that the behavior of both real and simulated engines are affected a lot by transients and that therefore the error found could have been higher than that found in the highest load conditions. In conclusion, we can affirm that the methodology of remaining in the error declared by EMEP-EEA (±20% for Fuel consumption and ±30% in port for NO_X essentially given by the uncertainty related to consumption data).

4.6. Discussion and conclusions

Developing simulation models for combustion engines with the capability of predicting emissions is an important target in the maritime sector also as regards the commitment to reducing emissions on a local and global scale. This work presents a simulation model of a 4-Stroke diesel engine used in the maritime field. The simulation results are calibrated with engine bench tests and validated with the experimental tests at sea. The results obtained in stationary conditions show a good fit with data from an experimental campaign carried out on board and encourage testing the model in other situations, characterized by transient situations during manouvres. In conclusion, it can be said that the built model has led to good results despite the lack of all the necessary data and despite the not always high quality of the data measured, especially in terms of emissions. In fact, it is emphasized that the experimental campaign carried out at the time doesn't have the characterization of polluting emissions or even the validation of a simulation model as its main purpose. Future developments of the model will see it interfacing with the SIMULINK environment with the aim of integrating the behavior of the ship both in navigation and in port.

The availability of a reliable numerical prediction could really make it possible to assess and the control emissions in those situations representing the largest risk for the health of inhabitants of the areas surrounding ports.

5. *Acoustic impact of ships in port*

Aims and scope

Another type of impact caused by ships affecting near-ports inhabited areas is certainly the acoustic one. As in the case of chemical pollution, the approach is twofold: experimental campaigns and simulation models. As regards predictive models for *the whole ship radiated noise, again the input data regarding the characterization of single acoustic sources on board may be derived by predictions or experiments. The final model of the whole ship is to be later validated by experiments.*

A first case study focuses on the acoustic impact originating from ***a ferryboat berthed in the port of Naples*** *and affecting the surrounding portion of the city. The aim is to obtain a tool able to investigate the acoustic impact of shipo perations in port and the effect of possible countermeasures against noise generation and propagation in the port area. In this case, the experimental campaigns and the simulations have been made on the port of Naples.*

*The second part of this work was carried out within a project developed, in the last two years of the PhD, in collaboration with the universities of Genoa and Trieste. The trigger for the project was the publication of the new additional class notation concerning the noise radiated into the air by ships in port ("**Procedure for the Determination of Airborne Noise Emissions from Marine Vessels"**, Lloyd's Register (2019)). The project was conceived as a first, preliminary application of the procedure, hypothesized by the LR document, to be used as a tool for evaluating the performance of an existing ship, but also as a control tool during the design and construction phases of ships. This project has allowed to explore an already previously addressed topic but with a definitely deeper level of detail. In particular, data from a ship and her main sources of external noise were available. The aim of the project has been to verify the possibility of using commercial software to study and effectively deliver the airborne noise radiation from the ship, which has been modeled as a complex acoustic source. Due to industrial confidentiality reasons it is not possible to publish the whole set of data, therefore graphs and tables will be presented in small amount and in non dimensional form.*

5.1. Motivations of the investigation

In recent years, airborne noise emissions from different transportation modes have become a major concern for environmental and governmental agencies due to the impact they have on inhabited areas. This is the result of an increasing concern about the environmental acoustical impact of anthropogenic activities and about the soundscape quality of modern cities. In addition to many other forms of environmental impact of shipping activities (see chapter 1), the **external airborne noise** emission by ships has therefore come to the attention of Regulatory Bodies. On the other hand, the objective presence of strong acoustic sources on board ships and the proximity of inhabited areas to areas of ship operation (port facilities and shipping lanes along the coast or in inland waters) represent the technical aspect of the problem. The airborne noise related to shipping activities indeed affects the population living near ports or close to straits and to navigation channels located along the coast or inland (see e.g. **Coppola et al., 2018**). Traditionally, mostly in Europe, many urban areas developed in close proximity of ports, particularly in the Mediterranean Sea. Perhaps also for these reasons, the European Union is particularly concerned with the harmful impact of airborne noise and is world leader in formulating guidelines and requirements to control noise (**NoMEPorts 2008**). In addition to other contributors to the whole noise levels in port (repair shipyards, gears for loading and unloading operation, truck, cars, trains, conveyors etc), ships are the most significant noise source and those generating the primary impact (**Badino et al., 2011; Badino et al., 2012; Badino et al., 2012a; WHO 1999**).

Despite that no specific acoustic requirements have been issued so far for ports, the problem of the acoustical impact of ports is going to pose technical, juridical and economic challenges to Port Authorities. In addition, the specific characteristics of noise emissions by ships (with strong low-frequency components) can make standard countermeasures placed in buildings ashore, like noise walls, soundproof windows and similarnot always effective in reducing the impact.

5.2. Technical problem

The overall external airborne noise emission from a ship is due to several single sources acting on the ship surface, the most relevant ones being funnels and inlets and outlets of ventilation and air-conditioning systems. In simple terms, noise sources correspond to all openings in the ship surface where an internal mechanical source (engine, compressor, actuator) is in acoustical contact with the outside atmosphere, often with an exchange of gases (air in input, air and exhausts in output). Given that the original source of noise is mechanical and due to running engines or plants, the airborne noise emitted by ships in port depends on the operations carried out by the vessel. In addition, the same plant can be run in different conditions, with different acoustical impact. For these reasons, the results presented in (**Ferdianelli et al., 2020**) were affected by large uncertainties.

While berthed, ships normally run auxiliary engines producing the electric power needed for hoteling service. The noise generated presents strong components at low frequencies propagating with long wavelength and making it quite annoying. Moreover, noise sources are located in different position on board, making the ship a complex noise source (**Badino et al., 2016**).

The development of **numerical models** for the prediction of noise propagation in air represents a favourable element for controlling the acoustic impact of ships. Ray-tracing software, using ISO 9613-2 to calculate outdoor propagation, have been successfully used for design. However, there are still some doubts regarding the accuracy of some of the various empirical algorithms used, such as algorithms for ground effects and reflections, source height, reflections by objects, and ground cover. Based upon these considerations, a comparison of different softwares has been promoted to compare results in terms of accuracy and also in terms of computational effort.

A preliminary but essential procedure for the development of a realistic simulation model of the acoustic impact of a ship is the creation of an **inventory of noise sources on board**. The inventory can be based on two types of data: **previsional or experimental data**. The first type of data is based on information provided by the manufacturers of the plant or the particular unit considered, while the second one is made of measurements carried out onboard the complete ship, with all the systems installed and in operation.

As mentioned, what is interesting for the acoustic analysis is the characterization of the strength of each source on the outer surface of the ship, but such strength depends in most cases on the running conditions of a machinery placed inside the ship. In this case, any source of noise with an airborne contact with the external atmosphere is to be considered as an external source and therefore is to be characterised in the position where the connecting duct reaches the external surface of the ship. The ending points of all systems having inlet or outlet grids or pipes are in focus. Based on what was mentioned above, with reference to the case of a passenger ship, for example, three main categories of external sources may be identified:

- **funnels** (as ending points of exhaust gases plants);
- **ventilation** inlets and outlets (ending point of the ventilation systems of technical spaces including machinery: here the original noise source may be the ventilation system, but also the other machinery present in the ventilated room);
- **air conditioning** inlets and outlets (ending points of HVAC systems of living spaces):
- **other external sources** (e.g, winches and other handling equipment for cables, anchors and chains): this category corresponds to sources radiating directly outside. It may generally be neglected in most operating conditions of interest.

Often, on a passenger ship, the external sources of noise are located on the upper decks, where the funnels and a large number of inlet/outled grids are placed. Other locations may include the ship sides below accommodation, on the lower decks above the waterline.

Taking a diesel running in an inner engine room as an example, the contribution to the total external radiated noise is mainly represented by all the transmission paths connecting the engine and its room with the outside atmosphere. The main part of this connection will occur through the fresh air inlets from the outside, through the exhaust gas duct ending on the funnel and via the outlet duct of the ventilation system. The noise transmitted through the (inlet/outlet) ventilation systems will be increased by the contributions due to the ventilators moving the air flow (in both directions), while the path through the exhaust gases duct will take advantage of a reduction of levels from the silencer. Any other internal piece of machinery or plant will in general have outside connections only through one or more aeration grids at the end of inlet/outlet ventilation systems.

A first strategy for the identification of the airborne noise external source is to model the whole chain starting from the original noise source and including all the items of the connecting path, coming to a prediction of the noise radiated outside. A different strategy is to characterize experimentally the external source by measuring the sound power levels directly at the inlet/outlet end. While the former predictive procedure takes advantage of a global knowledge of the plant, the experimental procedure minimizes all the uncertainties connected with the prediction and provides a sound basis for the external propagation study. On the other hand, the number of noise sources to be characterized on the outer surface of the ship makes the experimental campaign quite complex and the adoption of strict protocols mandatory to keep a good quality of the results. Experimental measurements carried out as part of our study have highlighted how uncertainties related to the number and type of sources that were measured often resulted in the impossibility of using effectively the measured data. It would therefore be good to schedule with care a measurement campaign on board with information about the position and characteristics of the single sources present.

A key point both in following the experimental and predictive procedures is to identify the running conditions of each plant in every situation, as the sound power radiated can in a first approximation be considered proportional to the power delivered by the plant.

5.3. Regulatory framework and investigations in the field

The development of a regulatory framework for airborne noise emissions in the shipping field has been delayed to some extent by the fact that **many Bodies** are potentially or in practice involved in the assessment of the acoustical impact of port activities (Shipowners, Class Societies, Port Authorities, Coast Guards, Health-Care Institutions, Municipalities) and this has prevented the development of a coherent set of requirements on the subject. In a few cases, some of these Institutions have issued local requirements on noise emissions, but a turning point in the regulatory process can be identified in the issue of Class Notations on the subject, implying the establishment of a first regulatory framework for the definition of performance standards and procedures for their verification.

For decades, airborne noise on board ships has been regulated to protect living and working spaces on board to benefit both the passengers and the crew, Figure 5-1. The **external acoustic impact on third parties** has recently been taken into consideration as well, in the forms of underwater noise, affecting the marine fauna, and of airborne noise, affecting the terrestrial fauna (humans, in particular), Figure 5-1 (**Coppola et al., 2019**).

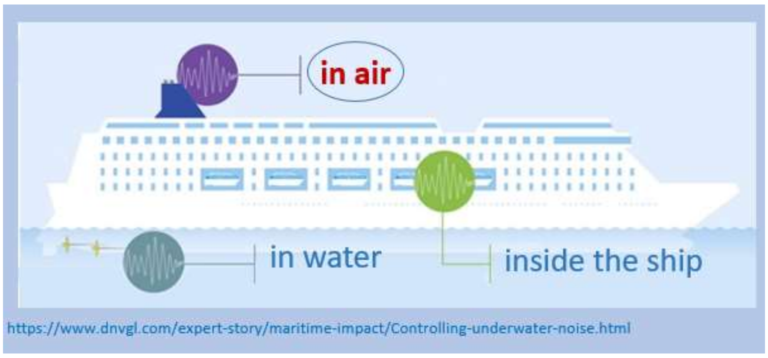

Figure 5-1 Acoustic impact of a ship

Maritime transportation would not exist without large ports representing focal points of the logistic chain responsible for the transportation of goods and passengers all over the world. Even though the European Union passed the European Noise Directive 2002/49/EC (END) (Directive E.U. 2002/49/EC), requiring member states to produce strategic noise maps and action plans for roads, railways, airports, and urban centers every five years, ports are excluded from these general requirements.

A few projects and studies on the characterization of **port sources and the acoustic mapping of harbours** have been carried out (see e.g **Alsina-Pagès et al., 2019; Eco.Port Project 2006; EcoPorts 2011;**

Herramienta Automática de Diagnóstico Ambiental, 2005; NoMEPorts 2008; SIMPYC 2008; Schenone et al., 2016). Projects addressing airborne noise from berthed ships have also been carried out in recent years. One of the most recent one is the NEPTUNE (Noise Exploration Program To Understand Noise Emitted by seagoing ships) project initiated by a number of ports in Europe and in the rest of the world with the goal of providing "tools to support a sustainable port development by reducing noise related to seagoing ships". The main results of the project have been a Measurement Protocol and a Best Practice Guide describing effective measures. Another reference project is the EU project SILENV which covered on-board, underwater, and external airborne noise (**SILENV 2012**). This project developed a measurement protocol for airborne external noise from ships. Another interesting news came from the decision of the World Port Sustainability Program (WPSP) to include, from 2020, airborne noise in the Environmental Ship Index (ESI) formula (see chapter 6). Local requirements for ships approaching the quay have been issued in specific ports, other ports have imposed fee reductions to control the acoustical performances of ships. The dispersion of responsibilities on the subject itself has probably prevented the issue of an international framework of requirements for ships, despite the fact that progress achieved by tools for acoustics and acoustical modelling and countermeasures has made the sector mature in regulation. The first sign of an inversion in the trend has been the issue, in the last two years, by two Classification Society, Lloyd's Register and DNV-GL, of voluntary class notations on airborne noise radiated by ships in port. This was the first time that a procedure for the characterization of the airborne noise by ships was defined, also defining limits to rank the overall acoustical performances of a ship. A new voluntary class notation, developed by DNV and known as "QUIET", addresses the vessels external airborne noise emission in port (**DNV QUIET 2019**). All types of vessel built in compliance with the requirements may be assigned the class notation QUIET. The second one, the Lloyd's Register class notation, will be analysed in the next subsection 5.3.2.

5.3.1. ISO standards

Depending on the ship type, the simulation model can be very complex with a significant number of sources of different kinds: point, surface etc. For a modern passenger ship, the total number of sources can easily be higher than a hundred. For these reasons, a check for the internal coherence model is needed. A possible way to carry out such a check is verifying that the total acoustic power of the ship equals the sum of the single acoustic powers of the sources used in input to the model. Different procedures can be used, but it is here suggested to apply to the numerical model two ISO standards aimed at assessing the acoustic power of complex sources given a series of measures of acoustic pressure at specific points. In particular, for the specific case of ships, ISO 8927:1994 and ISO 3744:2010 can be applied:

- **ISO 8297:1994** Acoustics —Determination of sound power levels of multisource industrial plants for evaluation of sound pressure levels in the environment —Engineering method;
- **ISO 3744:2010** Acoustics — Determination of sound power levels and sound energy levels of noise sources using sound pressure— Engineering methods for an essentially free field over a reflecting plane.

These procedures were used to evaluate the internal coherence of the propagation model. This verification also provides useful information on the effectiveness of the experimental procedure, which could be applied to the ship precisely to determine its overall sound power, without starting from the detail of the various sources. The comparative sound power values (i.e. used at the input to the model and subsequently checked with the sound pressure modeled at a distance) are the forecast ones. ISO 8927:1994 specifies an engineering method for determining the sound power level of multisource industrial plants that is relevant to the assessment of the noise around the plant. The basic assumptions and limitations are that the source radiates regularly in all horizontal directions; the procedure suggested is based on measuring the sound pressure level on a closed path (measurement contour) surrounding the plant and determining an appropriate measurement surface. The measurement points are located on a perimeter that surrounds the source. The share of the measuring points is taken as the average share of the individual sources of the plant. The spacing of the points is defined according to the plan dimensions of the ship. Another possible approach for the check on internal coherence of the model is to follow the procedure suggested in ISO 3744:2010. The standard describes methods for determining the sound power level or sound energy level of a noise source from sound pressure levels measured on a surface enveloping the noise source in an environment that approximates to an acoustic free field near one or more reflecting planes. The procedure is more complex than the ISO 8297 one but the main advantage is that the hypothesis of omnidirectional source used in 8297 is no more in place. Also in this procedure the distance between the various points depends on the size of the source. Once the measurement point's positions are determined, the sound pressure level for each frequency band must be calculated in those points and the total acoustic power is calculated following the standard procedure. The checks on the sound power levels are partially carried out both by families of sources (funnels, ventilation, and air conditioning) and on the total given by the sum of all sources on board.

5.3.2. Class notation (LR 2019)

The notation considered in this analysis is the Airborne Radiated Noise notation developed by Lloyd Register. The text of the requirement includes the procedure that is to be folled for awarding this notation (**Lloyd's Register, 2019**). The notation applies to new or existing self-propelled ships of greater or equal length of 24 m and may be awarded when the measured values fulfil the defined criteria. The notation identifies two principal operating conditions: the harbor moored and the free sailing conditions. In the *harbor-moored condition*, the ship is moored at pier with all equipment normally operating at harbor (including a possibly situation with power provided from shore) and the main propulsion system turned off. For ships with garages such as passenger ferries and ro-ro cargo/passenger ships the car deck ventilation shall be included while the noise directly emitted from cars/trucks and passengers during loading and unloading operations should not be included. The *free sailing condition* may correspond to the sailing inside port areas or along the coast in channels with all equipment normally operating during the navigation (main and auxiliary engines, ventilation systems in operation). The standard sailing speed is 5 knots. The assessment should at least be performed in the frequency range of 31.5–8000 Hz in 1/1-octave bands. The reference levels and parameters are:

- Sound pressure level (L_p) – 10 times the logarithm to the base 10 of the ratio of the square of the root-mean-square sound pressure, p_{rms}, to the square of a reference value, p_0, expressed in decibels (5-1):

5-1 Sound pressure level

$$L_p = 10 \log \left(\frac{p_{rms}^2}{p_0^2} \right), dB$$

where

p_{rms} = the root-mean-square sound pressure in Pa

p_0 = the reference sound pressure level (= 20 μPa)

- $L_{WA,ship}$ is the "Ship Sound Power Level" (5-3), the energy sum of all single-source sound power levels $L_{WA,i}$ (5-2) for given operating;

5-2 Single-source sound power levels

$$L_{WA,i} = 10 \log \left(\frac{P_i}{P_0} \right), dB$$

5-3 Ship sound power level

$$L_{Wa,ship} = 10 \log \left(\sum_{i=1}^{n} 10^{\frac{L_{WA,i}}{10}} \right), dB$$

where

- P_i = sound power of source number i, in W
- P_0 = the reference sound power (= 1 pW)
- i refers to single source number i
- n is the total number of single sources on a ship
- $L_{Aeq,T}$ is the "Equivalent Continuous A-Weighted Sound Pressure Level", the sound pressure levels (5-4)

5-4 Equivalent Continuous A-Weighted Sound Pressure Level

$$L_{Aeq,T} = 10 \log \left(\frac{1}{Tp_0} \int_0^T p_A(t)^2 \, dt \right), dB$$

where

- p_A = the instantaneous A-weighted sound pressure, in Pa;
- T = the specified time interval, in s.

- $L_{pAS,max}$ the maximum A-Weighted root-mean-square sound pressure level measured with constant SLOW during passage of the ship or during the defined operating condition, according to IEC 61672-1;
- d, Distance to shipside is the distance to the hull side in horizontal direction, Figure 5-2.

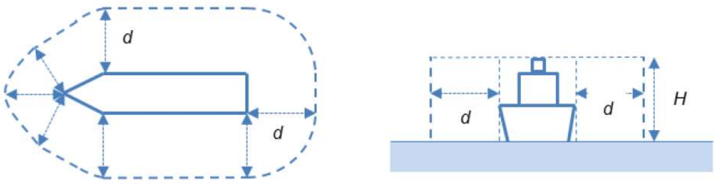

*Figure 5-2 Definition of distance **d** to ship side, in metres*

Table 5-1 shows the limit values for the assessment criteria:

Table 5-1 Assessment criteria values Lloyd's Register, 2019

Sound power	**Harbor moored**		**Free sailing**		**Distance to ship side**
	dB		dB		m
	$L_{WA,ship}$	$L_{Aeq,T}$	$L_{WA,ship}$	$L_{pAS,max}$	d
SQ	82	40	92	50	50
Q	88	40	98	50	100
S	96	40	106	50	250
IW	101	65	111	75	25
C	108	40	-	-	1000

The acronyms in the Table 5-1 correspond to notation levels: respectively *Super Quiet, Quiet, Standard, Inland Waterways and Commercial*. To obtain the ABN notation, the ship shall meet all four requirements at the same level. The ABN(*) notation at a given level may be awarded only if the measured airborne noise levels are less than the corresponding limit. The classification of a vessel therefore requires the correct evaluation of two different quantities (**Lloyd's Register, 2019**). On the one hand there are the ship sound power levels, $L_{WA,ship}$, as in energy-based sum of all single-source sound power levels. To determine the single source power levels of each source onboard the standards to be followed are ISO3744 or ISO9614. The second set of limits refers to the sound pressure level (in terms of $L_{Aeq,T}$ and $L_{pAS,max}$) measured at specific distances from the vessel. For new constructions, it is therefore recommended to create a 3D calculation model of the ship according to ISO 9613-2, see Figure 5-3.

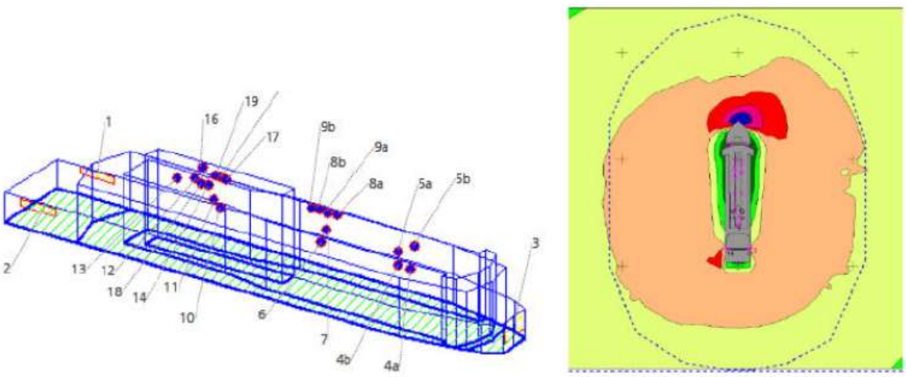

Figure 5-3 Example of 3D calculation model and noise contour map (left and right respectively)

This model shall include the main geometry and individual noise sources of the vessels, screenings, reflections and absorptions by the ship structure, in order to realize a model of the ship which will identify the specific Sound Pressure Levels values at given target points. Following this recommendation, each source shall be characterized by its sound power level and, if relevant, a directivity index. In the predictive model, the exhaust stacks and funnels of main and auxiliary engines, the ventilation air intakes and exhaust, all the external fans, any special equipment in operation (as cranes and/or cargo pumps) and, if relevant, the hull radiated noise are all considered main sources. The calculated noise emitted from the exhaust stacks shall also include, if present, silencers, scrubbers and filters (**Lloyd's Register, 2019**). The requirement also prescribes how to model the sources on board: small ventilation openings and exhaust stack openings may be in general be modeled as point sources, larger ventilation grilles shall be modeled as surface sources. The design stage calculation report shall primarily include: the selected assessment criteria in each operating condition, all user input according to ISO9613, the single source sound power levels, the determined ship sound power levels, any deviation from calculation method and calculated sound pressure levels as color-coded noise contour maps. On-site measured levels for the verification of compliance to the class notation should be carried out. For both the preset operating conditions, the notation mentions on-site measurements following preferably a "near-field" method (limited to a distance from the source equal to about a wavelength of sound or equal to three times the largest dimension of the sound source (whichever is the larger). The weather condition limits to carry out the measurements should not exceed 3 on the Beaufort scale and a Sea State 2. The ship under test should be ballasted to the design draught with all equipment, normally in operation, running. The sound pressure levels $L_{Aeq,T}$ and the $L_{pAS,max}$ shall be determined by updating the 3D calculation model with the single-source sound power levels and verifying at a relevant distance and at least two heights (3.5 m and at ship height above sea level) the compliance to the assessment criteria (**Lloyd's Register, 2019**).

5.3.1 Comments

As mentioned, the checks provided by the LR concern the total acoustic power emitted by the ship and the sound pressure radiated at certain reference distances and evaluated differently depending on the ship condition. The above described criteria do not depend in any way on the size of the ship. In this sense, a ship of larger dimensions is equated, in terms of sound power limits, to e.g a significantly smaller one, while it should be noted that in a large ship the availability of space and weight to be dedicated to sound propagation counter measures (applied at sources: limitation of the emitted sound power) is larger than on a smaller unit.

Another note about the LR notation concerns the difference in requirement levels for the conditions of the mooring and navigation ship: the ship that moves at 5 kn can radiate 10 times more acoustic power and sound pressure than the one moored.

5.4. Simulation software

The software used for this and for all the acoustic applications at UNINA is the Terrain Olive Tree Lab-Suite developed by Mediterranean Acoustics Research & Development (**PEMARD 2017)** [15] based on Ray Tracing approach implementing International Standard ISO 9613-2 methodology (**ISO 1993; ISO 1996**). This

ISO is a simple and practical empirical method to calculate outdoor propagation of sound from a point source to a receiver, it has been around since the year 1996 and it has been very useful for the acoustical engineering community. Other software dealing with outdoor sound propagation are VDI 2714, CONCAWE, Nord2000 and Harmonoise (**Nota et al., 2005**) among others. Nord2000 and Harmonoise are considered more advanced calculation software, since they apply more sophisticated propagation models (algorithms) based on physics, which give acceptable runtimes for engineering applications. All these methods can be described as 2.5 dimensional (more than 2, but less than a full 3 dimensional), calculating for each plane containing a ray between a source and a receiver. Nonetheless, one should offer criticism taking the empirical approach of the ISO 9613-2 standard (and other similar methods of the time) into consideration, it can be considered as true innovation in acoustical engineering, since it encapsulates the essence of outdoor sound propagation and it offers engineers the possibilities of calculating complicated scenarios in a spreadsheet format. Later, ISO 9613-2 was implemented in various ray-tracing software packages to make larger, more sophisticated, and more accurate models possible. For this application three softwares have been used and compared: Soundplan, Mithra and *Terrain* (University of Naples Federico II, UNINA). **OTL-Terrain** simulates and predicts sound propagation from a source to a receiver using wave based geometrical acoustics. It utilizes image source sound ray modelling in a proper 3D space that solves Helmholtz's sound wave equation, and thus calculates wave phenomena such as phase changes upon reflection due to finite reflector size and impedance, edge diffraction effects, turbulence, in resolutions below 0.001Hz, between 1 to 100 kHz **Lam (2005)**. The OTL- Terrain engine is based on a general geometrical acoustics ray model based on analytical solutions for various wave phenomena and can simulate sound propagation in arbitrary geometries. The software application calculation engine is based on the work of **Salomons (1997)** who applied a ray model using analytical solutions; spherical wave diffraction coefficients given by **Hadden and Pierce (1981)**; spherical wave reflection coefficients based on the work of **Chessel (1977)**, and complex ground impedance based on the **Delany and Bazley (1970)** model. Finite-size reflectors' Fresnel zones contribution is taken into account by applying the work of **Clay et al (1993)**. The atmospheric turbulence model used is based on Harmonoise (**Nota et al., 2005**) and atmospheric attenuation is based on ISO 9613-116. The Sound Path Explorer (SPE), a module in OTL-Terrain, is an in-house developed algorithm which detects valid diffraction and reflection sound paths from source to receiver in proper 3D. Sound path detection is based on the image-source method and the geometrical theory of diffraction according to **Keller (1962)**. **Economu & Charalampous (2013)** provide more information on the equations used by OTL-Terrain. The limitations of OTL-Terrain currently include: lack of directivity properties of noise sources; lack of atmospheric refraction; only multiple point and line sources.

It is expected that OTL-Terrain is able to give accurate results for long distances in a neutral atmosphere, and distances inferior to 200 m in typical atmospheres. Lastly, OTL-Terrain also includes the 9613-2 calculation method as an option for those who need to comply with regulations and for comparison purposes. The simulations carried out as part of this research are of two types. The first, on a port scale, with aims to obtain a tool able to investigate the acoustic impact of ships' port operations and the effect of possible countermeasures against noise generation and propagation in the port area. The second type of simulations, on the other hand, was carried out as part of a research project focused on a single unit in view of the new class notation of the LR.

5.5. Case study n.1: ferry boat in the port of Naples

Figure 5-4 shows the **3D model developed** to represent a ferry boat moored in the port of Naples and the buildings of the port and of the nearest city area. The source used was a dodecahedral type with a flat spectrum (see Figure 5-5); the receivers were placed in correspondence of the survey points (see Figure 5-5). The software also allows visualization of the incident rays as shown in Figure 5-6.

Figure 5-4 3D model of ship, port and buildings

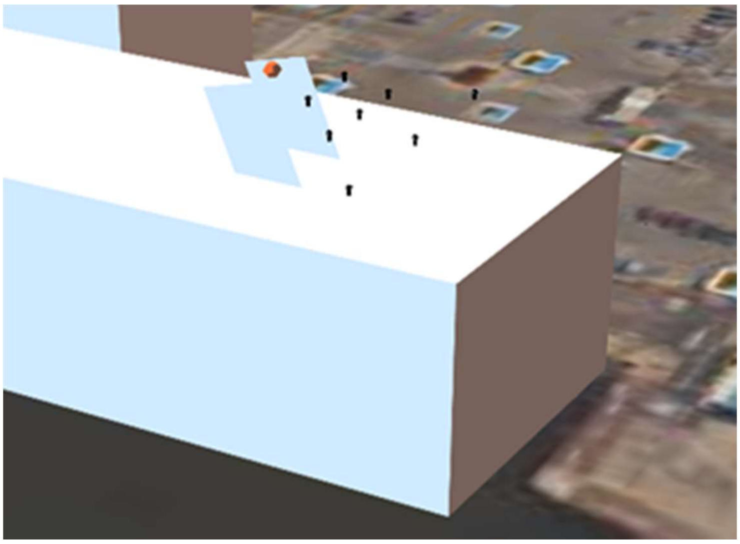

Figure 5-5 Funnel source and receptors

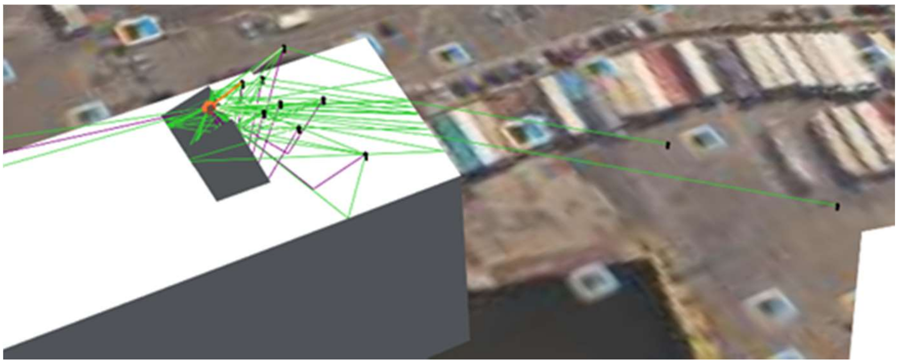

Figure 5-6 Acoustical rays modelling the propagation

The model thus constructed had to be clearly calibrated by means of experimental measurements, reported below. These measurements s have been realized precisely for this purpose and both during measurements and simulations, the only sources deemed relevant were the funnels.

5.5.1. Experimental campaign

The experimental campaign was carried out in the Port of Naples on May 11th 2017, aimed at acquiring data for the characterization of a passenger ship, see Table 5-2, as source of noise and for the calibration of a propagation model. The investigated source is a ferryboat arriving each day in Naples around 6 am and departing at 8 pm. When at berth, see Figure 5-7, the electric power generators of the ship constantly run to feed hoteling and hull services.

Table 5-2 Characteristics of the ship arriving in port during the experimental campaign

Characteristics	Value	Units
GT	33.366	[tsl]
Loa	161.25	[m]
B	29.60	[m]
Depth	16.2	[m]
Max speed	21.3	[kn]
Total power installed on board	19.600	[kW]

Figure 5-7 Position of the ship source after mooring

The experimental investigations were carried out through two sound level meters (LXT and Larson Davies 824) able to measure several quantities at the same time among Equivalent Sound Level (L_{eq}), max and minimum Sound Pressure Level (SPL), Sound Exposure Level (SEL). Phonometric surveys were carried out following the usual procedure, including calibration, carried out by means of a calibrator device and selection of the instrument settings. Measurements were made by directing the microphone towards the sound source at a height of about 1.5 m from the ground and at least 1 m from interfering surfaces such as walls, barriers and/or obstacles. Surveys were carried out in several points and at different distances from the ship to cover arrival, maneuver and mooring of the ship, see Figure 5-8. In area 1, see Figure 5-8, the receivers were located on the balcony of Stazione Marittima. In area 2, see Figure 5-8, the receivers were placed on the ground (SNAV service area. For a better characterization of the sources on board with ship at berth, other measurements were carried out on board the ship. Initial onboard surveys were carried out with running garage fans; noise levels were then recorded in the areas close to the ship's funnel. The last measurements were carried out in the Snav square. The measurement points on board were grouped by zones and for each of them the average levels were estimated in third octaves.

- Zone A (Level I, [lower level] around the funnel-stern);
- Zone B (Level II [medium level] around the funnel-stern);
- Zone C (Level III [upper level] around the funnel-stern);
- Zone D (Level III around the funnel-starboard);
- Zone E Level III around the funnel-port);
- Zone F (Level III around the funnel-bow).

Figure 5-8 Main locations of surveys

Table 5-3 Aquisition data (LXT)

Sound level meter	Decription of locations/phase	times	Leq [dB(A)]	SEL [dB]
824 SONORA	Arrival (from zone 3)	30	62,9	72,9
824 SONORA	Deck garage	30	88,6	98,6
824 SONORA	Deck garage	50	79,6	87,8
824 SONORA	Deck 6 Left	60	74,8	76,9
824 SONORA	Deck 6 Left	20	74,3	84,3
824 SONORA	Deck 6 Left	30	73,4	83,4
824 SONORA	Deck 6 Right	20	81,6	91,6
824 SONORA	Deck 6 Right	30	83,3	93,3
824 SONORA	Deck 6 Right	10	83,3	93,3
824 SONORA	Deck 6 Right	10	79,2	89,2
824 SONORA	Deck 6 Right	10	71,6	81,6
824 SONORA	Deck 5 Around the funnel	10	68	78
824 SONORA	Around the funnel (side)	10	74,7	84,8
824 SONORA	Around the funnel (bow)	20	78,6	88,6
824 SONORA	Around the funnel (bow)	0	76,3	86,4
824 SONORA	Around the funnel (side)	30	75,9	85,9
824 SONORA	Around the funnel (medium level)	30	77,7	87,7
824 SONORA	Around the funnel (lower level)	0	73,1	83,1
824 SONORA	Around the funnel (lower level)	0	71,3	81,4
824 SONORA	Square (M)	30	62,6	72,5
824 SONORA	Square (N)	40	66,3	76,3

Table 5-4 Aquisition data (SONORA)

Sound level meter	Decription of locations/phase	times	Leq [dB(A)]	SEL [dB]
824 VM	Arrival	30	84,9	94,9
824 VM	Arrival	30	73,1	83,1
824 VM	Deck 6 Right	20	71	81
824 VM	Deck 6 Right	6	72,7	82,7
824 VM	Deck 6 Right	30	71,8	81,8
824 VM	Deck 6 Right	30	82,2	92,2
824 VM	Deck 6 Right	10	83,7	93,8
824 VM	Deck 6 Right	30	82,4	92,4
824 VM	Deck 6 Right	20	81,3	91,3
824 VM	Deck 6 Right	40	76,1	76,7
824 VM	Deck 6 Right	30	64,8	74,8
824 VM	Around the funnel (side)	40	78,1	88,1
824 VM	Around the funnel (side)	10	76,4	86,4
824 VM	Around the funnel (side)	20	76,9	86,9
824 VM	Around the funnel (upper level)	30	80,4	90,4
824 VM	Around the funnel (upper level)	30	85,6	95,7
824 VM	Around the funnel (medium level)	20	78,4	88,4
824 VM	Around the funnel (medium level)	20	76,4	86,4
824 VM	Around the funnel (lower level)	10	73,6	83,6
824 VM	Square	20	63,1	73,1
824 VM	Square	40	68	78

The maneuvering ship entering the port was surveyed from area 1. Noise records with time duration of about 60 minutes (steps of 10 sec), were stored in third octave band spectra. In Figure 5-9, the equivalent sound pressure level is presented vs. time.

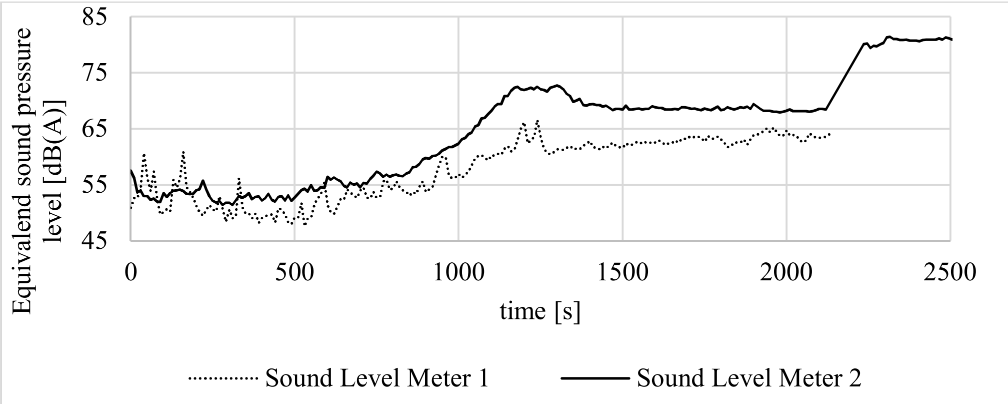

Figure 5-9 The equivalent sound pressure level vs. time for the entering in the port

Below the measurements obtained in the various areas on board are reported (from Figure 5-10 to Figure 5-15).

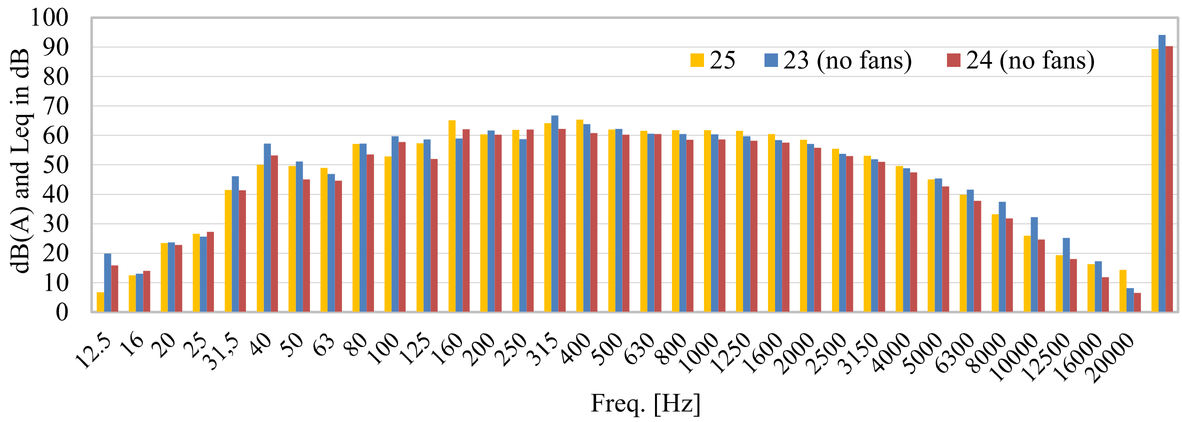

Figure 5-10 Zone A

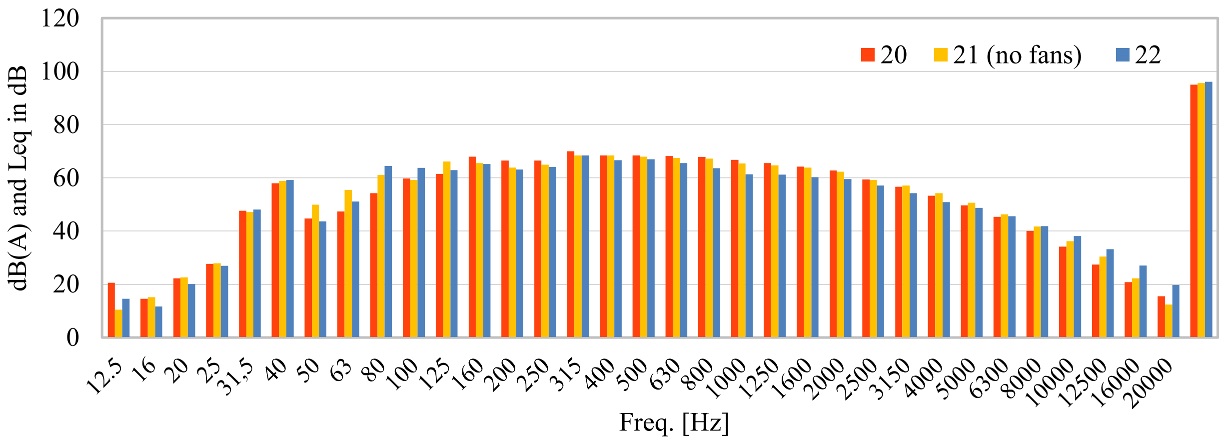

Figure 5-11 Zone B

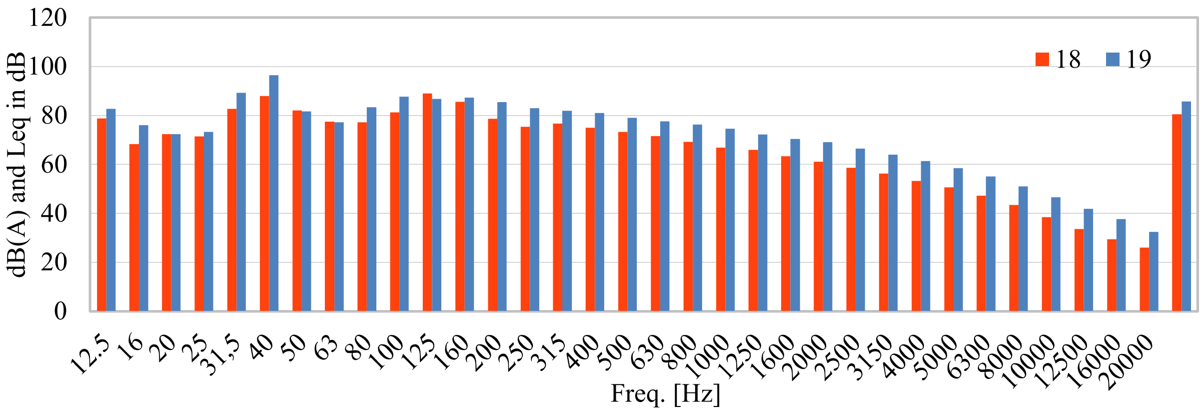

Figure 5-12 Zone C

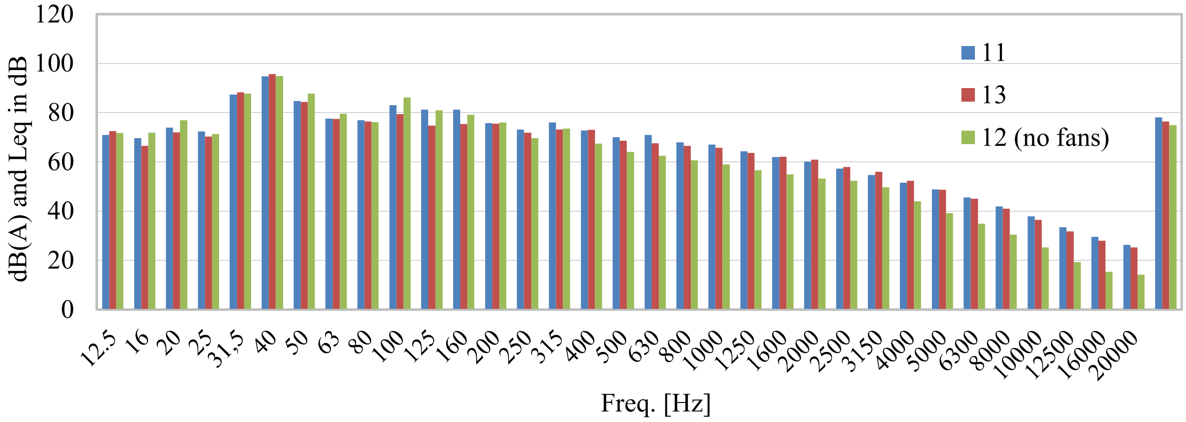

Figure 5-13 Zone D

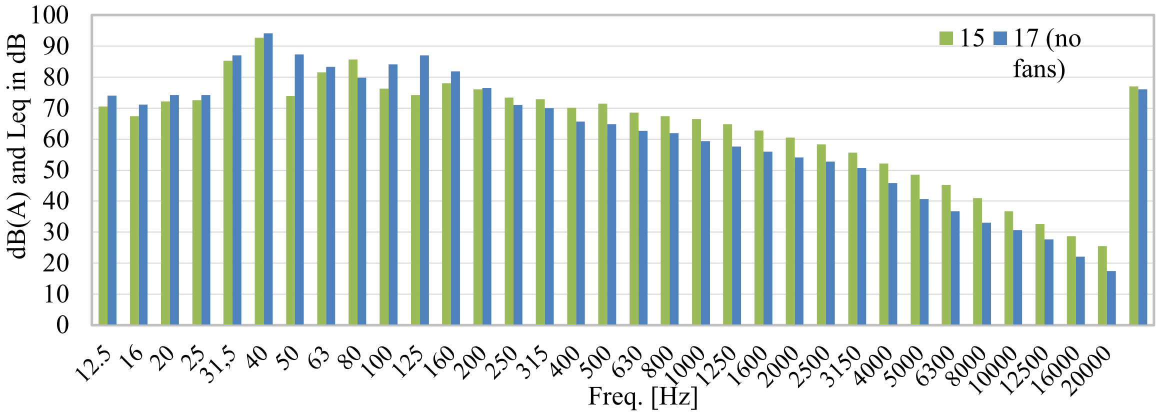

Figure 5-14 Zone E

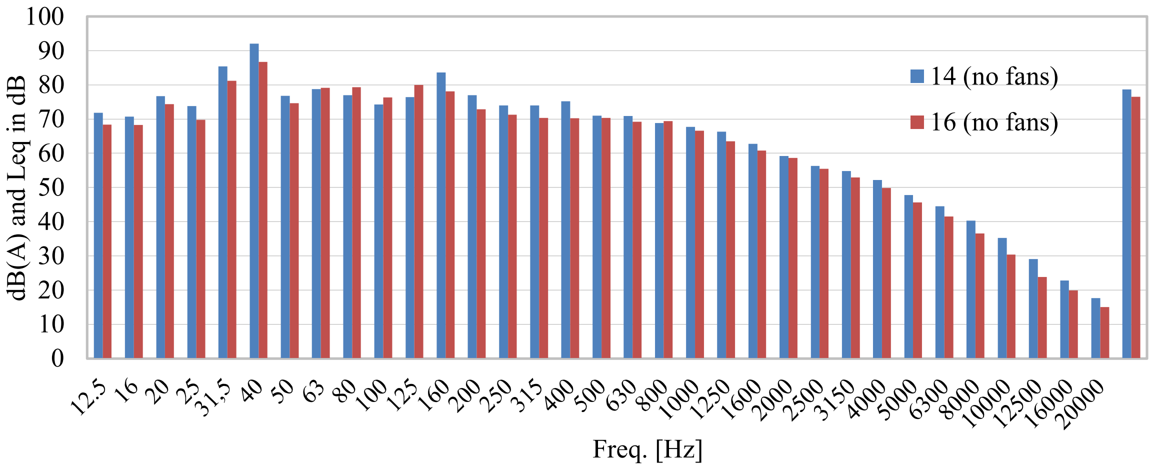

Figure 5-15 Zone F

An overall comparison is shown, in Figure 5-16, in among different measurement locations on board. The different profiles of the spectra show that there is quite a complex transmission in the proximity of the funnel.

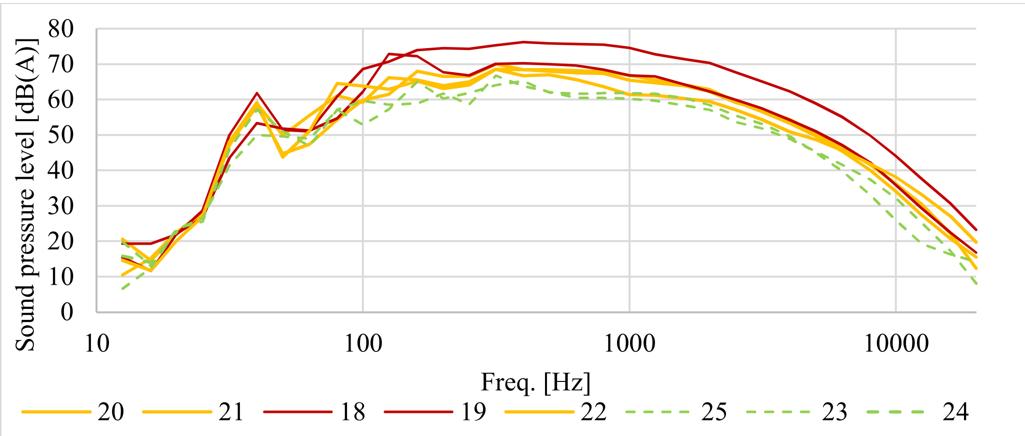

Figure 5-16 Overall comparison in among different measurement locations on board.

5.5.2. Simulation model: calibration and comparisons

The simulation model provided transmission losses from the source to the various receiving positions (in Figure 5-5 some of the nearest positions are shown in black). In order to derive the absolute value of noise radiation, the source strength was derived by back-computing it using the experimental value in a given position and the transmission losses calculated in the same point.

This calibration of the source strength was performed in each single survey point available on board, obtaining different characterizations of the sources. The various predicted levels were compared with the measurements (excluding the point used for calibration); this method provided info and data for optimizing the fitting between estimates and measurements. For the choice of the calibration point, all the points close to the funnel were tested, for which both the experimental measurements and the numerical results were available. Each calibration involves more or less significant errors depending on the frequency; these errors were grouped for each calibration and average and standard deviation were evaluated.

The minimum standard deviation data is obtained by calibration on receiver 20 or 21; the calibration at point 20, however, provides the lowest average error. As an example of the results obtained from the different calibrations, the calibration obtained on point 20 is reported in Figure 5-17.

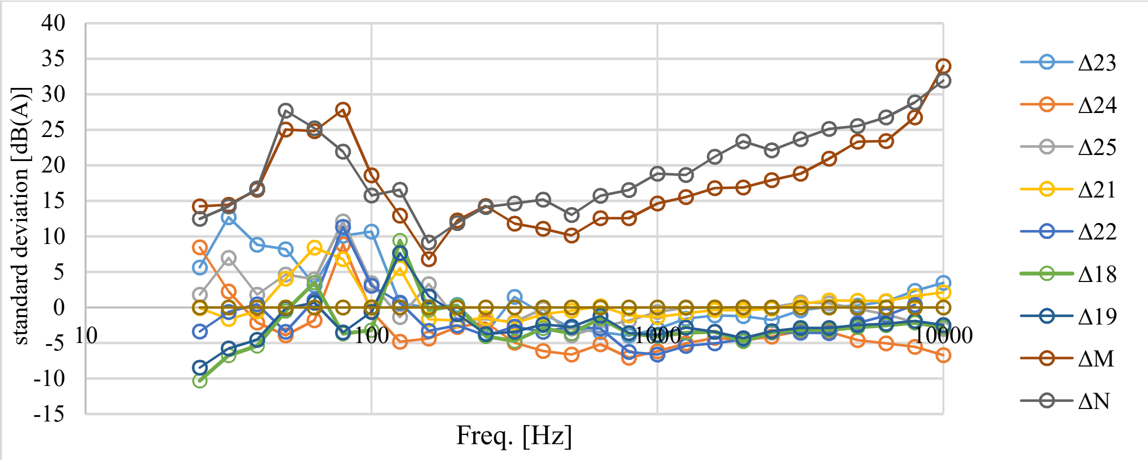

Figure 5-17 Calibration on point n. 20

Figure 5-18 below show the results of this exercise in terms of average difference and standard deviations between the predicted values and the experimental ones (a couple of values for each calibration point): the adoption of calibration in point 20 provided the lower BIAS and lower Standard deviation, respectively. The model has therefore been calibrated on this point.

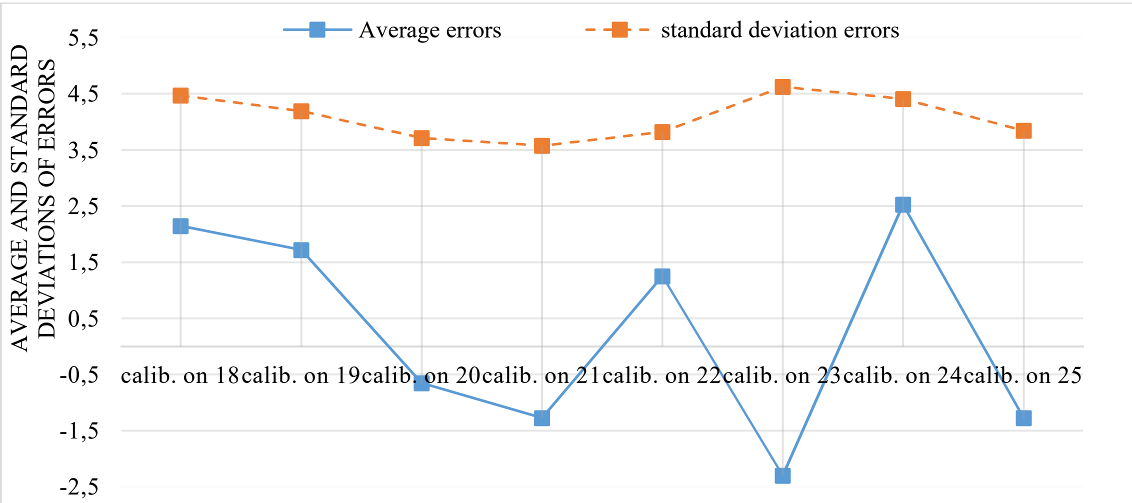

Figure 5-18 Average and standard deviations of differences between predicted and measured values (depending on the calibration point)

Table 5-5 reports the complete results with the calibration in point n.20. Results show a fairly good agreement in the zones close to the noise sources (and calibration point), but also quite disappointing results to the receiver 24 and on the points in the square SNAV, where experimental values are respectively lower and higher than predictions. In those positions, acoustical effects, not included in the model, seem to affect predictions.

Table 5-5 Expected against experimental values of the equivalent sound pressure

Position	Results L_{eq} [dB(A)] (Experimental value/ predicted value)
Receiver 18 (Level III)	80.5/82.6
Receiver 19 (Level III)	80.5/82.0
Receiver 20 (Level II)	78.4/78.4
Receiver 21 (Level II)	77.8/78.5
Receiver 22 (Level II)	76.5/79.5
Receiver 23 (Level I)	73.2/74.0
Receiver 24 (Level II)	71.5/76.2
Receiver 25 (Level I)	73.7/74.6
N (SNAV Service Area)	62.6/57.2
M (SNAV Service Area))	63.3/59.6

5.5.3. First approach to the new additional class notation

An application of the LR notation in this specific context by means of numerical models can be carried out by means of ray tracing-based methods. These methods, however, need to be applied with specific attention to the anthropomorphic characteristics of the area, because the specific geography of the port can produce discrepancies of results. In this regard, and given above all the need to analyze behavior over long distances, ad hoc simulations were carried out to read the data of an *old* measurements *campaign also carried out at the port of Naples by the Department of Industrial Engineering. These measures concern the same passenger ship moored at a different point. These measures were therefore used despite not being born with the aim of being used for applications relating to the LR regulation, obviously being antecedent.* In this case, the points of interest are those shown in the Figure 5-19. Points A, B, and C are inside the red area, point D in the yellow one, and E, F, and G in the green one.

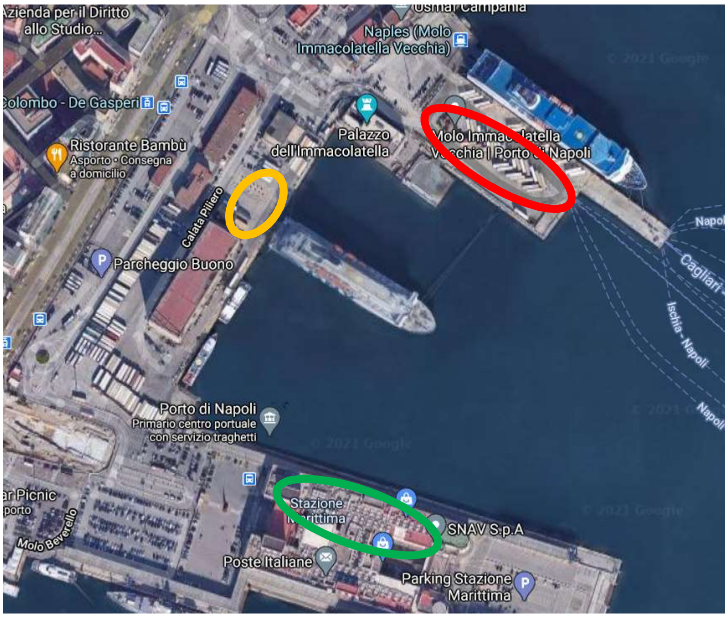

Figure 5-19 Measurement zone

The next picture,

Figure 5-20 , shows an example of the Terrain modeling when evaluating the acoustic footprint of a long-range ferry at quay.

Figure 5-20 Source

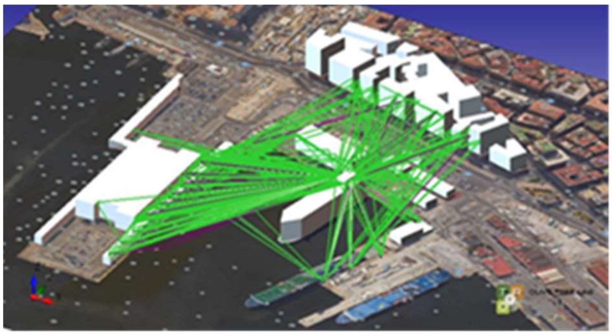

Figure 5-21 Numerical model transmission paths

Nevertheless, it appears evident that the noise transmission paths to the target receivers are strongly affected by the presence of surrounding buildings in the

Figure 5-21. Because of this, when verifying the ABN, different noise levels at similar distances from the source are produced. The next table, Table 5-6, shows a direct comparison of noise level estimated at the target point and relative experimental measurements.

Table 5-6 Comparison of noise level estimated at the target point and relative experimental measurement

Point	Experimental value	Numerical value	Difference
	dB	dB	dB
A	61	58	-3
B	64	64	0
C	65	67	2
D	71	65	-6
E	63	63	0
F	63	59	-4
G	60	55	-5

It must be kept in mind that points E, F and G are located along the balcony of Stazione Marittima on the right side of the ship, A, B and C are located on the opposite left side on the quay area and D is located on the back of the ship (see Figure 5-19). Numerical and experimental values are quite similar in some locations but significantly differ in other ones. This may be due to model uncertainties both in the characteristics of the source and of the environment. On the one hand, the source (in lack of more detailed information) was modelled as omnidirectional and this may turn out to be imprecise. On the other hand, the surrounding environment is definitely asymmetric and different effects affect the propagation in different directions (different interaction of direct, diffracted and reflected paths). This may imply a different degree of accuracy of predicted values along the various transmission paths.

5.6. Case study n.2 application of the LR class notation to a passenger ship

The publication of the class notation of the Lloyd Register, in addition to the port and civil regulations, may in the future lead to the request, by shipping companies, to certify the levels of airborne noise emitted by their ships. Among other things, this certification may be required to access particular areas of naturalistic interest or some ports particularly sensitive to environmental impact issues (see those in Northern Europe). *The purpose of this research is to predict the airborne noise emitted by a ship through the use of simulation models and compare it with the limits set by LR.*

The development of the project essentially involved four phases:

- the analysis of predictive data relating to the sources of external noise present on board the ship;
- experimental measurements on the same sources and comparison with predictions;
- the elaboration of the geometric model of the external surface of the ship starting from the drawings available;
- generation of the simulation model and internal consistency checks;
- verification of the limits of the notation.

The characterization of the sources went through several phases. A starting point in particular has been the forecast **data provided by the manufacturers** of ventilation and air conditioning systems as well as by the engine manufacturers. These prediction data characterized each grid on board in terms of power and/or sound pressure generally at 1m. Validation of these purely predictive data was made by comparing these sound pressure levels with a few **measurements** carried out onboard. A mix between predictions and experiments constituted the input for the simulation model. *For reasons of industrial confidentiality, it is not possible to explicitly mention all the sources on board and show the inherent data.*

Once the single sources were characterized and implemented in the geometric model, the following steps were realised:

- a validation of the internal coherency of the model by applying ISO 3744 and 8927;
- a comparison of the model results with the experimental measurements made at sea;
- an assessment of the ship's emission level according to the LR standard;

5.6.1. Sources: funnels

The noise levels related to the funnels can be derived by data provided by the Manufacturer of the engines themselves the main information necessary for a prediction are:

- the number of engines and of the funnels were exhausts are convoyed;

- the position of the funnels (deck, height above sea level, longitudinal and transversal position);
- the sound power level after turbocharger for each type of engine vs. the % of the load to the engines to which the pressure levels refer.
- The sound power level reduction achieved by silencer(s) and ducts.

5.6.2. Sources: ventilation and air conditioning systems

The characterization of the external airborne noise sources related to ventilation and conditioning systems requires careful cataloging of each individual grid or group of grids corresponding to the intake or exhaust of each unit on board. The positioning of all the listed sources requires particular attention and precision in the early stages of model building. In fact, for air conditioning and ventilation systems the number of sources to be positioned can easily exceed a hundreds. Each unit is made up of one or more grids arranged on horizontal or vertical planes of the external surface of the ship. The identification of the position on board should therefore be done by indicating, at least, the ship deck, the number of grids present, the orientation of the same, and, consequently, the area or the extension in ordinates of the total number of grids. Given the high number of sources to be characterized, it is good practice, therefore, to generate a strict characterization and positioning protocol for each source on board (each labelled with its own identification code).

Air conditioning units are generally placed on board in living spaces (where no other noise-generating machinery is present). The external noise emitted should be therefore predicted on the basis of the airflow, (in inpu or output), the sound powerlevels of the plant and attenuation due to ducts and silencers).

Ventilation systems connect potentially more noisy spaces with the outer atmosphere, so in principle also the contribution of the machinery running in the ventilated room is to be taken into account.

In both cases, the final information is the sound power level at the external grid, which can be predicted on the basis of the plant characteristics or directly measured in the proximity of the grid itself.

5.6.3. Measurements and comparison with predicted data

An initial validation of noise pressure level predicted on the basis of data provided by the Manufaturers was carried out by comparison with a first set of measurements available from a sister ship. The purpose of the comparison was to cross-check the accuracy of the predictions and the quality of the procedure followed in the experimental campaign.

Sources were grouped by type: air conditioning grids, ventilation grids and funnels. Within the first two groups (the most numerous ones) a few typical trends were identified in the experimental data. For example, in a group of measurements, a strong component was found, concentrated at low frequencies that was not present in other surveys of the same type. This raised the question of a possible contamination in surveys by other sources in the proximity. Another problem was the difficulty in associating a given survey to a specific source (grid).

What the above suggested to point out the need for a strict protocol in carrying out the surveys, with a precise identification of the measuring position (by means also of photos, for example). A second suggestion was to explore the possibility of separate tests with single sources active, in order to avoid contamination in the results. The small number of measurement points of this campaign and the impossibility of a one-on-one association between measurement and source allowed only preliminary comparisons between experimental and predicted levels, but the general trend identified was that predicted levels were lower than experimental ones.

A second, more extensive and more finalized campaign was carried out on the ship under analysis during sea trials. In this second campaign more attention was devoted to the identification of the relative position between the measurement and the source and in a few cases procedures for the sound power characterization of source were applied. Surveys regarding the funnels were carried out, too, even though at comparatively large distances. This second set of measurements confirmed in any case that predictions under evaluated the actual strength of sources on board.

In addition to the surveys devoted to the characterization of the single sources on board, a few measurements were carried out of the whole ship at distance. The reason for doing this during sea trials was to take advantage of a more silent environment in comparison with the shipyard, where background noise is quite high. It is noted that the LR experimental procedure for the survey of the ship noise levels at distance requires vey low background noise, in practice impossible to be realised in an active shipyard.

Measurementes in open sea, however, were carried out from a small boat and this affected results to some extent because of wave noise produced by the boat pitching.

5.6.4. Geometric model

In order to characterize the airborne noise emission from the ship, a geometric model of the ship body has to be generated in order to apply on it the noise sources characterized beforehand. Since the analysis focuses on the acoustic field radiated outside the ship, only the outer surfaces of the vessel are used to define the model. More specifically, the ship body model is a continuous surface enveloping all the closed volumes of hull and superstructures, with special attention to the funnel. While generating the model, a proper compromise between accuracy in the resulting noise free field and in the pre-processing and computation time should be found.

Historically, simulation software has been developed to evaluate the impact of noise pollution caused by industry, roads, railways and airports on residential areas. They are therefore focused on the modelling of buildings and typical environment of the civil and industrial sector: tools for the modelling of a complex body like that of a ship, characterized by an outer double-curved surface, are not implemented. This created some problems that was not possible to solve by importing the geometry from other types of software (e.g. F.E.M). In the end, the outer surface of the ship was modelled by a stepwise cylindrical surface with vertical walls, obtained by ‘extrusion’ upwards in the vertical direction from the perimetr of each deck to the following one with different dimensions. The surface discretization is implemented starting from the waterline up to the highest deck mainly on the basis of the ship’s general plans.

Only large local protrusions from the ship sides like wing decks or balconies were modelled. The resulting surface is relatively coarse, but this was not considered to affect results in terms of propagation at large distances, such those at which the sound pressure levels radiated by the ship are to be compared with the limits contained in the class notation.

From the viewpoint of sound propagation, an important effect of the external surface is the reflection of the noise into the surrounding environment. Sound reflection characteristics correspondent to a full reflection from a rigid body were set, as well as a full reflection was modelled by the flat surface of the sea.

After generating the geometrical model of the ship, point sources were placed on the surface, with position according to the actual position and strength corresponding to the measured sound power levels. For a limited number of sources, for which direct measurements were not available, levels were derived by analogy from similar sources or predictions were adopted.

5.6.5. Cross-checks of the internal coherence of the acoustical model (ISO)

As a further step of the acoustical model development, an internal coherence check was carried out according to ISO 8927 and ISO 3744 standards. These standards are actually aimed at deriving the total sound power of a complex source from sound pressure measurements carried out (a) on a plane line and (b) on a closed surface surrounding the source.

In the present case, pressure levels computed by the propagation model on the line and on the surface were used to derive a value of the total power radiated by the ship that was compared to the sum of the power assigned to the various local sources placed on the ship surface. The scope of this check was to exclude that input errors were made in the generation of the model and that the output sound field was coherent with the input data. The checked equivalence in total power levels indicate also that a characterization of the total acoustic power level emitted by the ship could be measured by a limited number of surveys (in locations relatively close to the ship) instead of deriving the same information from a larger number of measurements characterizing all the local surface point sources actually present on the surface.

According to the first coherency checks, the ISO curves have been calculated according to ISO 8927 and ISO 3744 starting from Sound Pressure Levels. UNINA's forecast data according to ISO8297, is close to that of the input curve, with extra deviations at low and high frequencies and less at medium frequencies. The data obtained with ISO 8927 would seem to indicate that a result similar to that relating to the measurement sources characterized on board could be generally obtained through measurements.

5.6.6. Comparisons between propagation decay laws

As in the formulation of any acoustical problem, where the scope is the represented by the control and mitigation of the perception of noise by the receiver, key points are the correct characterisations of the noise source strength and of the transmission loss acting on the noise signal during the propagation to the receiver. In this study, the source is represented by a large number of point sources placed on a complex surface in slow motion. The transmission path, instead, is relatively simple, being made of a semispace of a homogeneous medium (air), bounded from below by a flat and reflective surface (sea surface). A single stationary point source in an unbounded medium would have a spherical propagation, producing pressure levels with decreasing values according to the known law:

5-5 Spherical propagation law

$$Lev(r) = Lev\,(source) - 20\,Log(r)$$

The same source in motion would produce a cylindrical propagation in terms of max levels. If the point source is placed on one side of a reflective plane (the ship surface), the propagation can be still modelled with a spherical law, but with higher level (+3 dB) due to a higher concentration of the same acoustical energy in half space. Another enhancement in levels comes from the reflection from the sea surface placed at a distance from the source, in our case. In the present case study the total acoustic power of the ship is split among a number of incoherent point sources placed along the considerable large length of the vessel.

This situation differs from the simple acoustic schemes (spherical/cylinder) in that the acoustic power radiated from the various sources is not correlated in space and in time, even though the total emission is the same. An expected difference is in the propagation pattern, which should depart both from a spherical propagation and a cylindrical propagation.

In the LR Class notation document, requirements are set both at source and at a distance, the former in terms of total radiated power by the ship, the latter in terms of pressure levels at a given distance. These two classes of requirements are implicitly linked through an hypothesis about the propagation law.

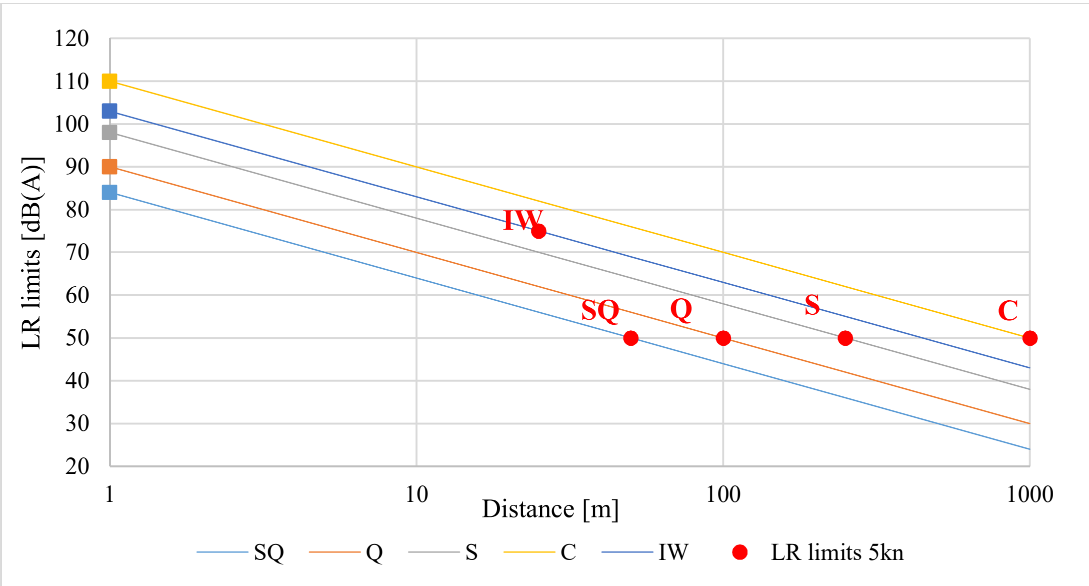

Figure 5-22 Interpretation of LR limits in function of the distance

In the Figure 5-22, the various requirements in terms of sound pressure levels at various distances (red dots) are interpreted as points on a straight line of slope -2 (in logarithmic scale), with starting point at a (distance of 1 m) corresponding to a pressure level 3 dB more of the one corresponding to a point source with the same total power of the ship radiating in an infinite space (square dots at 1 m). The two requirements are coherent with each other if the propagation scheme of a single point source of equal sound power in a half space is adopted for the ship. It should be noted that requirements are formulated in terms of distance from the shipside and not from any specific point on board (e.g. corresponding to an actual source). In this interpretation therefore, the reflecting plane corresponds to the ship side, and the single source is placed on such plane.

Figure 5-23 below compares the pressure levels computed by the UNINA propagation model with the spherical propagation law. Differences are very small.

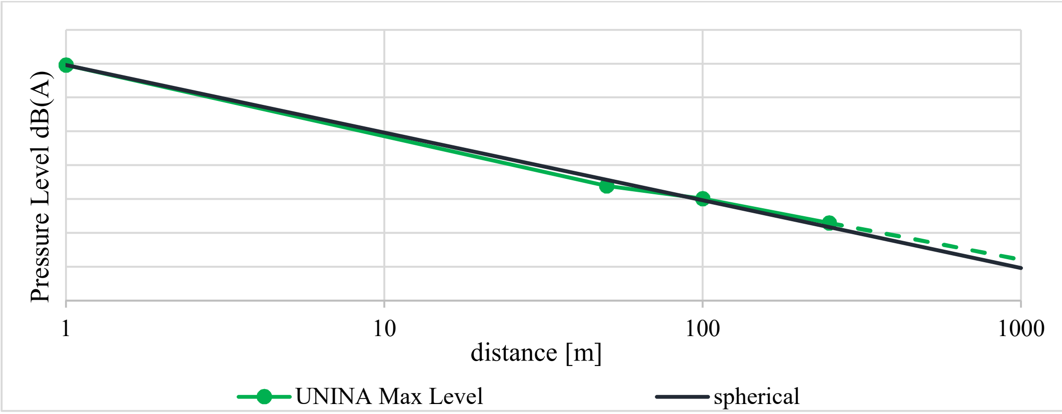

Figure 5-23Measured noise levels as a function of the distance NA (UNINA)

5.6.7. Propagation results

The following propagation predictions were made:

- on board, in the near-field, with the aim of investigating the effectiveness of propagation software in the near field and for the assessment of on-board comfort;
- at medium distance, with the purpose of a theoretical-experimental comparison in those positions, using the surveys carried out at sea;
- at larger distances, in the positions suggested by the LR procedure, in order to compare the results with the limits reported in LR.

5.6.7.1. Near-field propagation results

In graphs of Figure 5-24, a comparison of the data measured in two positions with the simulations results carried out in the same positions.

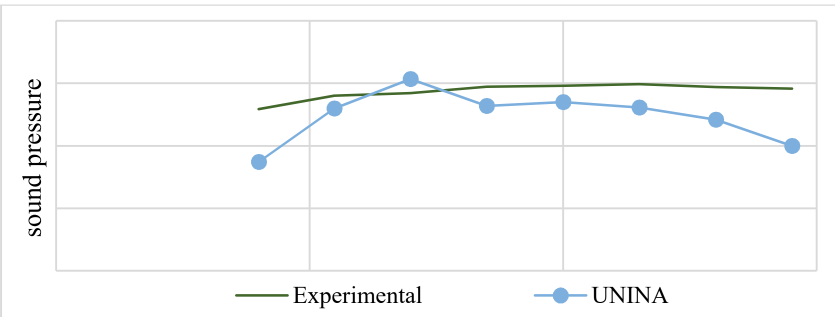

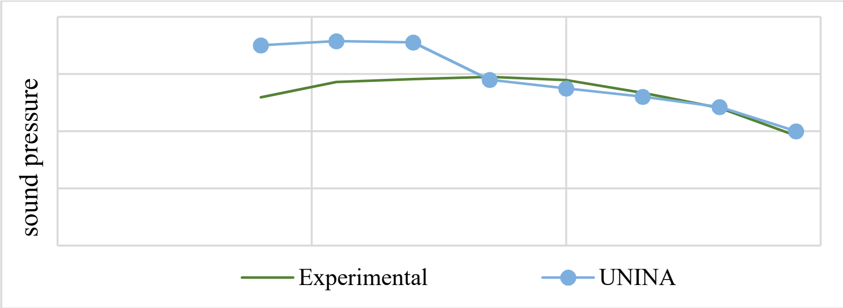

Figure 5-24 Comparisons in near-field

The simulation results are generally in line with the measurements. It is worth mentioning that the use of the class propagation software adopted in this study is not optimal for deriving levels at a short distance from the source.

5.6.7.2. Medium distance propagation results

This subsection compares the expected Sound Pressure Levels with those measured in positions on one side of the ship at certain distances during sea trials in Table 5-7. The predicted values are higher than those measured, but there are still uncertainties about the measured values. The Table 5-7 shows how the results obtained with the three simulation software are similar to each other; this comforts and confirms the reproducibility of the calculation methodology.

Table 5-7 Differences in dB between simulation and experimental results (standardized on Leq)

	Simulation results		
Point	UNIGE	UNITS	UNINA
1	2,3	-1,4	2,7
2	5,9	2,5	7,3
3	3,7	1,4	3,1
4	1,8	-0,4	0,9

5.6.8. Far-Field propagation results

According to LR, three distances have been chosen for the position of the receptors. For each of these distances, three heights above sea level, corresponding respectively to 3.5 m, H/2 and H, were chosen on both sides of the ship. These heights will be referred to as LOW, MID and TOP respectively. On each side of the ship, and for each height, sound pressure levels were calculated vs frequency. The calculations were developed on all the three softwares available to the three partner universities. Results are available in Table 5-8 for UNINA. A good congruence of the data can be observed for the maximum levels, intended as the envelope of the Max on all points equally distant from the ship (independently from the vertical position). For the above results, the fluctuation band is very low.

Table 5-8 Maximum levels expected at various distances and different heights (standardized at 50m low)

L_{Max}	UNINA		
d [m]	LOW	MID	TOP
50	0	1,4	1,3
100	-1,6	-3,7	-3,7
250	-10,6	-8,2	-10,4

The Table 5-8 also shows that for each distance (50, 100 and 250 m) the propagation is substantially flat since it varies little with the variation of the height (LOW, MID, TOP).

5.6.9. Discussion and conclusions

Presently, it is not typical that acoustic performances of the ship are set as design specifications, but the increasing interest on the acoustic impact of ships seems to indicate that the situation could soon change. If this should happen, the work carried out in this study indicates that the control of acoustic performance, needs to be implemented since the very early design stages. The key tool for such control is an acoustical model of the whole ship. However, in order to be reliable it should be based on solid predictions, effectively supported by reliable specification data but also by a robust database of experimental measurements systematically carried out onboard for the characterization of the sources.

6. Additional investigations on eco-friendly ports and on energy efficiency of cruise ships

Aims and scope

This chapter sets out three studies in order to keep on set the problem of emission of passenger ship in port, in a global scale context.

The first, in the wake of the ***EEOI and EEDI****, presents an analysis of the possible countermeasures that can be applied to the cruise ship fleet aimed at environmental safeguarding. These countermeasures will also be analyzed in terms of economic commitment and payback times. The application is aimed at evaluating the potential of a systematic application of energy saving techniques on the whole sector of cruise vessel. It is organized as follows: in the first part, the main concepts regarding EEDI and the methods of presenting costs related to the application of one or more particular emission reduction measures are recalled. The second part will concern the analysis of the spreadsheet in terms of basic hypotheses, inputs and outputs. Finally, an application on a set of cruise ships will be made.*

*The second work, on the other hand, concerns, the ports and the possible activities and initiatives to be implemented in order to host fleet of increasingly green and eco-sustainable ships (****Environmental Ship Index****). As it always will be, the case study is the port of Naples with its fleet of* ***cruise ships*** *arriving in the main busy periods. The obtained results will be compared with ports in Northern Europe that are particularly sensitive to environmental sustainability.*

Both applications, therefore, look at the same problem from different points of view: ports and ship owners.

*In the last subsection, a pilot experience carried out in the port of Naples has been presented. In this application, new technologies based on safe optical sensors for remote sensing (****LIDAR****) the* ***exhaust gases*** *emissions from internal combustion engines of ships proved to be ready for implementation in the context of a* ***port area****.*

6.1. Computer model application to the evaluation of Energy measures for cruise ships

6.1.1. Energy efficiency in maritime industry

Making the world’s fleet more and more efficient, with the aim of reducing emissions, is the challenge. The introduction of EEDI and EEOI (Energy Efficiency Operational Indicator) indices and inherent limits, respectively for new designs and operations in service ships, is an example of this effort that the maritime sector has been facing in recent years (**Smith et al., 2015**). The commitment to reduce emissions of which the maritime sector is responsible implies the adoption of operational measures aiming at reducing fuel consumption. Despite the fact that shipping is among the most efficient transportation means (**Wan et al., 2018**), the commitment taken by the IMO to fulfil the Paris Agreement for a reduction of emissions in all sectors has prompted a series of political and operational actions aimed at improving ship efficiency **(see f.i. Mocerino et al., 2018**). The definition of the EEDI aims at fostering design measures and technological innovations, leading to a continuous reduction of CO_2 emissions per mile. Data referring to 2010 estimated that the ships targeted by EEDI requirements account for about 72% of the CO_2 emissions of the maritime sector, covering the majority of the world fleet. In general, the fulfilment of requirements on the index should imply at obtaining increasingly more efficient fleets: +10% efficiency in 2015, +20% by 2020 and +30% by 2025. According to ICCT (International Council on Clean Transportation), if this roadmap were to be respected, 263 million tons of CO_2 per year could be saved by 2030 (**Hon & Wang 2011**). The EEOI focuses on efficiency and performances of a ship in operational conditions; the index can be used by ship-owners to monitor the overall performance of their fleets in terms of energy efficiency (**MEPC 2009**). Within the IMO-Marine Environment Division, a Project Coordination Unit (PCU) is dedicated to a particular project: the GloMEEP **(**Global Maritime Energy Efficiency Partnership) project; this collaboration between GEF (Global Environment Facility), UNDP (United Nations Development Programme) and IMO, has the main purpose of favouring the reduction of greenhouse gases connected to the maritime sector, see Figure 6-1.

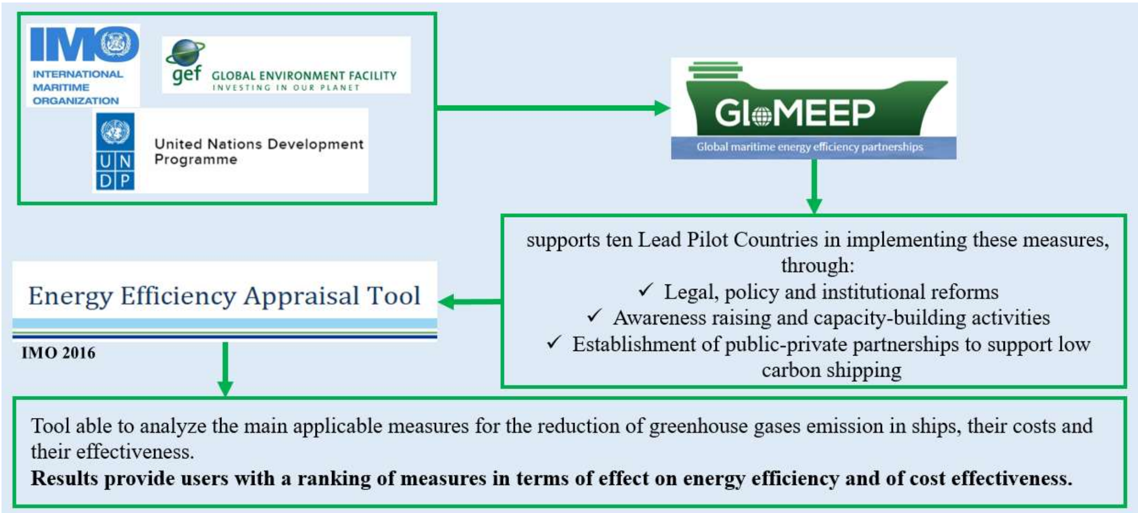

Figure 6-1 Energy Efficiency Appraisal Tool framework

The project supports adoption, on a global scale, and implementation of energy efficiency measures in the sea transport sector. Nowadays, 10 LPC (Lead Pilot Countries) have joined the project in order to implement policies to reduce their emissions through institutional reforms, enforcement of public awareness and the establishment of public-private partnerships for low-carbon navigation. The GIA (Global Industry Alliance) started in 2017, is an example of this partnership; members of this alliance are classification societies, engine and technology builders, suppliers, oil companies and ports. With the aim of providing a tool for costs and benefit analysis of these energy efficiency measures, DNV GL developed an interactive spreadsheet for IMO. The tool is meant to provide an assessment of the impact of the various possible energy efficiency measures. It computes the effects of these technical operational measures on both the EEDI and the EEOI, and also the Marginal Abatement Cost Curve. The calculation sheets used, “Energy Efficiency Appraisal Tool” (**EEA Tool**), are included in this project (**IMO 2016a**). *The purpose of these calculation sheets is to provide the operators of maritime sector with a tool able to analyze the main applicable measures for the reduction of greenhouse gases emissions in ships, their costs and their effectiveness in reduction. The results provide to the users the possibility of identifying the measures with the largest effect on energy efficiency and the highest cost* *effectiveness. This can result in important source of evaluation for Ship-owners, in view of the selection of a business strategy. In the present application, use, results and potential of the model have been exploited by using input data derived from the specific segment of cruise vessels. Therefore, the development of the EEDI and EEOI formulas will be based on this particular type of ship, taking into account that, to date, most cruise ships are equipped with electric diesel propulsion plants with azimuth thrusters.*

Implementing energy efficiency measures on these giants of the sea implies savings on operating costs, gains for the environment, compliance to regulations and an economic return in terms of positive advertising. For these reasons, many companies have already taken steps in the last years towards a policy for green ships. *Holland America Line* builds shorter routes to minimize fuel consumption, adopts silicone paint to reduce the drag of the hull, has taken steps to make the engine work more efficiently and has installed on many of its ships the OPS (On shore Power Supply).

The *Solstice* ship has built solar panels in the pool area on board reducing the load on the generators and 7000 LEDs replacing the classic bulbs to decrease electric consumption.

The *RMS Queen Mary 2* features an exhaust gas economizer using waste heat from engine to produce steam.

The *AIDA PRIMA* uses LNG in port since 2016; the *Viking Lines* have a rotor sail on board which uses wind power and dual fuel engines (**Underwood, 2009**).

Costa manages the European Commission co-funded Sustainable Cruise project to reduce and recycle solid waste on cruise ships and reuse or proper disposition of residual matter.

As of 2016, five of the Norwegian *Cruise* line vessels have been equipped with exhaust gas cleaning systems, which work to reduce sulfur oxide and particulate matter by scrubbing the ship's exhaust stream **[16]**.

6.1.2. EEDI

The evaluation and check of the EEDI has become mandatory for all new ships, or for those that have undergone major conversions, along with the SEEMP for all ships, with the MEPC.203 resolution (62) of 2011, with an adjustment to the Annex VI of the MARPOL (**MEPC 2012b**).

In 2014, MEPC extended the use of the index to new market segments, including cruise ships equipped with non-conventional propulsion. In the guidelines for the calculation of EEDI, the diesel-electric propulsion is, together with hybrid engines and turbines, included in the typology of nonconventional propulsion (*ncp*), to which reference is made in the following calculations (**MEPC 2012a**). EEDI characterizes each ship with a specific value, a ratio between the generation of CO_2 (g) and the transportation capacity, expressed as ship capacity*mile). In our case, it will be g_{CO2}/GT*mile, see Figure 6-2.

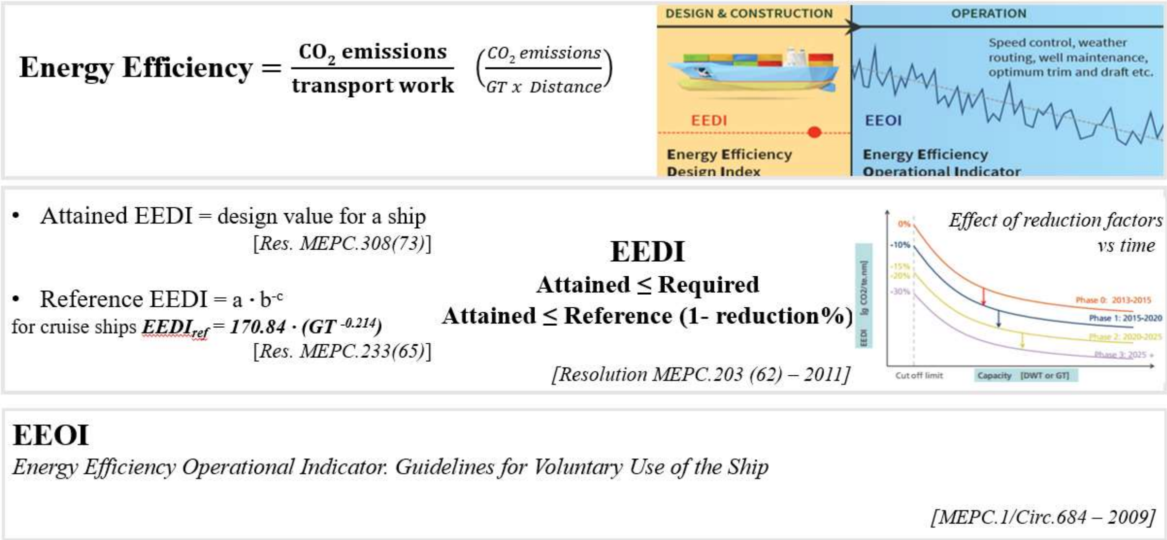

Figure 6-2 EEDI and EEOI framework

The guidelines for the calculation of EEDI on the attained energy efficiency index is, for new ships, in Annex 8 of MEPC.212 (63) adopted on March 2, 2012 (**MEPC 245(66) 2014, MEPC 308(73) 2018**). Each new vessel with more than 400 GT and operating in international waters features an EEDI, called attained EEDI, which must be *less or equal* to the required EEDI. The *required EEDI*, according to regulation 21 of MARPOL Annex VI, is calculated using the relevant *EEDI reference line* and *reduction factor* for a particular type of ship. The reference line shall be obtained as follows (6-1):

6-1 Reference Line Value

$$RLV = 170.84 \cdot (GT^{-0.214})$$

Where GT is the gross tonnage of cruise ships. Therefore, starting from Phase 0 (years 2013-2015), the scheduling to lower the reference line from Eq (6-1), which means ever-increasing efficiency of the cruise ships, is:

- phase 1 (2015-2020) with 5% of reduction factor;
- phase 2 (2020-2025) with 20% of reduction factor;
- phase 3 (2025 onwards) with 30% of reduction factor.

Small size ships are excluded from checking their EEDI, for some technical reasons. For cruise ships equipped with *ncp*, this cut-off limit is 25.000 DWT. The formula for calculating the attained EEDI has the **TW** (Transport Work) product of GT, and V_{ref} (knots), the speed of the ship in design load condition in deep water and absence of wind and wave, at the denominator. At the numerator, instead, there is the production of carbon dioxide that takes into account all the measures to reduce CO_2 emissions present on board: the specific consumption, engine power and conversion factors between fuel consumption and CO_2 emissions come into play.

6.1.3. Energy Efficiency Operational Indicator (EEOI)

The reference standard is MEPC.1/684 of 2009 (**MEPC 2009**), which introduces the methodology for the calculation of the EEOI. As defined for EEDI, the unit of measurement is, in our case, g_{CO2}/GT*mile. This index gives the idea of the behavior of the ship in service, providing a current value of CO_2 emissions resulting from the combustion of all types of fuels used on board both in port and in open sea. The denominator, as an expression of the Transport Work, is the product between the cargo carried (the number of passengers or the tonnage for a cruise ship) and the distance sailed in nautical miles for the voyage or period under consideration. The numerator is represented by the terms contributing to the quantification of the emissions, i.e. the mass of fuel burned (understood as the whole consumption, both in port and in navigation) and the conversion factors from fuel to emission, as defined for the EEDI.

6.1.4. MACC

The other output presented by the calculation tool is the Marginal Abatement Cost Curve (MACC). Abatement cost is defined as the cost for reducing the pollution of a unit (**Devanney & Beach 2010; Faber et al., 2011**). These abatement costs are provided in the graphic form as MACCs, which show the marginal cost of additional reductions in pollution, see Figure 6-3. The curves are a method of calculating the CO_2 reduction potential of a particular reduction measure; they present measures to reduce CO_2 emissions in order of cost and effectiveness. The curves are widely used as decision-making tools for policies aimed at reducing emissions (**Rehmatulla et al., 2013**).

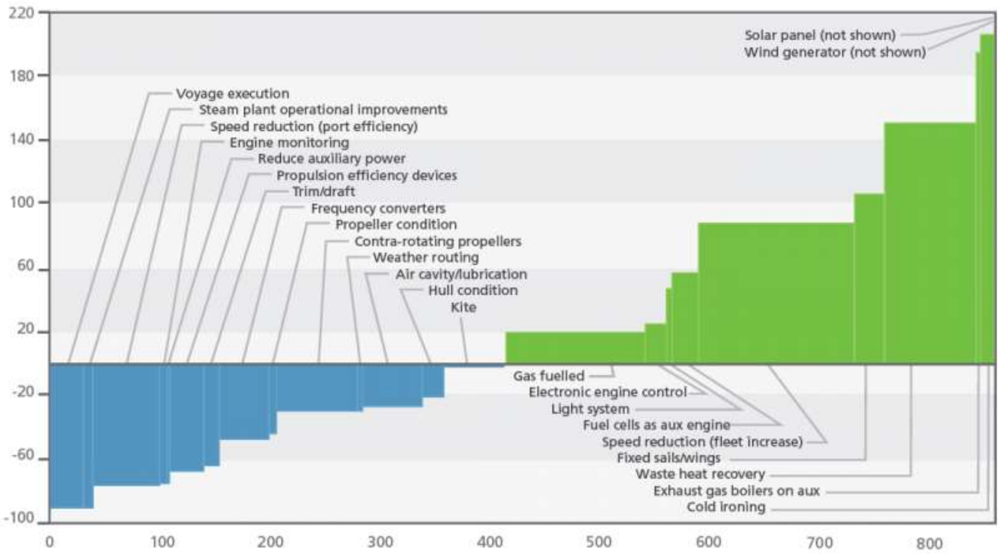

Figure 6-3 MACC curves

6.1.5. Energy Efficiency Appraisal Tool

6.1.6. Vessel segments and size categories

The types of ships on which the calculation of EEDI and EEOI is possible with the tool are Crude oil tankers, Product tankers, Chemical tankers, Dry bulk tankers, General cargo vessels, Container ships, Ro-ro ships, Passengers vessels, Ro-Pax vessels, and Cruise vessels (**DNV-GL 2016**). According to MEPC 245. (66) (**MEPC 2014**), which prescribes the use of GT for the calculation of EEDI, in this calculation tool, cruise ships are grouped by tonnage. In Table 6-1 the categories are presented with the symbol/ID adopted for the analysis.

Table 6-1. Size categories for the cruise ships

Size	Ships size ID
GT	
< 2.000	A
2.000; 9.999	B
10.000;59.999	C
60.000;99.999	D
>100.000	E

6.1.7. List of measures

The reduction measures taken into account in this tool may be grouped into *Technical Measures and Operational improvement*; some of them are *Alternative Energy Source*, see Table 6-2 (**DNV-GL 2016**).

Table 6-2 The list of measures

ID	Measures	Type	Uncertainty %
1	Waste Heat recovery	T	<10%
2	Solar panel (adoption)	T	>30%
3	Exhaust gas boilers on Auxiliary Engine	T	<10%
4	Trim & draft optimization	O	<10%
5	Propeller efficiency	O	<10%
6	Voyage execution (optimization)	O	10-30%
7	Hull coating optimization	O	<10%
8	Propulsion efficiency devices	T	<10%
9	(Energy efficient) frequency converter	T	10-30%
10	(Low energy) light systems	T	<10%
11	Air cavity lubrication	T	10-30%
12	Contra-rotating propellers	T	10-30%
13	Electronic engine control	T	<10%
14	Fixed sails or wings	T	>30%

Given that for all ships and for the considered categories in particular, the economic implications and the effects of each energy efficiency measure are different, uncertainties shall be considered (see Table 6-2). The uncertainties for each measure take cost and effectiveness of applying it on vessels into account. The uncertainties are the results of DNV GLs general knowledge on each measure, on its maturity in the maritime sector and on the experiences from other industrial applications. As an example, the alternative energy sources have high uncertainty due to their very limited adoption and experience in the maritime sector.

6.1.8. Input parameters and output

The EEA tool works in two modes: “Normal” and “Advanced”; in the Advanced mode the operational profile of the ship, the financial parameters, the effect of operational measures adopted, the fuel price development, and the fuel consumption can be specified by the user to obtain a more sensitive output (**DNV-GL 2016**). These parameters are automatically set in Normal mode (**DNV-GL 2016**).

The most important **assumptions** in the tool are 25 years of investment horizon, 8% of standard discount rate per annum and 3.114 g_{CO2}/g-fuel of Carbon content in the **HFO**, see Figure 6-4.

The results obtained are, for each measure considered, the effect of each measure on EEDI an EEOI [i.e. initial and new (post application of measures) EEDI and EEOI], an estimate of investment costs and payback time and a Marginal Abatement Cost Curve (MACC), see Figure 6-4.

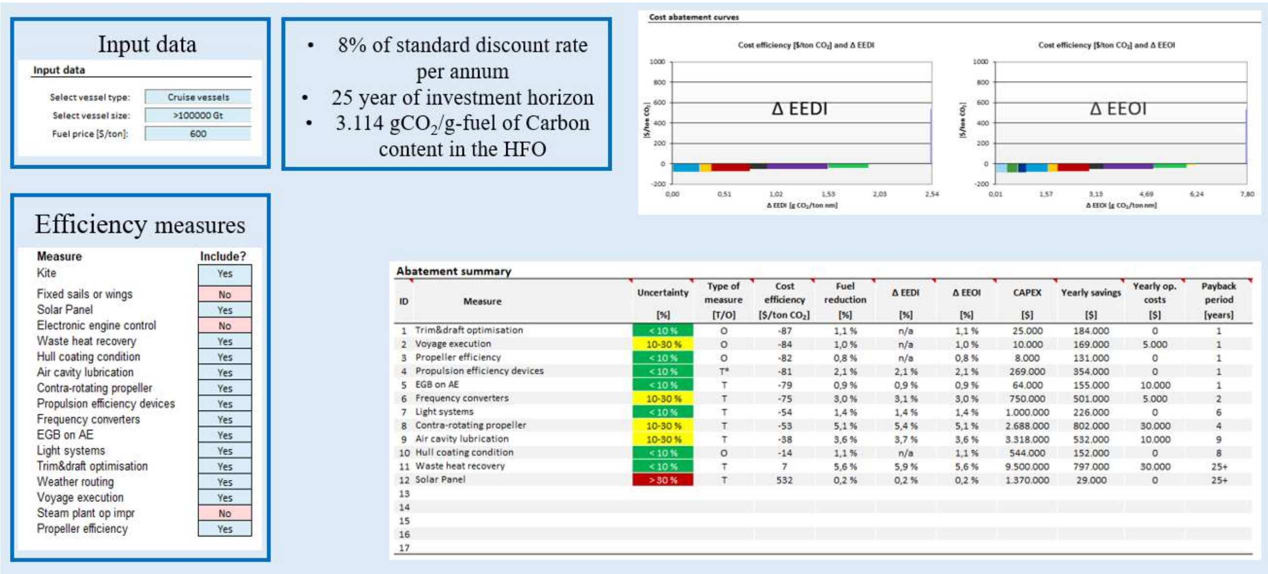

ID	Measure	Uncertainty [%]	Type of measure [T/O]	Cost efficiency [$/ton CO_2]	Fuel reduction [%]	Δ EEDI [%]	Δ EEOI [%]	CAPEX [$]	Yearly savings [$]	Yearly op. costs [$]	Payback period [years]
1	Trim&draft optimisation	< 10 %	O	-87	1,1 %	n/a	1,1 %	25.000	184.000	0	1
2	Voyage execution	10-30 %	O	-84	1,0 %	n/a	1,0 %	10.000	169.000	5.000	1
3	Propeller efficiency	< 10 %	O	-82	0,8 %	n/a	0,8 %	8.000	131.000	0	1
4	Propulsion efficiency devices	< 10 %	T*	-81	2,1 %	2,1 %	2,1 %	269.000	354.000	0	1
5	EGB on AE	< 10 %	T	-79	0,9 %	0,9 %	0,9 %	64.000	155.000	10.000	1
6	Frequency converters	10-30 %	T	-75	3,0 %	3,1 %	3,0 %	750.000	501.000	5.000	2
7	Light systems	< 10 %	T	-54	1,4 %	1,4 %	1,4 %	1.000.000	226.000	0	6
8	Contra-rotating propeller	10-30 %	T	-53	5,1 %	5,4 %	5,1 %	2.688.000	802.000	30.000	4
9	Air cavity lubrication	10-30 %	T	-38	3,6 %	3,7 %	3,6 %	3.318.000	532.000	10.000	9
10	Hull coating condition	< 10 %	O	-14	1,1 %	n/a	1,1 %	544.000	152.000	0	8
11	Waste heat recovery	< 10 %	T	7	5,6 %	5,9 %	5,6 %	9.500.000	797.000	30.000	25+
12	Solar Panel	> 30 %	T	532	0,2 %	0,2 %	0,2 %	1.370.000	29.000	0	25+
13											
14											
15											
16											
17											

Figure 6-4 Example of spreadsheet

6.1.9. Case study

The EEA Tool was used for all the categories of cruise ships in the dataset, ranging from 25.000 to over 220.000 GT and for all the measures considered in the tool. As a starting point, since not all the data was available for each ship to apply the exact formulation of the EEDI, a *concept* formula was used (6-2).

6-2 EEDI

$$EEDI_{Concept} = \frac{CO_{2emissions}}{TW}$$

The denominator contains the Transport Work, which is the product between gross tonnage and speed (6-3).

6-3 Transport Work

$$TW = GT * V$$

CO_2 emissions are obtained from the product between the emission factor (set to 3.114 t_{CO2}/t-fuel), the specific consumption, SFC (217 g/kWh) and the engine power (75% of the MCR) (6-4);

6-4 CO_2 emissions

$$CO_{2emission} = EF_{CO_2} \cdot SFC \cdot Power$$

The results obtained were inserted in a graph, Figure 6-5, with the tonnage on the *x-axis* and the values of the EEDI on the *y-axis*; the graph also shows the cut-off limit of the EEDI, 25.000 GT for the cruise, and the four reference curves depending on the reference phase.

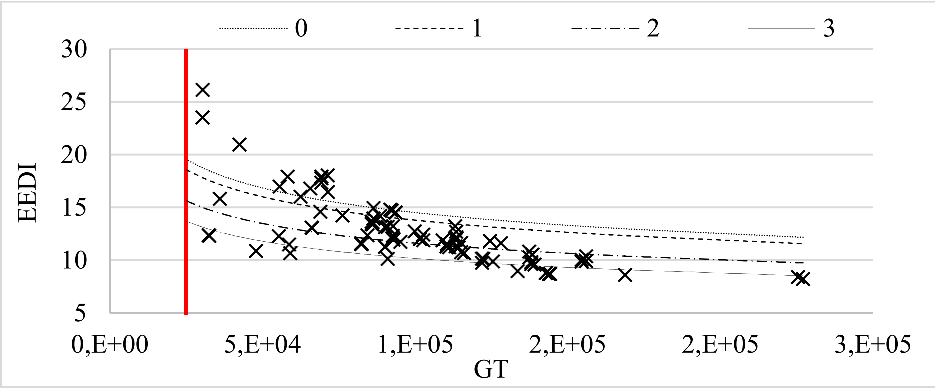

Figure 6-5 EEDI for the cruise ship data set

As it can be seen, by accepting the approximation of the used formula, many of the ships, especially those of small size, require the adoption of energy efficiency measures since they are not below the reference lines.

6.1.10. Results

The first results obtained were those related to TW and the quantity of saved fuel during a year of service (see

Figure 6-6); the tool returns two values for the EEDI, and two for the EEOI corresponding respectively to the value before and after the possible application of the energy efficiency measures, see Figure 6-7 and Figure 6-8.

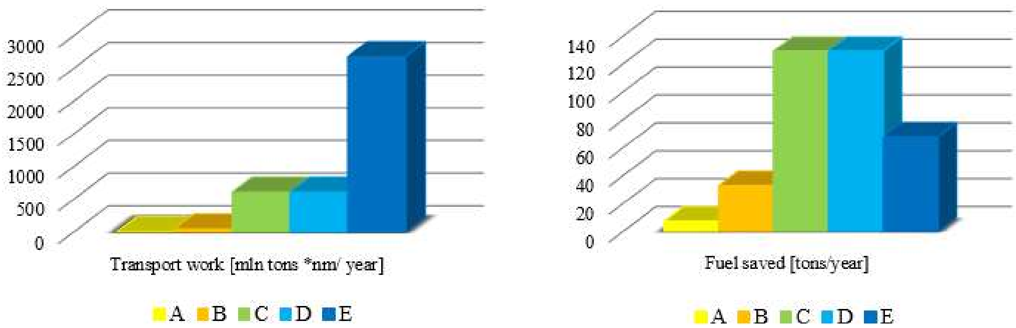

Figure 6-6 Transport Work (left) and saved fuel (right)

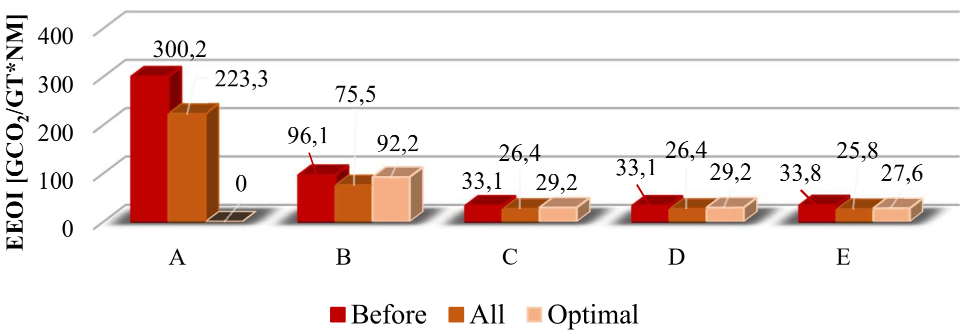

Figure 6-7 EEOI [$gCO_2/GT*nm$]

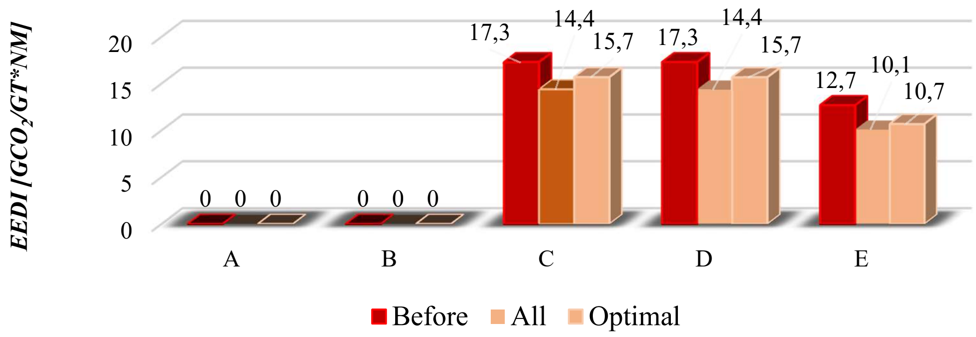

*Figure 6-8 EEDI [gCO$_2$/GT*nm]*

The Figure 6-7 and Figure 6-8 shows that the effects of applying the reduction measures are stronger in small ships. However, each emission reduction has its cost. To analyze the costs associated with the selected countermeasures, the reference is the Table 6-3, which made numbers out of the numerous MAC curves obtained through the carried out simulations. In the scenario, which sees the application of all possible countermeasures, the *cost efficiencies* in \$/ton$_{CO2}$ are indicated (see Table 6-3); negative values of cost efficiency indicate an economic saving achieved with the application of the measure. Analyzed by ship size, results show a considerable scale effect on costs:

- in category A, all emission reduction actions involve an additional cost (very high for the waste heat recovery for example: #1 in Table 6-3). The one with the greatest impact on emissions, in positive terms, is the use of fixed sails or wings (which entail an EEOI delta of 8.3% reduction in emissions: #14 in Table 6-4);
- in category B, as for the A one, evaluation of the EEDI is not yet required but some countermeasures, operational ones in particular, are nonetheless convenient in economic terms: trim & draft optimization (#4 in Table 6-3) and propulsion efficiency devices (#8 in Table 6-3). In this case, contra-rotating propellers are proved to be the most efficient means for EEOI reduction (#12 in Table 6-4);
- in category C, 58% of countermeasures imply economic gains and even those with positive costs are much more valuable than in other cases;
- in category D, 77% of the measures have a negative cost efficiency. The waste heat recovery system (#1 in Table 6-3) seems to be the most interesting measure. The most expensive, in terms of cost efficiency, i.e. the adoption of solar panels (#2 in Table 6-3), is clearly the one with lower percentage reduction, for both indices.

Particular attention has been given, for example, to the installation of an energy-saving lighting system (10 in Table 6-3), often applied in recent years on cruise ships; on average the percentage increase of the two indices linked to the light system is 1.5% (see Table 6-4). Cost efficiency goes from \$ 576/t$_{CO2}$ for small ships to savings of -\$ 54/t$_{CO2}$ for large cruise ships (see Table 6-3). In addition to the cost of efficiency, Table 6-4 shows the ΔEEOI (equal to the ΔEEDI at the first decimal place) of each countermeasure: each represents the percentage reduction from applying a specific measure.

Table 6-3. Cost efficiency

	Ship size ID				
	A	**B**	**C**	**D**	**E**
Meas.	[\$/ton $_{CO2}$]				
1	14581	2477	998	998	7
2	/	/	/	/	532
3	875	97	-48	-48	-79
4	17	-68	-83	-83	-87
5	599	21	-62	-62	-82
6	327	-14	-70	-70	-84
7	84	60	37	37	-14
8	74	-52	-74	-74	-81
9	92	69	33	33	-75
10	576	24	-19	-19	-54
11	254	118	53	53	-38
12	1046	125	-11	-11	-53
13	/	/	/	/	/
14	412	359	264	264	175

Table 6-4. Percentage reduction of the EEOI due to the single reduction

	Ship size ID				
	A	B	C	D	E
Meas.	[ΔEEOI %]				
1	2.0%	2.1%	2.1%	2.1%	5.6%
2	/	/	/	/	0.2%
3	0.9%	0.8%	0.9%	0.9%	0.9%
4	1.1%	1.1%	1.1%	1.1%	1.1%
5	0.7%	0.7%	0.7%	0.7%	0.8%
6	1.0%	1.0%	1.0%	1.0%	1.0%
7	1.0%	1.1%	1.1%	1.1%	1.1%
8	2.1%	2.1%	2.1%	2.1%	2.1%
9	3.1%	3.0%	3.1%	3.1%	3.0%
10	1.6%	1.6%	1.5%	1.5%	1.4%
11	2.1%	2.2%	2.1%	2.1%	3.6%
12	4.8%	5.0%	4.9%	4.9%	5.1%
13	/	/	/	/	/
14	8.3%	3.2%	1.5%	1.5%	0.6%

To complete the analysis from an economic point of view, the payback period of each countermeasure has been reported in Figure 6-9.

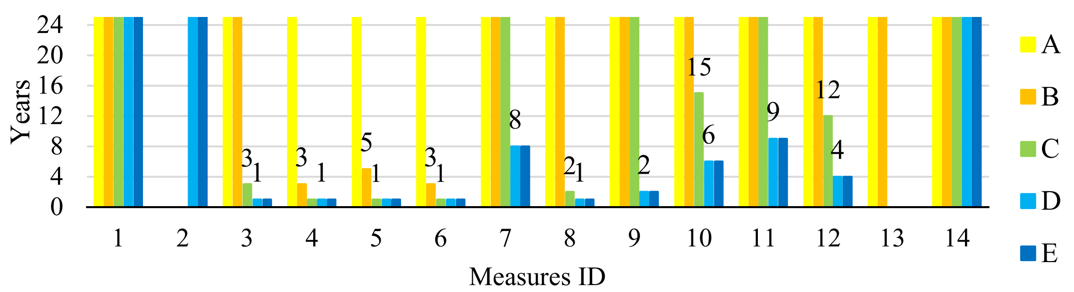

Figure 6-9. Payback period

Finally, a so-called “optimal condition” is derived for each size category of cruise ships, reporting the values of EEDI and EEOI predicted with the application of only the measures with a negative cost-efficiency (i.e. featuring intrinsic economical savings, see Figure 6-7 and Figure 6-8 and Table 6-5). These results are compared with the original EEOI and EEDI values and the ones predicted after the application of all measures.

From Table 6-5 it is clear that the choice of countermeasures which are convenient from only a purely economic perspective is not very effective on an energy efficiency perspective instead.

Table 6-5. “Optimal” combination

	EEOI			EEDI		
	[g_{CO2}/GT*nm]			[g_{CO2}/GT*nm]		
Ship Size ID	Before	All Meas.	Only Optimal	Before	All Meas.	Only Optimal
A	300,2	223,3	0	0	0	0
B	96,1	75,5	92,2	n/a	n/a	n/a
C	33,1	26,4	29,2	17,3	14,4	15,7
D	33,1	26,4	29,2	17,3	14,4	15,7
E	33,8	25,8	27,6	12,7	10,1	10,7

6.1.11. Effects on uncertainties

A final analysis was carried out by using the uncertainties introduced in Table 6-2, arbitrarily assuming that all countermeasures feature a percent reduction in their performances corresponding to half of their own uncertainty. The corresponding EEOI values have been estimated and are presented in Table 6-6 (A^*-E^* are the new results) in terms of new percent reductions (lower than the ones originally presented in Table 6-4).

It is clear from the comparisons that not only the EEDI percentage of reduction is affected by the application of the uncertainty, but the ranking of each countermeasure compared to the other ones (because of the different impact of uncertainties) as well.

Table 6-6. Delta EEOI obtained weighing the effect of uncertainties

	Ship size ID				
	A*	**B***	**C***	**D***	**E***
Measures	[ΔEEOI %]				
1	1,90%	2,00%	2,00%	2,00%	5,32%
2	/	/	/	/	0,17%
3	0,86%	0,76%	0,86%	0,86%	0,86%
4	1,05%	1,05%	1,05%	1,05%	1,05%
5	0,67%	0,67%	0,67%	0,67%	0,76%
6	0,85%	0,85%	0,85%	0,85%	0,85%
7	0,95%	1,05%	1,05%	1,05%	1,05%
8	2,00%	2,00%	2,00%	2,00%	2,00%
9	2,64%	2,55%	2,64%	2,64%	2,55%
10	1,52%	1,52%	1,43%	1,43%	1,33%
11	1,79%	1,87%	1,79%	1,79%	3,06%
12	4,08%	4,25%	4,17%	4,17%	4,34%
13	/	/	/	/	/
14	7,06%	2,72%	1,28%	1,28%	0,51%

6.1.12. Discussion and conclusions

The adoption and installation on board of countermeasures contributing all together to the reduction of the impact of ships on the environment is definitely the way to achieve the prescribed emission reduction targets in the shipping sector. Cruise ship data, filling the tool sheets provided by IMO for the assessment of the effectiveness of measures, exploited the potential of the tools themselves and of the attainable achievements. The application of the procedure supports the idea that target reductions in the emissions are feasible, in particular for this segment of ships (which probably has more degrees of freedom in comparison with other ship types). Results are however preliminary and need to be confirmed case by case, mostly because of the uncertainty affecting the performances evaluation. The list of measures could be integrated in future with other ones to be applied at a design stage, like the adoption of alternative fuels (LNG, bio fuels, hydrogen), hybridization, performance monitoring of the ships; improved aerodynamics of the superstructures etc. or even possibly adopted as retrofit solutions for existing ships.

6.2. Preliminary experimental campaign with the remote sensing- LIDAR

6.2.1. Framework and context

The identification and characterization of chemical and acoustical emissions from single sources and individual emitters is nowadays a necessary strategy for monitoring and controlling the emissions themselves. Transport infrastructures are called to implement policies for monitoring, identifying and fining transgressors. The maritime sector is not excluded from these strategies. The actual possibility for the local Authorities, such as Coast Guard, Port Authority, Municipality etc., of monitoring the emissions generated by single ship units is the first step to encourage the implementation of appropriate actions aimed at mitigating emissions and preserve the environment. For these reasons, a systematical monitoring of the emissions of ships at port is of extreme interest for implementing control policies. *The goal of this part of analysis is to exploit means for surveying ship emissions at harbor by remote sensing.* In the general context of shipping and port management, the focus on the source characterization represents an original aspect of the investigation, since the attention of monitoring activities is often concentrated on the final receiver. The trend is similar to what is taking place in road/rail transport infrastructures. Also in the context of EU Program Horizon 2020 (workprogramme ‘Smart, green and integrated transport’), a systematical monitoring of the emissions of ships operating in port area, in transient as well as in stationary conditions, is a matter of extreme interest. Surveys can be carried out in an intensive mode, but also in an extensive way, to characterize in real time the situation in the atmosphere above the port. A tool of this type would represent an asset for any Port Authority.

6.2.2. Surveying ship emissions

An average estimate of the emissions by ships in various operational conditions can be achieved by emission factors and dispersion model, see chapter 2 and 3 (**Papaefthimiou et al., 2016; Rodríguez et al., 2017**). Detailed surveys of ship emissions would require measures of both exit gas velocity and pollutant concentrations to obtain the mass flow rate of each pollutant. From a general point of view, the characterization problem for ship sources is quite similar to that of fixed point sources (e.g.; industrial chimneys) with additional complications:

- the large number of ships and then of sources (funnels) that change position all the time;
- the un-stationary regime in some operational phases;
- space limitations for the allocation of the monitoring equipment;
- maintenance of the dedicated equipment during navigation.

The different techniques for remote-monitoring ship emissions reported in literature may be classified as: land-based (generally inside port or urban areas), on board based, airborne (manned or unmanned rotary aircrafts) and satellite based.

In the first case, not the emission but the impact, generally at ground level (3-4 meters from ground level) is measured. These types of measurements are strongly influenced by the plume-like behavior of ship emissions with relatively short-time and intense peaks and for this they must be coupled with dispersion models or a statistical analysis (for source apportionment) in order to quantify the contribution of ship emissions. This determines a significant increase in the uncertainty of findings.

Land-based measurements include surveys of noxious gases, particulate matter, and chemical speciation (V, Ni, Fe) and are performed by using standard or innovative continuous analyzers or passive samplers. Even though data of air quality monitoring stations is often used to assess the impact of ship emissions in urban areas, specific monitoring campaigns are performed frequently.

Surveys of principal pollutants by continuous analyzers and passive samplers were carried out in the port of Naples (**Prati et al., 2015**) highlighting a non-critical situation inside the port area. Results shows how measured concentration levels were comparable with those observed at fixed monitoring stations in the urban area. This was probably due to the high emission height of funnels. Gaseous concentration of O_3, NO_X, and SO_2, were measured in the port of Brindisi (**Merico et al., 2016**) by using a mobile lab equipped with standard analyzers. The influence of ship emissions on airborne pollutant concentration was statistically relevant only when the receptor was placed downwind the ships. Similar results, even though less evident, were observed for particle number concentration and still less for particle mass concentration. Real-time single particle chemical measurement by an ATOFMS (Aerosol Time-Of-Flight Mass Spectrometer) were carried out in an urban site in Shangai (**Liu et al., 2017**) coupled with the hybrid single particle lagrangian integrated trajectory model (HYSPLIT-4). Results indicate that ships can contribute to 20-30% of the total PM 2.5 values during ship-plume-influenced periods. The results of these monitoring campaigns show the influence on land-based measures of the simultaneous occurrence of ship-plume emission periods and of the right wind direction blowing pollutants from the source to the receptor. The measures onboard are practically affected only by the difficulty that research centers and universities have in accessing onboard. In fact, most ship-owners hardly grant access or if they do, there are precise limitations; in addition, measurements of this type characterize only the particular ship available and therefore it should be carefully chosen to be at least representative of a particular category of ships. Airborne measurements could represent an alternative but they require the use of micro sensors to sample vessel exhaust gases in the plume. Depending on the *to be* analyzed molecule, micro sensors are based on different technologies such as electrochemical or Non-Dispersive Infrared (NDIR). The use of micro sensor technology has several advantages (**DEPA 2017**) low-cost, small size, lightweight transducers are easily fitted on a rotary aircraft, leveraging the ability of these platforms to navigate precisely in the plume and optimizing gas sampling. The Danish Environmental Protection Agency (**DEPA 2017**) used a set of micro sensors for measuring SO_2, CO_2, NO and NO_2 with the aim of determining individual vessel compliance with the international regulations. The inspections proved that, on a whole of 404 units measured, only 1:18 ships did not comply with regulations, burning fuel with Sulphur content min 50% higher than what allowed by law. In the last years, satellite based measurements of atmospheric trace gases have been used also to evaluate ship emissions. NO_X ship emissions were evaluated along the oceanic track connecting Sri Lanka to Indonesia (**Beirle et al., 2004**) using four spectrometers measuring the radiation reflected by the earth in the UV/VIS spectral range (240–790 nm) by applying the established Differential Optical Absorption Spectroscopy (DOAS). Due to the extension of ground pixel (about 10.000 km^2) the technique can be adopted only to estimate emissions in wide areas, like along oceanic tracks. Since ship emissions are modulated on their activities in ports and meteorological conditions can rapidly vary with time, it is necessary to know with accuracy the emissions of each ship during each activity. This goal cannot be achieved by land-based measurements due to the distance between the emission and the receptor. Nor can be actually achieved by using on-board measurements because it would be necessary to install detectors on each ship arriving at port. Satellite measures are not suitable as well, due to the insufficient resolution. The only practical and efficient technologies are the use of unmanned aircraft and of remote sensors.

6.2.3. Remote sensing and maritime sector

Several studies confirm the suitability of the remote sensing technique to assess mass flow rate of pollutants at ship funnels. The use of drones seems to be more suitable for an effective monitoring than for the evaluation of single ships emissions during the different activities in port (**Casazza et al., 2017**).

So far, remote analyses of the flow-rate of ship emissions were rarely carried out. Emissions from ships funnels were measured in the port of Brindisi using an UV-VIS remote sensing system (**Merico et al., 2016**). Uncertainties of estimated emissions were about 30% for SO_2 and 20% for NO_2. A good agreement between DOAS remote sensing measured emissions with inventory results is reported (**Merico et al., 2016**).

The principal techniques of remote surveys are spectroscopic and electromagnetic radiation detection. Within spectroscopy-based techniques, active and passive methods could be mentioned: the former use artificial light sources while the latter ones use sunlight, moonlight or starlight as energy source. Active systems normally use laser sources that, for applications aimed at detecting polluting emissions of exhausted gases, are capable of emitting high-power and narrow-band pulses of light. Another remote sensing technique for determining the concentrations and total amounts of atmospheric trace gases is the DOAS; the basic principle used in DOAS is the absorption spectroscopy. An interesting application of DOAS using sea scattered solar light as light source has been made by **Berg et al. (2012).** The results of this measurement from airborne platforms show that the sensitivity is sufficient to detect SO_2 and NO_2 in the ship plume for a 1s observation time (**Berg et al., 2012**). **Seyler et al. (2017)** showed the feasibility of long-term measurements of NO_2 and SO_2 using MAX-DOAS (Multi Axis Differential Optical Absorption Spectroscopy) instruments. **Masieri et al. (2009)** measured the mass per second of NO_2 and SO_2 (12.4 g/s and 4 g/s respectively) for single ship through the MAX-DOAS measurement in the Venice Lagoon.

6.2.4. Lidar Sensors

LIDAR, short for LIght Detection And Ranging, is an active remote sensing technique, based on the same principle of the Radar. It uses light pulses on a target to obtain range resolved measurement of the target properties in real time. A short pulse of light is emitted and the light reflected by the target is received with a telescope, spectrally selected, analyzed and detected. By measuring the time lapse between sending and receiving the light, the target distance can be obtained, while the spectral analysis and the intensity of the scattered light give information on optical and microphysical properties of the target and of the medium.

Lidar systems are among the most advanced methods for atmospheric studies, being able to give reliable information on particles distributions, on their optical properties and microphysical characterization with high resolution both in space and in time. LIDAR devices based on elastic backscatter represent the most common and simple method used in the study of aerosol and clouds, allowing to highlight the vertical structure of an aerosol layer and its geometrical features (base, top and thickness). Lidars with elastic/Raman capabilities give a better characterization of the aerosol, being able to measure their optical properties referred to the aerosol backscattering and extinction coefficients. Moreover, the Raman inelastic scattering is also used to measure atmospheric water vapor and vertical temperature profiles. The microphysics of particles can be inferred by advanced multi-wavelengths LIDAR systems, while changes of the polarization status of the backscattered radiation with respect to the transmitted one is used to identify different aerosol types, gaining information about the aerosol shape and identifying the presence of non-spherical particles with higher depolarization ratios (**Klett 1981**) in the atmospheric sample. One of the most promising survey methods for atmospheric gas concentration measurment and for monitoring of ships in port is a LIDAR technique based on the molecular absorption processes, the DIfferential Absorption Lidar (DIAL) technique. At the basis of DIAL is the detection of the different characteristics of the return waves characterized by two close wavelengths, only one of which is absorbed by the pollutant. The return signals analysis gives information about the present concentrations (**Celic et al., 2012**). Moreover, an application of the LIDAR technique based on the Doppler frequency shift is used to measure wind speed and direction along the vertical profile. Advanced Lidar systems make use of a combination of different methodologies and, if equipped with multi-wavelength and scanning capabilities, they allow to obtain a 4D (space and time) characterization of both the optical and microphysical properties of the aerosol. Nowadays, the LIDAR technology can be applied to a wide range of measurements concerning atmospheric and climatological studies, to vegetation monitoring as well as to archaeological and architectonical heritage monitoring, to range finding and terrain mapping, to bathymetry and to several other applications

6.3. Pilot experiences of LIDAR surveys

6.3.1. Organization of the measurement campaign

The preparatory phase to the port emission monitoring campaign is crucial to its success. Below is a list of the main aspects to be taken into account:

- *choice of suitable equipment and tools*: the sensors must be designed for the specific survey of one or more pollutant compounds and need to be calibrated on various concentrations. The possibility of a continuous (24 hours/day) operability and the use of eye safe light sources are key characteristics. A precise pointing system of the inspection light ray, with capability to track a moving source, is also important to follow a ship through all the operations in the port area;
- *choice of location;* the location should be in an upper position, suitable for monitoring a high number of vessels simultaneously present in port, with direct view on ships and funnels. Practical issues are also: gaining authorization to access the area, which is often under the jurisdiction of Coast Guard, or Port Authority; checking number and position of the sockets necessary to supply electric power to the instrumentation;
- *previous analysis of port traffic and calendar*; further valuable information about the incoming ships would also be main dimensions, height of the funnels on the sea level, etc.

6.3.2. Experimental campaign

An explorative measurement campaign was carried out in the port area of Naples to derive basic information about the feasibility of the adoption of Lidar system in this context. The adopted sensor was able to detect only particulate matter emissions but the main purpose of the campaign was to check the feasibility of the adoption of LIDAR systems in a port environment to survey ships funnels. A Lidar system in a transportable configuration was used to measure the soot and other particulate matter in the smoke plume emitted from vessels. Intensive measurements of the particulate matter emitted by single ships have been carried out during the phase of approach, maneuver, and mooring at quay. The measurements were performed during the period of September 24^{th} - 27^{th} 2018; in Table 6-7 is reported the timing of the measurements.

Table 6-7 Time and duration of the performed measurements

Date	UV-Lidar
24/09/18	16:15-17:15
25/09/18	03:06-08:42
26/09/18	03:21-13:37

The measurements were carried out using a portable scanning Lidar, developed by ALA s.r.l. (Advanced Lidar Applications srl) in the context of the I-AMICA (Infrastruttura ad Alta tecnologia per il Monitoraggio Integrato Climatico-Ambientale) project. The Lidar named μ-POLIS (Microjuole POrtable LIdar System) is a compact and portable Lidar system combining good accuracy, safety, portability, remote use autonomy and ease of operation (Figure 6-10). It is suited to carry out measurement in urban areas because it works in the eye-safe UV region and is proved to be effective in mapping emissions and identifying 'hotspots' through a horizontal scanning on the port. The following list contains the fundamental characteristics of Lidar System:

- laser source: repetition rate 1 KHz;
- laser source: average optical power at 355 nm of 0.04 W;
- receiver unit 20 cm Ritchey-Chrétien telescope;
- spatial resolution from 100 m to 15 km;
- temporal resolution 30 seconds.

Moreover, the system is equipped with a software for automatic continuous measurements and LIDAR data analysis.

Figure 6-10 Positioning of LIDAR instrumentation

The system swivels from vertical to horizontal plane by pointing the laser beam in the vertical plane from slightly below the horizon to the zenith. The receiver unit is designed to detect both the elastically diffused light with parallel and perpendicular polarization, i.e. the P and S components of the backscattered radiation. Moreover, it is equipped with a software for automatic continuous measurements and Lidar data analysis. Lidar data were analyzed in terms of particles backscatter coefficient (βp) and calibrated particles linear depolarization (δ_p) profiles. The former coefficient is related to the particles concentration while the latter one refers to particles shape, allowing to characterize the particulate size and to distinguish the contribution of solid and liquid particulate. The retrieval of the β_p coefficient was performed by using the Klett–Fernald algorithm (**Fernald 1984; Klett et al., 1981**). This method requires an assumption on the Lidar ratio (LR), a key parameter depending on the aerosol microphysical properties and typology. In the data analysis a constant value of 45sr was assumed for the LR along the beam profile (**Sicard et al., 2011**) and choosing a lower LR than the values obtained from Lidar measurements carried out in Naples in the frame of the EARLINET project (**Boselli et al., 2009**). Following the previously used approach for the characterization of volcanic emissions (**Scollo et al., 2015**), once β_p was measured, the particle mass concentration at emitting source can be obtained by (6-5):

6-5 The particle mass concentration

$$C = \sigma LR\beta_P\rho$$

where

- βp and LR refer to the Lidar signal measured in the plume,
- ρ is the mass density of particles generated by the combustion of diesel fuels
- σ is a conversion factor, function of the size distribution, which, for large values of the effective radius reff, is given by 2reff/3 (**Gasteiger et al., 2011; Schumann et al., 2011**).

A Doppler Lidar (WindCube WLS7 v2 by Leosphere) was made available by the CeSMA (Advanced Metrologic and Technological Services Center of the University of Naples "Federico II"). It has been used for wind profiles measurements, see Figure 6-11.

Figure 6-11 WindCube WLS7 v2 by Leosphere and LIDAR

This Lidar device is the referential remote sensor in the wind industry, providing accurate wind speed and direction profile measurements in the boundary layer. It emits 200 ns pulses of 10µJ energy at a wavelength of 1.54µm. The system, based on a heterodyne detection, is able to measure wind speed and direction profiles on 12 programmable altitudes in the range of 40–290 meters, with a spatial resolution of 20 meters and a sampling rate programmable between 1s to 10 minutes. With an unattended operation, data is automatically transmitted and stored. The instrument recorded the background of both the city and the port area before the arrival of the ship. The surveys were carried out at first in the direction of the city, with an elevation angle of about 7°, in order to obtain information on the state of the atmosphere around the port. Later, the Lidar was pointed in the direction of the sea, with the same elevation, carrying out measurements before the arrival of ships, in order to have information on the background situation. Upon the arrival of a ship, the Lidar was pointed in the direction of the plume, on the vertical of the funnel, following the ship through all the operations in port. Data was acquired with a time resolution of 30 seconds and a spatial resolution of 15 meters.

6.3.3. Results

Figure 6-12 and Figure 6-13 shows LIDAR profiles corresponding to measurements taken during Day 1 of the campaign with 1-minute time integration. The Figure 6-12 shows the plot of the β_p profiles acquired with 7.5° elevation and pointing at a specific passenger ship, (Ship A, passenger ship) approaching the port area. During the maneuvering phase, the values of β_p within the plume resulted about 4.0x 10^{-4}. These values were obtained when the ship was maneuvering at a distance of about 550 m from the LIDAR, with an angle of elevation of the laser beam of 7.5° from the horizontal plane, which corresponds to a height of about 75 m above sea level, on the vertical of the funnel. At shorter distances, the measured δ_p values resulted larger (20%) than the values measured at 570 m (<10%), this suggests a contribution of more spherical particles and the presence of water vapour in correspondence of the β_p picks. The Figure 6-13 corresponds to intensive measurements performed by pointing the laser beam towards the plume emitted from two passenger ships (ship A and ship B, both passenger ship) when they were moored. As it can be seen in the figure, the peak values of the backscattering coefficient are lower than those related to the maneuver phase of over a factor of 2 and correspond to the simultaneous emissions of two nearby moored ships. An important observation is that the depolarization of the plume was of about 10% in the maneuvering phase and of 20% in the stationary phase. Given the fact that a high depolarization corresponds to more irregular and generally larger particles, this observation is compatible with the identification of different operating regimes of the ship's engines. The color plot of Figure 6-14 shows the temporal evolution of the Range Corrected Signal (RCS), i.e. the Lidar signal corrected for the solid acceptance angle of the apparatus, and the particle depolarization, respectively, obtained from the elastic Lidar return at 355nm as a function of the time. Data is reported with a time resolution of 30 seconds and a spatial resolution of 15m; these measurements were carried out with an elevation of 5°. The spots at distances of about 0.5km and 1km, respectively, correspond to emission coming from two different ships, Ship A and Ship B (passenger ship), in the port area. As reported in Figure 6-15, asymmetrical and more depolarizing particles resulted from the more distant ship A, while water vapor could result from the nearer one B, the first one in stationary conditions, the second one in a maneuvering phase.

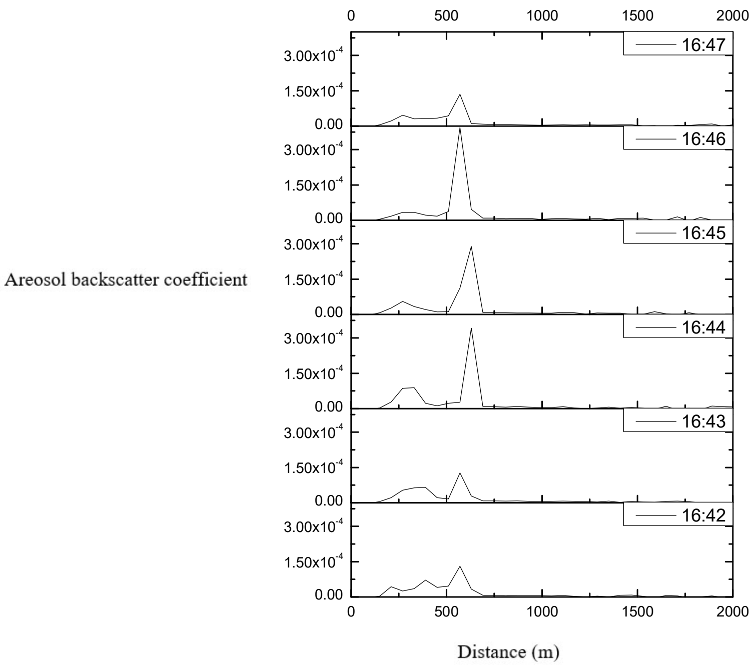

*Figure 6-12 Aerosol backscatter coefficient profiles measured on September 24th 2018 during the **maneuvering** phase of a ship* Areosol backscatter coefficient

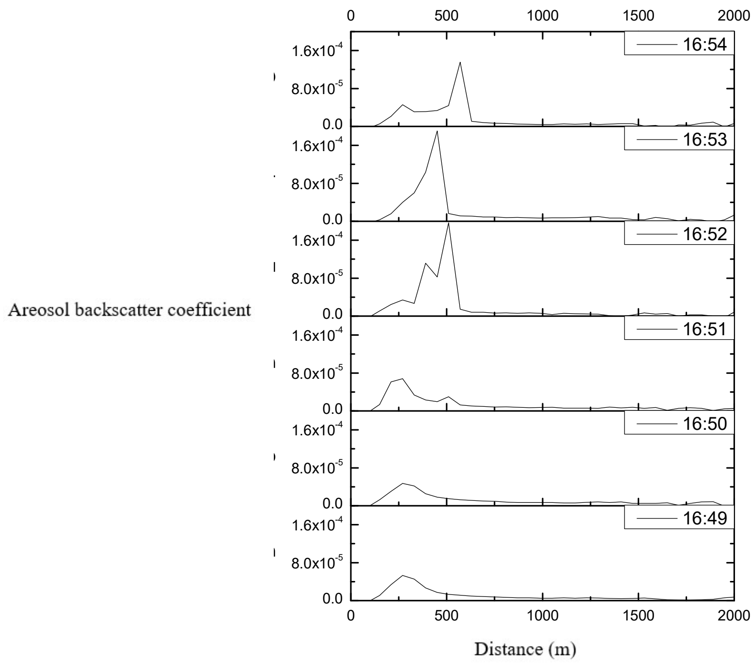

*Figure 6-13 Aerosol backscatter coefficient profiles measured on September 24th 2018 in the **stationary** phase of a ship*

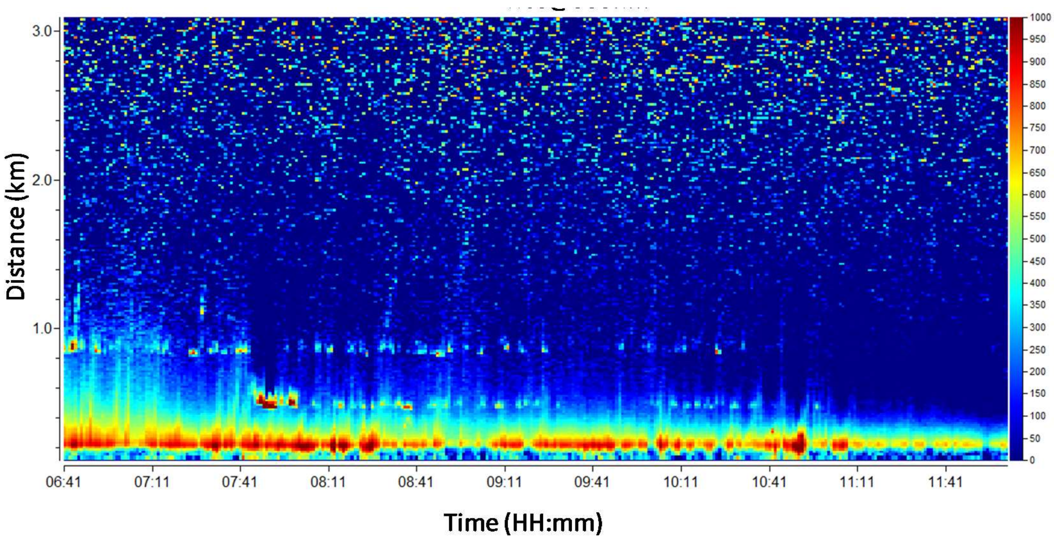

Figure 6-14 Color map of the RCS Lidar signal at 355nm. 27/09/2018 from 06:41 to 12:04

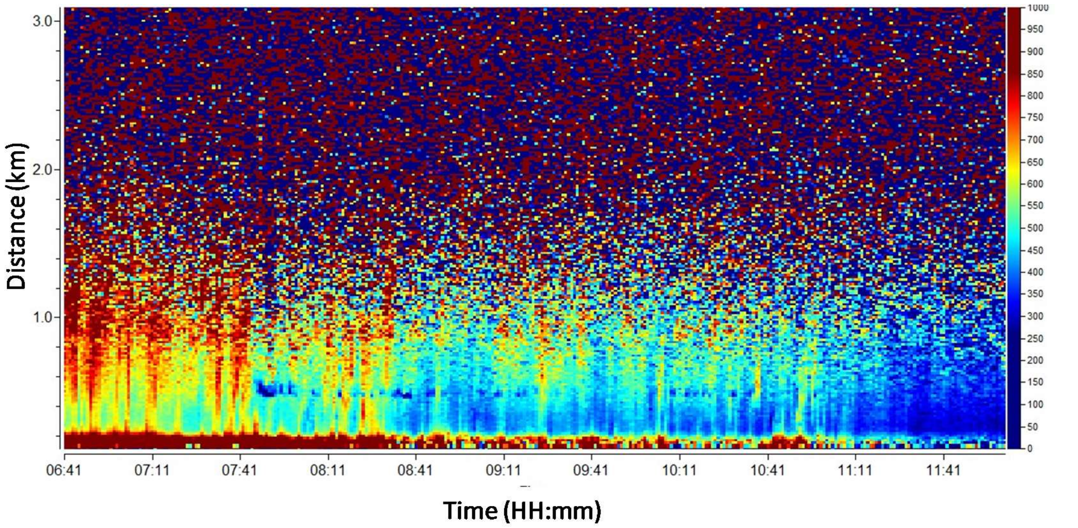

Figure 6-15 Color map of the particles depolarization at 355nm. 27/09/2018 from 06:41 to 12:04

The mass concentration at the emitting source has been calculated by means of Eq. 6-5 and considering a value of 2000 kg m^{-3} for the mass density ρ of the particles. The mass concentration at the emitting source was calculated by means of Eq. 6-5 while the main parameters are listed in the following Table 6-8.

Table 6-8 Parameters

Parameters	
Mass density ρ of the particles (kg m^{-3})	2000
Effective radius of emitted particles (m)	0.5 x 10^{-6}
Conversion factor (m)	3.3 x 10^{-7}
Mean β_p value ($m^{-1}sr^{-1}$)	1.2 $\cdot 10^{-4}$

The estimated mass concentration resulted: C≈ 8x10^{-5} kg/m^3 = 0.8 mg/m^3. Assuming the particle mass concentration C as constant in the plume and measuring the horizontal wind speed (vx) from wind profiles obtained with a Lidar Doppler, the flow rate of the particulate emissions was calculated. In particular, taking into account an angle of 45° of the plume from the vertical direction, we assumed the vertical speed of the emitted plume equaled the horizontal wind speed, which was 10 m/s. In these conditions, the flow rate of the particulate emissions can be calculated as the product between C and v_x and is equal to F_m = 17 mg/m^2s and F_s= 8 mg/m^2s for maneuvering and stationary phase, respectively.

Then, it must be remembered that the calculation refers to the evaluation of the concentration at the source, while the lidar measurements are carried out with the laser beam which flies over the funnel a few tens of meters above, where the plume is enlarged due to the dispersion, to such an extent that in the measurements made at a height of 75m, the width is greater than 50 m.

Therefore the concentration of 8x10^{-5} kg/m^3 is valid at an altitude at which the source has a diameter of 1-2 m. Remembering that the concentration goes as the square of the diameter of the section, the same concentration assumes a value of about 3.6x10^{-6} kg/m^3 at the vertical probing altitude at which the plume gives rise to a 15-30m wide peak.

6.3.4. Discussion and conclusions

Monitoring ports as well as other types of transport infrastructures and detecting the emission rates from single ships as well as single vehicles is a key point to enforce emission control policies and measures and to achieve on the long run an effective reduction of the environmental impact of such infrastructures. Real time experimental monitoring of the emissions of ships is considered a key issue for controlling the environmental impact of ports. While waiting for the implementation of specific sensors on board of each vehicle, remote sensing techniques embedded in the infrastructure seem to be the most promising way for pursuing the target.

The specific sensor adopted was able to detect particulate matter emissions, but similar optical techniques are available for the survey of other noxious compounds in the exhausts. The sensors tested showed to be capable of an effective action of identification, tracking and monitoring of the exhaust emissions by ships, both in transient and in stationary operational conditions. Further experiments are needed to calibrate and assess these other sensors, but the carried out campaign proves the possibility of developing an effective monitoring system of exhaust gases concentrations in a port.

6.4. The Environmental Ship Index (ESI)

The goal of reducing the environmental impact of maritime transport is to be achieved by both implementing sanctions against ships that do not respect the regulatory limits and perhaps above all, rewarding the ones that pay attention to the protection of the environment. The role of ports in worldwide policies is central; they play an important role supporting the economy but they are also key agents in favor of environmental policies on a global scale (**Bergqvist & Monios 2019**; **Fenton 2017; Gibbs et al., 2014**).

In 2008, the IAPH (International Association of Port and Harbors) launched the WPCI (World Port Climate Initiative) in order to support the ports to fight climate changes, see Figure 6-16. In 2010, in the framework WPCI, the ports of Rotterdam, Bremen, Le Havre, Antwerp, and Hamburg, developed the ESI (Environmental Ship Index) project, which is an emblematic example of how port authorities and service providers can inspire and encourage ship-owners to move in the direction of environmental sustainability, see Figure 6-16 [17] (**Svensson & Andersson 2012; WPCI 2010**).

In 2018, the IAPH launched the WPSP (World Ports Sustainability Program), which included the main ports of the world in a joint effort to reduce their impact on global pollution while maintaining their fundamental role of economic hotspots for transportation. The main partners of this initiative are the IAPH, the AAPA (American Association of Port Authorities), the ESPO (European Sea Ports Organization), the AIVP (Worldwide Network of Port Cities), and the PIANC (World Association for Waterborne Transport Infrastructure). The program is an extension of the WPCI, aiming once again at enhancing and assisting the global efforts toward sustainability.

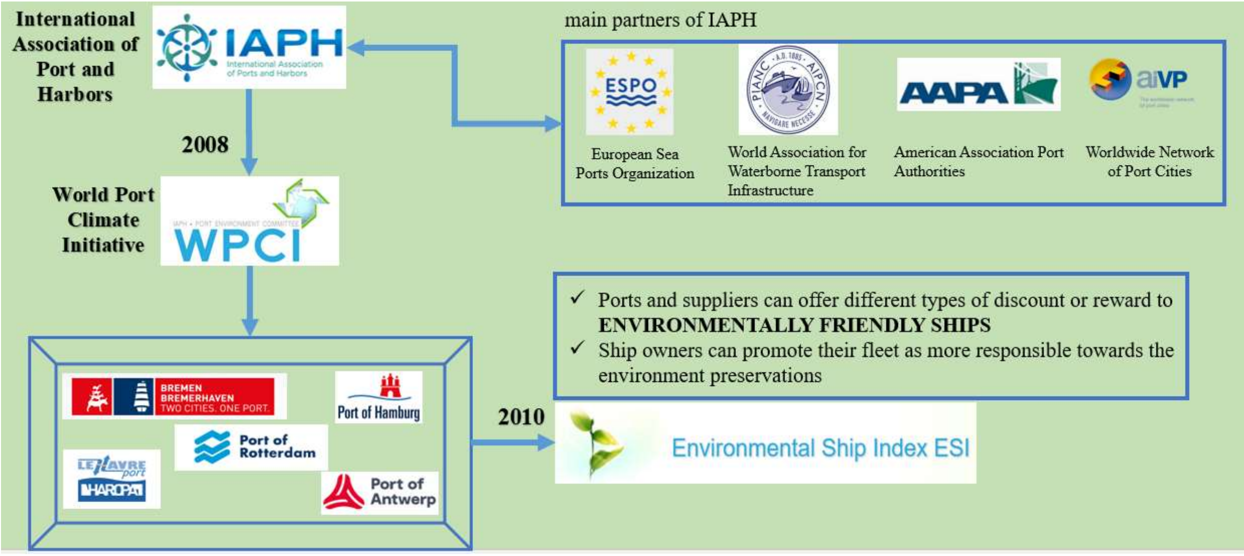

Figure 6-16 ESI framework

The adoption of the ESI is optional for ship owners yet strongly encouraged by ports and operators in the maritime segment. The potential uses of the index are several: while ports and suppliers can offer different types of rebates or rewards to environmentally friendly vessels, on the other hand, ship owners can promote their fleets as more responsible towards the environment protection. Each ship is characterized by an ESI score ranging from 0, for ships that just comply with existing regulation, to 100, for ships with virtually zero emissions and having also a system for monitoring and reporting their EEOI, see Figure 6-17 (Energy Efficiency Operational Index) performance (**Brodie 2013; WPCI 2011a; WPCI 2011b**).

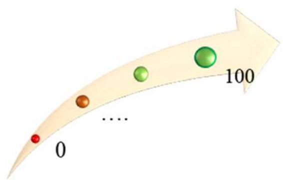

Figure 6-17 ESI range of score

Each ship owner can register his own ship and or fleet in the ESI database and the index is automatically calculated. The method for calculating the ESI score consist in a formula sum of three terms related to NO_X, SO_X and CO_2, to which an extra is added for ships with OPS (On-shore Power Supply) to obtain electrical power supply from land in ports equipped with appropriate infrastructures (**WPCI 2011a; WPCI 2011b**). For the calculation of the score of ESI linked to NO_X there are three requirements: the nominal power, the actual emission value for the main and auxiliary engines and the limit of the reference standard based on the rpm. These informations are normally available in the EIAPP (Engine International Air Pollution Prevention) certificate. For the calculation of the ESI score linked to SO_X instead, the necessary informations, which are the Sulphur content of the fuel and the average quantity of bunkered fuel during a year, are available on board in the BDN's (Bunker Delivery Notes). Normally used fuels are divided into three categories according to the percentage of Sulphur content, see Table 6-9.

Table 6-9 Typical Sulphur content in the fuel

Type	Range
High	0.50<S%<3.50
Mid	0.10<S%<0.50
Low	0.05<S%< 0.10

In Table 6-10 required data for ESI calculations are synthetized (**Hasan 2011**).

Table 6-10 Required data for ESI calculation

	NO_X	SO_X	$RRCO_2$
Information	Rated power and rpm (main and auxiliary); actual NO_X emission value (g/kWh)	Amount of bunkered fuel and average fuel sulphur content per kind and per delivery	Submission of EEOI.
Documentation	EIAPP certificate	BDN over 1 year	EEOI

6.4.1. ESI scores

The overall formula for the calculation of the ESI score is (6-6)

6-6 ESI formula

$$\mathrm{ESI_{overall}} = \frac{1}{3.1}\left(2\ \mathrm{ESI_{NO_X}} + \mathrm{ESI_{SO_X}}\right) + \mathrm{RRCO_2} + \mathrm{OPS}$$

The single terms are calculated separately and, if not possible to calculate one or more of these parts, 0 should replace them. The expressions concerning the formula are defined as follows:

For the **NO_X** sub points (The IMO TIER I is the baseline used for the analysis) (6-7).

6-7 NO_X sub points

$$ESI_{NO_X} = \frac{100}{\sum_{i=1}^{n} P_i} \cdot \sum_{i=1}^{n} \frac{\left(NO_{x_{limiit_{value_1}}} - NO_{xrating_i}\right) \cdot P_i}{NO_{x_{limiit_{valu\ 1}}}}$$

Where:

In reference to each engine on board (main or auxiliary):

- $NOx_{\_limitvalue}$ is the limit value expressed in g/kWh and is a function of rpm;
- NO_{x_rating} is the rating value expressed in g/kWh of each engine on board;
- P_i is the rated power of the single engine, in kW.

For the **SO_X** sub points (6-8)

6-8 SO_X sub points

$$ESI_{SO_X} = a\% \cdot 30 + b\% \cdot 35 + c\% \cdot 35$$

Where:

- the sulphur limits chosen for baseline are respectively 3.5% in high sea and 0.5% at berth and in ECA zones;
- a%, b% and c% stands for the reduction of the sulphur content respectively in high, mid and low fuels (see Table 2).

Generally, HIGH fuel oil is used in open sea while MID and LOW are adopted respectively in ECA zones and in ports areas. It is worth noting that, despite the foreseeable higher consumption for high sulfur fuel, used during navigation in open sea, the weight it has in the formula is less than the one of other categories of fuels. This is justified by the fact that the impact on human health is certainly lower compared to the case of use at port or near the coast. This choice of including the characteristics of the fuel burned at sea has basically been taken to sensitize ship owners. Considering that the ESI score is based on comparison with the regulatory limits, this formula has recently been updated and consists of two rates linked only to the middle and low categories for the percentage of sulfur contained in the fuel with an exception for ships equipped with Scrubber.

Additionally, ships equipped with On-shore Power Supply receive **10 points**. In regard to the score related to $\mathbf{CO_2}$, called $\mathbf{RRCO_2}$ (Reward for Reporting), the efficiency of ships is calculated over a 3-year period based on the reported totals of fuel consumption and navigated distance. By reporting these data every semester, **5 points** can be obtained and in addition, the efficiency increase in %, in the three year reference period, is added to the score (maximum **15 points**). Recently in the calculation of the ESI score a Noise-related score has been added. The total airborne noise score is the sum of three parts: the first function of the SPL (Sound Power Level) of the ship, the second of the total low frequencies airborne SPL of the ship and the last part consists of 20 points assigned to those ships that have Neptunes Measuremets reports. Therefore vessels that have carried out the NEPTUNES measurements can deliver a measurements report and can also get ESI-noise points, as a separate score.

6.4.2. ESI: incentive providers and ships

The ESI is an honorable indication of the environmental performance of vessels and will assist in identifying cleaner ships. Nowadays, 58 organizations, most of which are ports (see Figure 6-18), adopt ESI as a measure for providing ships with in Incentives (updated at July 2021) [17].

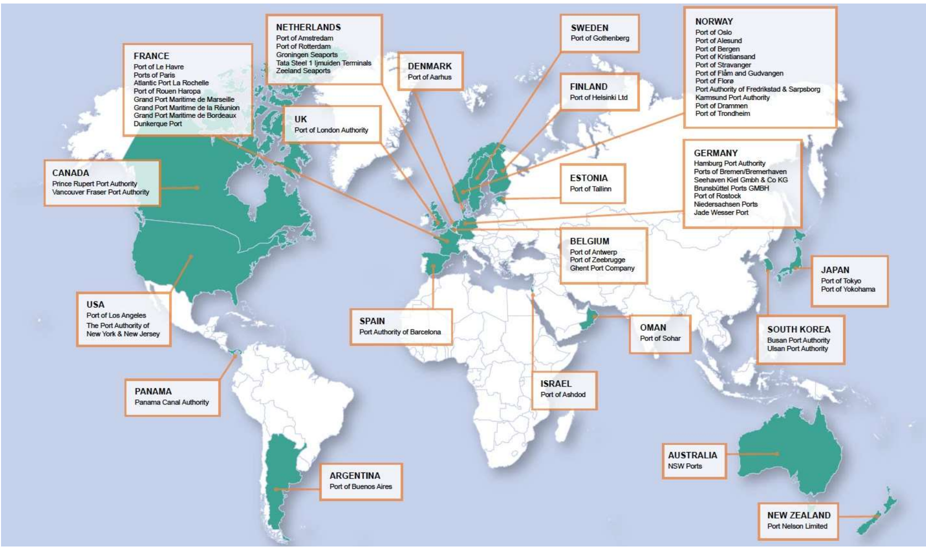

Figure 6-18 ESI Incentive providers

In Figure 6-19, the distribution of ports participating in the initiative grouped by country

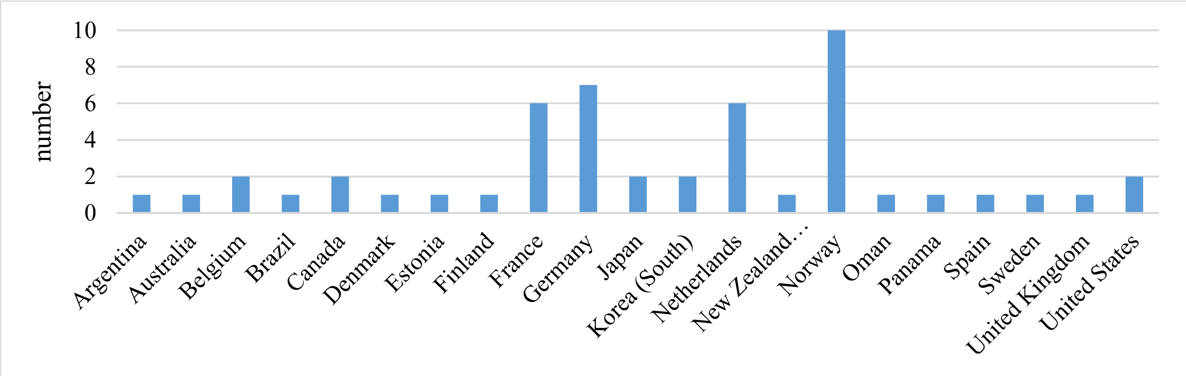

Figure 6-19 Number of port-incentive Providers

Northern European countries are the most active in terms of attention to environmental policies (Norway 10 ports, Netherlands 6 ports, Germany 7 ports). The types of incentives provided by ports typically include reductions on port taxes in percentages gradually increasing proportionally to the score realized. For example, the port of Antwerp offers a 5% discount on the tonnage tax rate with ESI between 31 and 50, a 10% discount for ships with ESI between 50.1 and 70 and a 15% with ESI from 70 on. Another recent example is the port of Bergen, where ships with a total ESI score between 30 and 50 points are granted a 20% rebate on ship harbor dues, ships with a total ESI score greater than 50 points are granted a 50% rebate. The port of Civitavecchia was the only Italian port participating to the initiative until 2019. The offered discount is on the indirect fee on waste collection service. The ships loaded on the database are 8426 to date (01/07/2020). The first 50 ships with highest ESI scores are supply vessels, offshore supply vessels, oil/chemical tankers, Ro-Ro passenger ships, and LNG tankers most of which with Norwegian or Swedish flag.

6.4.3. ESI: application to the case of the port of Naples

The chosen period for the evaluation in the port of Naples, are the months of maximum presence of ships for 2019. In particular, the months of May and September have been selected; the number of dockings are 62 and 53 respectively for May and September, see Table 6-11. Considering that numerous ships enter the port periodically, weekly for example, the number of different vessels obtained is of 26 y and 24 for May and September, see Table 6-11. The incoming ships have been verified on the portal of the ESI program and not all of them are registered on it; in Table 6-11 the number of ships featuring a valid ESI score.

Table 6-11. Docking data for the Port of Naples

	May 2019	**September 2019**
Docking	62	53
Vessels	26	24
Member vessels	38.5%	37.5%

The ESI scores of these ships are reported in Figure 6-20.

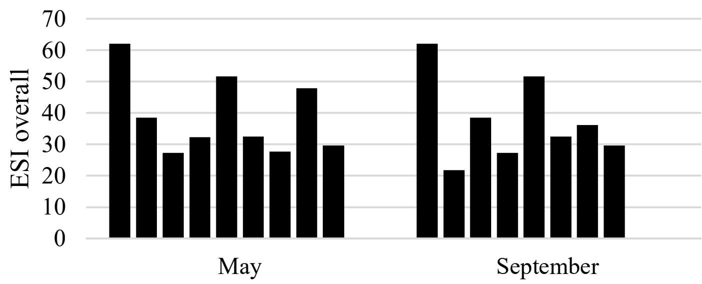

Figure 6-20. The overall ESI score

The below graph, Figure 6-21, shows for each ship the ESI sub points and the overall ESI. Starting from the bottom of each histogram bar, the ***NO_X***, the ***SO_X*** and the bonuses related to ***$RRCO_2$*** and ***OPS*** are reported. An analysis of the ESI scores of these ships shows that most of them are equipped with a CO_2 monitoring system and an OPS installation. As marked in the Table 6-11, despite the high number of dockings, the number of ships participating in the initiative is limited because this port, like many of the ports on their routes in Mediterranean and Southern Europe, does not provide financial incentives.

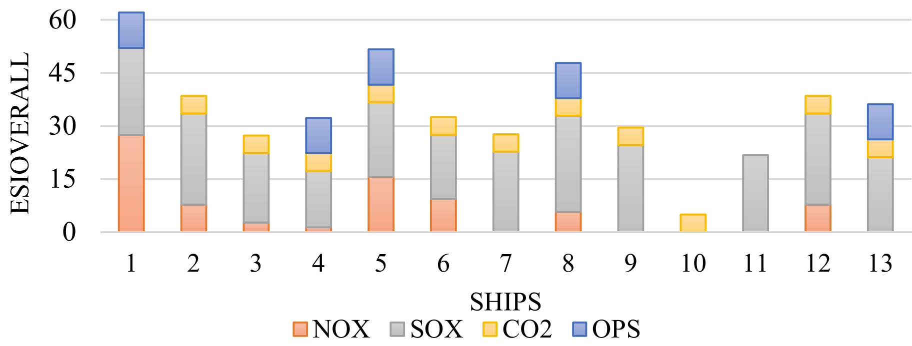

Figure 6-21. The ESI terms

For the calculation of the scores, the regulatory limit of nitrogen oxide, the g/kWh of NO_X emitted, and the sulphur content in the fuel used in the conditions of cruise, berth, and navigation in in ECA zones are necessary. Obviously, the information of the EIAPP certificates and those of the BDN are not available, while power and rpm of engines are known. The ESI scores have therefore been used in reverse mode: from the two aliquots of **NO_X** and **SO_X** sub points, available on the portal, the following results have respectively been obtained for each ship:

- declared emissions in g/kWh of nitrogen oxides, after calculating the limit value for the specific rpm;
- an estimate of the mean of fuel sulphur contents used in the various conditions.

Figure 6-22 shows the content of sulphur in the used fuels (continuous line in cruise mode, dotted line for ECA zones and points for berth), it is on average equal to 1% in port and 2% in cruise mode.

The results should be interpreted as an average value of the sulphur content: these values are, indeed, the function of the quality of different fuel on board obtained from different bunker operations in different parts of the world.

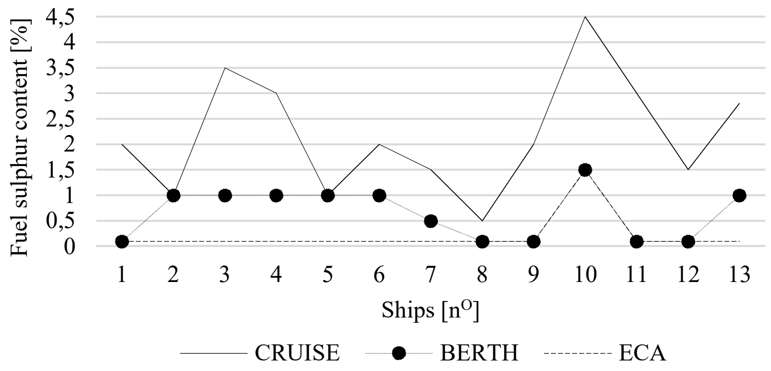

Figure 6-22. Results for the fuel Sulphur content.

The reverse analysis made For NO_X emissions, returns an average value 12.58 g/kWh (see Figure 6-23), in agreement with **Trozzi & Lauretis (2019)** indicating as standard for ships under consideration 13 g/kWh of NO_X.

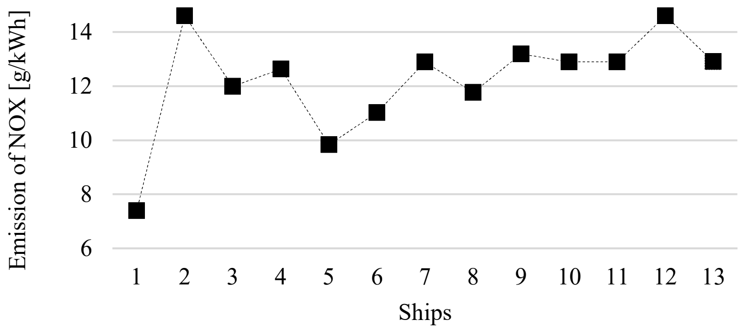

Figure 6-23. Results for the emission of NO_X

6.4.4. Comparison with northern Europe

The ships arriving in port have been compared with ships, of the main cruise companies, operating in the Northern Seas and in the Norwegian Fjords. First of all it is worth noting that a very limited number of ships makes those routes but also that sometimes the same ships, that reach Naples, are used for Baltic routes in different periods of the year. Thus excluding these overlapped ships, the ESI scores of some ships arriving in those zones with those that sail into the port of Naples has been analyzed. Comparisons in Figure 6-24 show how scores are on average equivalent. In the graph of Figure 6-24, comparisons related to NO_X and SO_X sub points are shown. The greatest difference in distribution is in the score linked to the CO_2 emissions (see Figure 6-25): almost 90% of the ships sailing in the northern seas obtain the bonus associated to high-energy efficiency standards (75% of ships docking in the port of Naples get this bonus).

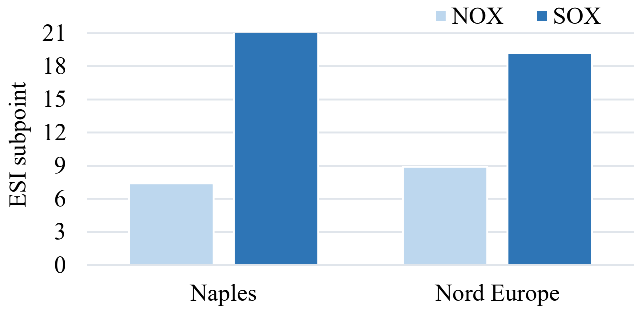

Figure 6-24 Comparisons related to NO_X and SO_X sub points

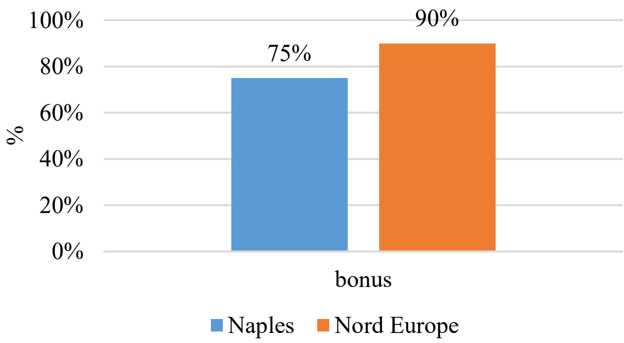

Figure 6-25 Comparison of emissions between port of Naples and North Europe

6.4.5. Discussion and conclusions

The aim of reducing the environmental impact of vessel traffic is to be achieved by both implementing sanctions against vessels not respecting the regulatory limits and perhaps above all rewarding those paying attention to the safeguarding of the planet. In this work, the application of the ESI index aimed at analyzing the quality of the environmental impact of the ships entering the port of Naples in the most crowded months. The first results show that the percentage of ships registered in the ESI portal is still low. The main cause is to be found in the fact that few of the ports of call of these ships offer advantages and tax incentives to the best performing ships. The teamwork that port authorities, ship owners and suppliers of naval services should carry out together must start from the bottom and right from initiatives like this. The extension of the use of the index to a larger number of ports will certainly lead to an increase in the number of ships registered in the portal, with advantages in monitoring and control of ship emissions, not only in port but also during navigation.

7. Conclusions

Environmental sustainability and reduction of emissions related to human activities are recognized worldwide as targets to be achieved by any means possible as soon as possible. The transport sector plays a major role in this challenge. Within the transport sector, merchant and passenger fleets of ships must do their part with their own means and in a way that is proportional to their emissions. In addition to the production of CO_2 and therefore of greenhouse effect pollutants, ships produce pollutants with a local impact (NO_X, PM and SO_X) altering the quality of the air we breathe. This thesis allows to investigate the issue of the environmental impact of passenger ships in port from different points of view. The focus is on ports located close to inhabited centers, for which the environmental and acoustic impact of the operations taking place at harbur affects directly the inhabited center. Experimental campaigns, simulations, and numerical applications have been carried out over the years of the PhD, leading to interesting conclusions about the role that passenger ships have within the port and the role that the port itself has in relation to the nearby city center. A co-operation with the chemistry department of the University of Naples "Federico II" has made it possible to deepen the emission description far beyond the hourly emissions of individual ships and to create detailed maps of the concentrations in the port area. Different approaches have been faced and compared with each other. Engine simulations made it possible to estimate emissions in more details than with the use of simple emission factors (characterized by a linear link with power). The experimental measurements of the acoustic impact of ships in port have proved useful for the validation of a numerical simulation model. Future developments of the topic will investigate aspects such as maneuvering in port, transients in simulation, and the interface between engine simulation and ship simulation software. Future analysis would deep some theoretical aspects regarding both emission and atmospheric dispersion. A more feasible assessment of emission factors requires the knowledge of the distribution of weight of ships in each macro-category and use of AIS data with the aim to better characterize the timing and the areas of manoeuvring in the port to model short-time albeit important, emission peaks. Moreover, the performances of the model adopted could be improved by the use of specific CFD simulations or wind-tunnel experiments to better define the parameters governing the dispersion phenomenon inside the urban area. Recently experimental measurements of pollutants concentrations in port have been carried out and will allow a more accurate validation of this bottom-up methodology. The concentrations of the main air pollutants in an area close to the piers and at high quotes (in accordance with what has been said in chapters 2 and 3) in two weeks in which the traffic of passenger ships is very scarce (due to covid) have been recorded. The same measures will be done in a moment of full-blown traffic. The first measure will act as a background value while the second one as a real validation. With regard to acoustics, on the other hand, further applications of experimental data will allow further analysis to be achieved such as, for example, the presence of numerous ships in port or the influence of the engine's loads on the acoustic impact.

8. *Acronyms*

AAPA American Association Port Authorities
AD Anderson-Darling statistics
AE Auxiliary Engine
AIS Automatic Identification Systems
AIVP Worldwide Network of Port Cities
ANFIS Adaptive Neuro-Fuzzy Inference System
ANN Artificial Neural Network
ARPAC Agenzia Regionale per la Protezione Ambientale in Campania
ATOFMS Aerosol Time-Of-Flight Mass Spectrometer
BAU Business As Usual
BDC Bottom Dead Center
BDN Bunker Delivery Notes
bmep Brake Mean Effective Pressure
CLIA Cruise Lines International Association
CSV Comma Separated Values
DEP Diesel Electric Propulsion
DEPA Danish Environmental Protection Agency
DIAL DIfferential Absorption Lidar
DOAS Differential Optical Absorption Spectroscopy
DWT Dead Weight
EEA Tool Energy Efficiency Appraisal Tool
ECA Emission Control Area
ECGS Exhaust Gse Cleaning Systems
EEA European Environment Agency
EEDI Energy Efficiency Design Index
EEOI Energy Efficiency Operational Index
EEXI Energy Efficiency Existing Ship Index
EF Emission Factor
EIAPP Engine International Air Pollution Prevention
EMEP European Monitoring and Evaluation Program
ESI Environmental Ship Index
ESPO European Sea Ports Organization
ETA Estimated Time of Arrival
EVC Exhaust Valve Close
EVO Exhaust Valve Open
fmep Friction Mean Effective Pressure
GEF Global Environment Facility
GHG Green House Gases
GIA Global Industry Alliance
GloMEEP Global Maritime Energy Efficiency Partnership
GT Gross Tonnage
HCN Hydrogen Cyanide
HFO Heavy Fuel Oil
HSD High Speed Diesel
HSFO High Sulphur Fuel Oil
IAPH International Association of Port and Harbors
ICAO International Civil Aviation Organization
ICCT International Council on Clean Transportation
imep Indicated Mean Effective Pressure
IMO International Maritime Organizations
IPCC Intergovernmental Panel on Climate Change
IVC Intake Valve Close
IVO Intake Valve Open

LIDAR LIght Detection And Ranging
LPC Lead Pilot Countries
MACC Marginal Abatement Cost Curve
MARPOL MARine POLlution
MAX-DOAS Multi Axis Differential Optical Absorption Spectroscopy
MBM Market-Based Measures
MCR Maximum Continous Rating
MDO Marine Diesel Oil
ME Main Engine
mep Mean Effective Pressure
MEPC Marine Environment Protection Committee
MGO Marine Gas Oil
MMSI Maritime Mobile Service Identities
MRV Monitoring, Reporting, Verification
MSD Medium Speed Diesel
NDR Non-Dispersive Infrared
OLS Ordinary Least Squares
OPS On-shore Power Supply
PCU Project Coordination Unit
PIANC World Association for Waterborne Transport Infrastructure
PM Particulate Matter
PPM Primary Particulate Matter
PRESS Predicted Residual Error Sum of Squares
RCPs Representative Concentration Pathways
RVL Reference Line Value
S-AIS Satellite-AIS
SAR Search And Rescue
SEEMP Ship Energy Efficiency Management Plan
SEL Sound Exposure Level
SFOC Specific Fuel Consumption
SIA Secondary Inorganic Aerosols
SOI Start of Injection
SPL Sound Power Level
SSD Slow Speed Diesel
SSPs Shared Socioeconomic Pathways
T-AIS Terrestrial-AIS
TDC Top Dead Center
TEU Twenty-foot Equivalent Unit
TW Transport Work
UNCTAD United Nations Conference on Trade and Development
UNDP United Nations Development Programme
UTC Universal Time Coordinated
UTM Universo Traverso Mercatore
VHF Very High Frequency
VIF Variance Inflation Factors
VOC Volatile Organic Compound
WHO World Health Organization
WNW West Nord West
WPCI World Port Climate Initiative
WPSP World Ports Sustainability Program

9. *List of Figures*

10. List of Tables

11. List of Equations

12. References

Adamo, F., G. Andria, G. Cavone, C. De Capua, A. Lanzolla, R. Morello, and M. Spadavecchia. (2014). Estimation of ship emissions in the port of Taranto. *Measurement* 14:982–988. doi:10.1016/j.measurement.2013.09.012.

Agrawal, H., Eden, R., Zhang, X., Fine, P. M., Katzenstein, A., Miller, J. W., ... & Cocker III, D. R, (2009). Primary particulate matter from ocean-going engines in the Southern California Air Basin. *Environmental science & technology*, 43(14), 5398-5402.

Alsina-Pagès, R. M., Socor, J. C., & Bergadà, P. (2019, September). The impact of man-made noise on the passenger transport stations of Port of Barcelona. In *INTER-NOISE and NOISE-CON Congress and Conference Proceedings* (Vol. 259, No. 3, pp. 6912-6922). Institute of Noise Control Engineering.

Altosole, M., Benvenuto, G., Campora, U., Laviola, M., & Zaccone, R. (2017). Simulation and performance comparison between diesel and natural gas engines for marine applications. *Proceedings of the Institution of Mechanical Engineers, Part M: Journal of Engineering for the Maritime Environment*, 231(2), 690-704.

Amsden, A.A., Ramshaw, J.D., O'Rourke, P.J. and Dukowicz, J.K. (1985), "KIVA: a computer program for two and three-dimensional fluid flow with chemical reactions and fuel sprays", Report LA-10245-MS, Los Alamos National Laboratory

Amsden, A.A., Butler, T.D. and O'Rourke, P.J. (1987), "KIVA-II computer program for transient multidimensional chemically reactive flows with sprays", Paper No. 872072, SAE, International Fall Fuels and Lubricants Meeting and Exhibition, November 1, doi: 10.4271/872072.

Anderson K., Bows A. (2012). Executing a Scharnow turn: reconciling shipping emissions with international commitments on climate change, *Carbon Management* 3:6 (2012), 615-628.

Arguedas, V. F., Pallotta, G., & Vespe, M. (2018). Maritime traffic networks: From historical positioning data to unsupervised maritime traffic monitoring. *IEEE Transactions on Intelligent Transportation Systems*, 19(3), 722–732.

ARPAV, 2014. La modellistica di dispersione ad alta risoluzione per lo studio dell'impatto delle navi crociera e passeggeri nella città di Venezia.

Ault, A.P., M.J. Moore, H. Furutani, and K.A. Prather. (2009). Impact of emissions from the Los Angeles port region on San Diego air quality during regional transport events. *Environ. Sci. Technol*. 43:3500–3506. doi:10.1021/es8018918.

Badino A., Borelli D., Gaggero T., Rizzuto E., Schenone C. 2011. Acoustic impact of ships: noise-related needs, quantification and justification, IMAM (2011), 14th *Congress of the Internat. Maritime Association of the Mediterranean*, Sept. 2011, Genoa, IT.

Badino A., Borelli D., Gaggero T., Rizzuto E. Schenone C. (2012). Noise emitted from ships: impact inside and outside the vessels *Procedia: Social & Behavioral Sciences*, Elsevier, Vol.48 pp 868-879.

Badino A., Borelli D., Gaggero T., Rizzuto E., Schenone C., (2012a.) Normative framework for Ship Noise: Present Situation and Future Trends *Noise Control Engineering Journal*, Institute of Noise Control Engineering Vol.60, pp 740-762.

Badino A., Borelli D., Gaggero T., Rizzuto E., Schenone, C. (2016). Airborne noise emissions from ships: experimental characterization of the source and propagation over land, *Applied Acoustics*, Elsevier, Vol. 104, March 2016, pp 158-171. Acoustics, Elsevier, Vol. 104, March 2016, pp 158-171.

Battistelli, L., Fantauzzi, M., Coppola, T., & Quaranta, F. (2012). Evaluation of the environmental impact of harbour activities: Problem analysis and possible solutions. In *Sustainable maritime transportation and exploitation of sea resources* (pp. 945-950). London: Taylor & Francis Group.

Badeke, R., V. Matthias, & D. Grawe, (2020). Parameterizing the vertical downward dispersion of ship exhaust gas in the near-field. *Atmospheric Chemistry and Physics Discussions*, 1-27.

Beirle, S., Platt, U., Von Glasow, R., Wenig, M., & Wagner, T. (2004). Estimate of nitrogen oxide emissions from shipping by satellite remote sensing. *Geophysical Research Letters*, *31*(18)

Benvenuto, G., Campora, U., Carrera, G., & Casoli, P. (1998). A two-zone diesel engine model for the simulation of marine propulsion plant transients. In *Proceedings of the 2nd International Conference on Marine Industry*, MARIND (Vol. 98).

Benvenuto, G., Campora, U., & Figari, M. (2000). Reduction of NOx Emissions From Marine Diesel Engines By Means of Exhaust Gas Recirculation Technique: A Numerical Approach. *In IX Congress IMAM* (pp. 2-4).

Berg, N., Mellqvist, J., Jalkanen, J. P., & Balzani, J. (2012). Ship emissions of SO2 and NO2: DOAS measurements from airborne platforms. *Atmospheric Measurement Techniques*, *5*(5), 1085-1098.

Berechman, J., & Tseng, P. H. (2012). Estimating the environmental costs of port related emissions: The case of Kaohsiung. *Transportation Research Part D: Transport and Environment*, *17*(1), 35-38.

Bergqvist, R., & Monios, J. (2019). Green Ports in Theory and Practice. In *Green Ports* (pp. 1-17). Elsevier.

Boselli, A., Armenante, M., D'Avino, L., D'Isidoro, M., Pisani, G., Spinelli, N., & Wang, X. (2009). Atmospheric aerosol characterization over Naples during 2000–2003 EARLINET project: Planetary boundary-layer evolution and layering. *Boundary-layer meteorology*, *132*(1), 151-165.

Bouman Evert A, Lindstad E., Rialland A.I., Strømman A. H. (2017). State-of-the-art technologies, measures, and potential for reducing GHG emissions from shipping – *A review, Transportation Research Part D* (52), 408–421.

Breithaupt, S. A., Copping, A., Tagestad, J., & Whiting, J. (2017). Maritime route delineation using AIS data from the atlantic coast of the US. *Journal of Navigation*, 70(2), 379–394.

Brodie, P. (2013). Dictionary of shipping terms. Informa Law from Routledge.

Casazza, M., Varchetta, G., Pirozzi, N., Teta, R., Ulgiati, S., & Lega, M. (2017). A survey method towards an effective emission monitoring within the urban environment: a case study in the port of Naples (Italy). *International Journal of Environmental Impacts*, *1*(1), 1-13.

Ćelić, J., Cuculić, A., & Valčić, M. (2012). Remote Sensing for Ship Emission Monitoring in Adriatic Ports: An Approach. *Proceedings Elmar 2012*, 263.

Cesari, D., Genga, A., Ielpo, P., Siciliano, M., Mascolo, G., Grasso, F. M., & Contini, D. (2014). Source apportionment of PM2. 5 in the harbour–industrial area of Brindisi (Italy): Identification and estimation of the contribution of in-port ship emissions. *Science of the total environment*, *497*, 392-400.

Chessell, C. I. (1977). Propagation of noise along a finite impedance boundary. The *Journal of the Acoustical Society of America,* 62(4), 825-834.

Chen, D., Zhao, N., Lang, J., Zhou, Y., Wang, X., Li, Y., ... & Guo, X., (2018). Contribution of ship emissions to the concentration of PM2. 5: A comprehensive study using AIS data and WRF/Chem model in Bohai Rim Region, China. *Science of the Total Environment*, 610, 1476-1486.

Chidambaram, K., & Thulasi, V. (2016). *Two zone modeling of combustion, performance and emission characteristics of a cylinder head porous medium engine with experimental validation*. Multidiscipline Modeling in Materials and Structures.

Clay, C. S., Chu, D., & Li, S. (1993). Specular reflections of transient pressures from finite width plane facets. *The Journal of the Acoustical Society of America*, 94(4), 2279-2286.

CLIA, (2014). Cruise Line International Association (CLIA). 2016 CLIA cruise market overview. Retrived from, https://cruising.org/en-gb/news-and-research/research, on 21/04/21.

CLIA, (2016). Cruise Line International Association (CLIA). 2014 CLIA Annual report. Retrived from, https://cruising.org/en-gb/news-and-research/research, on 21/04/21.

CLIA, (2020). Cruise Line International Association (CLIA). 2020 CLIA Annual report. Retrived from, https://cruising.org/en-gb/news-and-research/research, on 21/04/21.

CONCAWE. "The propagation of noise from petroleum and petrochemical complexes to neighboring communities," CONCAWE Report No. 4/81, Den Haag 1981).

Contini, D., Gambaro, A., Belosi, F., De Pieri, S., Cairns, W. R. L., Donateo, A., ... & Citron, M. (2011). The direct influence of ship traffic on atmospheric PM2. 5, PM10 and PAH in Venice. *Journal of Environmental Management, 92(9), 2119-2129.*

Cooper, D. A. (2001). Exhaust emissions from high-speed passenger ferries. *Atmospheric Environment*, 35(24), 4189-4200

Coppola, T., Mocerino, L., Rizzuto, E., Viscardi, M., & Siano, D. (2018, June). Airborne Noise Prediction of a Ro/Ro Pax Ferry in the Port of Naples. In *Technology and Science for the Ships of the Future: Proceedings of NAV 2018: 19th International Conference on Ship & Maritime Research* (p. 157). IOS Press.

Coppola, T., Lorenzo, F. D., & Mocerino, L. (2019, November). The Irradiated Noise Underwater by the Ships: A State of the Art. In *Nautical and Maritime Culture, from the Past to the Future: Proceedings of the 3rd International Conference on Nautical and Maritime Culture* (Vol. 3, p. 90). IOS Press.

Corbett, J. J., Winebrake, J. J., Green, E. H., Kasibhatla, P., Eyring, V., & Lauer, A. (2007). Mortality from ship emissions: a global assessment. Environmental science & technology, 41(24), 8512-8518.

Damian, V., Sandu, A., Damian, M., Potra, F.A., Carmichael, G.R., (2017). *Kinetic preprocessor*. http://people.cs.vt.edu/asandu/Software/Kpp/.

Delany, M. E., & Bazley, E. N. (1970). Acoustical properties of fibrous absorbent materials. *Applied acoustics*, 3(2), 105-116.

De Melo Rodríguez G.; Martin-Alcalde E.; Murcia-González J.C.; Saurí S., (2017). Evaluating air emission inventories and indicators from cruise vessels at ports. *WMU J Marit Affairs* (2017) DOI 10.1007/s13437-016-0122-8.

DEPA 20107. The Danish Environmental Protection Agency / Airborne Monitoring of Sulphur Emissions from Ships - 2017 Campaign Results www.explicit.dk.

Devanney, J., & Beach, S. (2010). Efficient, safe reduction of CO_2 emissions from Shipping. Retrieved (June 2010) from Http://www. c4tx. org/ctx/pub/tax_vs_ets. Pdf.

Dobrucali, E., & Ergin, S. (2019). An investigation of exhaust smoke dispersion for a generic frigate by numerical analysis and experiment. Proceedings of the Institution of Mechanical Engineers, *Part M: Journal of Engineering for the Maritime Environment*, 233(1), 310-324.

Dong Yang, Lingxiao Wu, Shuaian Wang, Haiying Jia & Kevin X. Li (2019) How big data enriches maritime research – a critical review of Automatic Identification System (AIS) data applications, *Transport Reviews*, 39:6, 755-773.

DNV, G., Safer, S. M. A. R. T. E. R., & Greener, D. (2018). *Global sulphur cap 2020. How to move ahead*.

DNV-GL (2016), *EE Appraisal Tool For Imo Project Report*, Dnv Gl As Maritime.

DNV QUIET (2019), Available online: https://www.dnvgl.com. (accessed on 4 December 2020).

Durmaz, M., Kalender, S. S., & Ergin, S. (2017). Experimental study on the effects of ultra-low sulfur diesel fuel to the exhaust emissions of a ferry. *Fresenius Environmental Bulletin*, 26(10), 5833-5840.

Economou, P., & Charalampous, P. (2013). The significance of sound diffraction effects in simulating acoustics in Ancient Theatres. *Acta Acustica united with Acustica*, 99(1), 48-57.

EcoPort Project 2006. EU Co-Financed Project through the European Regional Development Fund (ERDF) in the Framework of the Adriatic New Neighbourhood Program INTER-REG/CARDS-PHARE 2000–2006. Available online: https://www.port.venice.it/it/progetto-eco-port.html (accessed on 1 July 2020).

EcoPorts 2011. EcoPorts Project, Information Exchange and Impact Assessment for Enhanced Environmental-Conscious Operations in European Ports and Terminals, FP5. Available online: http://cordis.europa.eu/project/rcn/87079_en.html (accessed on 1 July 2020).

EMEP/EEA (2013): Air Pollutant Emission Inventory Guidebook International Maritime Navigation. *European Environment Agency* (2013).

EMEP/EEA (2016). Air Pollutant Emission Inventory Guidebook 2016: technical guidance to prepare national emission inventories. *EEA-Report*, 2016, 21.

Entec UK Limited, (2002). Quantification of Emissions from Ships Associated with Ship Movements Between Ports in the European Community. Entec UK Limited, Nortwich.10.1080/01441647.2019.1649315.

Ergin, S. (2008). A Study on Exhaust Emissions Reduction System for Marine Diesel Engines. *Proceedings of 12th Int. Congress of the Int. Maritime Assoc. of the Mediterranean* (IMAM 2007) Varna, Bulgaria. Maritime Industry, Ocean Engineering and Coastal Resources, 2008, Taylor & Francis Group, London, ISBN 978-0-415-45523-7.

Eyring, V., Köhler, H., van Aardenne, J., Lauer, A., (2005). Emissions from international shipping: 1. The last 50 years. *Journal of Geophysical Research* 110, D17305. doi:10.1029/2004JD005619.

E.U. Directive 2002/49/EC of the European parliament and the Council of 25 June 2002 relating to the assessment and management of environmental noise. *Off. J. Eur. Communities* L 2002, 189, 2002.

Faber, J., Wang, H., Nelissen, D., Russell, B., & Amand, D. (2011). *Marginal abatement costs and cost effectiveness of energy-efficiency measures*. International Maritime Organization, London, UK.

Fan, Q., Zhang, Y., Ma, W., Ma, H., Feng, J., Yu, Q., ... & Chen, L. (2016). Spatial and seasonal dynamics of ship emissions over the Yangtze River Delta and East China Sea and their potential environmental influence. *Environmental science & technology*, *50*(3), 1322-1329.

Fenimore, C. P. (1971, January). Formation of nitric oxide in premixed hydrocarbon flames. In *Symposium (International) on Combustion* (Vol. 13, No. 1, pp. 373-380). Elsevier.

Fenton, P. (2017). The role of port cities and transnational municipal networks in efforts to reduce greenhouse gas emissions on land and at sea from shipping–an assess-ment of the World Ports Climate Initiative. *Marine Policy*, 75, 271-277.

Fredianelli, L., Nastasi, M., Bernardini, M., Fidecaro, F., & Licitra, G. (2020). Pass-by characterization of noise emitted by different categories of seagoing ships in ports. *Sustainability*, 12(5), 1740.

Fernald, F. G. (1984). Analysis of atmospheric lidar observations: some comments. *Applied optics*, 23(5), 652-653.

Fuglestvedt, J., Eyring, V., Isaken I., Lee D., Sausen R., (2009). Shipping Emissions: From Cooling to Warming of Climates-and Reducing Impacts on Health, *Environ. Sci. Technol*. 43 (2009), 9057–9062.

Fumo, N., & Biswas, M. R. (2015). Regression analysis for prediction of residential energy consumption. *Renewable and sustainable energy re-views*, 47, 332-343.

Gariazzo, C., Papaleo, V., Pelliccioni, A., Calori, G., Radice, P., & Tinarelli, G. (2007). Application of a Lagrangian particle model to assess the impact of harbour, industrial and urban activities on air quality in the Taranto area, Italy. *Atmospheric Environment*, *41*(30), 6432-6444.

Gasteiger, J., Groß, S., Freudenthaler, V., & Wiegner, M. (2011). Volcanic ash from Iceland over Munich: mass concentration retrieved from ground-based remote sensing measurements. *Atmospheric chemistry and physics*, 11(5), 2209-2223.

Gibbs, D., Rigot-Muller, P., Mangan, J., & Lalwani, C. (2014). The role of sea ports in end-to-end maritime transport chain emissions. *Energy Policy*, 64, 337-348.

Giernalczyk, M., Górski, Z., & Kowalczyk, B. (2010). Estimation method of ship main propulsion power, onboard power station electric power and boilers capacity by means of statistics. *Journal of Polish CIMAC*, 5(1), 33-42.

Goodwin, D.G., Moffat, H.K., Speth, R.L., (2017). Cantera: an object-oriented software toolkit for chemical kinetics, thermodynamics, and transport processes. http://www.cantera.org version 2.3.0.

Hadden Jr, W. J., & Pierce, A. D. (1981). Sound diffraction around screens and wedges for arbitrary point source locations. *The Journal of the Acoustical Society of America*, 69(5), 1266-1276.

Hansen, J. F., Ådnanes, A. K., & Fossen, T. I. (2001). Mathematical modelling of diesel-electric propulsion systems for marine vessels. *Mathematical and Computer Modelling of Dynamical Systems*, 7(3), 323-355.

Harati-Mokhtari, A., Wall, A., Brooks, P., & Wang, J. (2007). Automatic Identification System (AIS): Data reliability and human error implications. *Journal of Navigation*, 60(3), 373–389.

Hasan, S. M. (2011). Impact of EEDI on Ship Design and Hy-drodynamics A Study of the Energy Efficiency Design Index and Other Related Emission Control Indexes. Master of Science Thesis. Gothenburg, Sweden, (Report No. X-11/272).

Heywood, J. B. (1988). *Combustion engine fundamentals.* 1ª Edição. Estados Unidos.

Herramienta Automática de Diagnóstico Ambiental (Automatic Tool for Environmental Diagnosis), LIFE02 ENV/E/000274; Environment-LIFE: Brussels, Belgium, 2005.

Hon, G., & Wang, H. (2011). *The Energy Efficiency Design Index (EEDI) for New Ships.* ICCT Policy Update, 1-9.

Hosoz, M., Ertunc, H. M., Karabektas, M., & Ergen, G. (2013). ANFIS modelling of the performance and emissions of a diesel engine using diesel fuel and biodiesel blends. *Applied Thermal Engineering*, 60(1-2), 24-32.

IALA. (2004). IALA guideline no. 1028 on the Automatic Identification System (AIS) volume 1, part I operational issues edition 1.3. Retrieved from https://www.e-navigation.nl/sites/default/files/ universal-automatic-identification-ais-volume-1-part-1-operational-issues-1028.pdf

IMO (1988), *International Maritime Organization 1998, Annex VI of MARPOL 73/78 and NOx Technical Code*, IMO-664E ed.,150 pp., International Maritime Organization, London, UK.

IMO (2003), *Guidelines for the installation of a shipborne automatic identification system*, SN/Circ.227.

IMO (2007), International Maritime Organization 2007, *Review of MARPOL Annex VI and the NOx Technical Code; Report on the outcome of the Informal Cross Government/Industry Scientific Group of Experts established to evaluate the effects of the different fuel options proposed under the revision of MARPOL Annex VI*, p. 48.

IMO (2008),International Maritime Organization, and Marine Environment Protection Committee 2008, *Report of the Working Group on Annex VI and the NOx Technical Code*, edited by B. Wood-Thomas, London.

IMO (2014), *Guidelines on the Method of Calculation of the Attained Energy Efficiency Design Index (EEDI) For New Ships- Annex 5*, MEPC66, 2014.

IMO (2016), *Guidelines for the Development of a Ship Energy Efficiency Management Plan (SEEMP)*- Annex 10, MEPC70 2016.

IPCC (2007), *Climate Change: Mitigation. Contribution of Working Group III to the Fourth Assessment Report of the Intergovernmental Panel on Climate Change*, Cambridge University Press, Cambridge, United Kingdom and New York, NY, USA, 2007.

IPCC (2014), *Climate Change 2014: Mitigation of Climate Change. Contribution of Working Group III to the Fifth Assessment Report of the Intergovernmental Panel on Climate Change*, Cambridge University Press, Cambridge, United Kingdom and New York, NY, USA, 2014

IPCC (2014a), Climate Change 2014: Synthesis Report. Contribution of Working Groups I, II and III to the Fifth Assessment Report of the Intergovernmental Panel on Climate Change, IPCC, Geneva, Switzerland, 151 pp, 2014.

Ishida M., Ueki H., Matsumura N., Chen Z. L (1996). Diesel Combustion Analysis Based on Two-Zone Model. JSME *International Journal*, Series B, Vol. 39. No. 3.

ISO (1993). Attenuation of sound during propagation outdoors Part 1: Calculation of the absorption of sound by atmosphere Standard ISO 9613-1 International Organization for Standardization, Geneva, CH

ISO (1996). Attenuation of sound during propagation outdoors Part 2: General method of calculation, Standard ISO 9613-2 International Organization for Standardization, Geneva, CH.

ISO 8297:1994 Acoustics —Determination of sound power levels of multisource industrial plants for evaluation of sound pressure levels in the environment —Engineering method

ISO 3744:2010 Acoustics — Determination of sound power levels and sound energy levels of noise sources using sound pressure— Engineering methods for an essentially free field over a reflecting plane

Jalkanen, J. P., A. Brink, J. Kalli, H. Pettersson, J. Kukkonen, & T Stipa. (2009). A modelling system for the exhaust emissions of marine traffic and its application in the Baltic Sea area. *Atmospheric Chemistry & Physics*, 9(23).

Jinghong Gao, Sari Kovats, Sotiris Vardoulakis, Paul Wilkinson, AlistairWoodward, Jing Li, Shaohua Gu, Xiaobo Liu, Haixia Wua, JunWang, Xiaoqin Song, Yunkai Zhai, Jie Zhao, Qiyong Liua (2018). Public health co-benefits of greenhouse gas emissions reduction: A systematic review, *Science of the Total Environment* 627 (2018), 388–402.

Johansson L., Jalkanen J., Kukkonen J. (2017). Global assessment of shipping emission in 2015 on high spatial and temporal resolution, *Atmospheric Environment* 167 (2017), 403-415.

Judd, C. M., McClelland, G. H., & Ryan, C. S. (2011). Data analysis: A model comparison approach. Routledge.

Jukka-Pekka Jalkanen, Lasse Johansson and Jaakko Kukkonen. (2014). 'A Comprehensive Inventory of the Ship Traffic Exhaust Emissions in the Baltic Sea from 2006 to 2009'. In: *AMBIO* 43.3 (Apr. 2014), pp. 311– 324.

Kalender, S. S., & Ergin, S. (2017). An experimental investigation into the particulate emissions of a ferry fuelled with ultra-low sulfur diesel. *Journal of Marine Science and Technology*, 25(5), 499-507.

Kaluza, P., Kölzsch, A., Gastner, M. T., & Blasius, B. (2010). The complex network of global cargo ship movements. *Journal of the Royal Society Interface*, 7(48), 1093–1103.

Kee, R. J., Rupley, F. M., Meeks, E., and Miller, J. A., (1996), Chemkin III User Manual, Reaction Design, San Diego, CA.

Keller, J. B. (1962). Geometrical theory of diffraction. *Josa*, 52(2), 116-130.

Klett JD (1981). Stable analytical inversion solution for processing lidar returns. *Applied optics* 20.2: 211-220

Kivekäs, N., Massling, A., Grythe, H., Lange, R., Rusnak, V., Carreno, S.,…Kristensson, A. (2014). Contribution of ship traffic to aerosol particle concentrations downwind of a major shipping lane. *Atmospheric Chemistry and Physics*, 14(16), 8255–8267.

Kuiken, K. (2008). *Diesel engines for ship propulsion and power plants*, vol. 1. I1, Onnen, the Netherland, 314-333.

Kuzu, S. L., L. Bilgili, &, A Kiliç. (2020). Estimation and dispersion analysis of shipping emissions in Bandirma Port, Turkey. *Environment, Development and Sustainability*, 1-21.

Kristensen, H.O. (2012). *Energy demand and exhaust gas emissions of marine engines*. Technical University of Denmark: Univertsity of southern Denmark.

Lam, Y. W. (2005). Issues for computer modelling of room acoustics in non-concert hall settings. *Acoustical science and technology,* 26(2), 145-155.

Lamb, T. (2003). *Ship design and construction*. Editor Thomas Lamb, Published by: The SNAME, ISBN: 0-939773-40-6.

Larkin A., Smith T., Wrobel P. (2017). Shipping in changing climates, *Marine Policy* 75 (2017), 188–190.

Lavoie GA, Heywood JB, Keck JC, (1970). Experimental and theoretical study of nitric oxide formation in internal combustion engines. *Combust Sci Technol* 1970;1:313–26.

Lepore, A., dos Reis, M. S., Palumbo, B., Rendall, R., & Capezza, C. (2017). A comparison of advanced regression techniques for predicting ship CO_2 emissions. *Quality and Reliability Engineering International*, 33(6), 1281-1292.

Lee, J. G., Han, J., & Whang, K. Y. (2007). Trajectory clustering: A partition-and-group framework. In Proceedings of the 2007 ACM SIGMOD *International Conference on Management of Data* (pp. 593–604). ACM.

Liu, Z., Lu., X, Feng, J., Fan, Q., Zhang, Y., Yang, X.: Influence of Ship Emissions on Urban Air Quality, (2017). A Comprehensive Study Using Highly Time-Resolved Online Measurements and Numerical Simulation in Shanghai. *Environ Sci Technol*. 51(1), 202-211

Lloyd's Register, (2019). Design and Construction Additional Design and Construction, *Procedure for the Determination of Airborne Noise Emissions from Marine Vessels*, Lloyd's Register Group Limited 2019 Published by Lloyd's Register Group Limited.

Lonati, G., Cernuschi, S., & Sidi, S. (2010). Air quality impact assessment of at-berth ship emissions: Case-study for the project of a new freight port. *Science of the Total Environment*, *409*(1), 192-200.

Masieri, S., Premuda, M., Bortoli, D., Kostadinov, I., Petritoli, A., Ravegnani, F., & Giovanelli, G. (2009). Cruise ships flow rate emission evaluated by means of a passive DOAS instrument. In *Remote Sensing for Environmental Monitoring*, GIS Applications, and Geology IX (Vol. 7478, p. 74781S). International Society for Optics and Photonics.

Mazzarella, F., Alessandrini, A., Greidanus, H., Alvarez, M., Argentieri, P., Nappo, D., & Ziemba, L. (2013). Data fusion for wide-area maritime surveillance. In Proceedings of the COST MOVE workshop on moving objects at sea, Brest, France (pp. 27–28).

MEPC (2009). MEPC 1./Circ.684. Guidelines for voluntary use of the ship energy efficiency operational indicator (EEOI).

MEPC (2012a). Guidelines on the method of calculation of the attained Energy Efficiency Design Index (EEDI) for new ships. Resolution MECP 212 (63/23), Annex 8, March 2012, http://www.imo.org/en/OurWork/Environment/PollutionPrevention/AirPollution/Documents/212(63).pdf.

MEPC (2012b). MEPC 1./Circ.213 (63). *Guidelines for the development of a Ship Energy Efficiency Management Plan (SEEMP).*

MEPC 245(66). (2014). Guidelines on the method of calculation of the attained Energy Efficiency Design Index (EEDI) for new ships adopted by resolution.

MEPC, (2014). Reduction of GHG Emissions from Ships, Third IMO GHG Study 2014 Final Report. Tech. Rep. MEPC 67/INF.3. Marine Environment Protection Committee, London, UK.

MEPC 308(73)/19/Add.1 2018 Guidelines On The Method Of Calculation Of The Attained Energy Efficiency Design Index (EEDI) For New Ships

Merico, E., Donateo, A., Gambaro, A., Cesari, D., Gregori, E., Barbaro, E., Dinoi, A., Giovanelli, G., Masieri, S., Contini, D., (2016). Influence of in-port ships emissions to gaseous atmospheric pollutants and to particulate matter of different sizes in a Mediterranean harbour in Italy. *Atmospheric Environment* 139, 1-10

Merico, E., Gambaro, A., Argiriou, A., Alebic-Juretic, A., Barbaro, E., Cesari, D., Chasapidis, L., Dimopoulos, S., Dinoi, A., Donateo, A., Giannaros, C., Gregoris, E., Karagiannidis, A., Konstandopoulos, A.G., Ivoševic´, T., Liora, N., Melas, D., Mifka, B., Orlic´, I., Poupkou, A., Sarovic, K., Tsakis, A., Giua, R., Pastorel, T., Nocioni, A., Contini, D., (2017). Atmospheric impact of ship traffic in four Adriatic-Ionian port-cities: Comparison and harmonization of different Approaches. *Transportation Research Part D* 50 (2017) 431–445

Merico, E., Dinoi, A., & Contini, D. (2019). Development of an integrated modelling-measurement system for near-real-time estimates of harbour activity impact to atmospheric pollution in coastal cities. *Transportation Research Part D: Transport and Environment*, *73*, 108-119.

Minitab: Meet for Windows, (2007).

Miola, A., & Ciuffo, B. (2011). Estimating air emissions from ships: Meta-analysis of modelling approaches and available data sources. *Atmospheric environment*, *45*(13), 2242-2251.

Mitchell, K. N., & Scully, B. (2014). Waterway performance monitoring with Automatic Identification System data. *Transportation Research Record: Journal of the Transportation Research Board*, 2426, 20–26.

Mocerino, L., Quaranta, F., & Rizzuto, E. (2018). Climate changes and maritime transportation: A state of the art. *In NAV International Conference on Ship and Shipping Research*, (221499). https://doi. org/10.3233/978-1-61499-870-9-1005.

Mocerino, L., Murena, F., Quaranta, F., Toscano, D. (2020). A methodology for the design of an effective air quality monitoring network in port areas. *Scientific Reports*, 10(1), 1-10.

Molland, A. F. (Ed.). (2011). *The maritime engineering reference book: a guide to ship design, construction and operation.* Elsevier.

Morris, R. E., Kessler, R. C., Douglas, S. G., Styles, K. R., & Moore, G. E., (1988). Rocky Mountain acid-deposition model assessment: Acid Rain Mmountain Mesoscale Model (ARM3). Final report (No. PB-89-124408/XAB). Systems Applications, Inc., San Rafael, CA (USA).

Murena, F., Prati, M. V., & Quaranta, F. (2014). Monitoring the quality of air in the port of Naples. *Developments in maritime transportation and exploitation of sea resources*, 835-833.

Murena, F., Prati, M.V., Quaranta, F. (2017). Assessment of the impact of ship emissions on the air quality in Naples. *IMAM 2017.*

Murena, F., Mocerino, L., Quaranta, F., Toscano, D., (2018). Impact on air quality of cruise ship emissions in Naples, Italy. *Atmospheric Environment*, 187, 70-83.

Neptunes Project. Available online: https://www.neptunes.pro/ (accessed on 4 December 2020).

NoMEPorts (2008). Noise Management in European Ports, LIFE05 ENV/NL/000018, Good Practice Guide on Port Area Noise Mapping and Management. Technical Annex; Environment-LIFE: Brussels, Belgium, 2008.

Nota R., Barelds R., van Maercke D., (2005). “Harmonoise WP 3 engineering method for road traffic and railway noise after validation and fine-tuning,” (HARMONOISE, WP3, 2005).

Olive, D. J. (2017). *Multiple linear regression. In Linear regression* (pp. 17-83). Springer, Cham.

Papaefthimiou, S., Maragkogianni, A., & Andriosopoulos, K. (2016). Evaluation of cruise ships emissions in the Mediterranean basin: The case of Greek ports. *International Journal of Sustainable Transportation*, *10*(10), 985-994.

PEMARD 2017. Olive Tree Lab Suite: An integrated acoustics software for indoors and outdoors. Mediterranean Acoustic Research Development Ltd., Limassol CY http://www.mediterraneanacoustics.com/olive-tree-lab-suite.html.

Perera, L. P., Oliveira, P., & Guedes Soares, C. (2012). Maritime traffic monitoring based on vessel detection, tracking, state estimation, and trajectory prediction. *IEEE Transactions on Intelligent Transportation Systems*, 13(3), 1188–1200.

Poplawski, K., Setton, E., McEwen, B., Hrebenyk, D., Graham, M., & Keller, P. (2011). Impact of cruise ship emissions in Victoria, BC, Canada. *Atmospheric Environment*, *45*(4), 824-833.

Prati, M. V., Costagliola, M. A., Quaranta, F., & Murena, F. (2015). Assessment of ambient air quality in the port of Naples. *Journal of the Air & Waste Management Association*, *65*(8), 970-979.

Quaranta, F., Fantauzzi, M., Coppola, T., Battistelli, L. (2012). The environmental impact of cruise ships in the port of Naples: analysis of the pollution level and possible solutions. *Journal of Maritime Research*, 9(3): 81-86.

Reaction Design, (2017). Chemkin. http://www.reactiondesign.com/products/chemkin/ chemkin-2/.

Raptotasios SI et al (2015). Application of a multi-zone combustion model to investigate the NOx reduction potential of twostroke marine diesel engines using EGR. *Appl Energy* 2015, http://dx.doi.org/10.1016/j.apenergy.2014.12.041.

Rehmatulla, N., Smith, T., & Wrobel, P. (2013). *Implementation barriers to low carbon shipping.*

Rodríguez, G. D. M., Martin-Alcalde, E., Murcia-González, J. C., & Saurí, S. (2017). Evaluating air emission inventories and indicators from cruise vessels at ports. *WMU Journal of Maritime Affairs*, 16(3), 405-4204.

Rong, H.; Teixeira, A. P., and Guedes Soares, C. Ship trajectory uncertainty prediction based on a Gaussian Process model . Ocean Engineering. 2019; 182499-511.

Rong, H.; Teixeira, A. P., and Guedes Soares, C. Data mining approach to shipping route characterization and anomaly detection based on AIS data . *Ocean Engineering* . 2020; 198106936

Salomons, E. M. (1997). Sound propagation in complex outdoor situations with a non-refracting atmosphere: model based on analytical solutions for diffraction and reflection. *Acta Acustica united with Acustica*, 83(3), 436-454.

Saxe, H., & Larsen, T. (2004). Air pollution from ships in three Danish ports. *Atmospheric environment*, *38*(24), 4057-4067.

Schenone, C., Pittaluga, I., Borelli, D., Kamali, W., El Moghrabi, Y. (2016). The impact of environmental noise generated from ports: Outcome of MESP project. *Noise Mapp*. 2016, 3.

Scire, J.S., Strimaitis, D.G., Yamartino, R.J., (2000). A User’s Guide for the CALPUFF Dispersion Model. Earth Tech Inc, Long Beach, CA.

Scollo, S., Boselli, A., Coltelli, M., Leto, G., Pisani, G., Prestifilippo, M., ... & Wang, X. (2015). Volcanic ash concentration during the 12 August 2011 Etna eruption. *Geophysical Research Letters*, *42*(8), 2634-2641.

Scully, B. M., & Mitchell, K. N. (2017). Underkeel clearance reliability model for dredged navigation channels. *Transportation Research Record: Journal of the Transportation Research Board*, 2611, 41–49.
Schumann, U., Weinzierl, B., Reitebuch, O., Schlager, H., Minikin, A., Forster, C., ... & Sturm, K. (2011). Airborne observations of the Eyjafjalla volcano ash cloud over Europe during air space closure in April and May 2010. *Atmospheric Chemistry and Physics*, 11(5), 2245-2279.
Seyler, A., Wittrock, F., Kattner, L., Mathieu-Üffing, B., Peters, E., Richter, A., ... & Burrows, J. P. (2017). Monitoring shipping emissions in the German Bight using MAX-DOAS measurements. *Atmospheric Chemistry and Physics*, *17*(18), 10997-11023.
Skamarock, W. C., & Klemp, J. B. (2005). A description of the Advanced Research WRF version 3. NCAR Tech. Note NCAR/TN-4751STR, 113 pp., doi: 10.5065/D68S4MVH.
Shi Y., (2016). Reducing greenhouse gas emissions from international shipping: Is it time to consider market- based measures?, *Marine Policy*, (2016), 64 123–134.
Sicard, M., Rocadenbosch, F., Reba, M. N. M., Comerón, A., Tomás, S., García-Vízcaino, D., ... & Baldasano, J. M. (2011). Seasonal variability of aerosol optical properties observed by means of a Raman lidar at an EARLINET site over Northeastern Spain. *Atmospheric Chemistry and Physics*, 11(1), 175-190.
SILENV (2012).Ships oriented Innovative soLutions to rEduce Noise and Vibrations, FP7. ⟨http://www.silenv.eu/⟩.
Simonen, P., Dal Maso, M., & Kangasniemi, O. (2020). THE SCIPPER PROJECT. Shipping Contributions to Inland Pollution Push for the Enforcement of Regulations. EUROPEAN COMMISSION, Horizon 2020 No. 814893.
SIMPYC (2008). Sistema de Integración Medioambiental de Puertos y Ciudades (Environmental integration for ports and cities), LIFE04 ENV/ES/000216; Environment-LIFE: Brussels, Belgium, 2008.
Sims R., R. Schaeffer, F. Creutzig, X. Cruz-Núñez, M. D'Agosto, D. Dimitriu, M. J. Figueroa Meza, L. Fulton, S. Kobayashi, O.Lah, A. McKinnon, P. Newman, M. Ouyang, J. J. Schauer, D. Sperling, and G. Tiwari, (2014). *Transport In: Climate Change 2014: Mitigation of Climate Change. Contribution of Working Group III to the Fifth Assessment Report of the Intergovernmental Panel on Climate Change*, Cambridge University Press, Cambridge, United Kingdom and New York, NY, USA (2014), 599-670.
Smith, T.W.P., Jalkanen, J.P., Anderson, B.A., Corbett, J.J., Faber, J., Hanayama, S., O'Keeffe, E., Parker, S., Johansson, L., Aldous, L., Raucci, C., Traut, M., Ettinger, S., Nelissen, D., Lee, D.S., Ng, S., Agrawal, A., Winebrake, J.J., Hoen, M., Chesworth, S., Pandey, A., (2014). *Third IMO GHG Study 2014*. International Maritime Organization (IMO), London, UK, pp. 2014 (June).
Solomon, S. (2007, December). IPCC (2007). Climate change the physical science basis. In *Agu fall meeting abstracts* (Vol. 2007, pp. U43D-01).
Svensson, E., & Andersson, K. (2012). Inventory and evaluation of environmental performance indices for shipping. Chalmers University of Technology.
Szelangiewicz, T., & Żelazny, K. (2015). An approximate method for calculating total ship resistance on a given shipping route under statistical weather conditions and its application in the initial design of container ships. Zeszyty Naukowe Akademii Morskiej w Szczecinie.).
Tadros, M., Ventura, M., & Guedes Soares, C. (2015). 'Numerical simulation of a two-stroke marine diesel engine' in *Towards Green Marine Technology and Transport*. CRC Press, Taylor & Francis Group, London Guedes Soares, C., Dejhalla, R., Pavletic, D. (Eds.), pp. 609-617, 2015.
Tadros, M., Ventura, M., & Guedes Soares, C. (2015). Numerical simulation of a two-stroke marine diesel engine. *Towards Green Marine Technology and Transport*. Taylor & Francis Group, London, 609-617.
Tadros, M., Ventura, M., & Guedes Soares, C. (2016). Assessment of the performance and the exhaust emissions of a marine diesel engine for different start angles of combustion. *Maritime Technology and Engineering*, 3, 769-775.
Tadros, M., Ventura, M., & Guedes Soares, C.2018. Surrogate models of the performance and exhaust emissions of marine diesel engines for ship conceptual design. *Transport*, 2, 1.
Tadros, M., Ventura, M., Guedes Soares, C.., & Lampreia, S. (2019a). Predicting the performance of a sequentially turbocharged marine diesel engine using ANFIS. In: *Georgiev, P. & Guedes Soares C., (Eds.). Sustainable Development and Innovations in Marine Technologies.* Engineering 3, Guedes Soares, C. & Santos T. A., (Eds.); London, UK Taylor & Francis Group; pp. 769-775.
Tadros, M., Ventura, M., & Guedes Soares, C. (2019). Optimization procedure to minimize fuel consumption of a four-stroke marine turbocharged diesel engine. *Energy*, 168, 897-908. (B)
Tadros, M., Ventura, M., & Guedes Soares, C. (2020). Data Driven In-Cylinder Pressure Diagram Based Optimization Procedure. *Journal of Marine Science and Engineering*, 8(4), 294.
Tichavska, M., B. Tovar, (2015). Port-city exhaust emission model: an application to cruise and ferry operations in Las Palmas port. *Transp. Res. A Policy Pract*. 78, 347–360.
Trodden, D. G., & Haroutunian, M. (2018). Effects of ship manœuvring motion on NO_X formation. *Ocean Engineering*, 150, 234-242.
Trozzi, C., & De Lauretis, R. (2016). EMEP/EEA Air Pollutant Emission Inventory Guidebook 2016 (Technical guidance to prepare national emission inventory), ISBN 978-92-9213-806-6, European Environment Agency.

Trozzi, C., & De Lauretis, R. (2019). EMEP/EEA Air Pollutant Emission Inventory Guidebook 2019, European Environment Agency.
UNCTAD (2013). *Review of Maritime Transport 2013, United Nations Publication*, 2013.
UNCTAD (2017*). Review of Maritime Transport 2017, United Nations Publication*, 2017.
UNCTAD (2019). *Review of Maritime Transport 2017, United Nations Publication*, 2019.
Underwood, K., (2009). *Ocean-Friendly Eco Cruises Hit-ting the High Seas*, www.treehugger.com.
UNFCC (2012). *Doha amendment to the Kyoto Protocol*, Doha, 2012.
UNFCC (2015). Negotiating text, Agenda item 3-Implementation of all the elements of decision 1/CP.17, Ad Hoc Working Group on the Durban Platform for Enhanced Action, Second session, part eight Geneva, 8–13 February 2015
VDI 2714, "Outdoor sound propagation" (Beuth-Verlag, Berlin, 1988) (in German), and VDI 2720 – Part 1, "Noise control by barriers outdoors" (Beuth-Verlag, Berlin, 1997).
Vettor, R., Tadros, M., Ventura, M., & Guedes Soares, C. (2018). Influence of main engine control strategies on fuel consumption and emissions. *Progress in Maritime Technology and Engineering*. Guedes Soares, C. & Santos T. A., (Eds.), London: Taylor & Francis Group, 157-163.
Viana, M., P. Hammingh, A. Colette, X. Querol, B. Degraeuwe, I. de Vlieger, and J. van Aardennee. (2014). Impact of maritime transport emissions on coastal air quality in Europe. *Atmos. Environ*. 90:96–105. doi: 10.1016/j.atmosenv.2014.03.046.
Wade W. R., Hunter C. E., Trinker F. H., Cikanek H. A. (1988). Reduction of NOx and Particulate Emissions in the Diesel Combustion Proces - *ASME Transaction, Journal of Engineering for Gas Turbines and Power*, Vol. 109, October, pp 426-434, 1987.
Wang, J., Zhu, C., Zhou, Y., & Zhang, W. (2017). Vessel spatio-temporal knowledge discovery with AIS trajectories using co-clustering. *Journal of Navigation*, 70(6), 1383–1400.
Watson, R. T., Holm, H., & Lind, M. (2015). Green steaming: A methodology for estimating carbon emissions avoided. Thirty Sixth International Conference on Information Systems, Fort Worth, the U.S.A.
Weisberg, S. (2005). *Applied linear regression* (Vol. 528). John Wiley & Sons.
WHO (1999). Guidelines for Community Noise, Berglund B., Lindvall T. & Schwela D. Edts. World Health Organization, Occupational and Environmental Health Team, Copenhagen DK http://www.who.int/docstore/peh/noise/guidelines2.html.
WHO, (2016). Health risk assessment of air pollution – general principles. http://www. euro.who.int/__data/assets/pdf_file/0006/298482/Health-risk-assessment-air-pollut ion-General-principles-en.pdf
Winnis, H., and Fridell, E., (2010). Emissions of NOx and particles from manoeuvring ships. *Transportation Research Part D* 15204-211
Winther, M., Christensen, J. H., Plejdrup, M. S., Ravn, E. S., Eriksson, Ó. F., & Kristensen, H. O. (2014). Emission inventories for ships in the Arctic based on satellite sampled AIS data. *Atmospheric Environment*, 91, 1–14.
Vitali, N.; Prpic-Oršic, J., and Guedes Soares, C. Coupling voyage and weather data to estimate speed loss of container ships in realistic conditions. Ocean Engineering. 2020; 210106758
WPCI, World Ports Climate Initiative. (2010). Environmental ship index. www.wpci-esi.org/Public/Home.
WPCI, World Ports Climate Initiative. (2011a). Environmen-tal Ship Index, ESI: Introduction. http://esi.wpci.nl/Public/Home.
WPCI, World Ports Climate Initiative. (2011b). The Main Characteristics of ESI. http://esi.wpci.nl/Public/Home/AboutESI.
WPCI, *World Ports Climate Initiative*. (2011c). ESI Formulas. http://esi.wpci.nl/Public/Home/ESIFormulas.
Xu, H. T.; Rong, H., and Guedes Soares, C. Use of AIS data for guidance and control of path-following autonomous vessels. *Ocean Engineering*. 2019; 194106635
Zhang, L., Meng, Q., & Fang, T. F. (2017). Big AIS data based spatial-temporal analyses of ship traffic in Singapore port waters. *Transportation Research Part E: Logistics and Transportation Review*. doi:10.1016/j.tre.2017.07.011
Zel'dovich YB (1946). The oxidation of nitrogen in combustion explosions. *Acta Physicochim* URS 1946; 21: 577–628.
Zetterdahl, M. (2016). *Particle emissions from ships: measurements on exhausts from different marine fuels* (No. 4064).

13. Sitography

[1] https://19january2017snapshot.epa.gov/climatechange/social-cost-carbon_.html
[2] https://news.stanford.edu/2015/01/12/emissions-social-costs-011215/
[3] http://www.consilium.europa.eu, Accordo di Parigi sui cambiamenti climatici, 2018.
[4] https://cop24.gov.pl/
[5] http://www.imo.org/en/OurWork/Safety/Navigation/Pages/AIS.aspx
[6] http://www.minitab.com
[7] https://support.minitab.com
[8] https://adsptirrenocentrale.it
[9] https://adsptirrenocentrale.it/wp-content/uploads/2020/12/10_Bollettino-statistico-10-mesi-2020.pdf
[10] https://www.visitnaples.eu/en/neapolitanity/discover-naples/the-port-of-naples-from-birth-to-its-change-over-the-centuries
[11] http://www.arpacampania.it
[12] https://spire.com/spirepedia/automatic-identification-system/
[13] http://www.naviecapitani.it
[14] https://ec.europa.eu/environment/air/pdf/chapter2_ship_emissions.pdf
[15] https://www.mediterraneanacoustics.com/
[16] https://www.cruisecritic.co.uk/articles.cfm?ID=528
[17] https://www.environmentalshipindex.org/

ta tcam